Modeling Atmospheric Mercury Deposition to the Great Lakes: Examination of the Influence of Variations in Model Inputs, Parameters, and Algorithms on Model Results

Final Report
for work conducted with FY2011 funding from the
Great Lakes Restoration Initiative

June 30, 2013

Mark Cohen, Roland Draxler, Richard Artz
NOAA Air Resources Laboratory
College Park, MD, USA

Contents

Executive Summary

This study examined the influence of variations in inputs, parameters, and algorithms on the estimated 2005 atmospheric mercury deposition to the Great Lakes with the HYSPLIT-Hg model. It represents an extension of the baseline analysis carried out with FY2010 Great Lakes Restoration Initiative (GLRI) funding (Cohen et al., 2011). The overall objective of this FY2011-funded 2nd phase of the project was to determine how robust the model results are with respect to various uncertainties in the analysis.

As described in the baseline analysis report, the overall modeling methodology is based on a series of unit emissions (1 g/hr) simulations of Hg(0), Hg(II), and Hg(p) from a number of standard source locations (SSL's). Each simulation with the HYSPLIT-Hg model was for 15 months, representing 3 months of "model spin up" before the start of 2005 and the 12 months of 2005. Results from the unit emissions simulations are then used, through spatial and chemical interpolation, to estimate the 2005 impacts on the Great Lakes and other key receptors from each source in the emissions inventory used in the analysis. In the baseline analysis, a total of 408 15-month HYSPLIT-Hg unit-emissions simulations were carried out to provide the basis for the analysis. As described below, a total of 828 additional 15-month HYSPLIT-Hg simulations were carried out in this 2nd phase of the project.

Due to computational resource constraints, only a few different overall variations in the "full" analysis could be undertaken. However, numerous variations were examined for a subset of five "illustrative" standard source locations (SSL's), representing local, regional, national/continental, and global sources. Several different types of variations were investigated for these illustrative source locations, including input meteorological data, and dispersion, deposition, and chemical transformation methodologies. A total of 320 different 15-month HYSPLIT-Hg simulations were carried out. The variations that were generally found to have the biggest influence on the simulations were: (a) the choice of input meteorological data [NARR (North American Regional Reanalysis) vs. EDAS (Eta Data Assimilation System)]; (b) variations in a particular model parameter affecting the wet deposition of atmospheric particles; and (c) variations in the emissions release height, primarily for the "local" impacts examined. Other variations examined, in numerous dispersion and chemical transformation parameters, generally had relatively small impacts on the simulations.

As discussed in the report, the NARR meteorological dataset is believed to be more accurate than then comparable EDAS dataset for 2005, and so the changes resulting from the use of the NARR rather than EDAS dataset to drive the HYSPLIT-Hg model can be viewed more as an "improvement" in the results rather than strictly a representation of the uncertainty associated with the choice of meteorological data.

Similarly, the impacts associated with variations in release height, while significant for near-field deposition impacts, should not be thought of strictly as an uncertainty. This is because the emissions release height used as the default was chosen to be representative of the mercury sources with the largest impacts. Thus, while a different (e.g., lower) release height was found to influence the results immediately downwind of the source, this would generally affect sources with relatively small impacts.

Moreover, most of the emissions impacting the Great Lakes are not immediately upwind of a given lake. Therefore, this issue is not expected to have an overly significant impact on the overall results.

The variation if the particle-wet-deposition parameter (WETR), found to exert significant influence over the modeling results in some cases, does represent more of an uncertainty in the simulation. The "true" value of this parameter is not known accurately. However, variations in this parameter primarily affected emissions of Hg(p), which accounted for only 2% of the total emissions used as input for the analysis. Therefore, the impact on the overall results of this uncertainty is not expected to be significant.

An additional 154 HYSPLIT-Hg 15-month simulations were carried out examining the impact of range of numerical issues on the modeling results. Numerical issues examined included changes in operating systems and compilers, changes in optimization schemes employed by the compiler, and changes in array handling algorithms within the HYSPLIT-Hg model. This analysis, presented in the Appendix, showed that these numerical issues did not generally cause changes in any key results greater than a few percent. In most cases, the numerically-related deviations in results – e.g., the modeled deposition to a given Great Lake -- were smaller than 1%

The variations examined for the full analysis, requiring 354 additional 15-month HYSPLIT-Hg simulations, were: (a) the use of NARR vs. EDAS meteorological data to drive the HYSPLIT-Hg model; (b) the use of additional standard source locations (SSL's) to reduce errors in spatial interpolation; (c) variation in the mercury re-emissions rate; and (d) variations in the spatial interpolation methodology.

Doubling the mercury re-emissions rate increased the model-estimated deposition to the Great Lakes by about ~25%. Additional SSL's and variations in spatial interpolation methodology were not found to influence the model results significantly. The NARR-based analysis had results that were more consistent with mercury wet deposition measurement in the Great Lakes region. However, while improved, the model performance for 12 sites in the eastern Great Lakes region did not improve significantly, and the tendency of the modeling analysis to over-predict the wet deposition flux at these sites remained. The overall results from the NARR-based analysis for Great Lakes deposition were somewhat different than those from the EDAS-based analysis. The most common difference was a decrease in model-estimated deposition from local and regional sources in the NARR-based simulations relative to the EDAS-based simulations.

An overall summary of the modeling results is provided below in Figure 1, which shows the overall source-attribution results for the largest variations in "full-analysis" modeling methodology, i.e., NARR vs. EDAS, and doubling the mercury re-emissions rate. While the overall fractions of the deposition contributed by key source types and regions were impacted somewhat by the simulation variations, the relative source-attribution results were not dramatically affected. This suggests that the results are reasonably robust, at least from the perspective of the relative importance of different source types and source regions to the deposition of mercury to the Great Lakes basin.

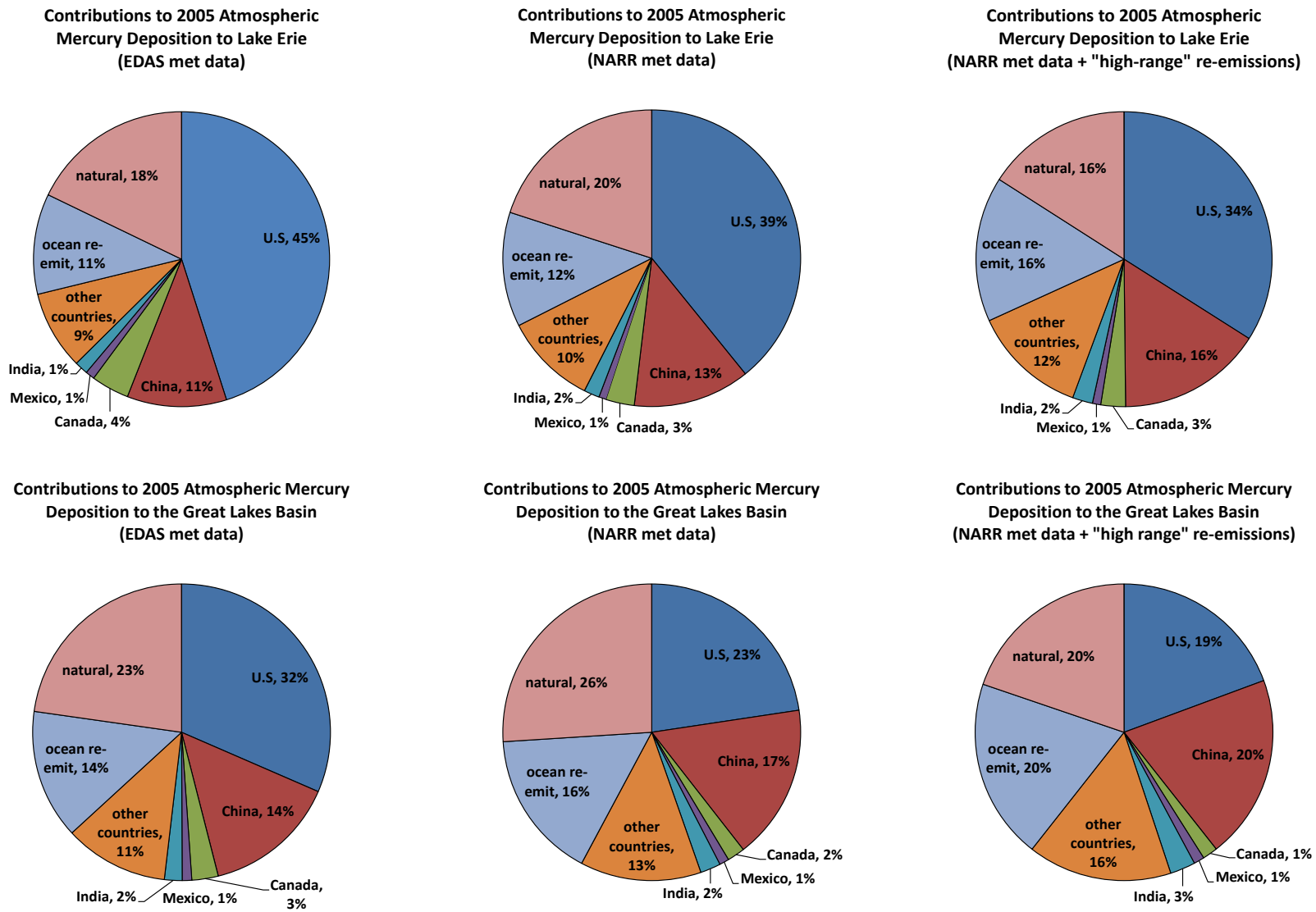

Figure 1. Overall source attribution results for Lake Erie (top row) and the Great Lakes Basin (bottom row) for largest variations in modeling methodology; 2005 baseline (left); key variations showing the largest differences (center & right)

1. Introduction

Mercury contamination in the Great Lakes Basin remains an important public and wildlife health concern as well as an economic issue (Evers et al, 2011ab). This report describes work done with FY2011 Great Lakes Restoration Initiative (GLRI) funding. Work done with FY2010 GLRI funding was summarized in Cohen et al. (2011), the "FY2010 report". In that FY2010 work, a 2005 baseline analysis of atmospheric deposition to the Great Lakes was carried out, including source-attribution for the model-estimated deposition. The modeling results were found to be consistent with measurements of mercury wet deposition in the Great Lakes region.

The overarching goal of the FY2011 work was to examine the sensitivity of the results to uncertainties in key inputs and model parameters.

In this report we will refer to three "kinds" of atmospheric mercury: (i) elemental mercury, or Hg(0); (ii) soluble oxidized mercury (Hg(II)), also referred to as reactive gaseous mercury (RGM); and (iii) particulate mercury, or Hg(p). Except where noted, results presented in this report are for total mercury (the sum of the three different forms), for simplicity and brevity's sake, even though the entire modeling analysis has been done with explicit treatment of the different mercury forms. This FY2011-funded work can be conceptually divided into two main sections:

(a) **Detailed sensitivity analysis for illustrative sources**. Since any given "full" analysis, e.g., with a given set of input data and parameters, took on the order of 2.5 months to carry out with the available computational resources, it was not possible to carry out multiple "full analyses" as part of the sensitivity analysis. Therefore, we decided to carry out detailed sensitivity analyses for five illustrative sources, examining numerous variations in modeling methodology.

(b) **Sensitivity analysis of "full results", including model evaluation**. Two primary variations were selected for examination of effects on the full analysis. One involved using a different choice for input meteorological data. The second involved using additional "standard source locations" in the analysis. For each variation studied, the impact on model evaluation – i.e., the degree of consistency of the modeling predictions with observations – and deposition was analyzed.

2. Detailed sensitivity analysis for illustrative sources

2.1. Selection of illustrative source locations

As discussed in detail in the FY2010 report, the modeling analysis is based on carrying out simulations of unit mercury emissions (i.e., 1 gram/hour) from numerous discrete source locations, called "standard source locations". Based on these simulations, the impacts on the Great Lakes of each source in the input emissions inventory is estimated using spatial and chemical interpolation. In the 2005 baseline analysis carried out previously, 136 such *standard source location*s ("SSL's") were used. The basic overall analysis requires three simulations from each location – for unit emissions of just Hg(0), for just Hg(II), and for just Hg(p). Therefore, a total of 408 separate simulations were required. With the computational resources available, this took ~2.5 months. For this reason, it was impractical to consider carrying out a detailed sensitivity analysis of comparable "full analyses" for a number of different variations. A few variations of the full analysis were carried out, and this is presented below, in Section 0. In the present section, a small number (5) of illustrative locations were selected and a detailed sensitivity analysis was carried out for these few locations. The locations of the 136 SSL's used in the FY2010 work and the five locations chosen for the sensitivity analysis here are shown in Table 1 and Figure 2.

Table 1. Five standard source locations for which a detailed sensitivity analysis was carried out

Standard source location number	Location	Lati-tude	Longi-tude	Distance (km) from centroids of the Great Lakes				
				Erie	Ontario	Michigan	Huron	Superior
8	western shore of Lake Erie, near Toledo, OH	41.70	-83.44	187	494	387	353	763
6	western Ohio River Valley	37.68	-87.13	704	1,015	703	886	1,122
11	north-eastern Texas	32.65	-94.88	1,600	1,915	1,437	1,735	1,778
13	eastern China, at the centroid of emissions inventory grid square with the highest reported 2005 emissions in China	31.25	121.25	18,094	17,643	18,392	17,892	18,044
48	north-eastern India, at the centroid of the emissions inventory grid square with the 2nd highest reported 2005 emissions in India	22.75	88.25	16,050	15,641	16,441	15,950	16,242

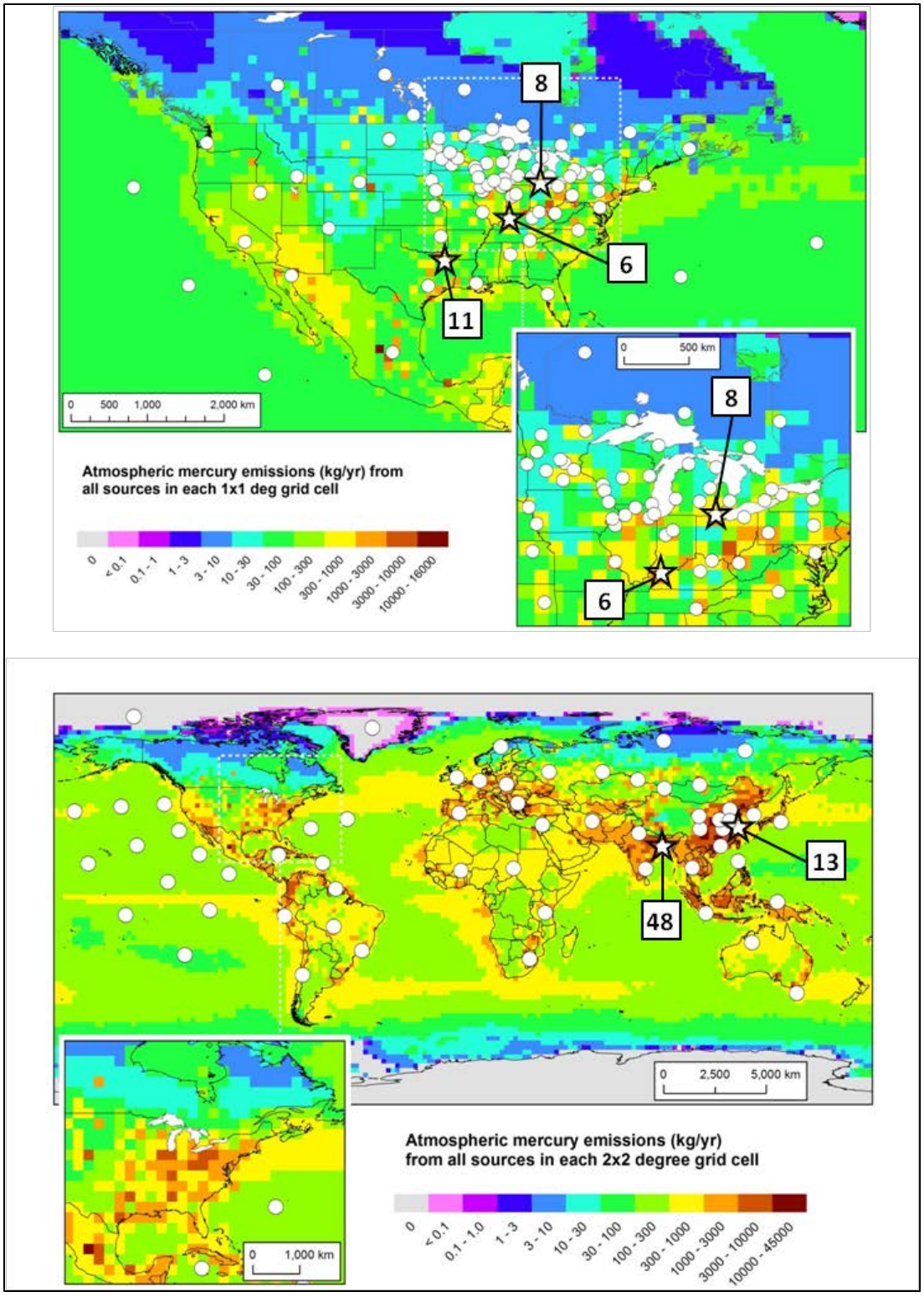

Figure 2. Five standard source locations for which a detailed sensitivity analysis was carried out

Several variations in model configuration, inputs, and parameters were examined in the detailed sensitivity analysis at these five locations. The different sensitivity "elements" were divided into several main categories:

- Meteorological input data
- Dispersion methodology
- Deposition methodology
- Chemistry-related parameters
- Numerical issues

2.2. Types of Simulations

Before describing the various sensitivity analyses performed, a summary of the different types of simulations carried out is needed. There were three basic types of simulations carried out, referred to here as "PUF", "GEM", and "COM".

- PUF simulations were done for Hg(II) and Hg(p) emissions from standard source locations (SSL's) in the continental U.S. (CONUS) and nearby adjacent regions in Canada and Mexico. In these simulations, 3-dimensional puffs of pollutants were emitted from the source and tracked as they were blown downwind, based on the meteorological data used. The maximum lifetime of a puff was chosen to be 504 hours (3 weeks) (parameter KHMAX, described below). The reason for limiting the lifetime of the puffs is that as the puffs age, they grow, and when a puff gets large enough relative to the meteorological grid size, it splits. This consequence of this puff splitting is that substantial numerical resources are needed to simulate any given emitted puff for any extended length of time. The 504-hour limit was believed to be sufficient to allow the emitted puff to impact any receptors – i.e., the Great Lakes and their watersheds – but that by the end of this time, the emitted material would be blown "past" the receptors and there would be no further impact. The PUF-type simulations examined in detail were Hg(II) and Hg(p) emissions from SSL-6 (western Ohio River Valley), SSL-8 (western shore of Lake Erie), and SSL-11 (northeastern Texas).

- GEM – "Global Eulerian Model" -- simulations were done for all SSL's outside of CONUS (and nearby regions in Mexico and Canada). In these simulations, the emitted mercury was immediately transferred to a global Eulerian grid, and the fate and transport simulated on that grid. The grid used for this simulation is by default the grid used for the global meteorological data, which in our case was the 2.5 degree NCEP-NCAR Global Reanalysis. This relatively coarse simulation was believed to be sufficient to capture the major characteristics of the source-receptor relationships between distant sources (e.g., in China) and the Great Lakes. The GEM-type simulations examined in detail were Hg(0), Hg(II), and Hg(p) emissions from SSL-13 (eastern China) and SSL-48 (northeastern India).

- COM – “Combined PUF and GEM” – simulations were done for Hg(0) emissions from SSL’s in CONUS and nearby adjacent regions in Canada and Mexico. In these simulations, puffs were emitted and simulated as puffs for 504 hours (3 weeks), after which the material in the puffs was transferred to the global Eulerian grid and simulated on that grid from then on. The reason why this approach was taken for Hg(0) -- as opposed to the PUF simulations described above for Hg(II) and Hg(p) – was that Hg(0) has a relatively long atmospheric lifetime and long-term impacts can be relatively large. The COM-type simulations examined in detail were Hg(0) emissions from SSL-6 (western Ohio River Valley), SSL-8 (western shore of Lake Erie), and SSL-11 (northeastern Texas).

With the above overall framework in mind, the various sensitivity analyses can be described. Throughout this section, we will refer to any given simulation by the name of the pure mercury form being emitted (“elem”, “HgII”, or “Hgpt”), the standard source location (“006”, “008”, “011”, “013”, or “048”) and the type of simulation performed (“PUF”, “COM”, or “GEM”). So, for example, the simulation referred to as “HgII_008_PUF” is a simulation of pure Hg(II) emissions, from SSL-8 (western shore of Lake Erie), using the “PUF” transport and dispersion methodology as described above.

2.3. Sensitivity to meteorological input data

In the FY2010 analysis, the EDAS dataset (with 40km resolution) was used over the Continental US (incl. southern Canada and northern Mexico), and the NCEP-NCAR Global Reanalysis dataset (with 2.5 degree) resolution was used outside of this region. To investigate the influence of input meteorological data, i.e., the data provided to the HYSPLIT-Hg model during the simulation, the NCEP-NCAR North American Regional Reanalysis ("NARR") dataset (with 36km resolution) was used instead of the EDAS dataset. The global dataset used, i.e., the NCEP-NCAR Global Reanalysis, was not changed. Due to systematic problems in the EDAS dataset (Rogers, 2011), the NARR dataset is believed to have more accurate precipitation data during 2005, and this was examined in the next section. It is noted that the precipitation issues in the EDAS data have reportedly been resolved and so the use these data may be very useful for analysis of more recent years.

2.3.1. Precipitation estimates in different meteorological datasets

The hypothesis that the NARR dataset was more accurate than the EDAS dataset for precipitation in 2005 was tested by comparing each model's predicted precipitation with observations at mercury wet deposition measurement sites in the Great Lakes region (Figure 3).

As can be seen in Figure 3, the EDAS dataset shows a systematic underprediction of precipitation at these key model evaluation sites. In contrast, the NARR dataset is shows precipitation that is more consistent with measured precipitation at these sites. Given the importance of this issue, it will be examined in more detail in the following.

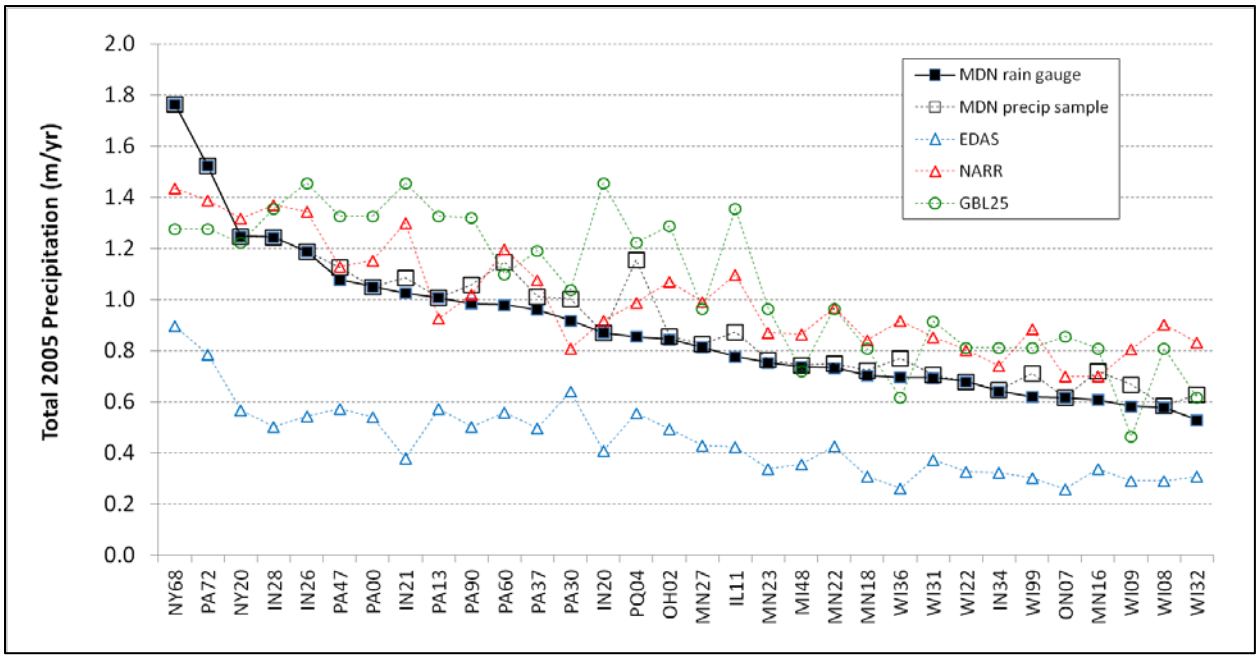

Figure 3. Total 2005 precipitation at mercury wet deposition measurement sites in the Great Lakes region

First, it is noted that there is some uncertainty in the "measured" precipitation at the MDN sites. The precipitation at the sites is reported in two ways: (a) based on a precipitation gauge at the site and (b) based on the amount of precipitation collected in the sample. Ideally, the two measures of precipitation would be identical, but they are sometimes different. These two measures of precipitation are compared in Figure 4 for all 86 MDN sites with "complete" data for 2005, including those outside of the Great Lakes region. The rain gauge measure is believed to be the most accurate, but the difference between the two for some of the sites suggests some degree of uncertainty in the precipitation measurement itself and/or in the measurement of mercury wet deposition.

In Figure 5, the rain-gauge based precipitation measurements at these 86 sites are compared against the values in the gridded EDAS meteorological dataset. It can be seen that there is an underprediction of precipitation for most sites, consistent with the situation with the Great Lakes sites (only) shown in Figure 3 above.

In Figure 6, the same comparison -- at 86 MDN sites with complete 2005 data -- is made with the gridded NARR meteorological dataset. It is seen that the 2005 NARR precipitation values – while certainly not perfect -- appear to be more consistent with measurements than the EDAS values at MDN sites. A comparable comparison with the NCEP-NCAR Global Reanalysis is shown in Figure 7. Given the relatively coarse grid of the global data (2.5 degrees, or roughly 250 km), it would not be expected that the modeled and measured precipitation would be overly consistent. Therefore, the degree of consistency found is somewhat unexpected. Finally, all of the above comparisons are shown in a combined fashion in Figure 8.

With the finding that the NARR data appear to be "better" than the EDAS data, at least with regard to precipitation data for 2005 – the year of this analysis – it was decided to use the NARR data as a new baseline for the sensitivity analysis. That is, we carried out the sensitivity analysis comparing all variations against a baseline NARR-based simulation. A comparison of this new baseline with the earlier EDAS-based simulation was then just one of the sensitivity elements explored.

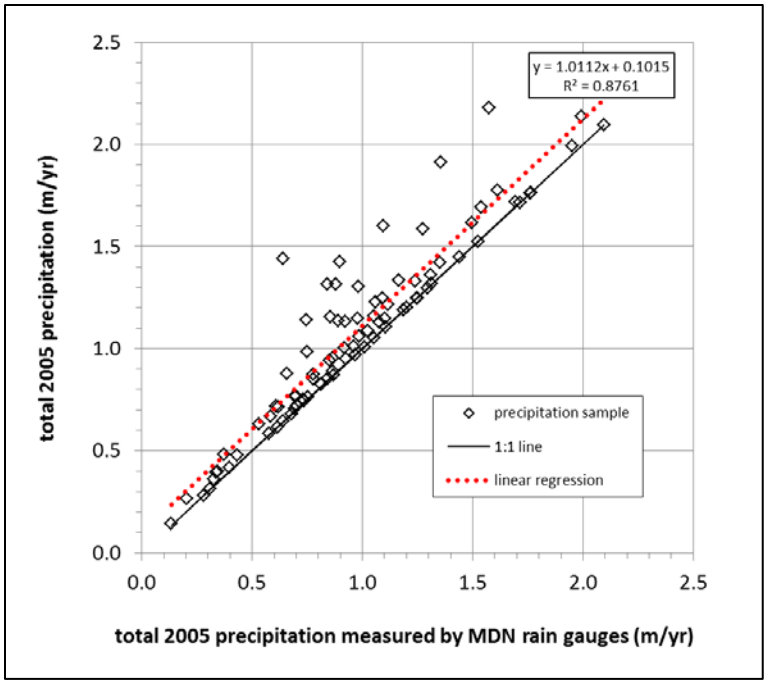

Figure 4. Comparison of precipitation measured by rain gauges at MDN sites with that estimated by sample volume

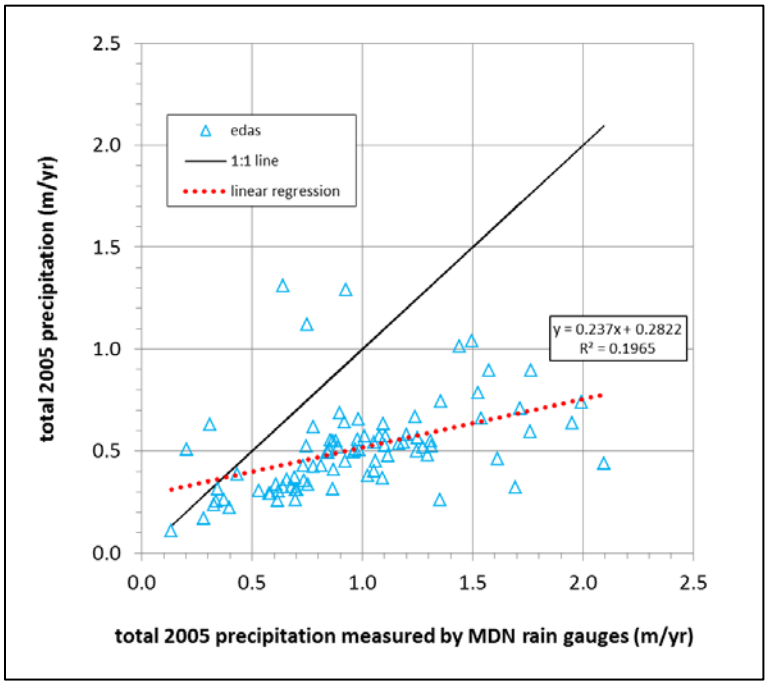

Figure 5. Comparison of precipitation measured by rain gauges at MDN sites with that in the EDAS meteorological dataset

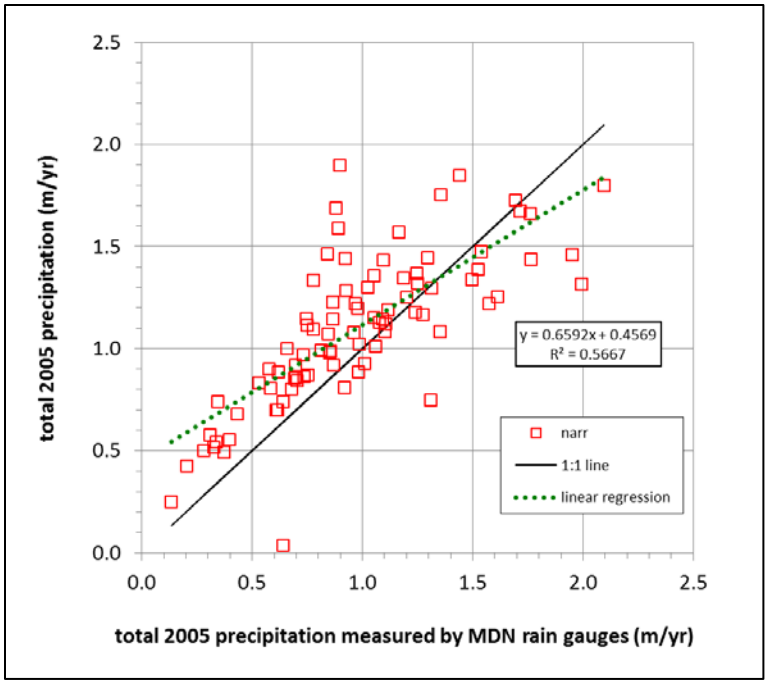

Figure 6. Comparison of precipitation measured by rain gauges at MDN sites with that in the NARR meteorological dataset

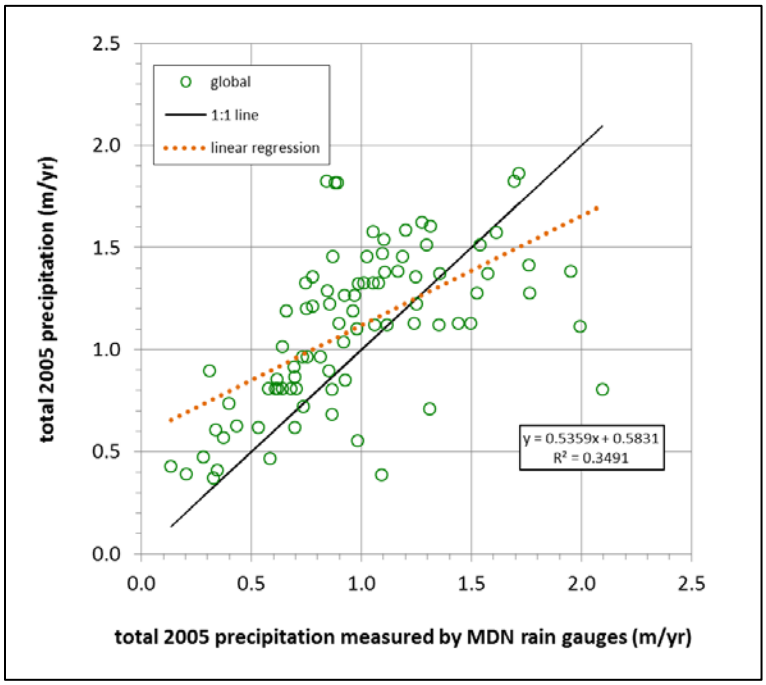

Figure 7. Comparison of precipitation measured by rain gauges at MDN sites with that in the NCEP-NCAR Global Reanalysis meteorological dataset

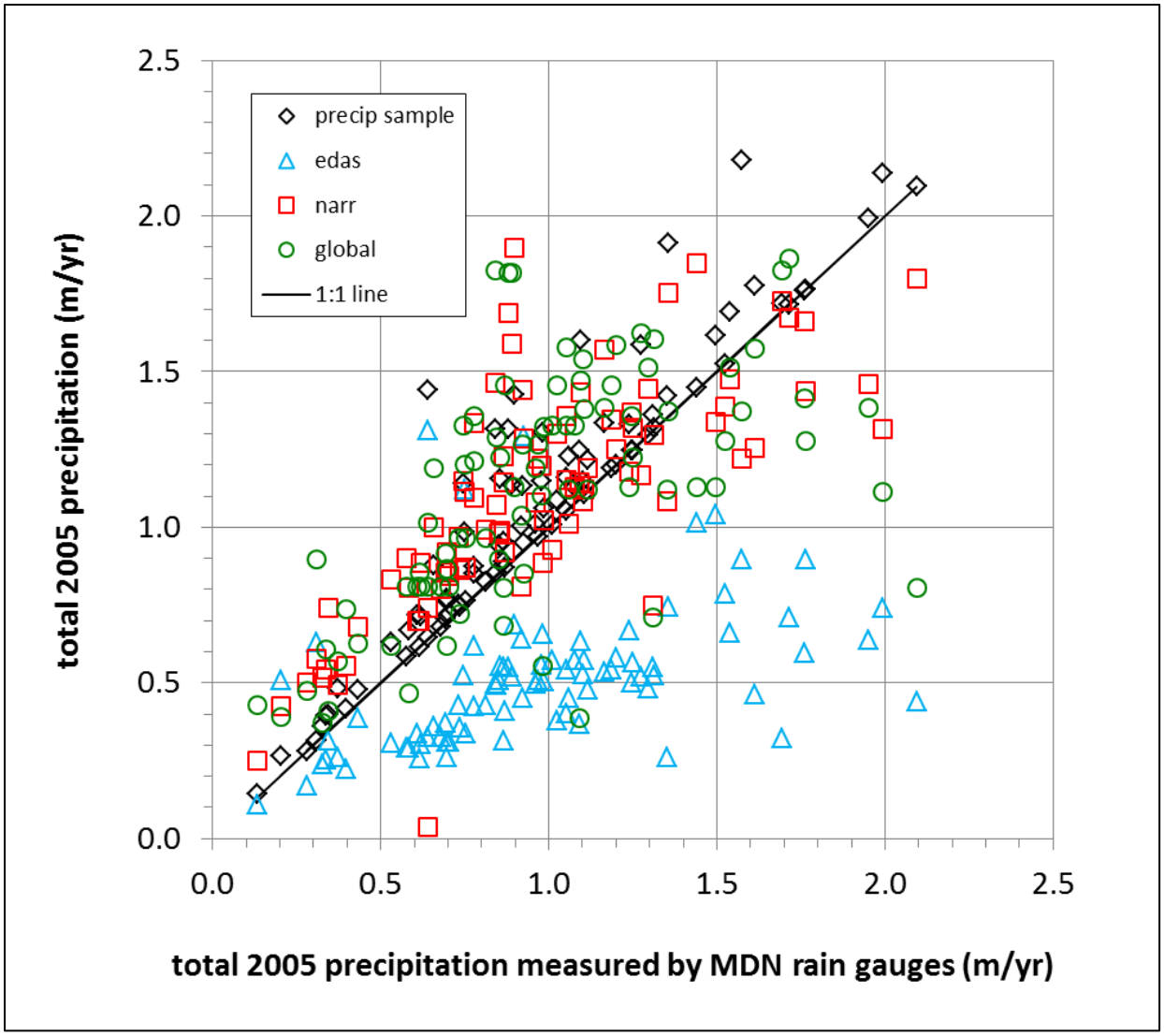

Figure 8. Comparison of precipitation measured by rain gauges at MDN sites with that in other datasets

2.3.2. Sensitivity to meteorological data inputs for simulations of illustrative sources

In Figure 9, the 2005 deposition to Lake Erie from standard source locations (SSL's) 6, 8, and 11 are shown for emissions of Hg(II), Hg(p), and Hg(0). Only these three source locations are shown (out of the five being studied in detail here), as they are the ones in which NARR or EDAS data are used. For the other two source locations, global Eulerian model ("GEM-type") simulations were performed that only utilized global meteorological data. It can be seen that there are significant difference between the NARR-based simulation and the EDAS-based simulation in many cases. Most notably, there is a relatively big difference in the largest impact – the Hg(II) emissions from SSL-8, on the western shore of Lake Erie: the atmospheric deposition to Lake Erie from a 1 gram/hour source of Hg(II) from this location was 554 g/yr using the EDAS data, and only 353 g/yr using the NARR data, a difference of 44%. The other comparisons showed somewhat smaller fractional differences, from 5% - 39%. In most cases the deposition was greater with EDAS than NARR, but the reverse was true for two of the comparisons (Hg(p) emissions from SSL-6 and Hg(II) emissions from SSL-11).

Comparable graphs for Lake Michigan, Lake Superior, Lake Huron, and Lake Ontario are shown in Figure 10 through Figure 13. One view of an overall summary of the data in this series of figures is shown in Figure 14, where the fractional difference between the NARR and EDAS simulations are shown for all of the lakes and source-location / emissions species simulations. Note that in some cases, the large fractional differences are the result of small differences between small numbers, i.e., the overall impacts are small, and the actual amount of difference between the NARR and EDAS simulations is relatively small.

Another view of an overall summary of these deposition data is shown in Figure 15, where the NARR estimates and EDAS estimates are plotted on an x-y scatterplot. It can be seen from this figure that the differences are both positive and negative, and that generally, the largest deviations are in the simulations of Hg(II) emissions (red symbols).

A final summary is shown in Figure 16, in which the NARR vs. EDAS analysis is applied to MDN sites in the Great Lakes region. It is seen that the simulations driven by EDAS meteorological data tend to predict lower mercury wet deposition fluxes at these MDN sites, with the greatest impact seen for simulations of Hg(II) emissions (red symbols).

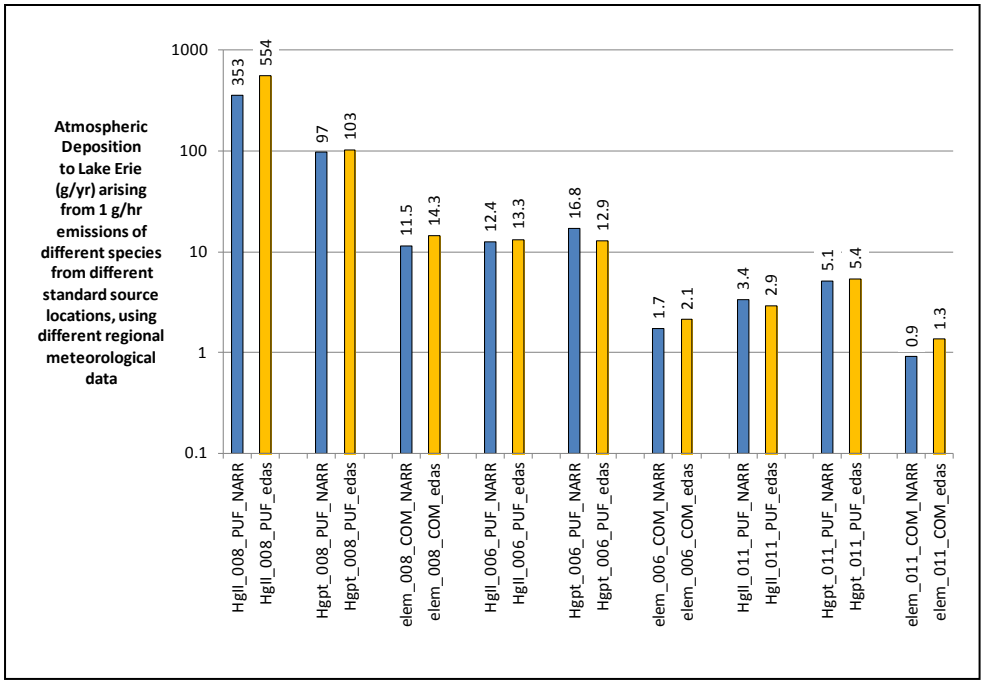

Figure 9. Atmospheric deposition to Lake Erie from standard source locations 6,8, and 11 using NARR and EDAS meteorological data

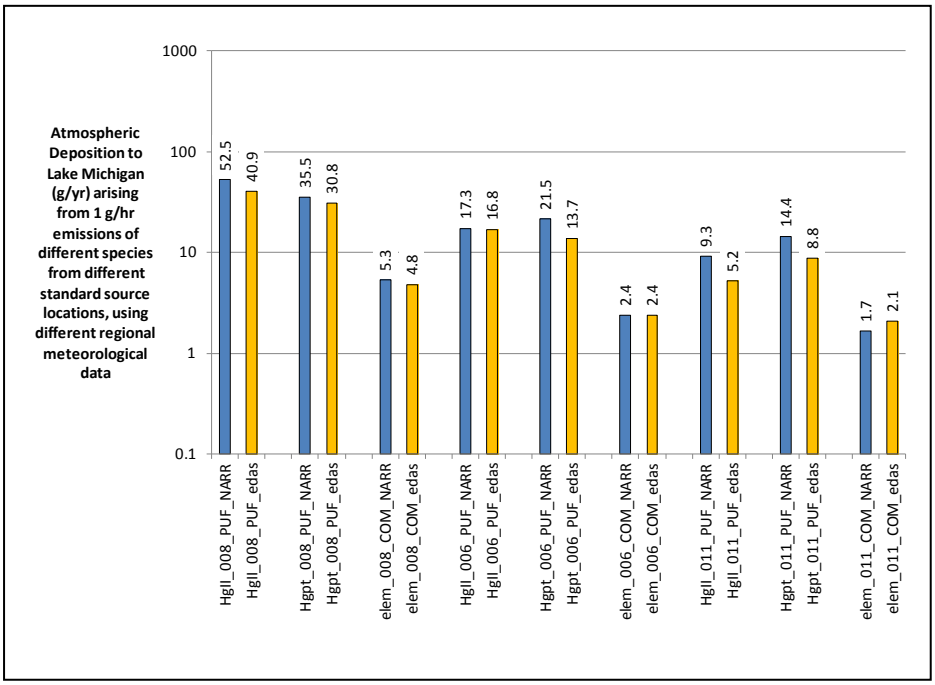

Figure 10. Atmospheric deposition to Lake Michigan from standard source locations 6,8, and 11 using NARR and EDAS meteorological data

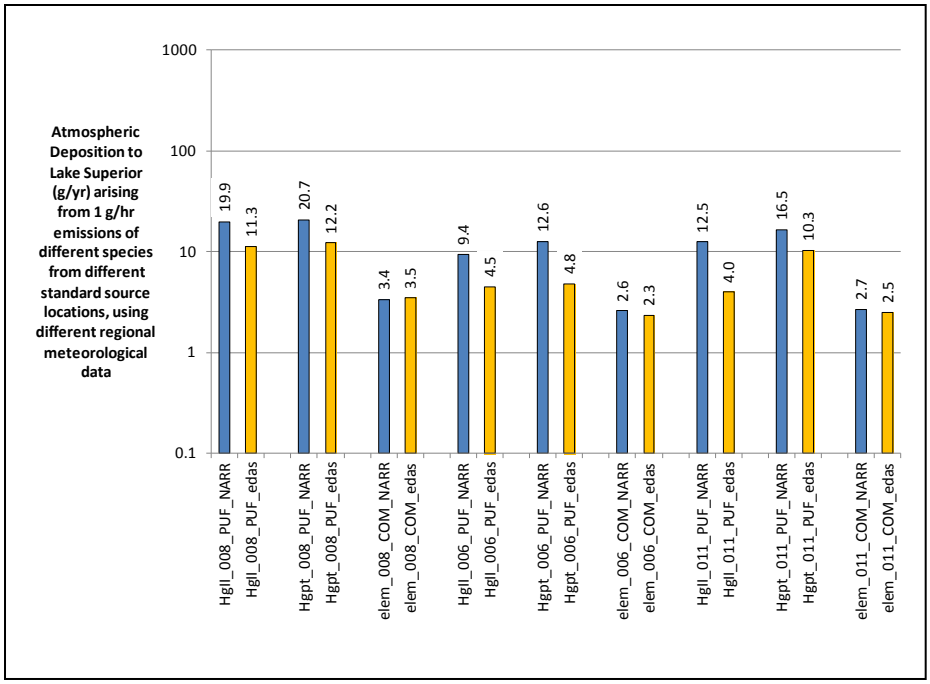

Figure 11. Atmospheric deposition to Lake Superior from standard source locations 6,8, and 11 using NARR and EDAS meteorological data

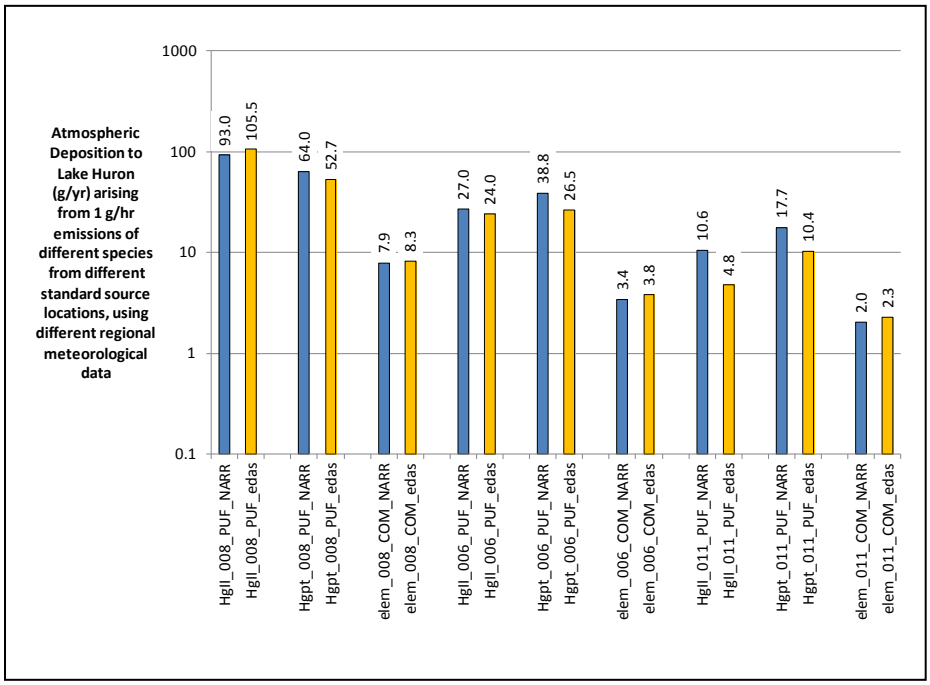

Figure 12. Atmospheric deposition to Lake Huron from standard source locations 6,8, and 11 using NARR and EDAS meteorological data

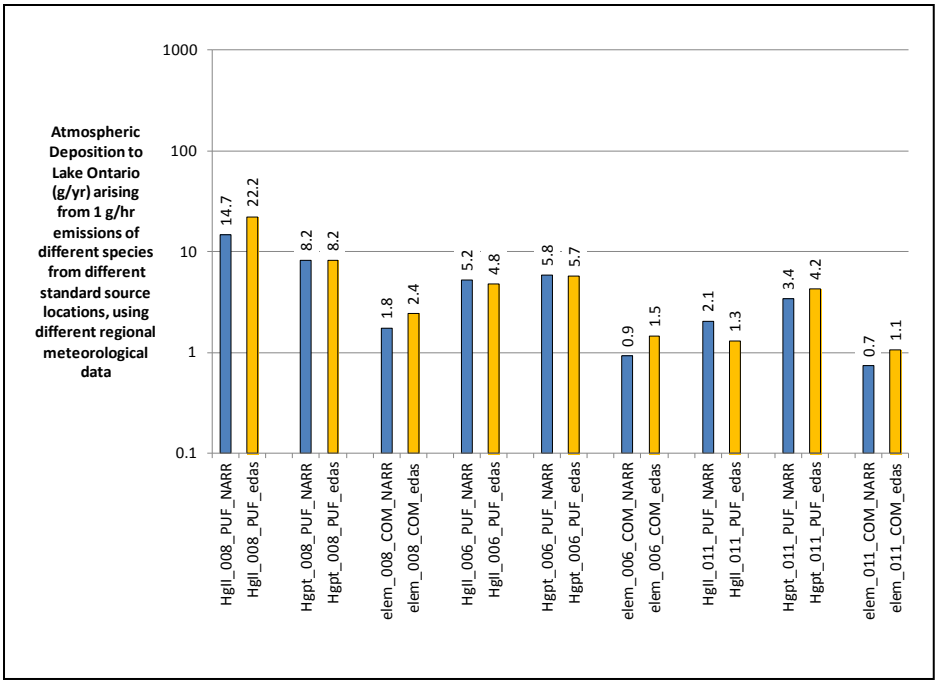

Figure 13. Atmospheric deposition to Lake Ontario from standard source locations 6,8, and 11 using NARR and EDAS meteorological data

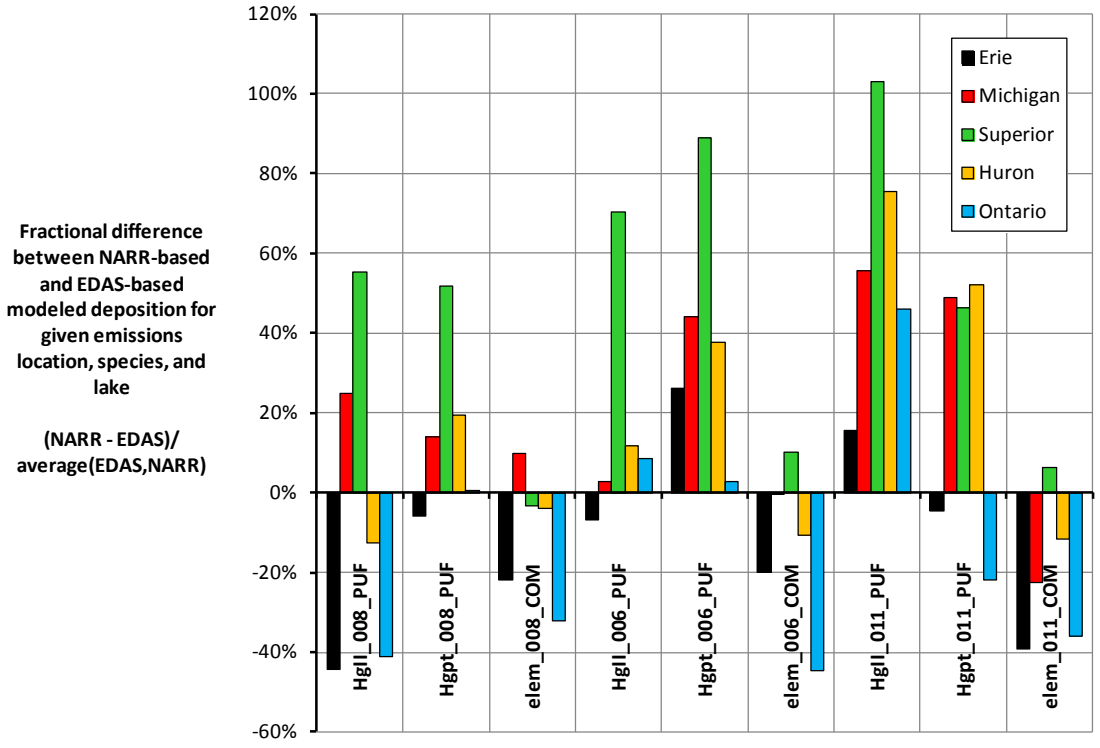

Figure 14. Summary (a) of atmospheric deposition differences between NARR and EDAS simulations from standard source locations 6,8, and 11 using NARR and EDAS meteorological data

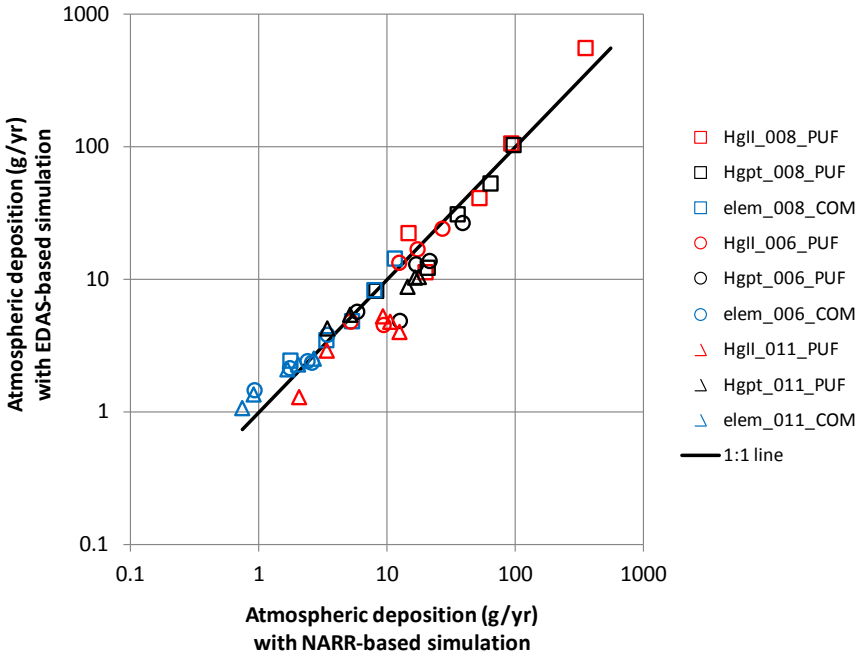

Figure 15. Summary (b) of atmospheric deposition differences between NARR and EDAS simulations from standard source locations 6,8, and 11 using NARR and EDAS meteorological data

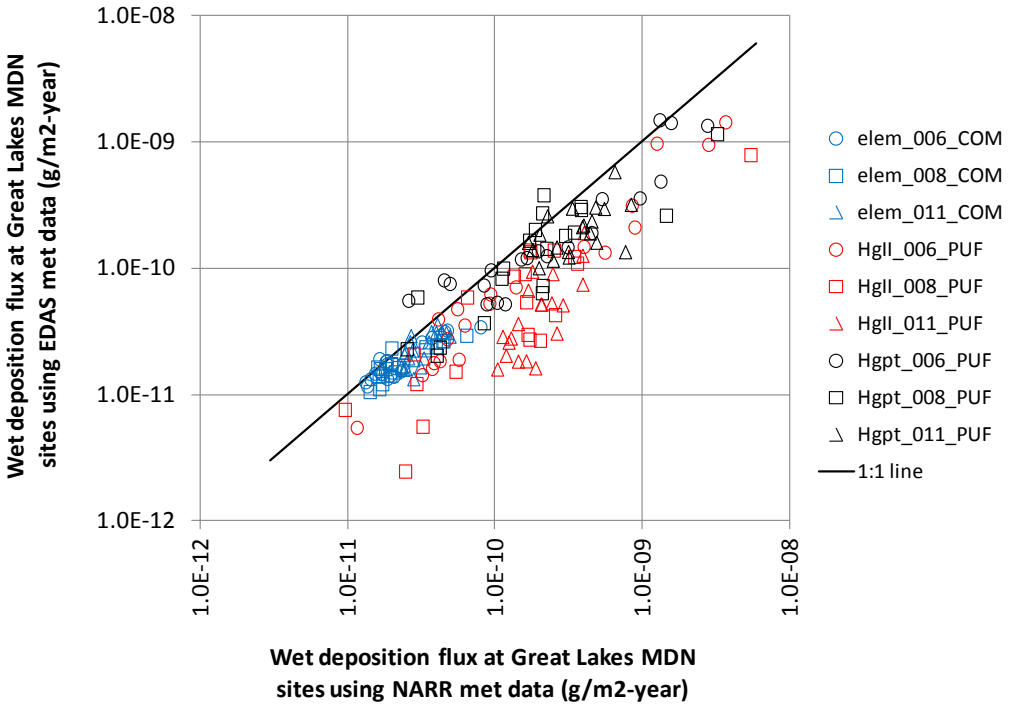

Figure 16. Comparison of mercury wet deposition fluxes at MDN sites in the Great Lakes region arising from emissions from 3 illustrative standard source locations using NARR and EDAS meteorological data

2.3.3. Sensitivity to meteorological data inputs for all 136 standard source locations

Because the meteorological data used to drive the HYSPLIT mercury simulations is such a fundamental model input, and because the differences between the NARR and EDAS datasets for 2005 appear to be significant, NARR simulations for each of the standard source locations (SSL's) that utilized these data were carried out. Of the 136 SSL's used in the baseline analysis, 75 were simulated using the PUF/COM approach, and 61 employed the GEM approach. In the PUF/COM approach, NARR or EDAS data are used until the pollutant is transported out of the data's domain. In the GEM approach, the NCAR/NCEP global reanalysis dataset is used throughout the simulation. The new NARR simulations for the 75 PUF/COM SSL's can be compared with the baseline analysis using EDAS data. Here we will simply show the basic results from each SSL, and examine the differences between the NARR- and EDAS-driven simulations. The overall impact on deposition to the Great Lakes after applying chemical and spatial interpolation is presented in Section **Error! Reference source not found.**, below.

Comparisons for each of the Great Lakes and the Great Lakes Basin as a whole are shown in Figure 17 through Figure 22. The general tendencies evident in all of these figures include the following:

- For Hg(0) emissions, modeled deposition is relatively low, and there is little difference between the EDAS- and NARR-driven simulations; because there is little wet deposition arising from Hg(0) emissions, differences in precipitation between the two datasets don't influence the results very much.

- For Hg(II) emissions, when the deposition is low, e.g., because the source location is relatively far from the receptor, the NARR-driven simulation results in a higher flux than the EDAS-driven simulation. However, when the deposition flux is high, the NARR-driven simulation generally shows a lower flux than the EDAS-driven simulation. There is no simple explanation for this trend, as the results are dependent on the fate and transport of the emitted pollutant for each source, and the precipitation differences exhibit complex, time-dependent and location-dependent patterns. For example, increased deposition might arise because the precipitation is greater over the receptor, but it also might arise because there was less precipitation affecting the pollutant as it made its way to the receptor.

- For Hg(p) emissions, the NARR- and EDAS-driven simulations are relatively consistent, but the NARR-driven fluxes tend to be slightly higher than the EDAS-driven fluxes. As for Hg(II), it is not possible to provide a simple explanation for the differences observed.

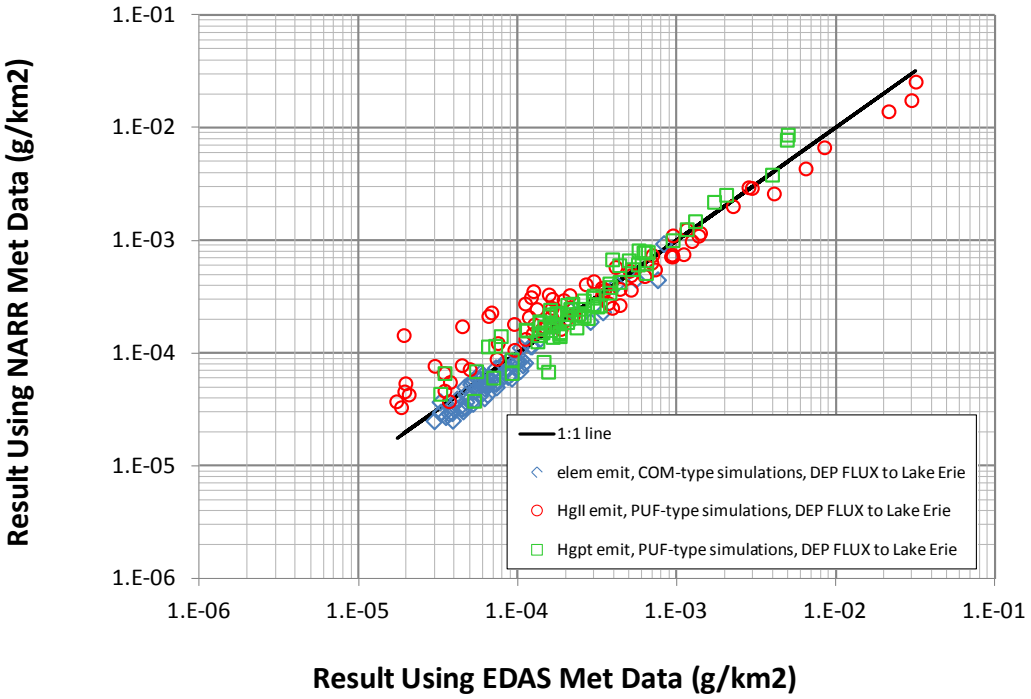

Figure 17. Annual (2005) mercury deposition flux to Lake Erie from 75 standard source locations, comparing NARR- and EDAS-driven simulations, for 1 g/hr emissions of Hg(0), Hg(II), and Hg(p).

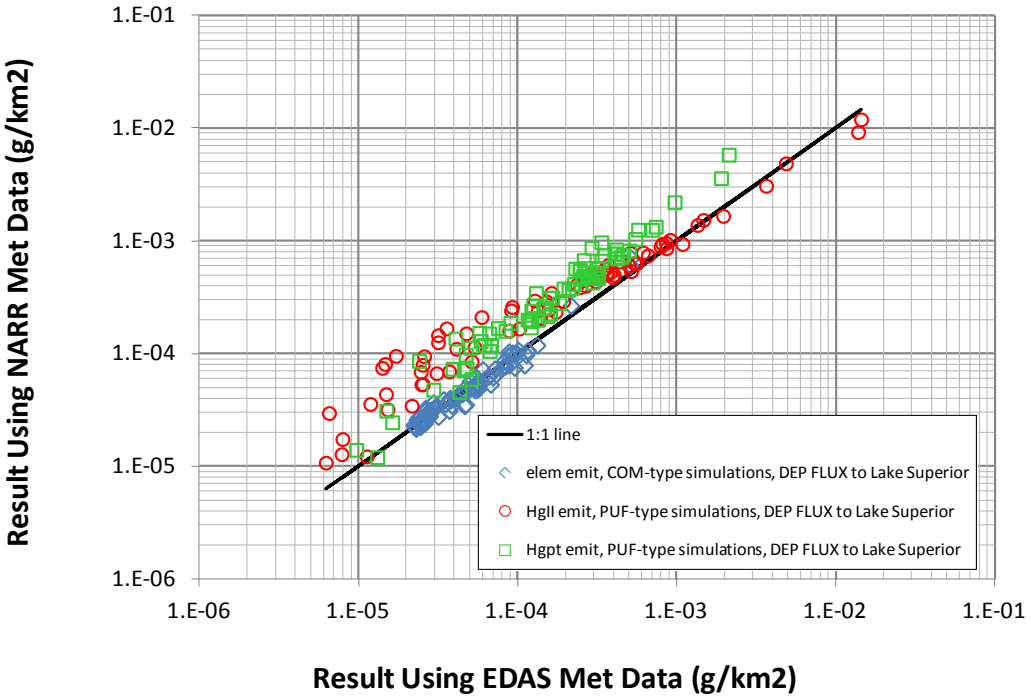

Figure 18. Annual (2005) mercury deposition flux to Lake Superior from 75 standard source locations, comparing NARR- and EDAS-driven simulations, for 1 g/hr emissions of Hg(0), Hg(II), and Hg(p).

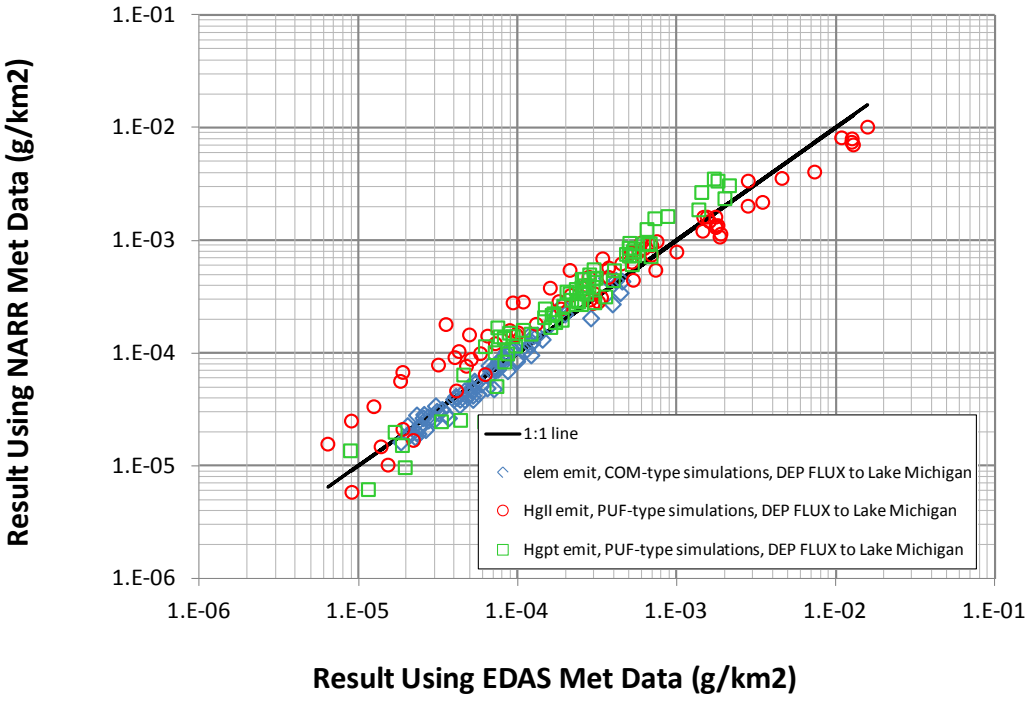

Figure 19. Annual (2005) mercury deposition flux to Lake Michigan from 75 standard source locations, comparing NARR- and EDAS-driven simulations, for 1 g/hr emissions of Hg(0), Hg(II), and Hg(p).

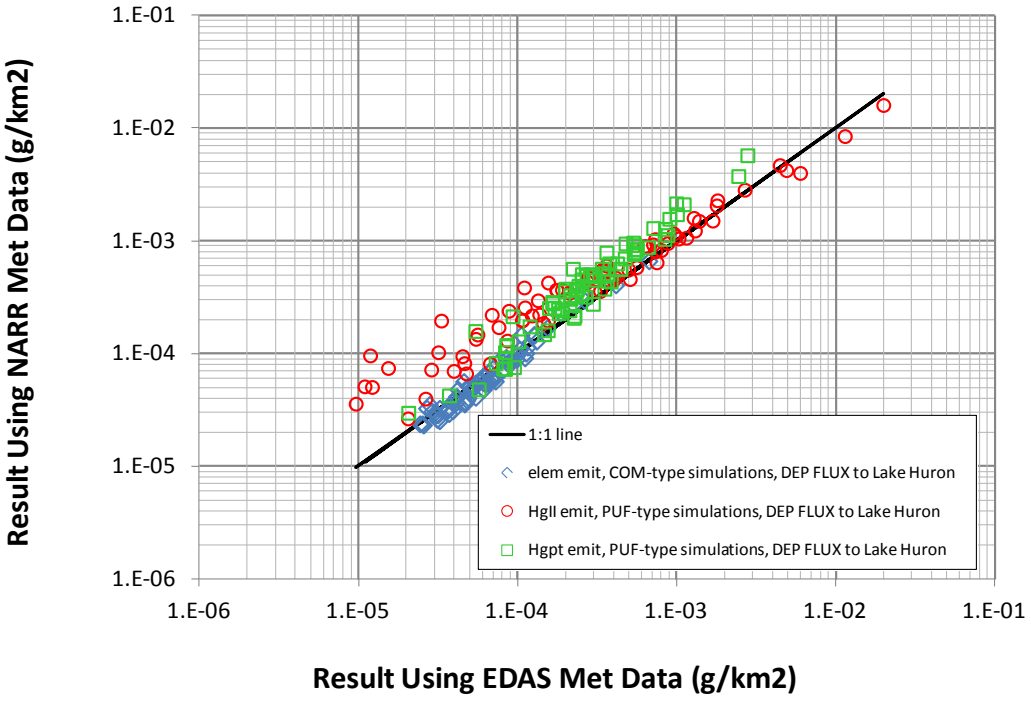

Figure 20. Annual (2005) mercury deposition flux to Lake Huron from 75 standard source locations, comparing NARR- and EDAS-driven simulations, for 1 g/hr emissions of Hg(0), Hg(II), and Hg(p).

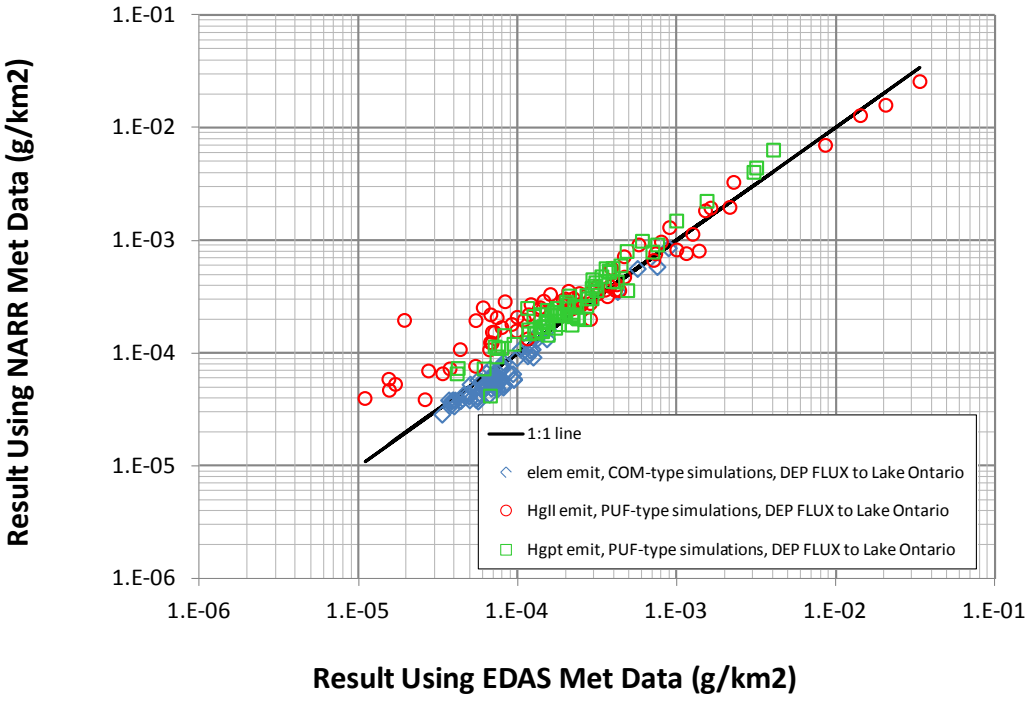

Figure 21. Annual (2005) mercury deposition flux to Lake Ontario from 75 standard source locations, comparing NARR- and EDAS-driven simulations, for 1 g/hr emissions of Hg(0), Hg(II), and Hg(p).

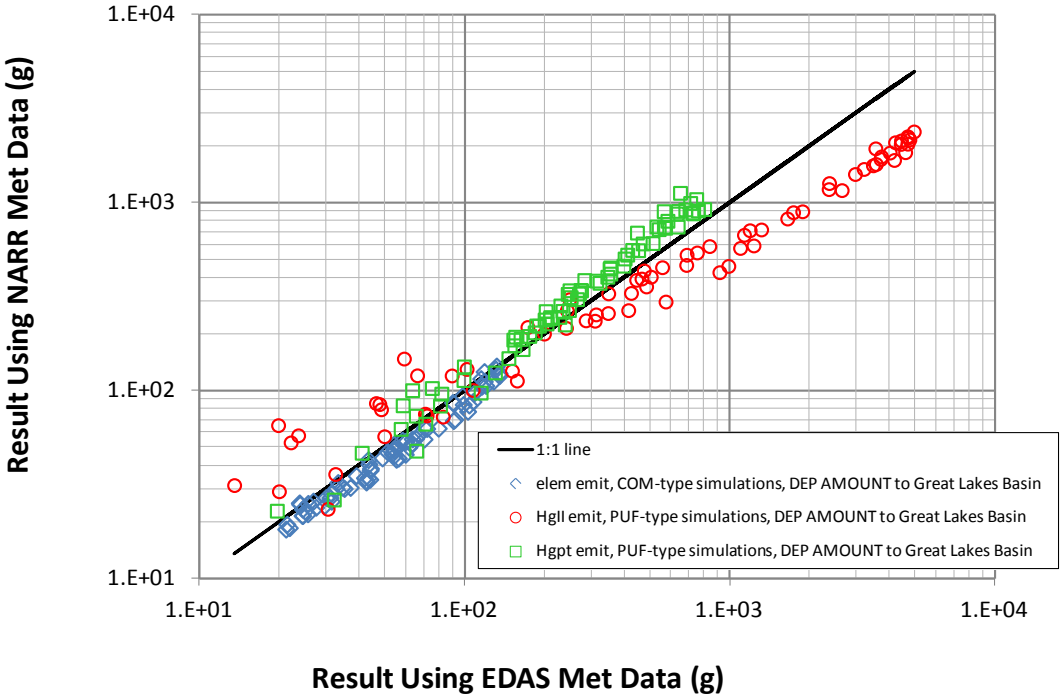

Figure 22. Annual (2005) mercury deposition flux to the Great Lakes Basin from 75 standard source locations, comparing NARR- and EDAS-driven simulations, for 1 g/hr emissions of Hg(0), Hg(II), and Hg(p).

2.4. Sensitivity to dispersion methodologies

2.4.1. Introduction

In the HYSPLIT model – as well the HYSPLIT-Hg model used in this analysis – there are a number of alternative dispersion methodologies and parameter variations that can be employed. A large group of different simulation variations was explored for the five selected illustrative standard source locations. Each of these parameter or methodological variations, and their influence on the fate and transport of emitted mercury, will be described and presented here.

2.4.2. KHMAX

The KHMAX parameter is the number of hours that any given emitted material is tracked in the PUF simulations. At this number of hours past emission, the material is removed from the simulation. As noted above, the baseline value used was 504 hours (3 weeks). The reason why this limitation is imposed is that increasingly large amounts of computational resources are required to track puffs as they age, due to puff-splitting. As the puffs age and grow, they split whenever their size becomes comparable to the meteorological grid size. Once they split, they will split again when the fragment again attains a size comparable to the meteorological grid size. For emission of Hg(II) and Hg(p), the reasoning is that if the deposition to a given receptor has not occurred within this time, then it is likely that the pollutant has already been deposited, or, that it has been transported out of the Great Lakes region.

To examine the influence of this parameter on the simulations, PUF-type simulations were carried out with KHMAX values of 336 hours (2 weeks) and 672 hours (4 weeks) to see what impact this would have on the simulation results. As described above, the only PUF-type simulation being examined in detail were emissions of Hg(II) and Hg(p) from SSL-6 (western Ohio River Valley), SSL-8 (western shore of Lake Erie), and SSL-11 (northeastern Texas). Emissions of Hg(0) at these locations were simulated with a COM-type simulation and were not affected by the KHMAX parameter variations. The overall results for deposition to the Great Lakes arising from 1 gram/hr emissions are shown in Figure 23. It can be seen that variation in KHMAX does not significantly impact the modeling results.

The small differences that do exist – slight *decreases* in deposition with longer KHMAX – are perhaps counterintuitive. One would generally expect that allowing the emitted material to last longer in the simulation would result in the *same or more* deposition, all things being equal. To consider this further, data from these same simulations for deposition to the Great Lakes and their watersheds are shown in Figure 25, in which the deposition flux (g/km2-year) results for variations in KHMAX are shown compared to the default value. The left panel gives results for KHMAX = 336, and the right panel shows results for KHMAX = 672. It can be seen that there is perhaps a slight tendency towards increased deposition flux with KHMAX = 336 and a slight tendency towards decreased deposition flux with KHMAX = 672, but, these slight tendencies are present only in the lower estimated fluxes. The estimates for the

highest impacts, i.e., the highest deposition fluxes, do not seem to be influenced at all. This type of result illustrates a general philosophy adopted in this analysis: since small differences in the "small impacts" will not have a big impact on the overall results, they are relatively unimportant. As long as there are not significant differences in the "big impacts", the overall results will not be strongly affected.

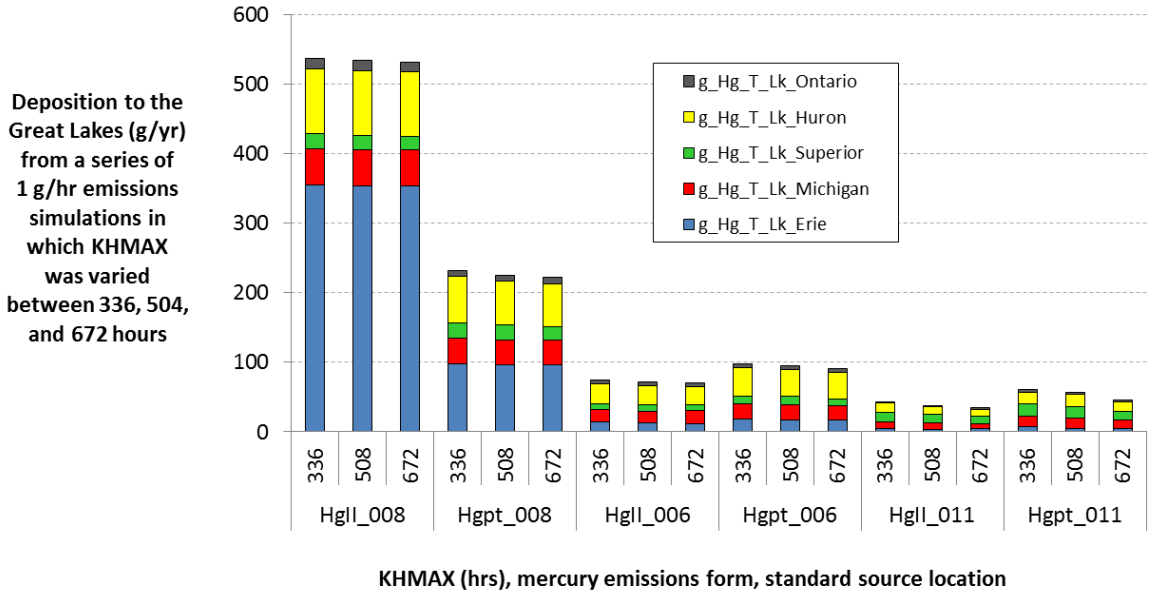

Figure 23. Variations in modeled deposition to the Great Lakes arising from variations in KHMAX (hrs)

In Figure 24. Variations in modeled wet deposition to MDN sites in the Great Lakes region arising from variations in KHMAX (hrs)Figure 24, the same types of comparisons are shown for wet deposition to MDN sites in the Great Lakes region. It is seen that there are moderate differences in wet deposition among the simulations with different KHMAX values. The largest differences occur for SSL-11 (NE Texas) which is the furthest of the illustrative locations from the Great Lakes. It is seen that with higher values of KHMAX, the deposition decreases. This is a counterintuitive result, as one would expect that if anything, the deposition would increase when puffs were allowed to impact the receptors for a longer time. The reason why the deposition decreases is likely a reflection of reductions in puff splitting due to the increased computational load of tracking the puffs for a longer time. In running HYSPLIT, one sets a maximum number of puffs that can exist in the simulation. With a higher value of KHMAX, more of this computational array is spent tracking older puffs, and this also affects the transport and dispersion of younger puffs. The finding that the deposition decreases with higher values of KHMAX suggests that if such a higher value was used, a higher maximum number of puffs would have to be used to keep a comparable accuracy in the simulation.

In Figure 25 and Figure 26, all of the data from the illustrative simulations for the Great Lakes and the MDN sites in the Great Lakes region are shown, respectively. In these figures, the left panel shows a comparison between the KHMAX=508 hr default and the KHMAX=336 variation, and the right panel

shows a comparable comparison between the default and KHMAX=672 hrs. It can be seen that there are no obvious or systematic tendencies in these comparisons.

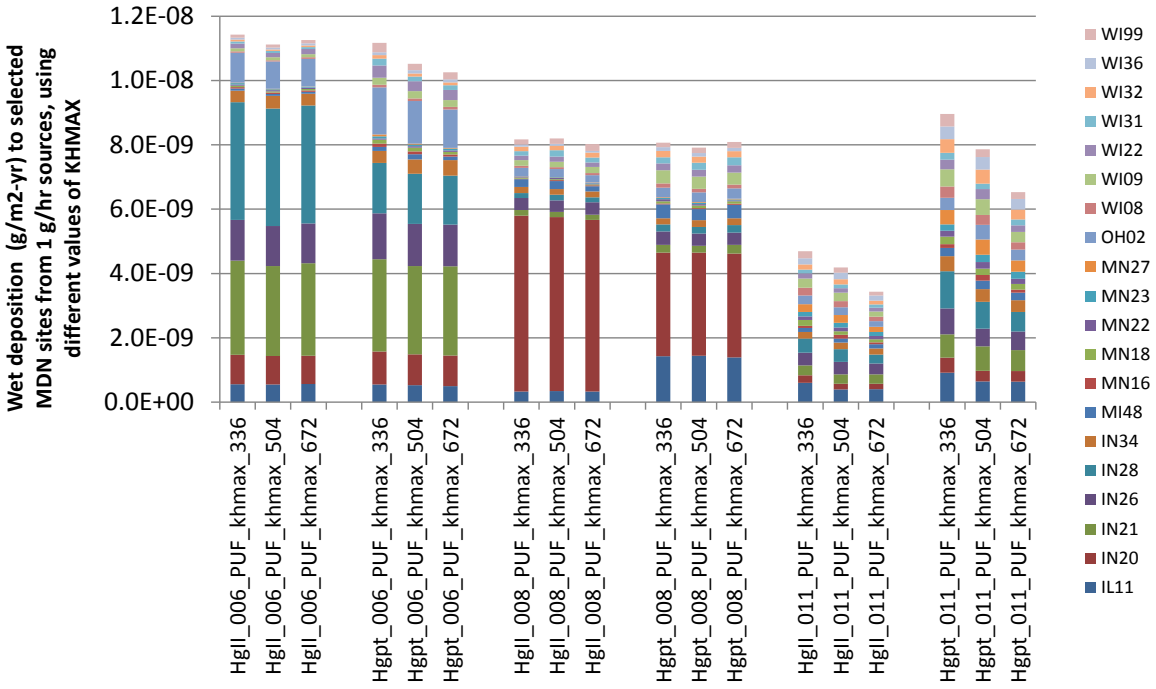

Figure 24. Variations in modeled wet deposition to MDN sites in the Great Lakes region arising from variations in KHMAX (hrs)

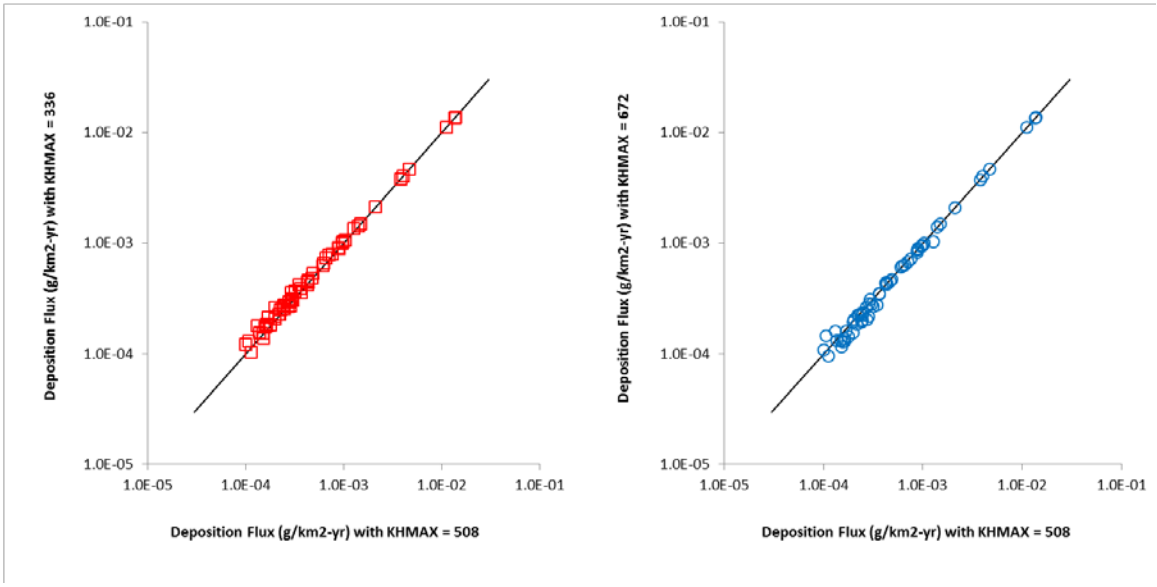

Figure 25. Deposition fluxes estimated with KHMAX = 336 and KHMAX = 672, relative to the default value of 508 hours, for the Great Lakes and their watersheds

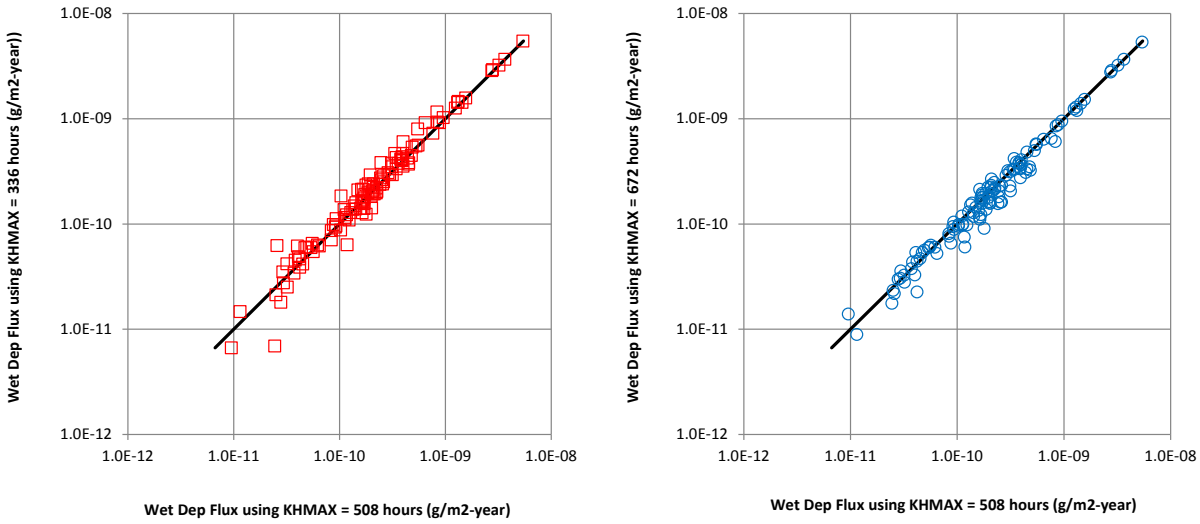

Figure 26. Deposition fluxes estimated with KHMAX = 336 and KHMAX = 672, relative to the default value of 508 hours, for MDN sites in the Great Lakes region

2.4.3. PUF vs. COM simulation

As discussed above in Section 2.2 (page 12), there were two types of simulations performed for standard source locations in the Continental U.S. and surrounding regions in Canada and Mexico. For Hg(II) and Hg(p) emissions, PUF-type simulations were carried out. For Hg(0), COM-type simulations were used, in which the emitted pollutant was tracked using 3-D puffs for 504 hours (3 weeks), and then any remaining pollutant at that time was converted over to a global Eulerian grid and tracked from that point forward on that global grid. In this section, we show comparisons between PUF and COM simulations for all emitted pollutants.

In Figure 27, the fractional difference between PUF-type and COM-type simulations are shown for emissions of Hg(0) ("elem"), Hg(II) ("HgII"), and Hg(p) ("Hgpt"), for the relevant illustrative standard source locations (SSL-6, SSL-8, and SSL-11). Inspection of the figure shows why this differential approach was taken. It can be seen that for elemental mercury, there is a big fractional difference between the estimated COM-type deposition and the comparable PUF-type deposition. In essence, the long atmospheric lifetime of Hg(0) means that the simulation must track the emitted pollutant for a comparably long time. For Hg(II) and Hg(p), there are only minor differences between the PUF- and COM-types simulations, and this is expected as the atmospheric lifetimes of these emitted pollutants is much less than that of Hg(0). These examples show that tracking Hg(II) or Hg(p) using only 3-D puffs for 3 weeks is sufficient for sources in CONUS and the nearby regions for predicting their impact on the Great Lakes.

It should be noted, however, that the deposition arising from Hg(0) emissions in these simulations is relatively small. This can be seen in Figure 28, showing the total (wet + dry) mercury deposition to each of the Great Lakes and their watersheds, individually, simulated with COM-type vs. PUF-type methodologies, from the three relevant illustrative SSL's (6,8, and 11). This figure shows that the simulations of pure Hg(0) emissions (blue symbols) are much less that the impacts of Hg(II) and Hg(p) emissions. Thus, while the fractional differences between COM vs. PUF methodologies for simulating Hg(0) emissions are large (Figure 27), the magnitudes of the differences are actually relatively small.

In Figure 29 and Figure 30, it can be seen that the same general finding applies to wet deposition at MDN sites in the Great Lakes region. The biggest fractional impact occurs for elemental mercury emission simulations, but the magnitudes of the differences are relatively small for these Hg(0) simulations, as well as for the Hg(II) and Hg(p) simulations. Even though the magnitudes of the differences between PUF and COM-type simulations were small for Hg(0), and even though the COM-type simulations required approximately 3 times as much computational resources, it was decided to use the COM-type simulation for all of the SSL's in the CONUS and surrounding regions.

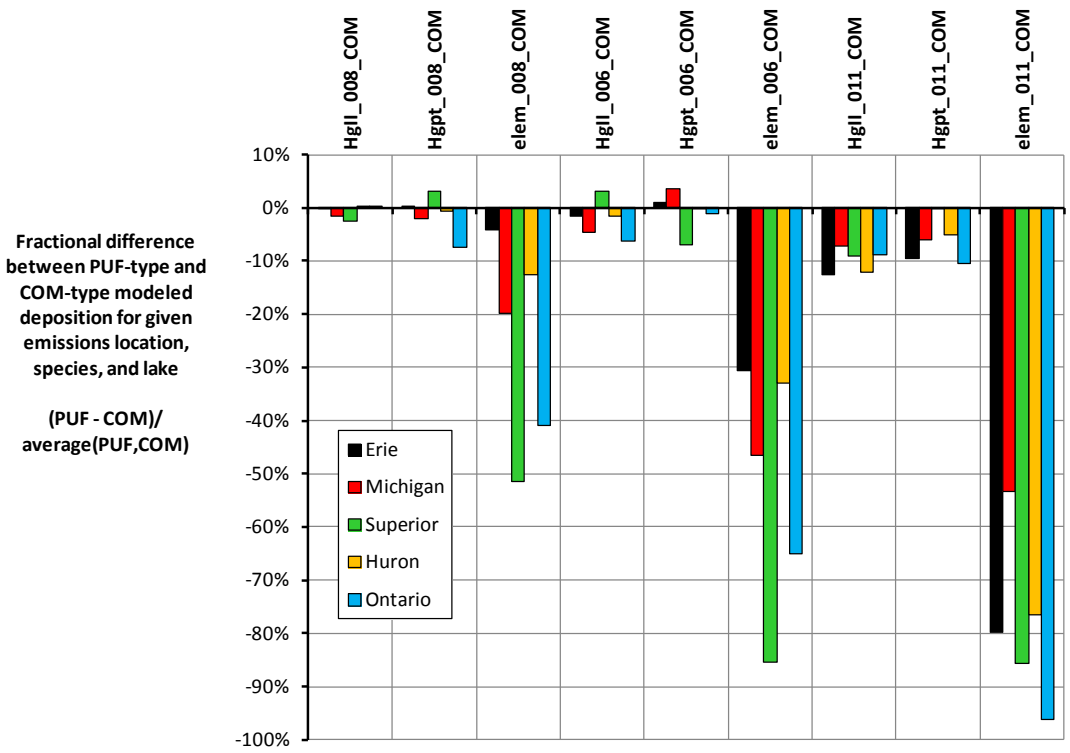

Figure 27. Fractional difference between estimated Great Lakes deposition from PUF-type and COM-type simulations, for 3 illustrative standard source locations.

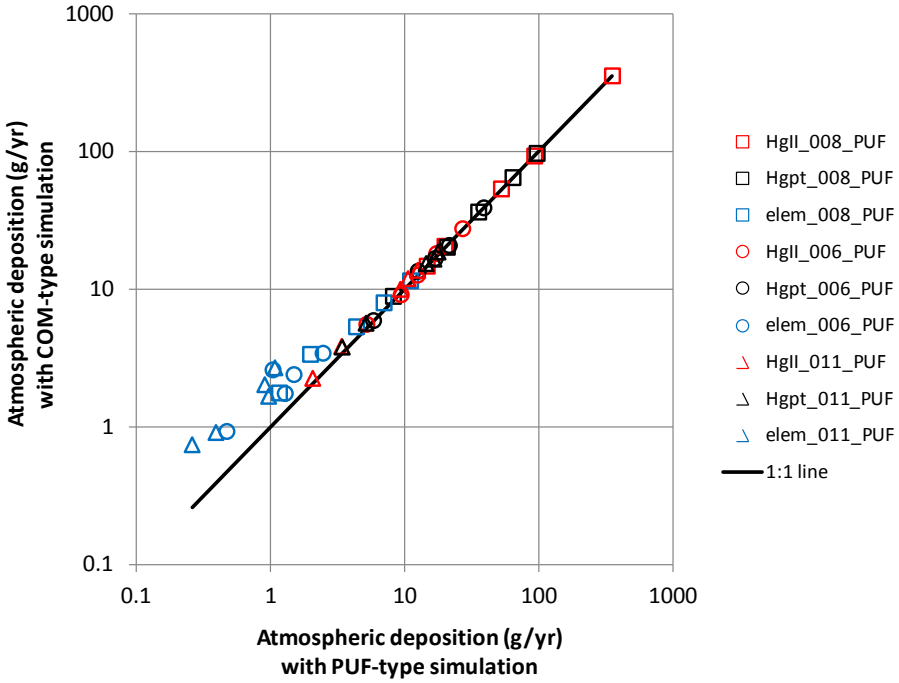

Figure 28. Total mercury deposition to individual Great Lakes and their watersheds using PUF- or COM-type simulation methodologies

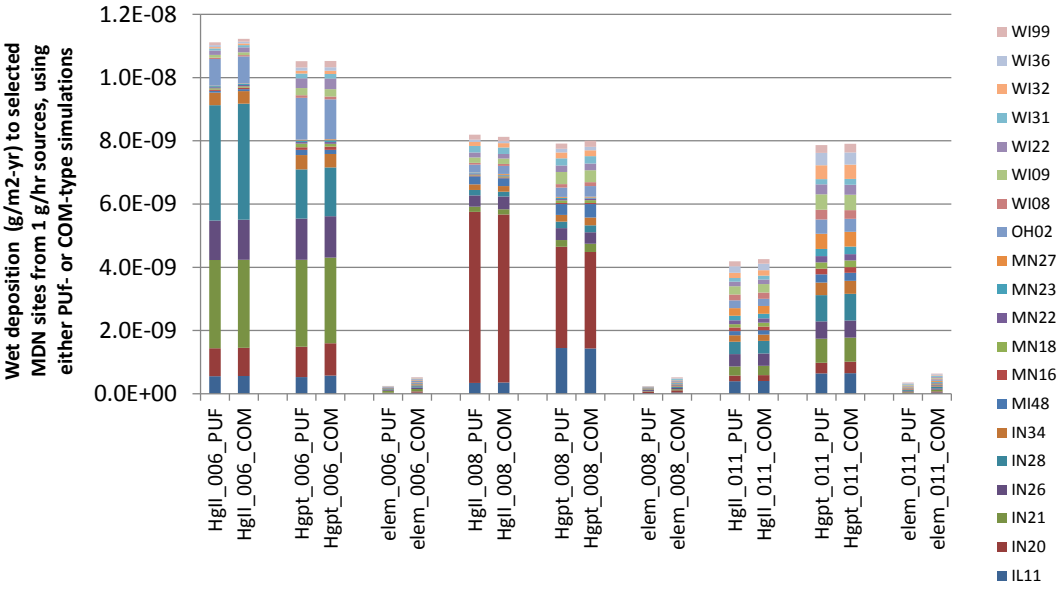

Figure 29. Wet deposition at MDN sites in the Great Lakes region using PUF- or COM-type simulation methodologies (stacked bar graph)

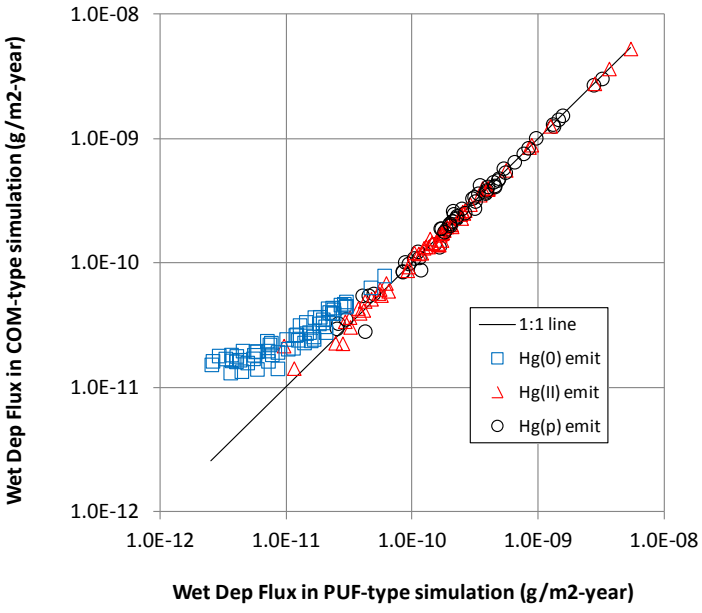

Figure 30. Wet deposition at MDN sites in the Great Lakes region using PUF-type vs. COM-type simulation methodologies (scatterplot)

2.4.4. Model time step

In HYSPLIT simulations, the time-step is fixed at 60 minutes for GEM simulations, but for any simulation involving 3-D puffs, one has the option of specifying a fixed time-step or to let the model adjust the time step. In either case, the maximum time-step is 60 minutes, and the minimum time-step is 1 minute. In carrying out the HYSPLIT-Hg PUF-type and COM-type simulations in this study, the fixed time-step approach was used. For any given simulation, the time-step for any given simulation was chosen to be small enough that emitted puffs would not "leapfrog" any key receptors. Computational resources for any simulation were strongly influenced by model time-step used, and so the goal was to use a time-step small enough to avoid leapfrogging, but not overly small, to optimize computational resources. In practice, this meant that for many of the standard source locations, a 60 minute time-step was determined to sufficient. The minimum time-step used for any standard source location was 12 minutes. In this section, results are presented for time-steps shorter or longer than the default, for the three illustrative PUF- or COM-type standard source locations being investigated (SSL-6, SSL-8, and SSL-11).

Results for total mercury 2005 deposition to Lake Erie are shown in Figure 31 for the default time-steps used, as well as time-steps shorter and longer than the default. It is seen that the differences arising from variations in model time-step are generally small. Results for all of the Great Lakes for deposition arising from SSL-8 (western shore of Lake Erie) are shown in Figure 32, where the non-default time-step results are plotted against the default time-step results. It is seen that the choice of time step does not significantly affect the modeled deposition.

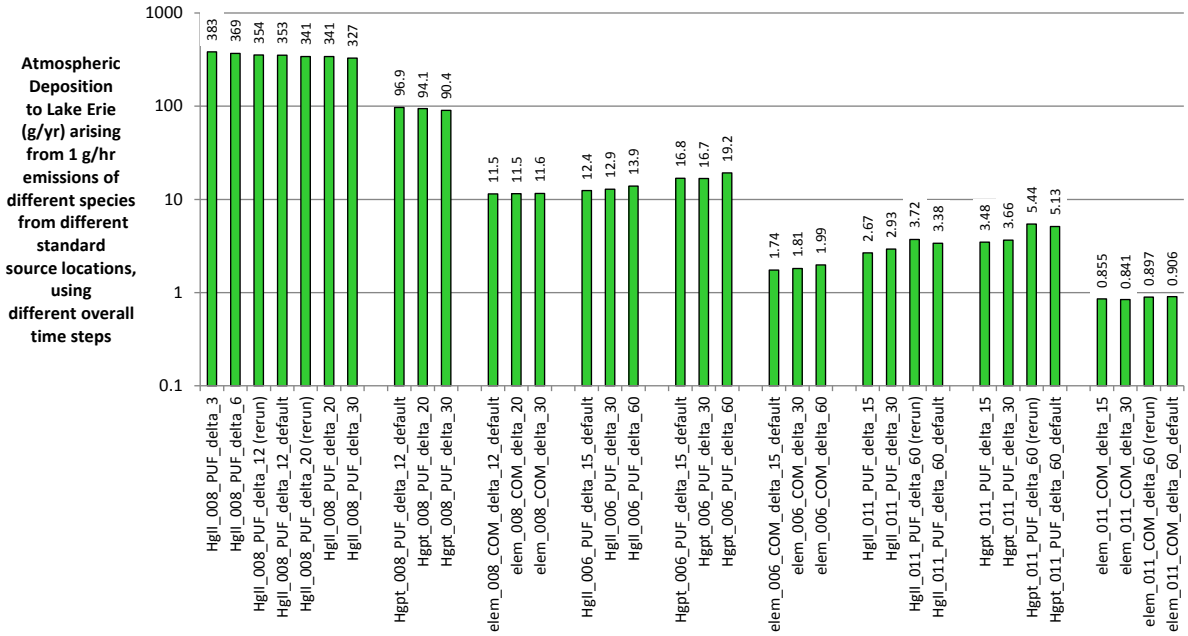

Figure 31. Modeled mercury deposition to Lake Erie from three illustrative standard source locations using different model time steps (minutes) (note: the time steps in the run labels are denoted by "delta", and the default value is also indicated)

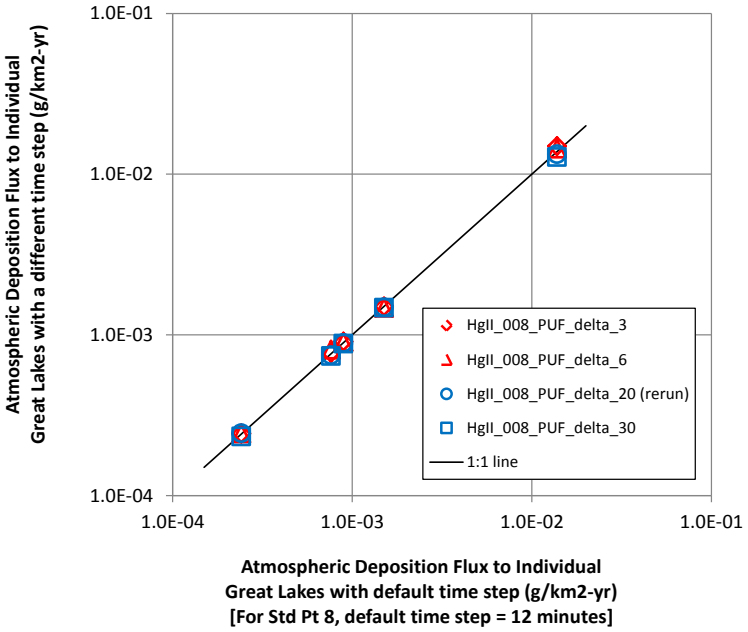

Figure 32. Modeled mercury deposition flux to individual Great Lakes from SSL-8 (western shore of Lake Erie) with different time steps

2.4.5. Maximum number of puffs

As discussed above, in Section 2.2 (page 12), HYSPLIT simulations with 3-D puffs requires that the maximum number of puffs allowed be specified by the user ("MAXPUFF"). When the number of puffs approaches this limit, puff-splitting is turned off. The program takes care to leave enough room for new puffs to be emitted. The computational resources required for any PUF-type or COM-type simulation are strongly influenced by this specified MAXPUFF parameter. In all PUF-type and COM-type simulations, the default value used was 20,000. Splitting was allowed to occur once every 24 hours, and puffs were released throughout the simulation every 3 hours.

In Figure 33, the total modeled mercury deposition to Lake Erie, from SSL-8 (western shore of the lake) is shown for the default value of MAXPUFF (20,000) and values of 10,000 and 40,000. It can be seen that there is very little influence on the overall modeled deposition. The largest fractional difference is seen for SSL-11 (NE Texas), but the deposition is relatively small and the magnitudes of the differences are very small. The differences observed for this case make sense, as the changes in puff splitting – due to different values of MAXPUFF -- would likely affect receptors further away from the source to a greater extent. The impact could be increased or decreased deposition, and would depend on the paths and fate of individual puffs that either split or didn't split in any given simulation. Figure 34 shows comparable data for deposition to each of the Great Lakes individually, and Figure 35 shows comparisons for wet deposition at MDN sites in the Great Lakes region. The results shown in both of these figures are consistent with the general finding that the MAXPUFF variations investigated did not have a significant impact on the results.

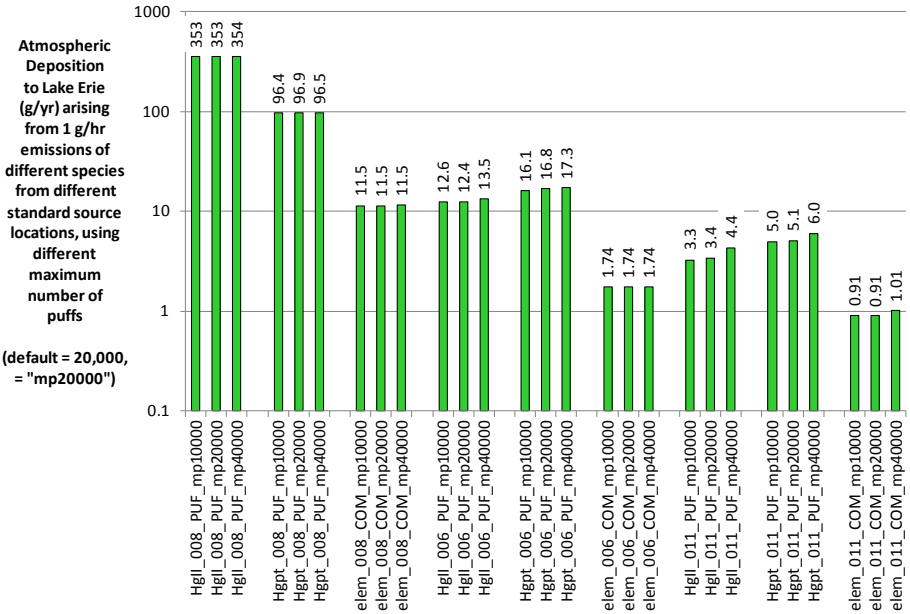

Figure 33. Modeled mercury deposition to Lake Erie from three illustrative standard source locations using different MAXPUFF values (note: the MAXPUFF values in the labels are denoted by "mp", e.g., mp10000 indicates that MAXPUFF for that simulation was 10,000)

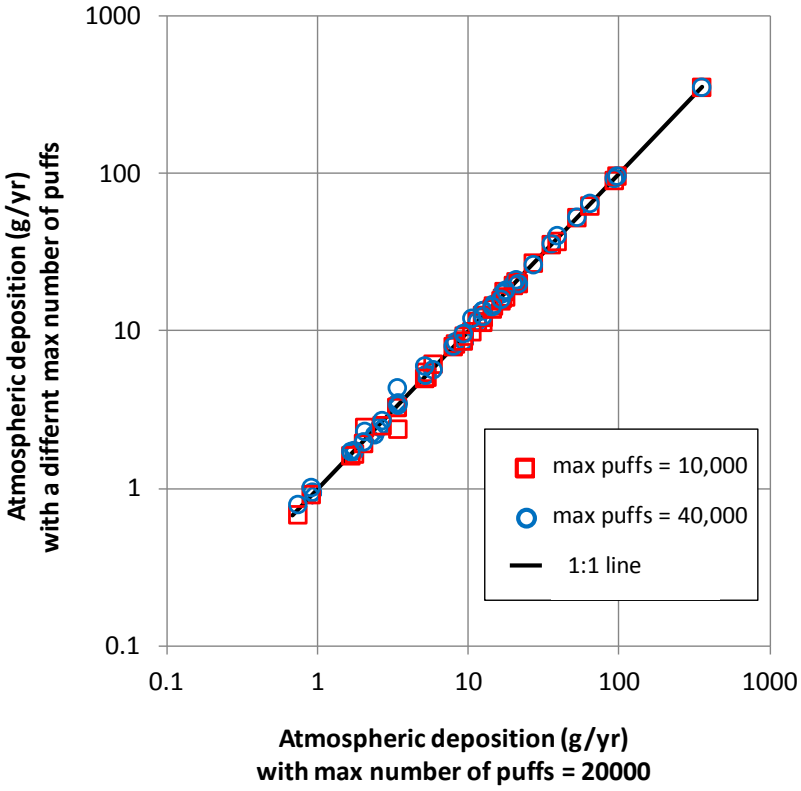

Figure 34. Modeled mercury deposition to individual Great Lakes using different MAXPUFF values

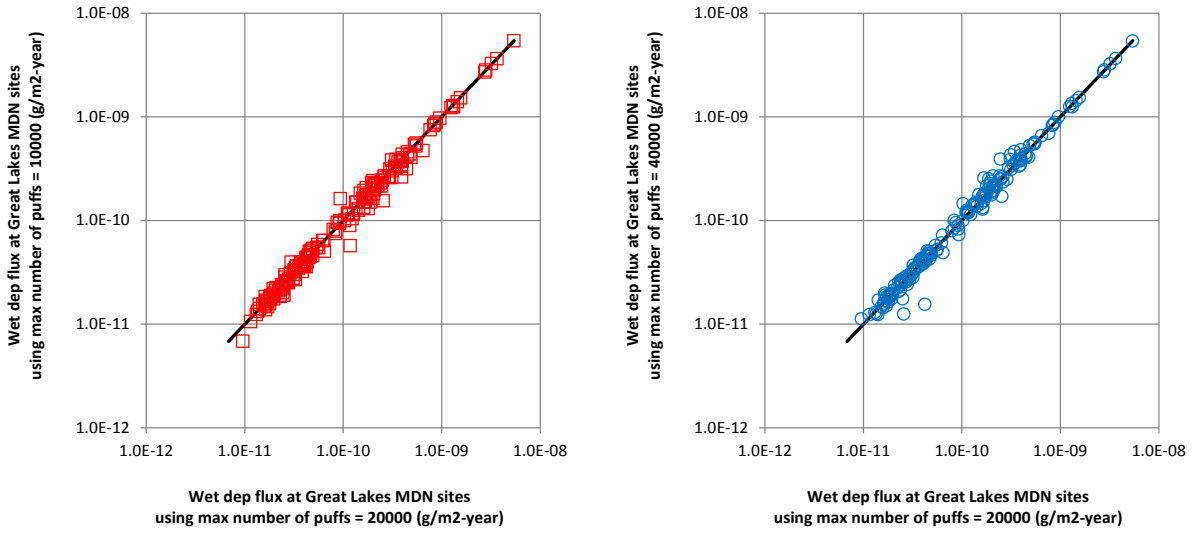

Figure 35. Modeled mercury wet deposition to MDN sites in the Great Lakes region using different MAXPUFF values (10000 vs. 20000 in left panel; 40000 vs. 20000 in right panel)

2.4.6. Frequency of puff releases and splitting

In carrying out HYSPLIT simulations, the frequency of pollutant emissions can be specified. The frequency can be hourly or more or less often. In the default PUF-type and COM-type simulations, pollutants were released once every three hours. A total of 3 grams of pollutant were emitted during each hour of release, so that the resulting average emissions amount would be 1 gram/hr for any given simulation. A series of simulations were carried out for Hg(II) emissions from SSL-11 (northeast Texas) using a range of release frequencies, from once every hour up through once every 7 hours. In each case, puff splitting was allowed to occur once every 24 hours. In any given variation, the MAXPUFF parameter was adjusted in order to compensate for the change in number of puffs emitted. For example, with puffs being emitted every hour, 3 times as many puffs would be emitted as compared to the default case, and so a MAXPUFF limit of 60,000 puffs was used in the simulation. Further, the emissions intensity in each simulation was adjusted so that the average emissions rate would be the same. So, for example, in the case with emissions every 6 hours, the emissions rate was 6 g/hr. The results for atmospheric mercury deposition flux to each of the Great Lakes with these different emissions frequencies are shown in Figure 36. It can be seen that there is moderate variations (on the order of +/- 10%), but no consistent pattern as the frequency is varied.

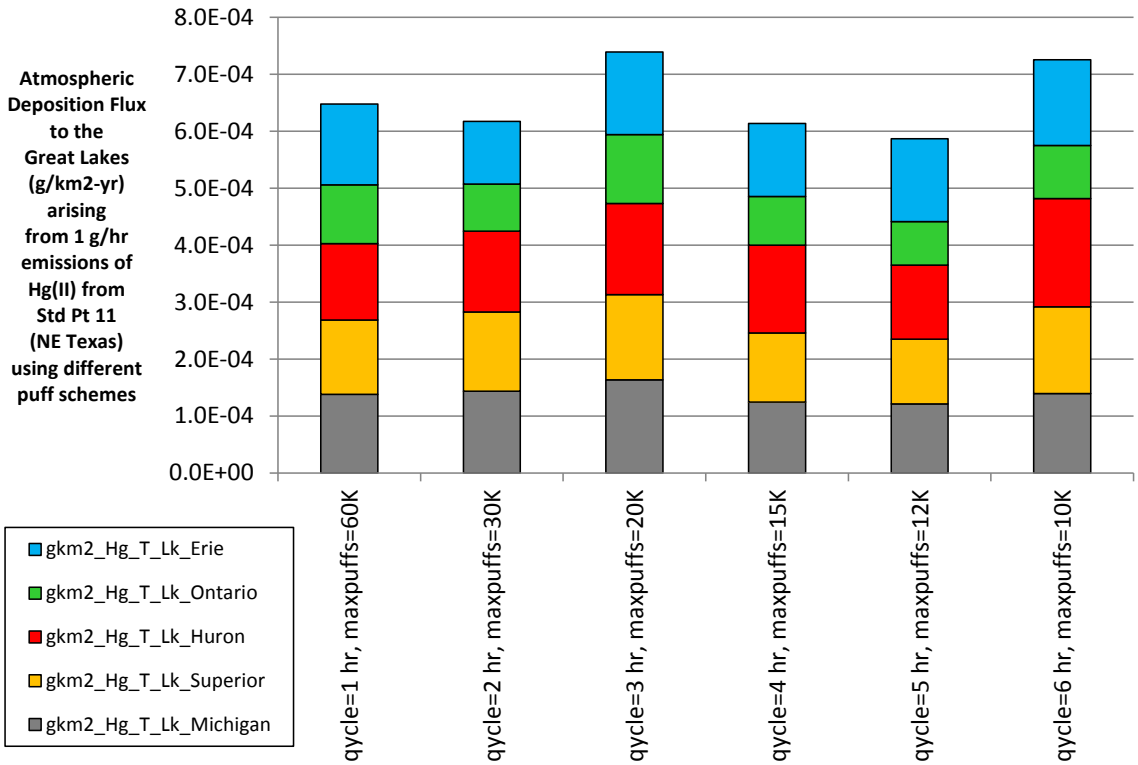

Figure 36. Atmospheric mercury deposition flux to the Great Lakes arising from Hg(II) emissions from SSL-11 using different puff-emission frequencies (in the labels, the frequency is indicated by "qcycle", e.g., qcycle=4 hr means that one puff was emitted every 4 hours)

An additional parameter is the frequency of puff splitting, with the default in these simulations being 24 hours. In the default simulations as described above, puff-scheme #11 was used, in which puffs were emitted every 3 hours and splitting was allowed to occur every 24 hours. In one of the variations, puff-scheme #10, emissions occurred every 7 hours, and splitting was also allowed to occur every 7 hours. In a second variation, emissions occurred every 7 hours but splitting was allowed to occur only once every 48 hours. The influence of these variations for model predicted wet deposition at MDN sites in the Great Lakes region is shown in Figure 37 and Figure 38. It can be seen that again, there is moderate influence, on the order of +/- 20%, but that there is no obvious trend, especially in the overall perspective offered by Figure 38.

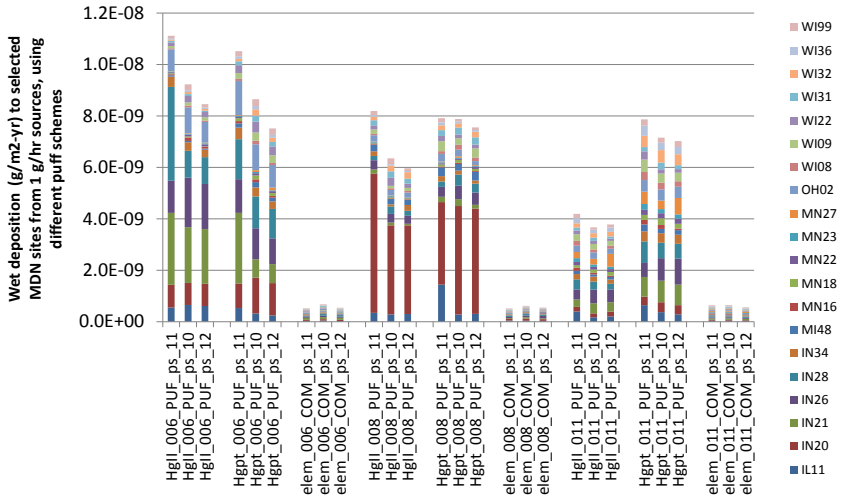

Figure 37. Modeled wet deposition at MDN sites in the Great Lakes region using different puff schemes (stacked bar graph)

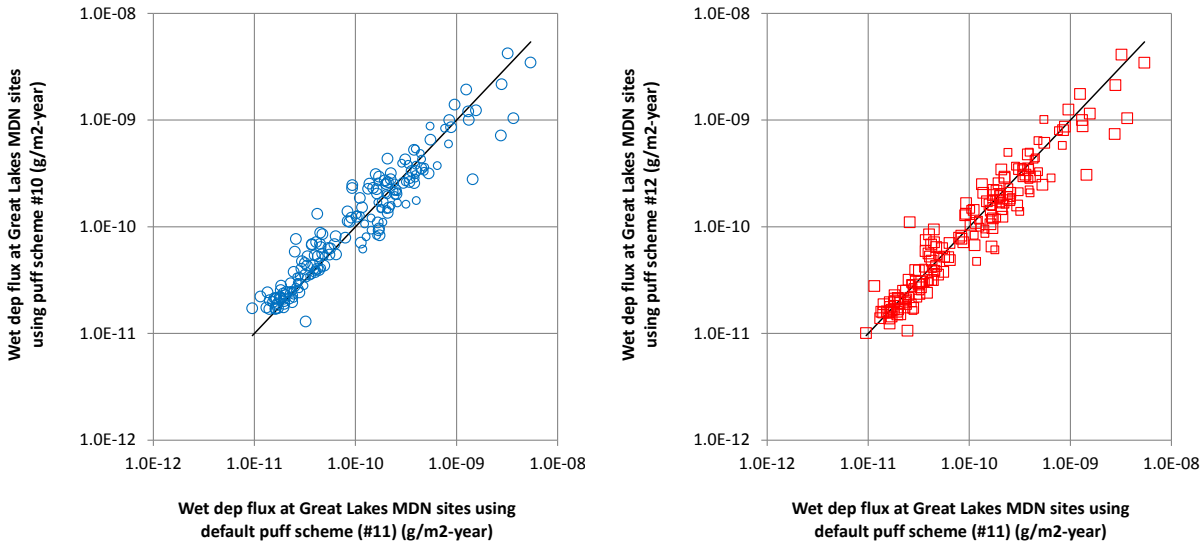

Figure 38. Modeled wet deposition at MDN sites in the Great Lakes region using different puff schemes (scatterplot)

2.4.7. Release height

In HYSPLIT simulations, one of the fundamental emissions parameters is the release height. In this work, a constant release height of 250 meters was assumed. A constant release height was used so that only one "set" of simulations at standard source locations would be needed to carry out the interpolation for all sources. Additional sets of SSL-simulations could have been carried out, for releases at different elevations, but each such set would mean an additional 2-3 months of computational resources. The fixed height of 250 meters was chosen as this is a common height for stacks at coal-fired power plants and other sources with large emissions. Stacks this high are commonly employed at such sources to reduce the adverse impacts in the immediate vicinity of the facility. The reasoning is that by the time the emissions plume reaches the ground, dispersion will have reduced its atmospheric concentrations significantly. It is recognized that not all sources have stacks this high. The decision to use this release height was made with the aim of characterizing the largest sources well, and accepting some loss of accuracy for emissions with much lower release heights. How big of an influence does this assumption have?

In Figure 39, the atmospheric mercury deposition to Lake Erie for 2005 is shown arising from each of the five illustrative standard source locations, for each of the 3 emitted mercury forms. This is the first parameter variation for which results for the two "global" illustrative locations are shown: SSL-13 (China) and SSL-48 (India). It can be seen from this figure that for the nearby source – SSL-8 – on the western shore of Lake Erie – there is a substantial influence of release height on the results. For emissions of Hg(II), the modeled deposition increases by almost a factor of 3. For sources further away from the lake, the influence of the release height is much less. This result is expected, but it does indicate that the height specification will have an important influence on the result. The importance of nearby sources with effective release heights less than 250 meters has likely been underestimated. But, as discussed above, it is hoped that the largest sources will have been reasonably well characterized.

In Figure 40, the model estimated deposition to each of the individual Great Lakes from each of the 5 SSL's is shown, as a scatterplot with 50m release-height results plotted against 250m results. It is seen that except for SSL-8's impact on Lake Erie – an expected, large influence – the influence of release height on the modeled deposition is very small. Figure 41 and Figure 42 show cumulative wet deposition at MDN sites in the Great Lakes region for 250m and 50m release heights for SSL's 6,8, and 11 and SSL's 13 and 48, respectively. For SSL-6 and SSL-8, which are inside the Great Lakes region, the choice of release height has a moderate influence. This is expected, as some of the MDN sites are relatively close to these SSL's.

However, it can be seen from Figure 43 that there is not a dramatic trend one way or another for the modeled wet deposition as a function of release height. The change from 250m to 50m release height results in lower wet deposition at some MDN sites and higher wet deposition at other sites. It is also seen in this figure that the greatest differences occur for the largest impacts, i.e., sources that are relatively close to the MDN sites.

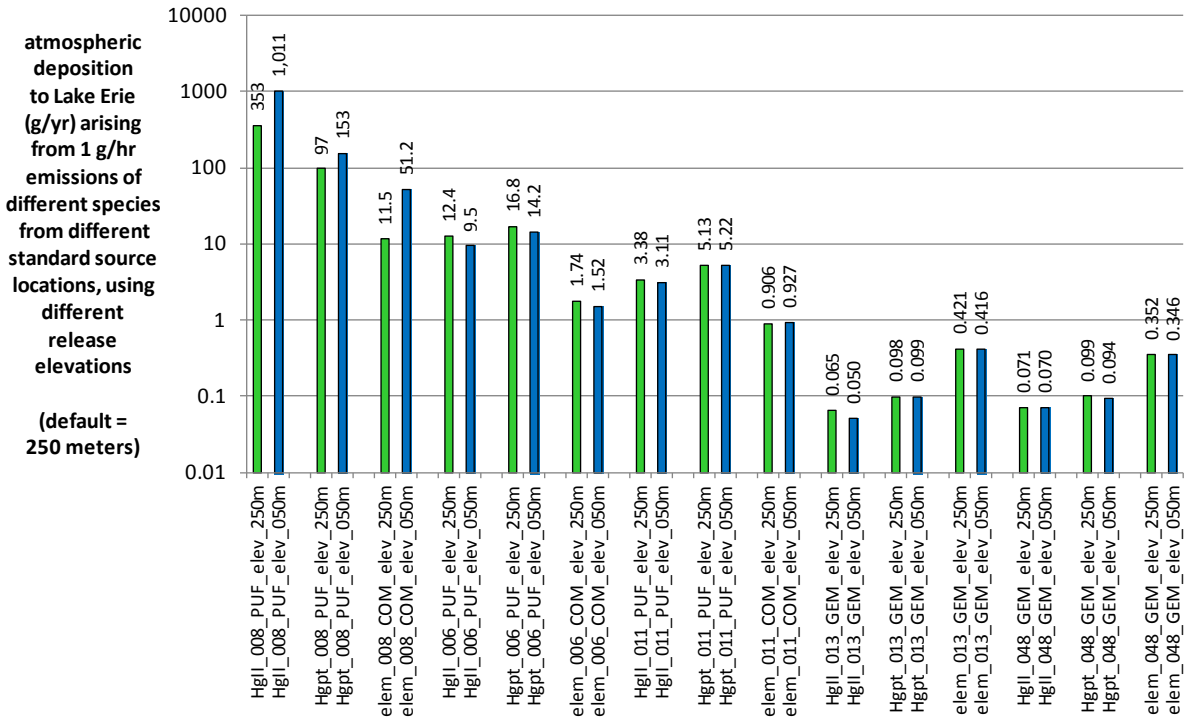

Figure 39. Atmospheric mercury deposition to Lake Erie from illustrative standard source locations with 250m and 50m release heights

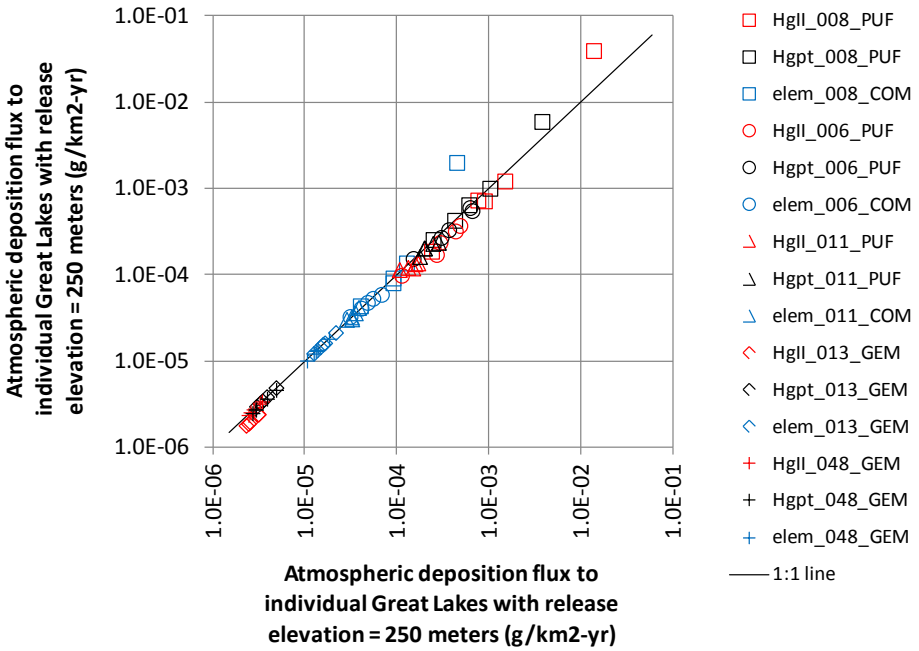

Figure 40. Atmospheric mercury deposition flux to individual Great Lakes using 250m and 50m release heights

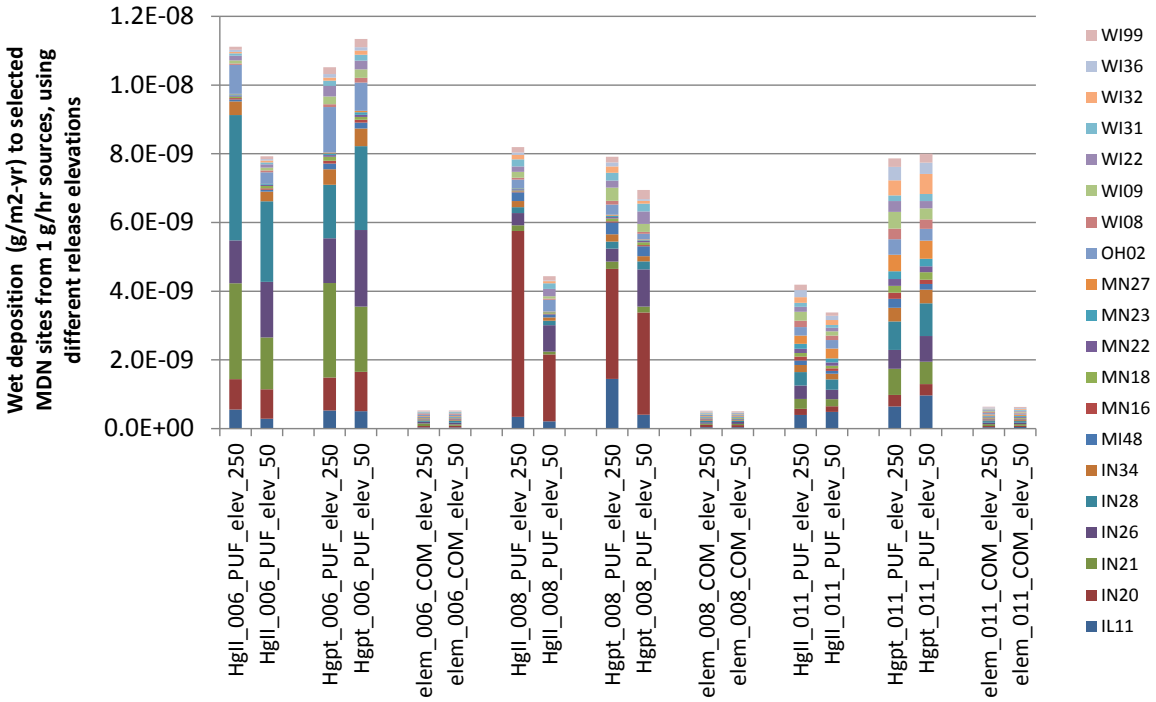

Figure 41. Atmospheric mercury wet deposition flux to MDN sites in the Great Lakes region from SSL's 6,8, and 11 (US) using release heights of 250m and 50m

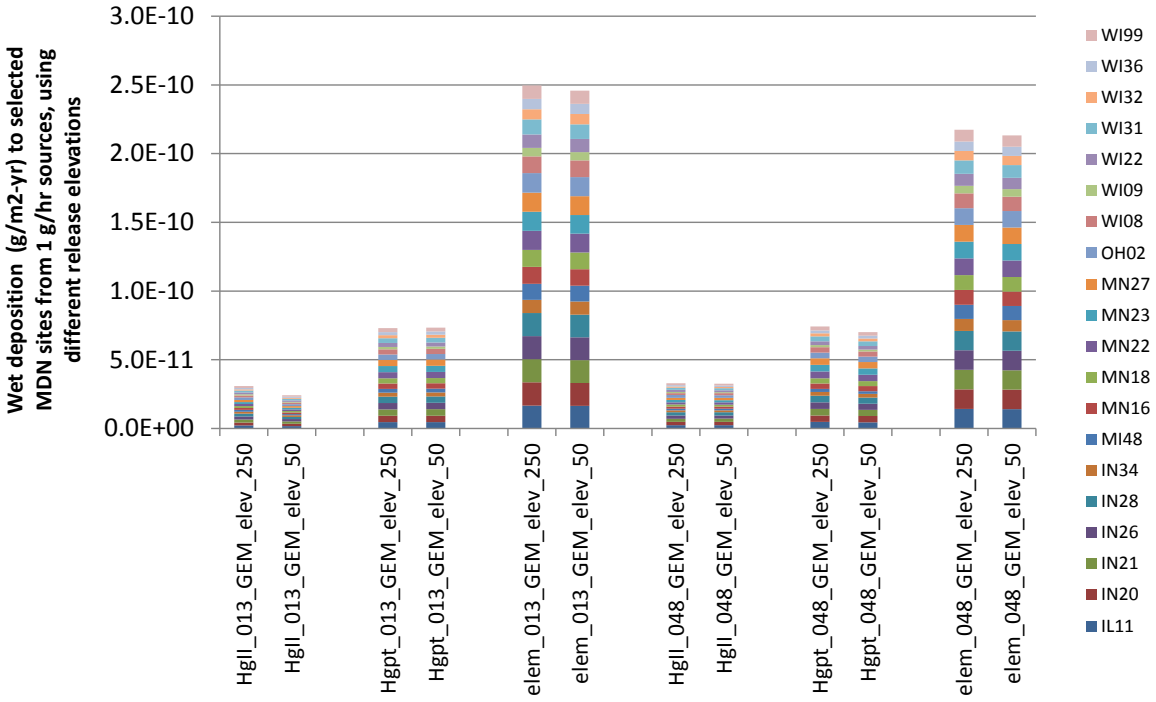

Figure 42. Atmospheric mercury wet deposition flux to MDN sites in the Great Lakes region from SSL-13 (China) and SSL-48 (India) using release heights of 250m and 50m

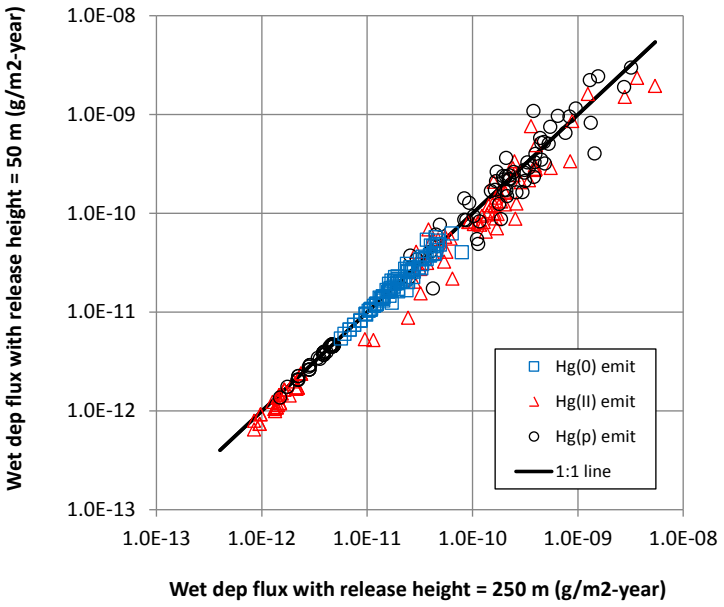

Figure 43. Atmospheric mercury wet deposition flux to MDN sites in the Great Lakes region from all five illustrative standard source locations with release heights of 250m and 50m

2.5. Sensitivity to deposition methodologies

2.5.1. Introduction

After puffs are released in the HYSPLIT model, they are advected downwind, expanded due to dispersion, and the pollutants contained within them are subject to dry and wet deposition phenomena. There are two basic types of wet deposition processes simulated in the HYSPLIT model: within-cloud and below-cloud. In the within-cloud process, gaseous and particulate pollutants are incorporated into precipitation, which then subsequently falls to the earth's surface. In the below-cloud process, pollutants are incorporated into falling precipitation. Dry deposition of gaseous and particulate pollutants is applied to pollutants if they are in the lowest model layer. The rate is based on a dry deposition velocity estimated with a resistance-based approach. A description of the algorithms used in these estimates is provided by Draxler and Hess (1998, 2010). In this section we will investigate the influence of different parameterizations and methodologies for estimating the rate of these deposition phenomena.

2.5.2. WETR

The WETR parameter governs the incorporation of particle-phase pollutant in within-cloud wet deposition processes. It is the "scavenging coefficient", the ratio of the pollutants concentration in water to its concentration in air. The default value used in these simulations was 40,000 [(g/m^3-water) / (g/m^3-air)] = 40,000 m^3-air / m^3-water. To investigate the influence of this parameter value on the modeling results, a value of 10,000 m^3/m^3 and a value of 160,000 m^3/m^3 were used and compared with the results using the default value of 40,000 m^3/m^3.

Figure 44 shows the total modeled mercury deposition to Lake Erie from each of the five illustrative standard source locations, for each form of mercury emitted, using the different values of WETR. As might be expected, the largest impacts are for the emissions of Hg(p). This can be seen more clearly by comparing Figure 45 [for emissions of Hg(p)] with Figure 46 [for emissions of Hg(II)] and Figure 47 [for emissions of Hg(0)]. It is clear from these figures that the largest differences are seen for emissions of Hg(p). As the WETR parameter is directly related to wet deposition of particles, this is not surprising. Differences do arise in the simulations of Hg(0) and Hg(II) emissions, as there is some conversion to Hg(p) in these simulations due to chemical and physical processes.

Figure 48, Figure 49, Figure 50 show the influence of the WETR value on modeled wet deposition to MDN sites in the Great Lakes region. As with deposition to the Great Lakes, the largest differences are generally seen for the simulations in which Hg(p) is emitted.

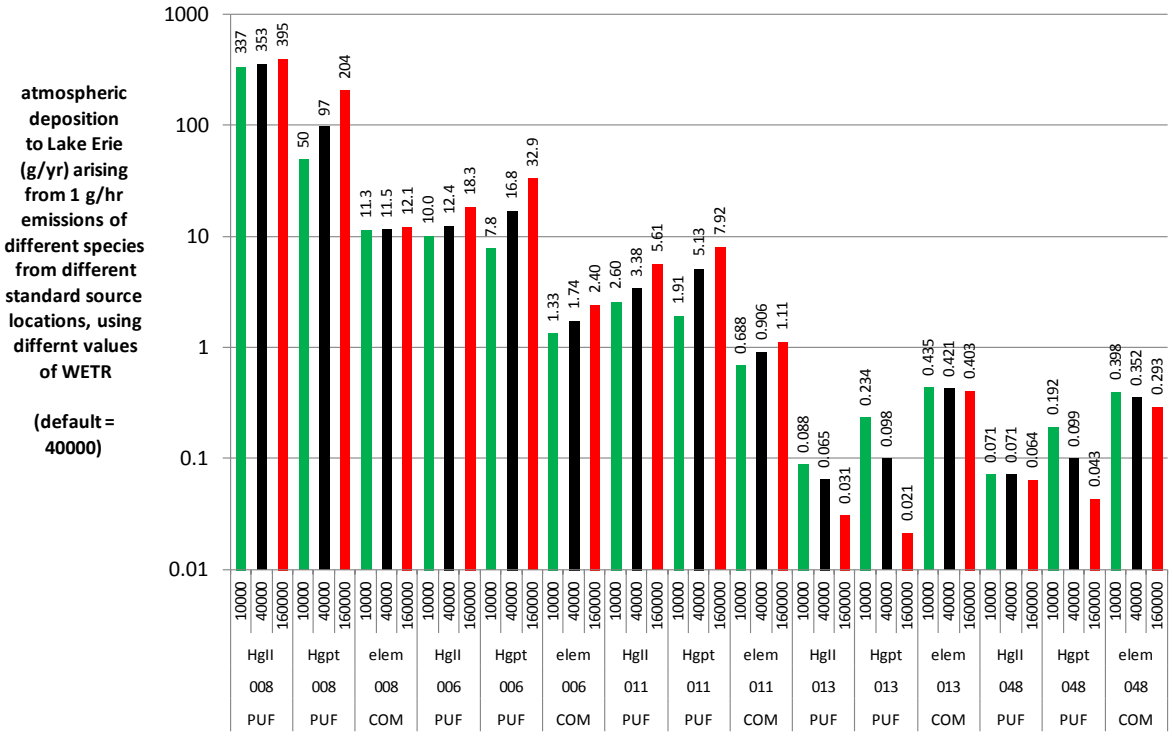

Figure 44. Modeled atmospheric mercury deposition to Lake Erie using different values of the within-cloud particle scavenging ratio, WETR

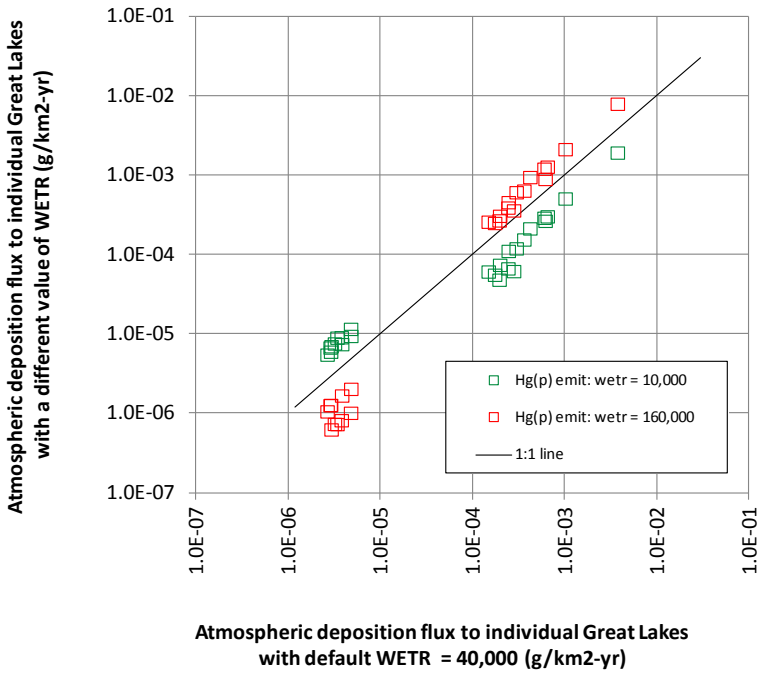

Figure 45. Modeled atmospheric mercury deposition to individual Great Lakes using different values of the within-cloud particle scavenging ratio, WETR, for emissions of Hg(p) from five illustrative standard source locations

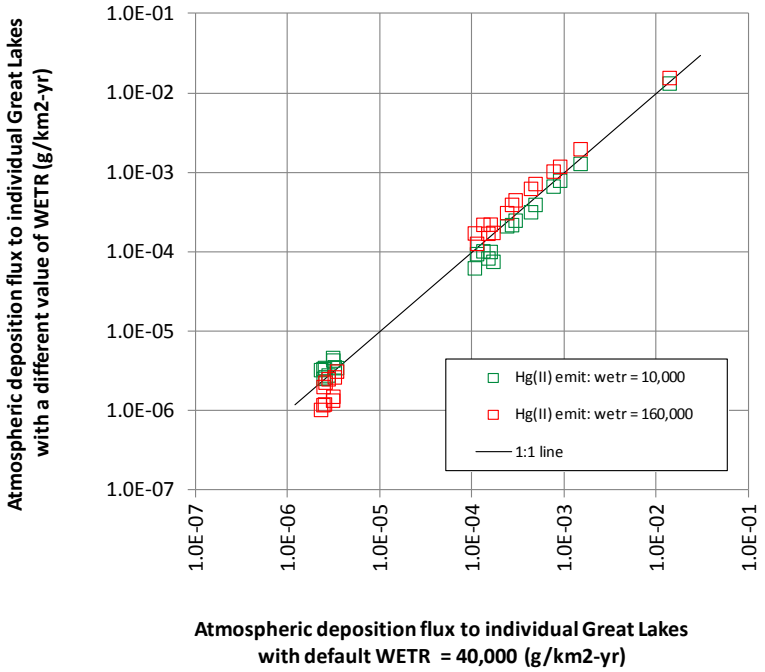

Figure 46. Modeled atmospheric mercury deposition to individual Great Lakes using different values of the within-cloud particle scavenging ratio, WETR, for emissions of Hg(II) from five illustrative standard source locations

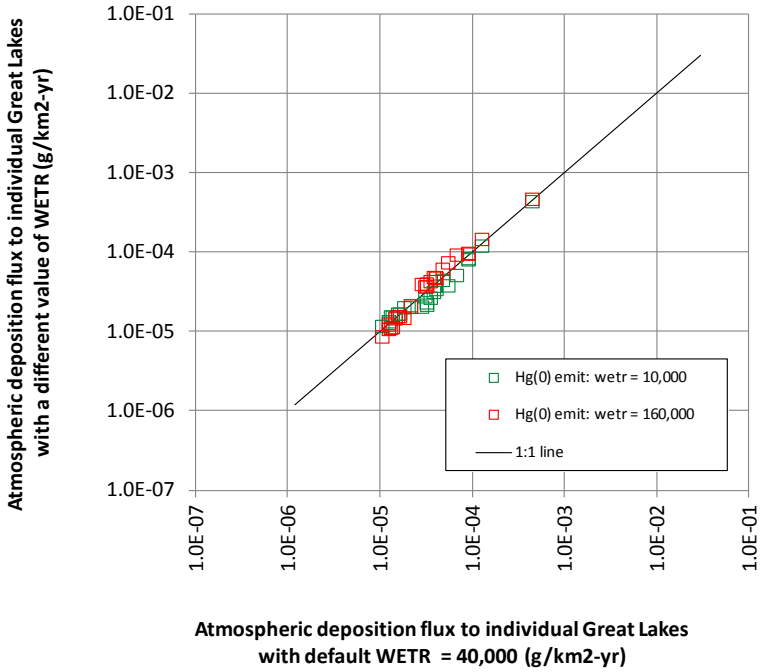

Figure 47. Modeled atmospheric mercury deposition to individual Great Lakes using different values of the within-cloud particle scavenging ratio, WETR, for emissions of Hg(0) from five illustrative standard source locations

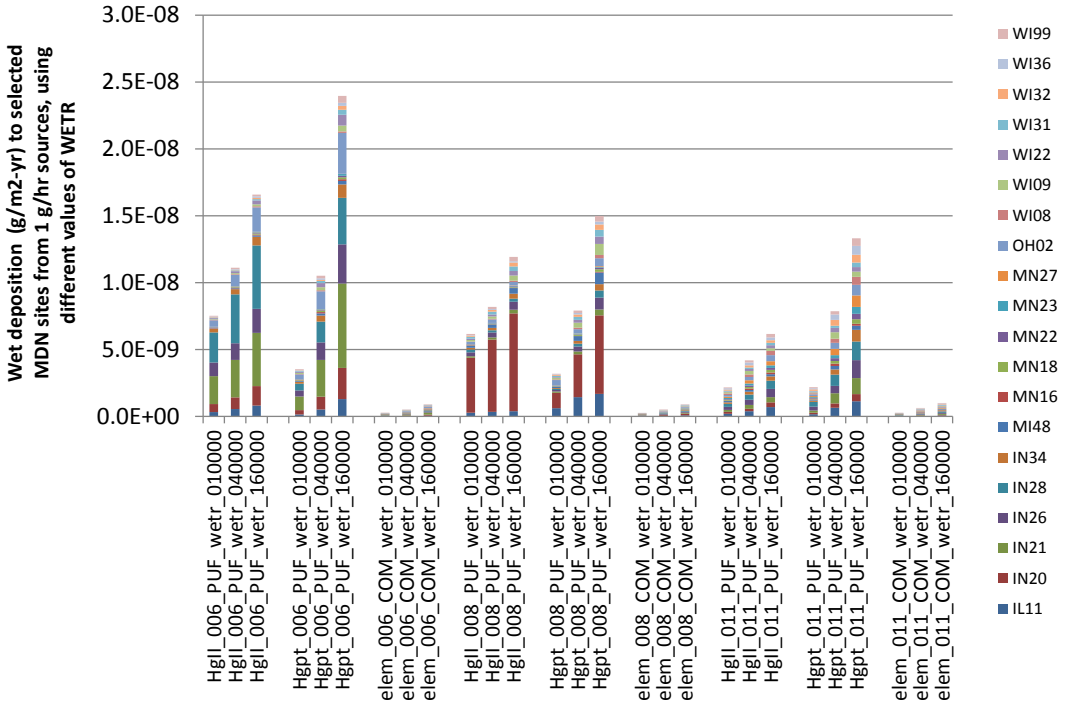

Figure 48. Modeled atmospheric mercury wet deposition to MDN sites in the Great Lakes region using different values of the within-cloud particle scavenging ratio, WETR, for standard source locations 6, 8, and 11 (U.S.)

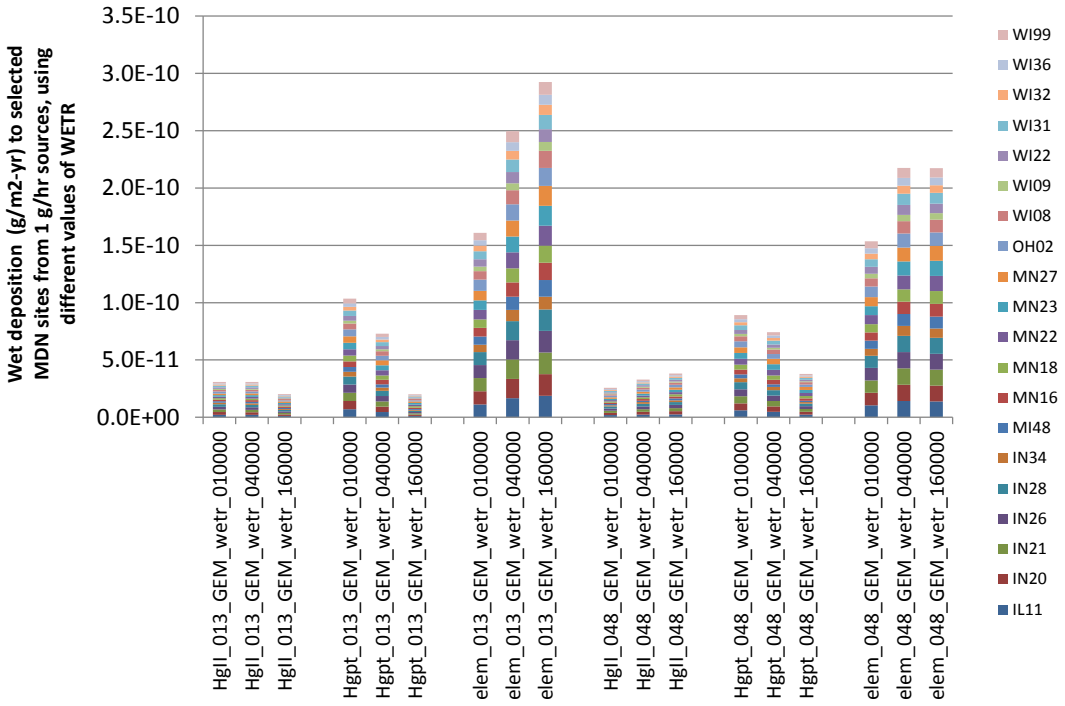

Figure 49. Modeled atmospheric mercury wet deposition to MDN sites in the Great Lakes region using different values of the within-cloud particle scavenging ratio, WETR, for standard source locations 13 (China) & 48 (India)

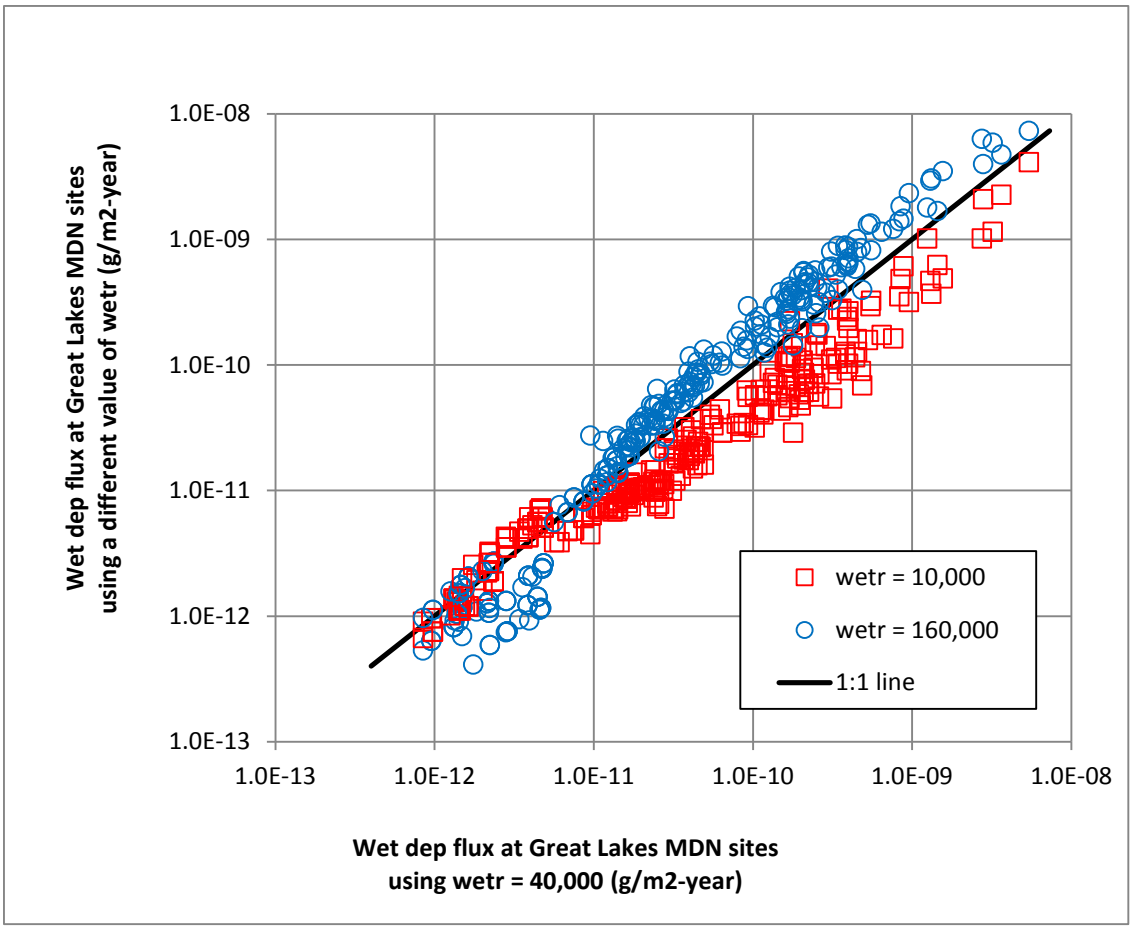

Figure 50. Modeled atmospheric mercury wet deposition to MDN sites in the Great Lakes region for all five illustrative standard source locations: non-default WETR results vs. default WETR results

2.5.3. Hg(0) deposition

In the default simulations using HYSPLIT-Hg, each form of mercury is subjected to wet and dry deposition processes. There are significant uncertainties in the rate of dry deposition of elemental mercury due to its bidirectional nature. To explore the influence of this uncertainty, simulations were done in which the dry deposition of Hg(0) was artificially set to "0", and these simulations were compared with those in which the dry deposition of Hg(0) was estimated via the normal HYSPLIT-Hg procedure involving a resistance-based deposition velocity.

Figure 51 shows the results of this comparison for the simulated deposition of mercury to Lake Erie, from each of the five illustrative standard source locations. It is seen that the largest differences are for simulations of Hg(0) emissions, as would be expected. It is also noted that the deposition arising from these emissions is generally much smaller than that arising from Hg(II) or Hg(p) emissions – for any given standard source location – and so the magnitude of the differences is relatively small. For example, the largest difference seen in this example is that for elemental mercury emissions from SSL-8, on the western shore of Lake Erie. The simulated deposition from 1 g/hr emissions of Hg(0) from this location is 11.5 g/year to Lake Erie. With Hg(0) dry deposition set to zero, the simulated deposition is 1.1 g/year, a difference of ~10 g/year. This difference can be compared with the deposition arising from analogous emissions of Hg(II) and Hg(p) with modeled deposition of ~350 g/year and ~100 g/year, respectively. Figure 52 through Figure 55 show analogous comparisons for individual Great Lakes and for MDN sites in the Great Lakes region. The overall influence of this variation in Hg(0) dry deposition is relatively small, although there are larger fractional differences seen in some of the Hg(0) emissions simulations.

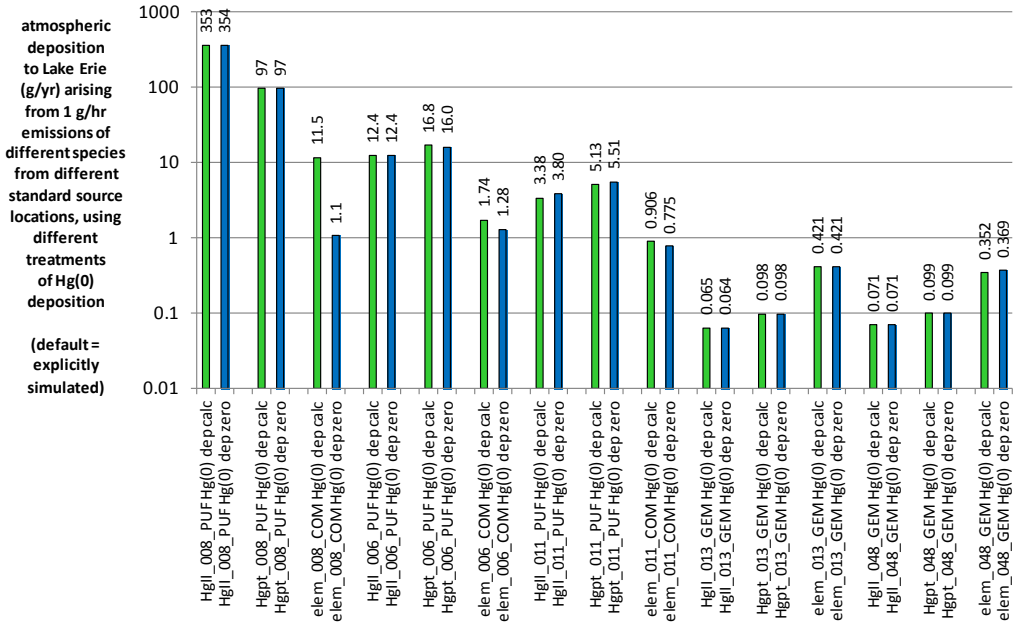

Figure 51. Atmospheric mercury deposition to Lake Erie arising from emissions of three different forms of emitted mercury from five illustrative standard source locations: results for default simulation and results of simulations with Hg(0) set to 0

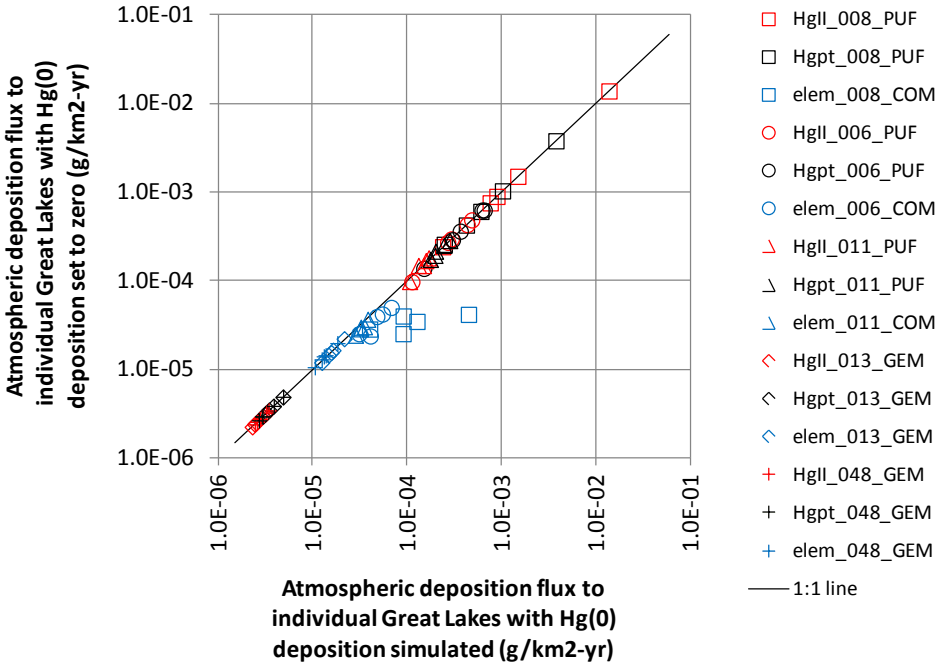

Figure 52. Atmospheric mercury deposition to individual Great Lakes arising from emissions of three different forms of emitted mercury from five illustrative standard source locations: results for default simulation and results of simulations with Hg(0) set to 0

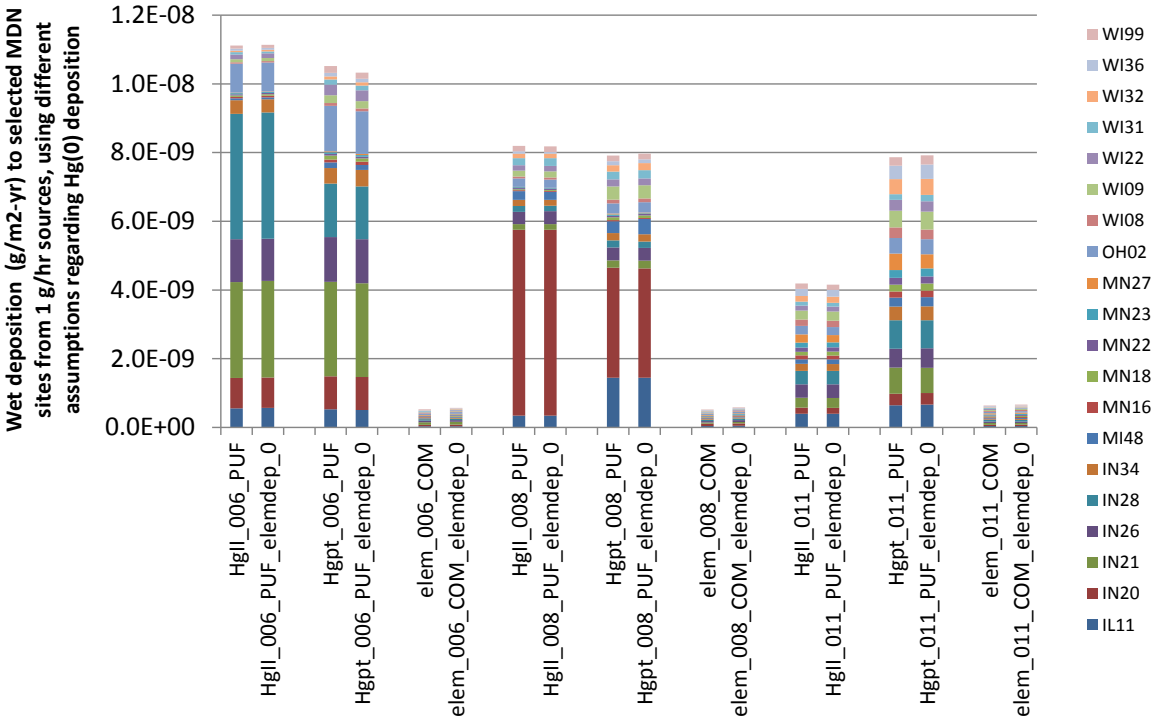

Figure 53. Atmospheric wet mercury deposition to MDN sites in the Great Lakes region from SSL's 6,8, and 11 (US) with and without Hg(0) dry deposition

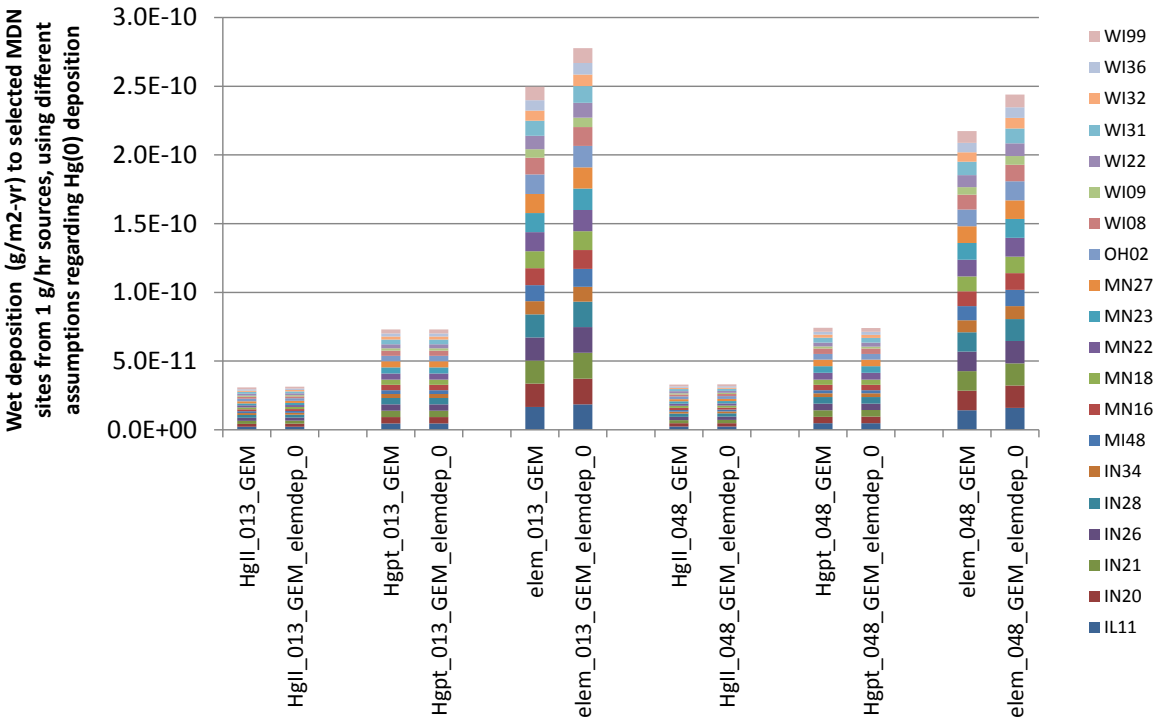

Figure 54. Atmospheric wet mercury deposition to MDN sites in the Great Lakes region from SSL-13 (China) and SSL-48 (India) with and without Hg(0) dry deposition

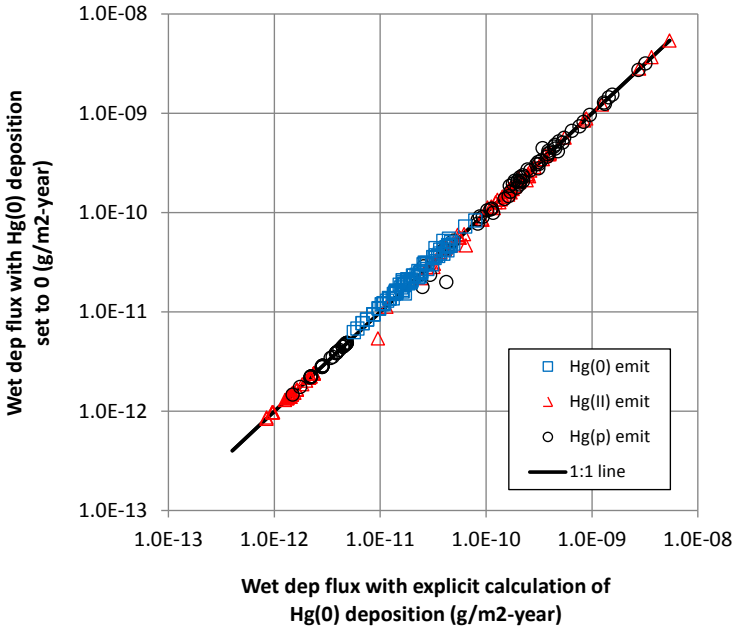

Figure 55. Atmospheric wet mercury deposition to MDN sites in the Great Lakes region from all SSL's Hg(0): dry deposition = 0 vs. default Hg(0) dry deposition

2.6. Sensitivity to chemical transformation methodologies

2.6.1. Introduction

In the HYSPLIT-Hg model, atmospheric mercury can be transformed by chemical and physical processes from one form to another. In the model, there are four forms of mercury tracked: Hg(0), Hg(II), Hg(p), and Hg(II) adsorbed to soot, which is abbreviated "Hg2s". The chemical transformations in the gas and liquid phase, as well as the process of Hg(II)-aqueous sorption to aqueous soot, are shown in Figure 56 and Table 2. In this section, the reaction rates and parameters shown in Table 2 were varied and the influence on the results was examined. In essentially every case, the variations chosen were ½ the default value and twice the default value.

As can be seen from close inspection of Table 2 and Figure 56, there are no processes in the model in which Hg(p) is transformed to another form of atmospheric mercury. Thus, for simulations of pure Hg(p) emissions, there should be no sensitivity to these chemical reaction parameters, and concentrations and deposition of the other mercury forms should all be zero. As a preliminary check, this will be examined in the next section.

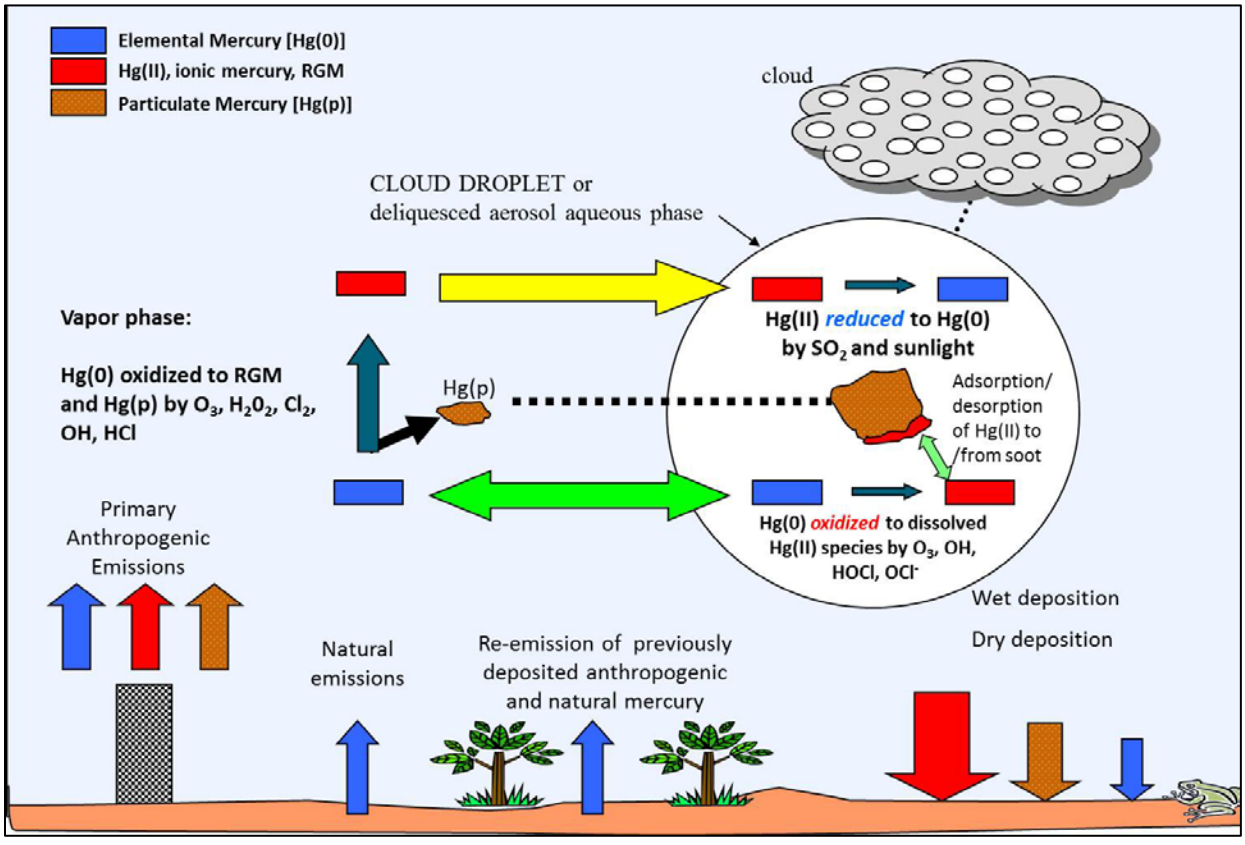

Figure 56. Schematic of mercury transformations in the HYSPLIT-Hg model

Table 2. Chemical Transformations in the HYSPLIT-Hg Model

Reaction	Rate	Units	Reference
GAS PHASE REACTIONS			
$Hg^0 + O_3 \rightarrow Hg(p)$	3.0E-20	cm^3/molec-sec	Hall (1995)
$Hg^0 + HCl \rightarrow HgCl_2$	1.0E-19	cm^3/molec-sec	Hall and Bloom (1993)
$Hg^0 + H_2O_2 \rightarrow Hg(p)$	8.5E-19	cm^3/molec-sec	Tokos et al. (1998) (upper limit based on experiments)
$Hg^0 + Cl_2 \rightarrow HgCl_2$	4.0E-18	cm^3/molec-sec	Calhoun and Prestbo (2001)
$Hg^0 + OH \rightarrow Hg(p)$	8.7E-14	cm^3/molec-sec	Sommar et al. (2001)
AQUEOUS PHASE REACTIONS			
$Hg^0 + O_3 \rightarrow Hg^{+2}$	4.7E+7	$(molar\text{-}sec)^{-1}$	Munthe (1992)
$Hg^0 + OH \rightarrow Hg^{+2}$	2.0E+9	$(molar\text{-}sec)^{-1}$	Lin and Pehkonen(1997)
$HgSO_3 \rightarrow Hg^0$	$T*e^{((31.971*T)-12595.0)/T)}$ sec^{-1} [T = temperature (K)]		Van Loon et al. (2002)
$Hg(II) + HO_2 \rightarrow Hg^0$	~ 0	$(molar\text{-}sec)^{-1}$	Gardfeldt & Jonnson (2003)
$Hg^0 + HOCl \rightarrow Hg^{+2}$	2.1E+6	$(molar\text{-}sec)^{-1}$	Lin and Pehkonen(1998)
$Hg^0 + OCl^{-1} \rightarrow Hg^{+2}$	2.0E+6	$(molar\text{-}sec)^{-1}$	Lin and Pehkonen(1998)
$Hg(II) \leftrightarrow Hg(II)_{(soot)}$	9.0E+2	liters/gram; t = 1/hour	eqlbrm: Seigneur et al. (1998) rate: Bullock & Brehme (2002).
$Hg^{+2} + hv \rightarrow Hg^0$	6.0E-7	$(sec)^{-1}$ (maximum)	Xiao et al. (1994); Bullock and Brehme (2002)

2.6.2. Check Hg(p) not influenced by chemical parameters

As discussed immediately above, the fate and transport of Hg(p) emissions should not be influenced by variations in the HYSPLIT-Hg chemical transformation rates and parameters being examined here. This was tested by carrying out a simulation in which all of the rates and parameters were adjusted. All oxidation reaction rates were multiplied by 2, and all reduction reaction rates were divided by 2, creating a "maximum oxidation" variation (often shown as "max oxid" in the figures below).

In Figure 57 through Figure 61, below, numerous comparisons are presented, showing the results of simulations of Hg(p) emissions with default and "maximum oxidation" chemical rate parameters. It can be seen in all of the figures that the deposition to the Great Lakes and the wet deposition to MDN sites in the Great Lakes region are identical. This is the expected result, and it serves as a useful QA/QC check on the simulation.

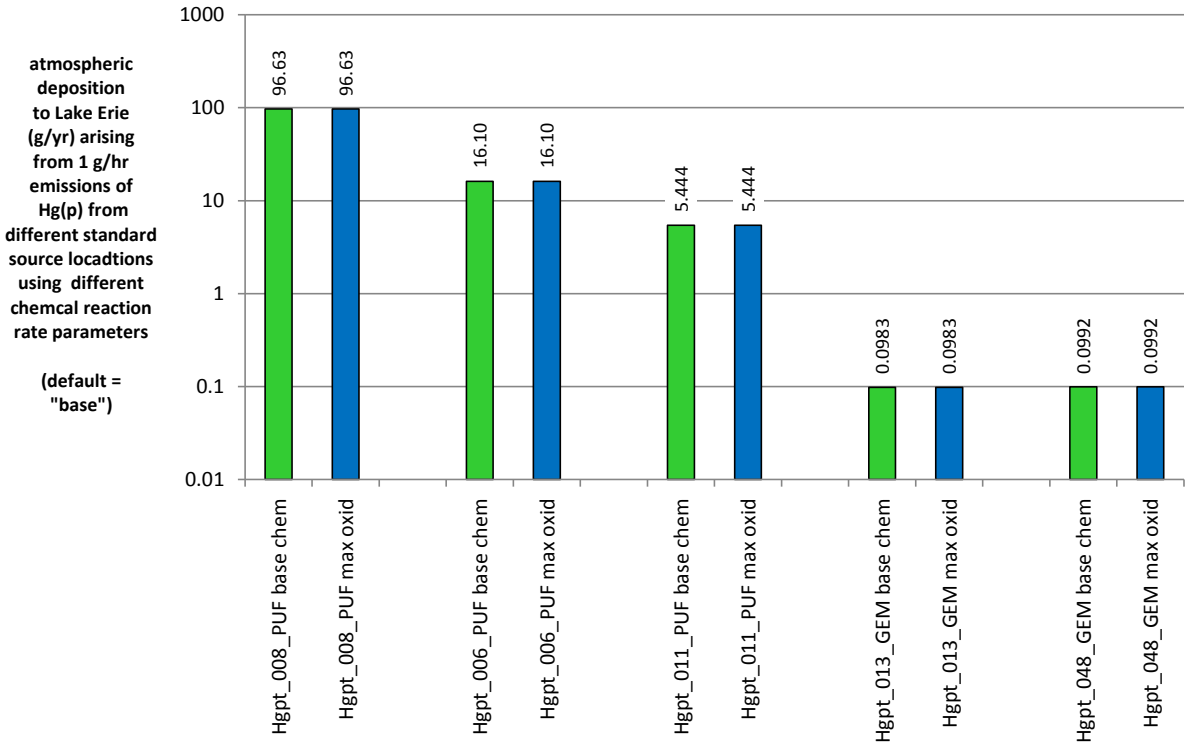

Figure 57. Atmospheric deposition to Lake Erie arising from Hg(p) emissions with "maximum oxidation" parameters vs. default chemical rate parameters

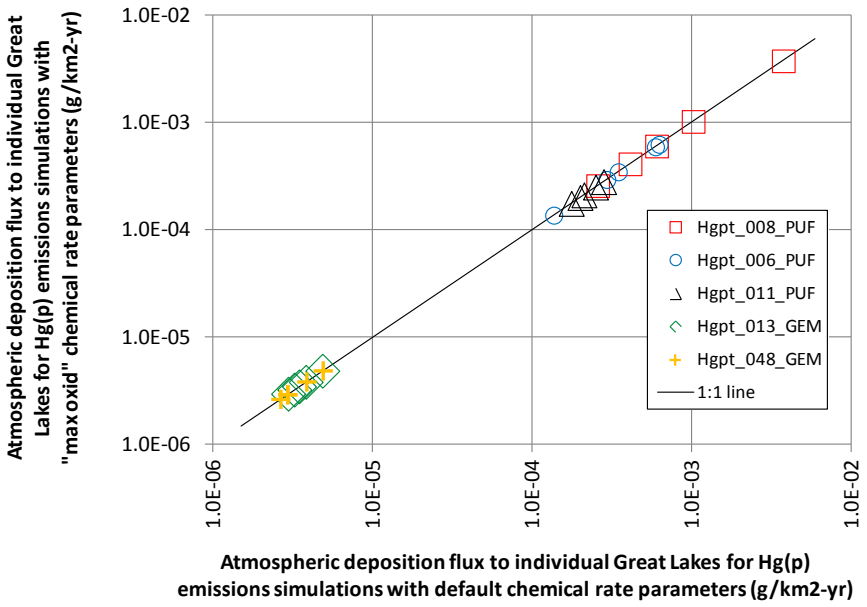

Figure 58. Atmospheric deposition to individual Great Lakes arising from Hg(p) emissions with "maximum oxidation" parameters vs. default chemical rate parameters

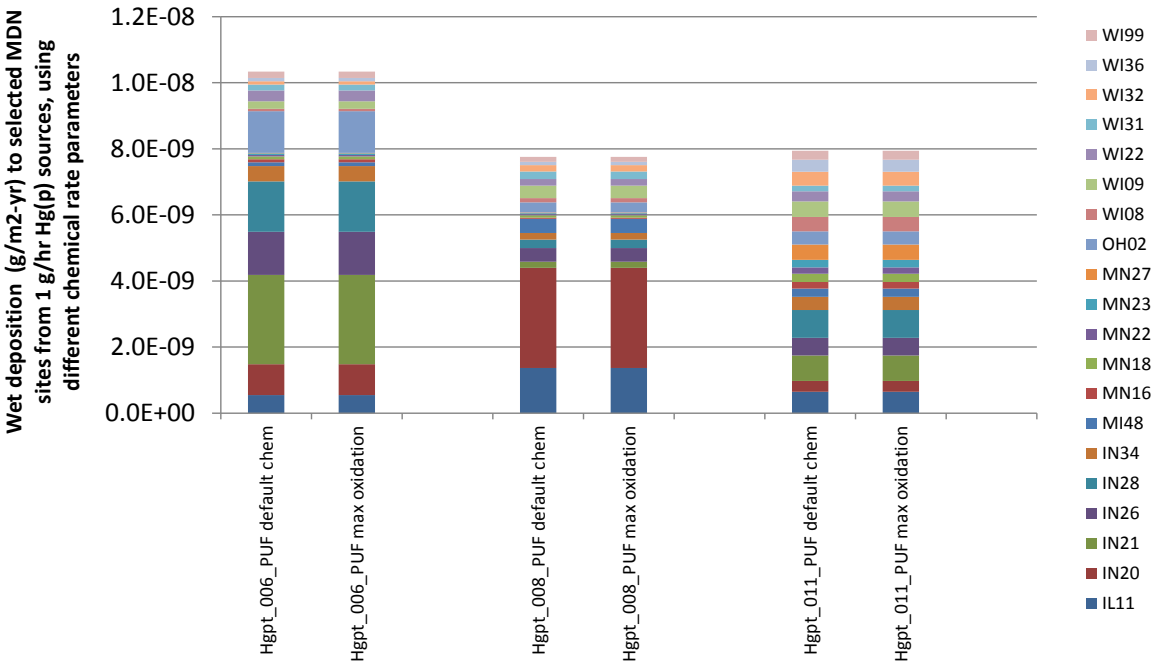

Figure 59. Atmospheric wet deposition to MDN sites in the Great Lakes region arising from Hg(p) emissions with "maximum oxidation" parameters vs. default chemical rate parameters, from SSL's 6,8, and 11 (U.S.)

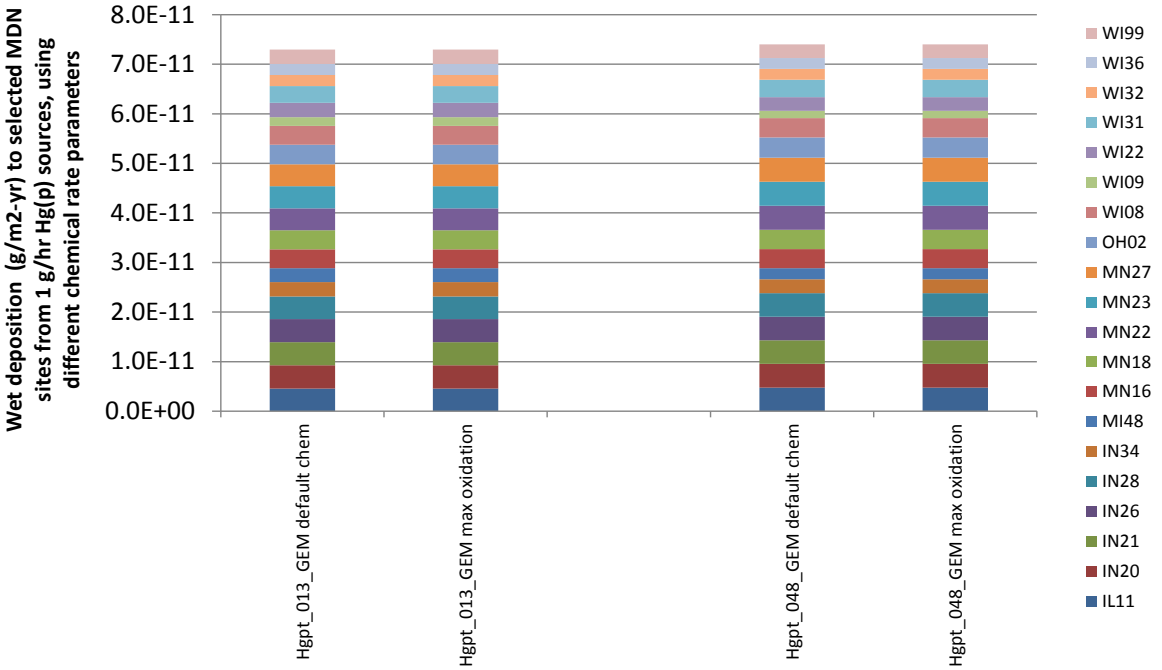

Figure 60. Atmospheric wet deposition to MDN sites in the Great Lakes region arising from Hg(p) emissions with "maximum oxidation" parameters vs. default chemical rate parameters, from SSL-13 (China) and SSL-48 (India)

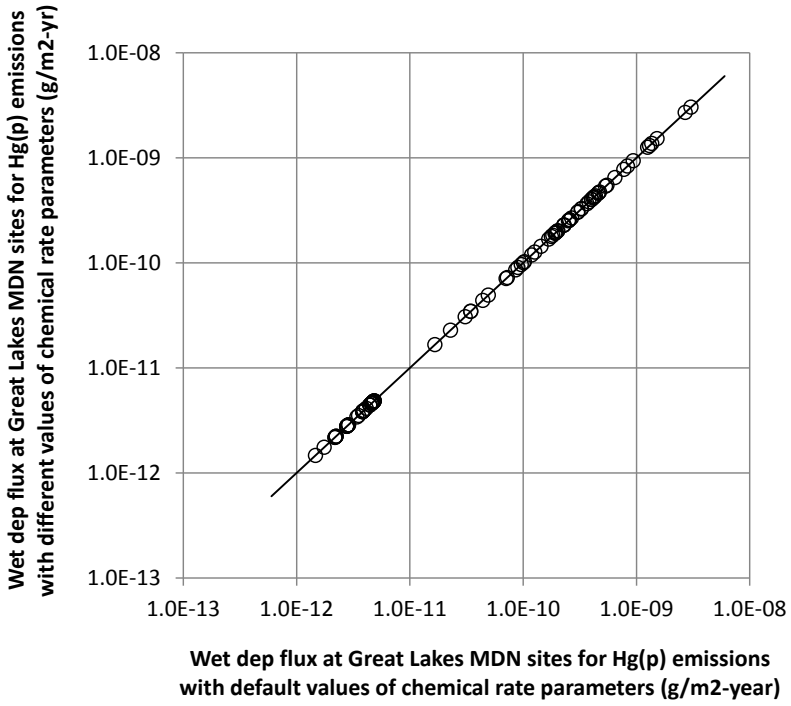

Figure 61. Atmospheric wet deposition to MDN sites in the Great Lakes region arising from Hg(p) emissions with "maximum oxidation" parameters vs. default chemical rate parameters, for all five illustrative SSL's

2.6.3. Aqueous-phase reduction of Hg(II) by hv

In this section, the rate of aqueous phase reduction of Hg(II) by sunlight is varied, and the influence on the modeled fate and transport of emitted mercury is examined. It can be seen in Figure 62 through Figure 66 that the variation in this chemical reduction rate has little effect on the modeled fate and transport of emitted mercury, in almost every case. Note that only simulations for Hg(0) and Hg(II) emissions are shown. As discussed earlier, emissions of Hg(p) are not affected by this process.

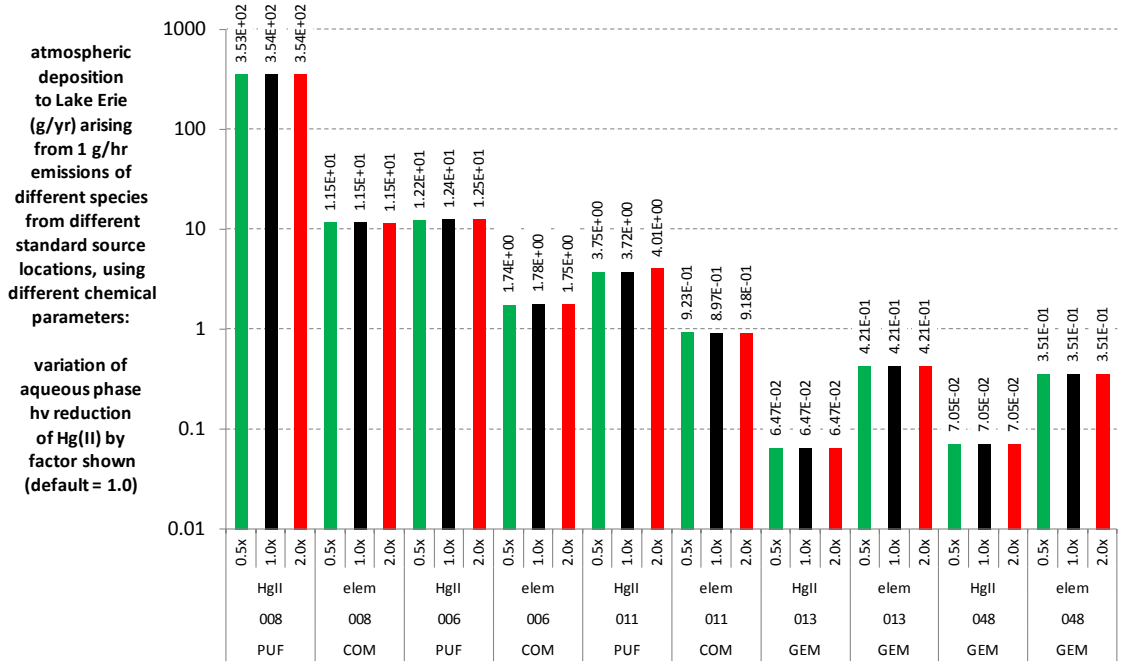

Figure 62. Atmospheric deposition to Lake Erie with Hg(II)-aq reduction at 0.5, 1.0, and 2.0x the default rate

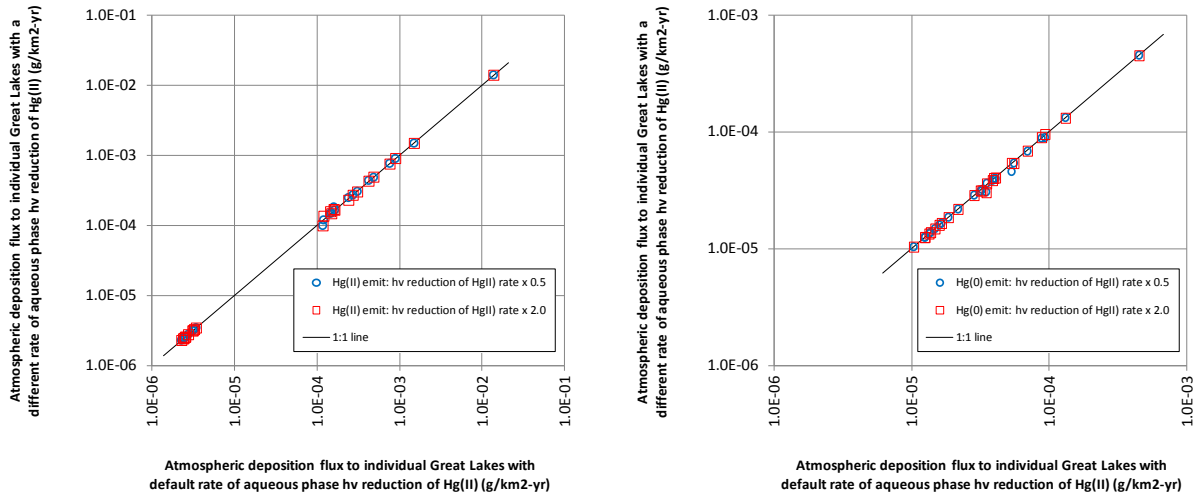

Figure 63. Atmospheric deposition to individual Great Lakes with different rates of sunlight-mediated Hg(II)-aq reduction for Hg(II) emissions (left) and Hg(0) emissions (right)

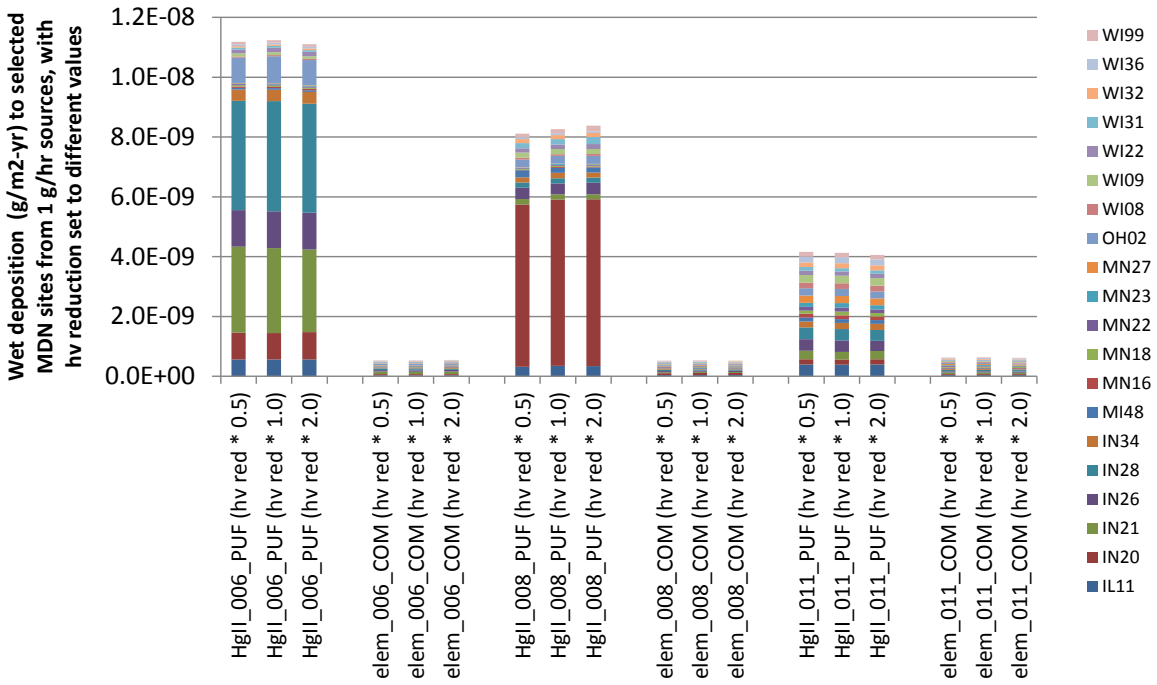

Figure 64. Atmospheric wet deposition to MDN sites in the Great Lakes region with different rates of sunlight-mediated Hg(II)-aq reduction for SSL's 6,8, and 11 (U.S.)

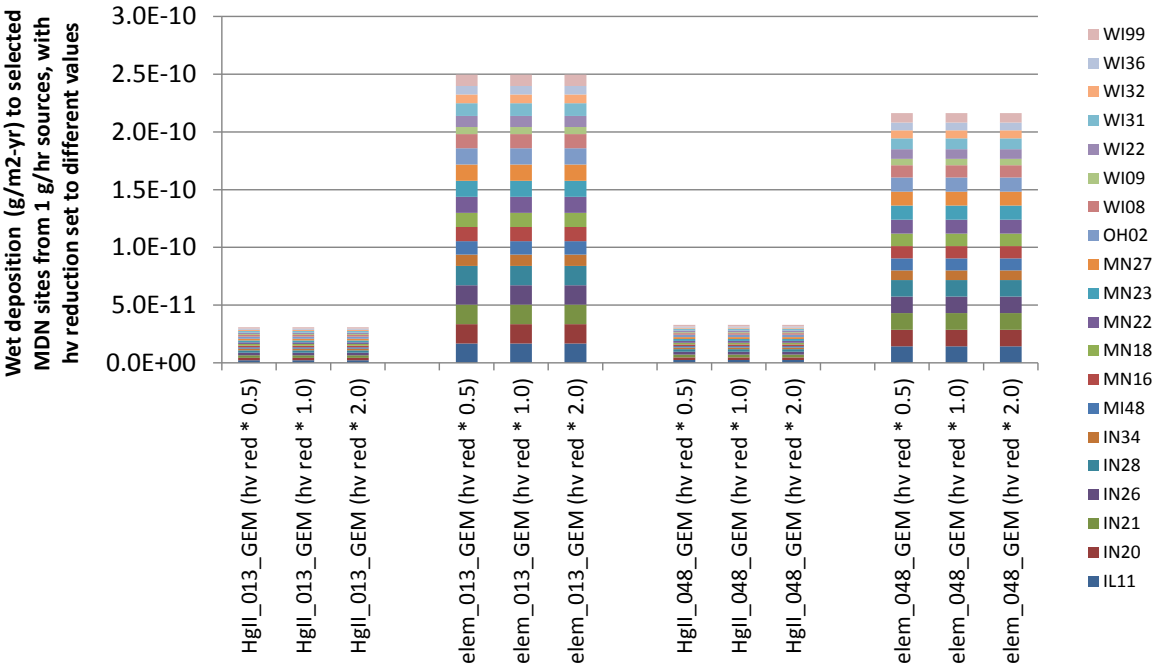

Figure 65. Atmospheric wet deposition to MDN sites in the Great Lakes region with different rates of sunlight-mediated Hg(II)-aq reduction for SSL-13 (China) and SSL-48 (India)

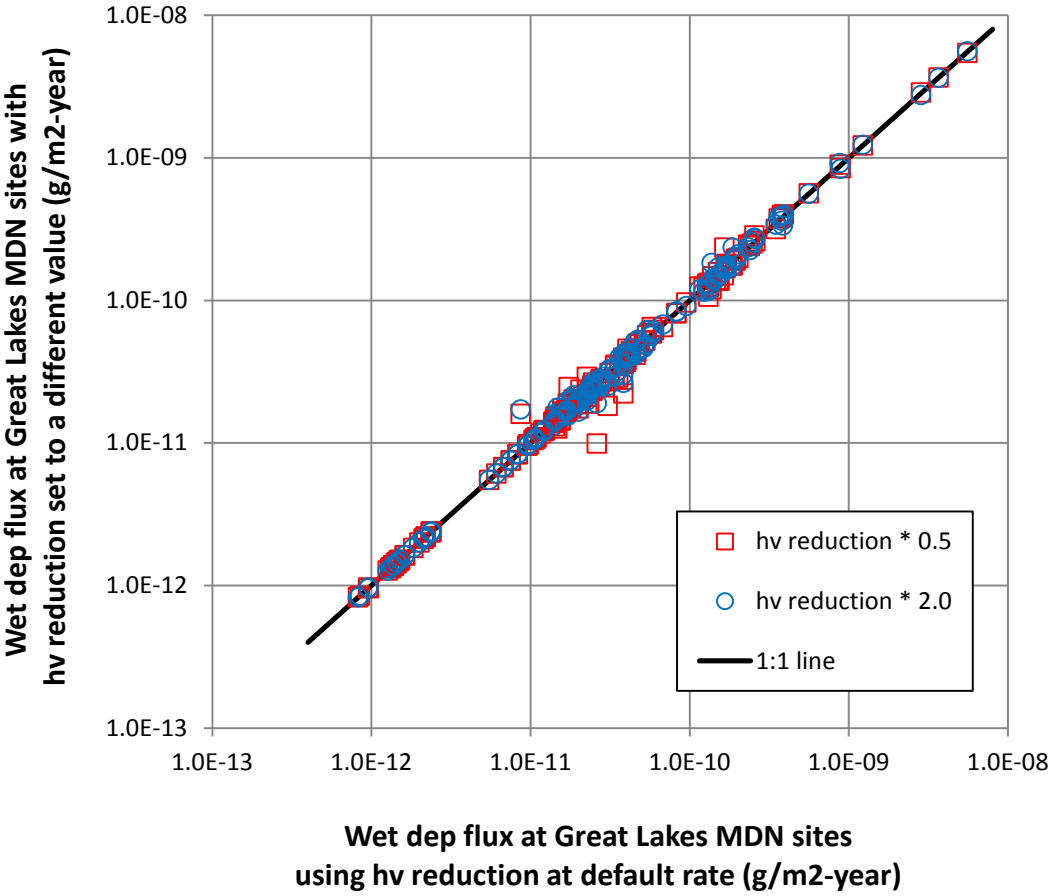

Figure 66. Atmospheric wet deposition to MDN sites in the Great Lakes region with different rates of sunlight-mediated Hg(II)-aq reduction for all five illustrative SSL's (scatterplot)

2.6.4. Gas-phase oxidation of Hg(0) by O3

In this section, the rate of gas-phase oxidation of Hg(0) by ozone is varied, and the influence of this variation on the fate and transport of emitted Hg(0) and Hg(II) is examined. It can be seen from Figure 67 through Figure 71 that the variation of this rate has little effect on the fate and transport of emitted Hg(0) or Hg(II). As discussed earlier, emissions of Hg(p) are not affected by this parameter.

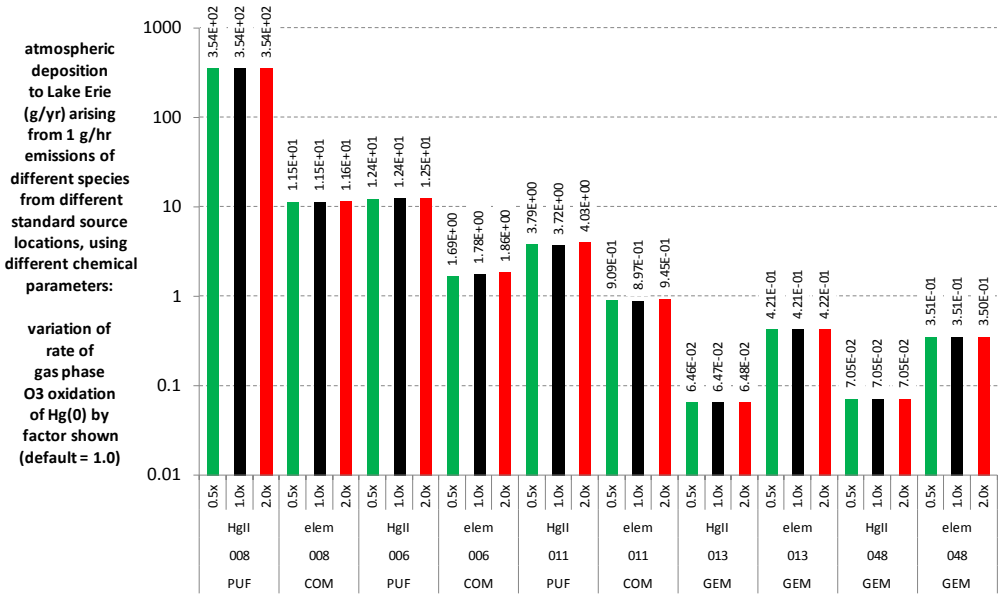

Figure 67. Atmospheric deposition to Lake Erie with gas-phase oxidation of Hg(0) by ozone at 0.5, 1.0, and 2.0x the default rate, for emissions of Hg(II) and Hg(0), from all five illustrative standard source locations

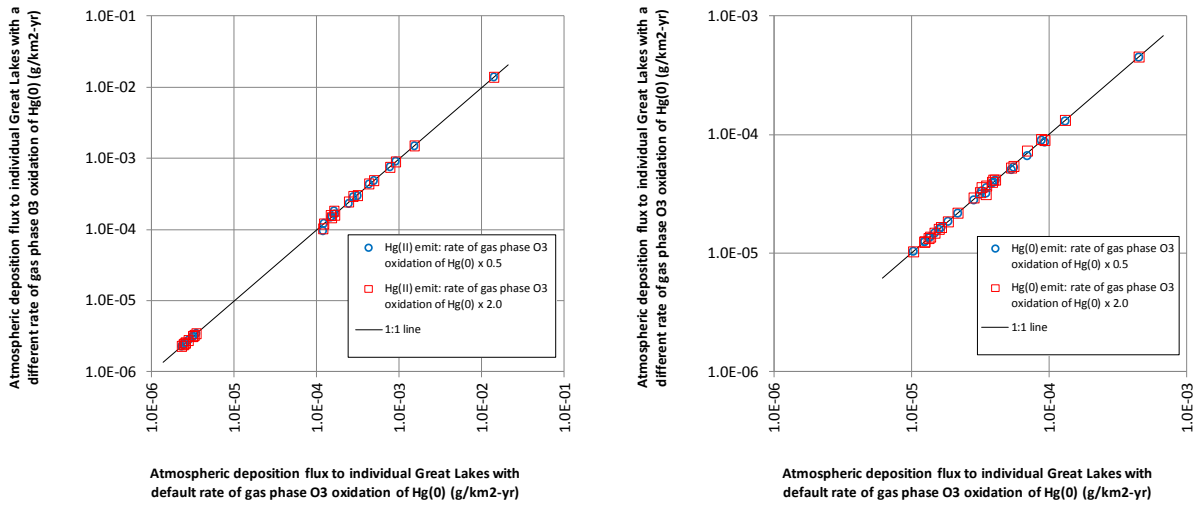

Figure 68. Atmospheric deposition to individual Great Lakes with gas-phase oxidation of Hg(0) by ozone at 0.5, 1.0, and 2.0x the default rate, for emissions of Hg(II) and Hg(0), from all five illustrative standard source locations (scatterplots)

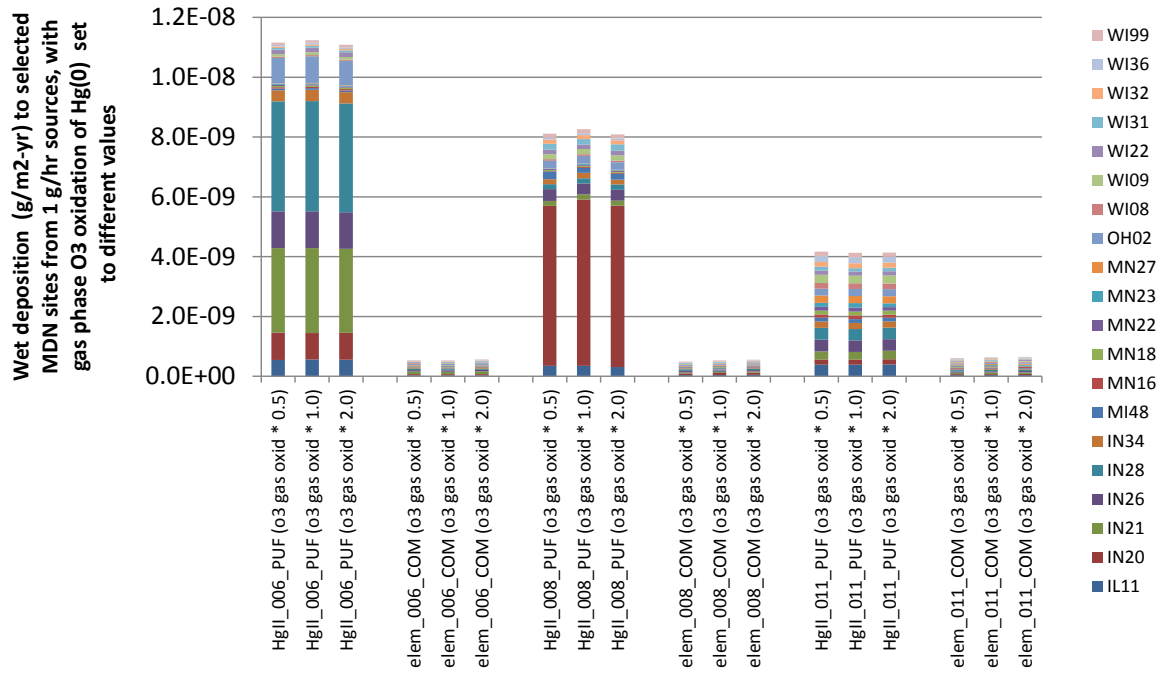

Figure 69. Atmospheric wet deposition to MDN sites in the Great Lakes region with gas-phase oxidation of Hg(0) by O_3 at 0.5, 1.0, and 2.0x the default rate, for emissions of Hg(II) and Hg(0), from the 3 U.S. illustrative SSL's

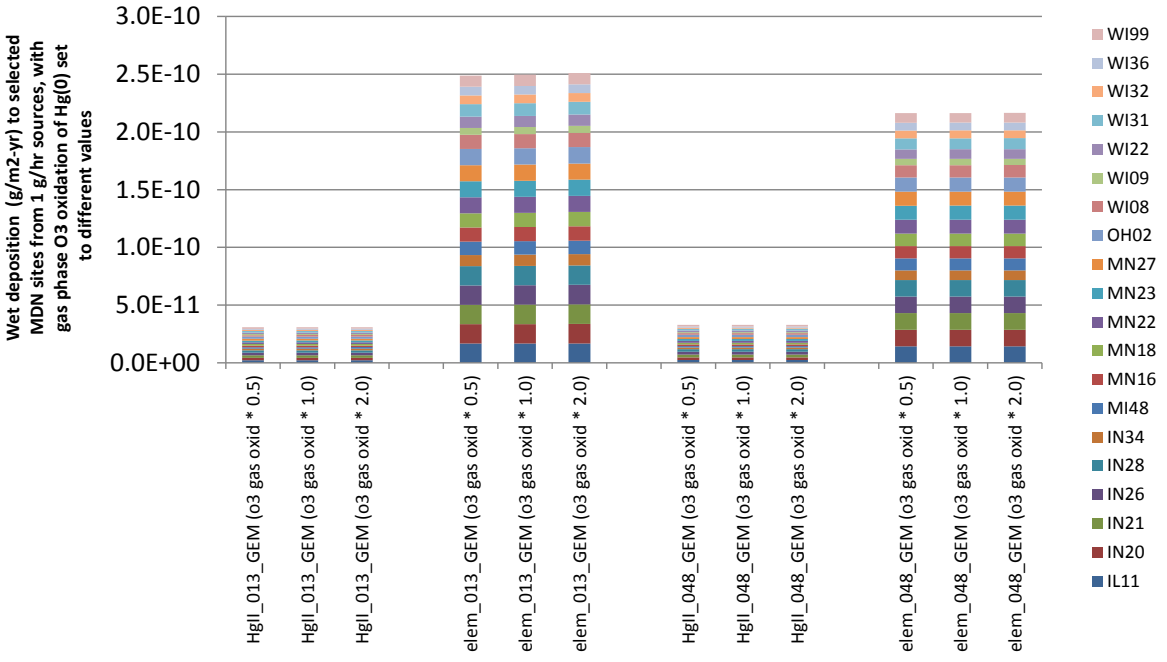

Figure 70. Atmospheric wet deposition to MDN sites in the Great Lakes region with gas-phase oxidation of Hg(0) by O_3 at 0.5, 1.0, and 2.0x the default rate, for emissions of Hg(II) & Hg(0), from SSL-13 (China) & SSL-48 (India)

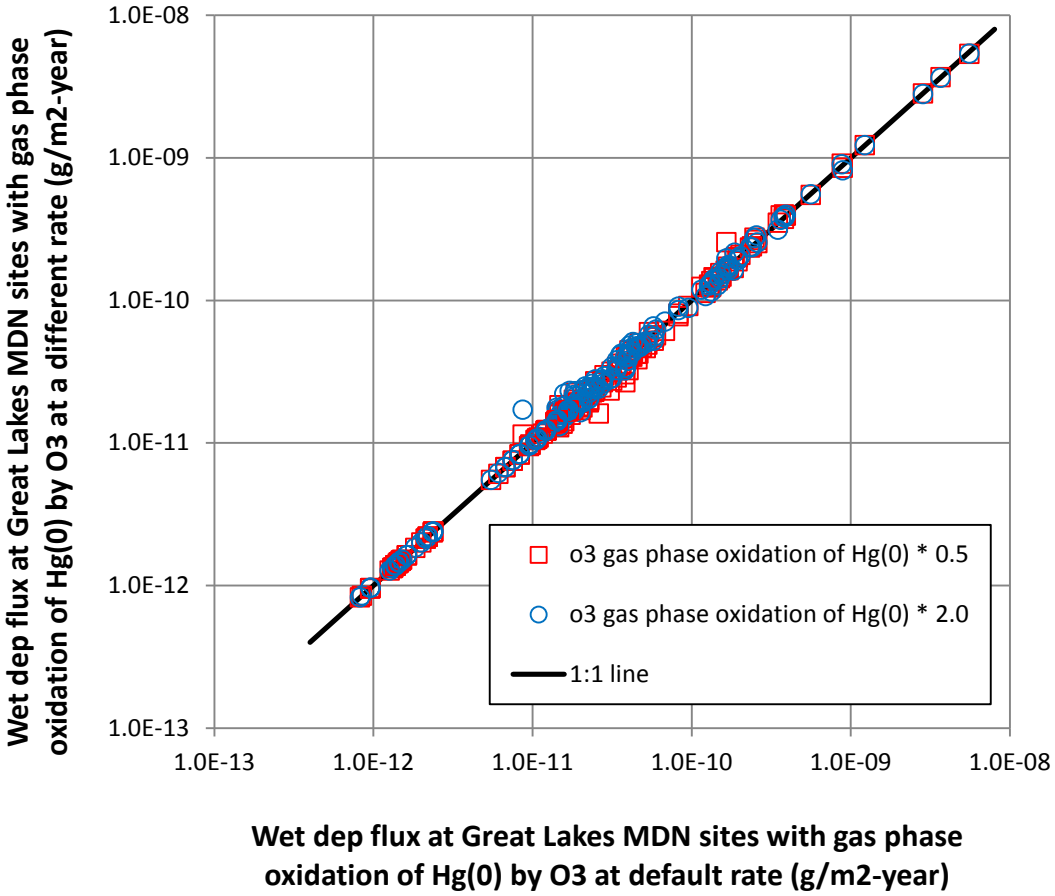

Figure 71. Atmospheric wet deposition to MDN sites in the Great Lakes region with gas-phase oxidation of Hg(0) by ozone at 0.5, 1.0, and 2.0x the default rate, for emissions of Hg(II) and Hg(0), from all 5 illustrative SSL's (scatterplot)

2.6.5. Aqueous-phase oxidation of Hg(0) by OH

In this section, the rate of aqueous-phase oxidation of Hg(0) by hydroxyl radical is varied, and the influence of this variation on the fate and transport of emitted Hg(0) and Hg(II) is examined. It can be seen from Figure 72 through Figure 76 that the variation of this rate has little effect on the fate and transport of emitted Hg(0) or Hg(II). As discussed earlier, emissions of Hg(p) are not affected by this parameter.

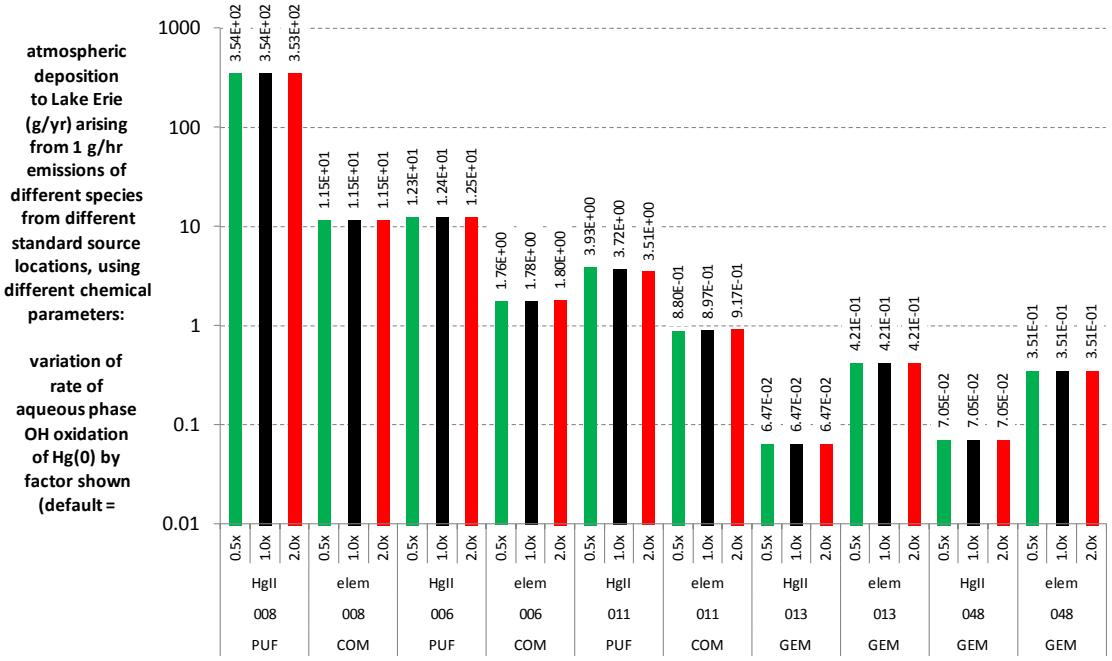

Figure 72. Atmospheric deposition to Lake Erie with aqueous-phase oxidation of Hg(0) by OH at 0.5, 1.0, and 2.0x the default rate, for emissions of Hg(II) and Hg(0), from all five illustrative standard source locations

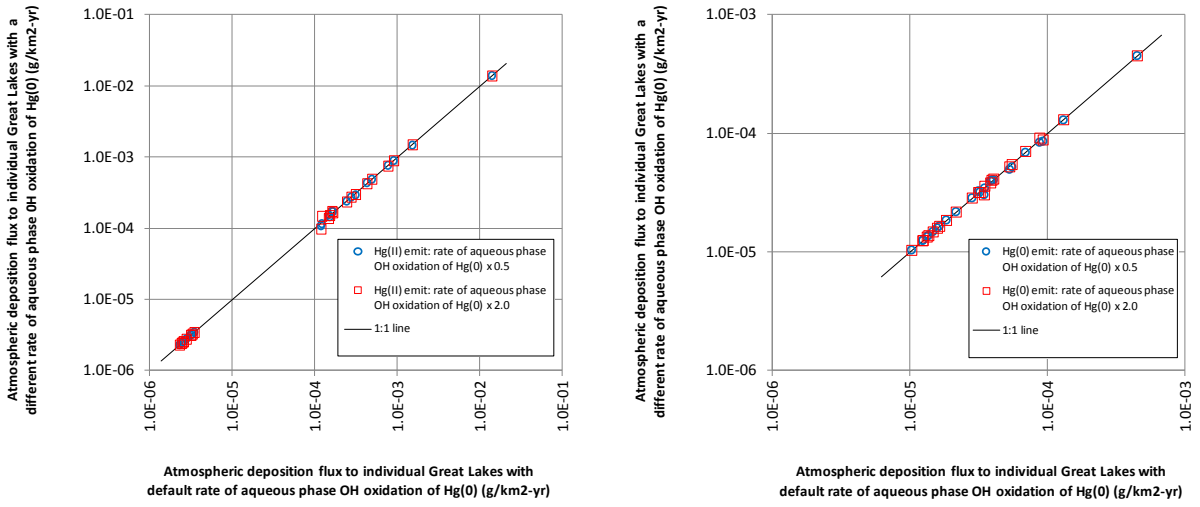

Figure 73. Atmospheric deposition to individual Great Lakes with aqueous-phase oxidation of Hg(0) by OH at 0.5, 1.0, and 2.0x the default rate, for emissions of Hg(II) and Hg(0), from all five illustrative standard source locations (scatterplots)

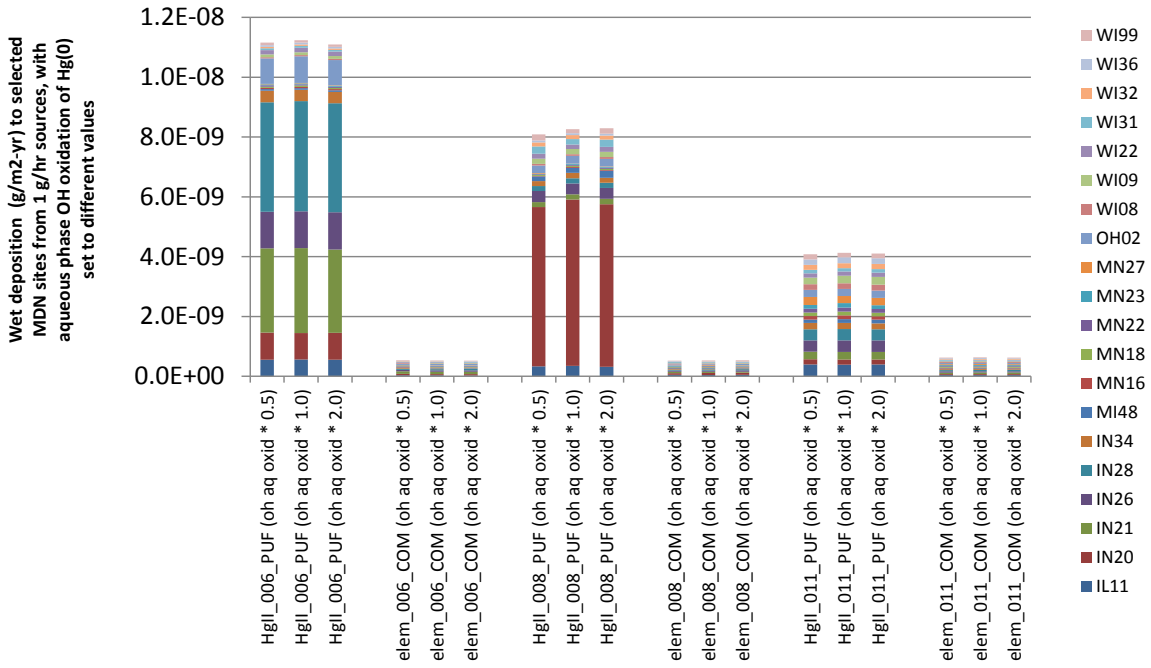

Figure 74. Atmospheric wet deposition to MDN sites in the Great Lakes region with aqueous-phase oxidation of Hg(0) by OH at 0.5, 1.0, and 2.0x the default rate, for emissions of Hg(II) & Hg(0), from the 3 U.S. illustrative SSL's

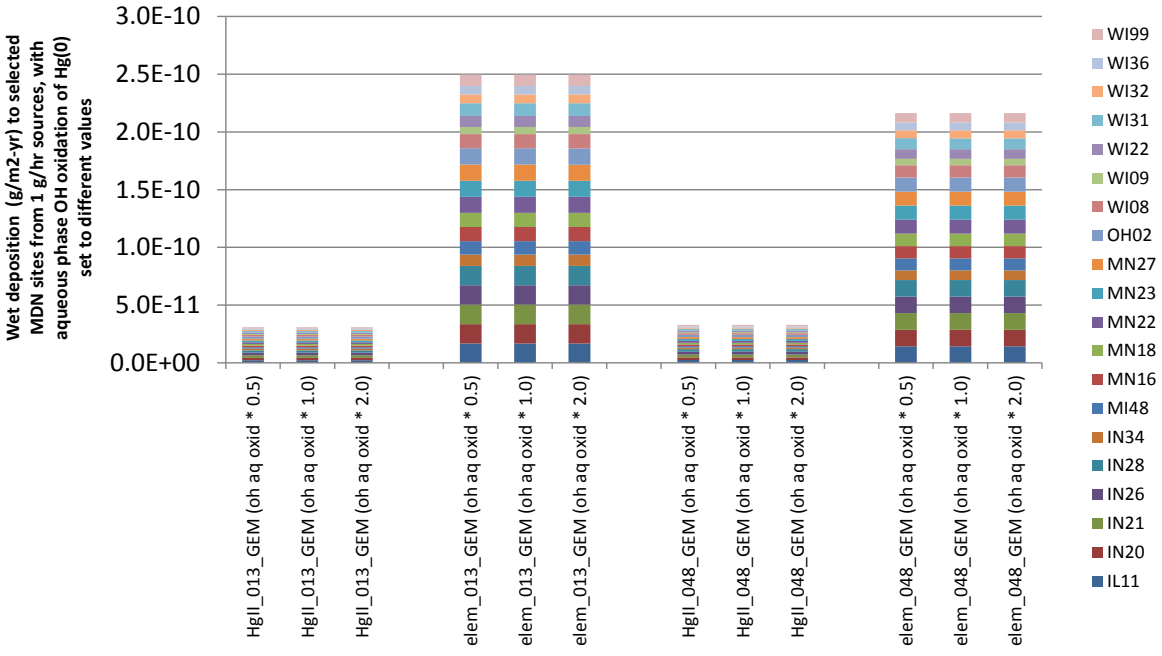

Figure 75. Atmospheric wet deposition to MDN sites in the Great Lakes region with aqueous-phase oxid. of Hg(0) by OH at 0.5, 1.0, & 2.0x the default rate, for emissions of Hg(II) & Hg(0), from SSL-13 (China) & SSL-48 (India)

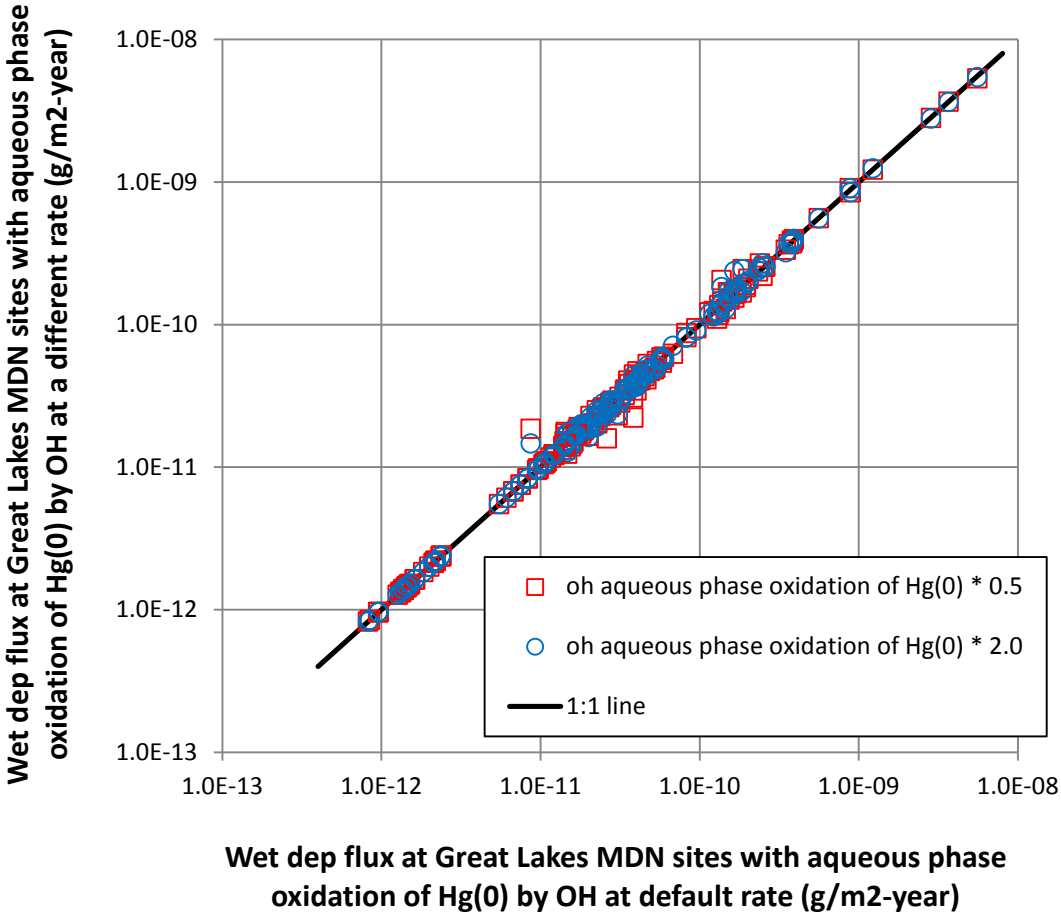

Figure 76. Atmospheric wet deposition to MDN sites in the Great Lakes region with aqueous-phase oxidation of Hg(0) by OH at 0.5, 1.0, and 2.0x the default rate, for emissions of Hg(II) & Hg(0), from all 5 illustrative SSL's (scatterplot)

2.6.6. Gas-phase oxidation of Hg(0) by OH radical

In this section, the rate of gas-phase oxidation of Hg(0) by hydroxyl radical is varied, and the influence of this variation on the fate and transport of emitted Hg(0) and Hg(II) is examined. It can be seen from Figure 77 through Figure 81 that the variation of this rate has little effect on the fate and transport of emitted Hg(0) or Hg(II). As discussed earlier, emissions of Hg(p) are not affected by this parameter.

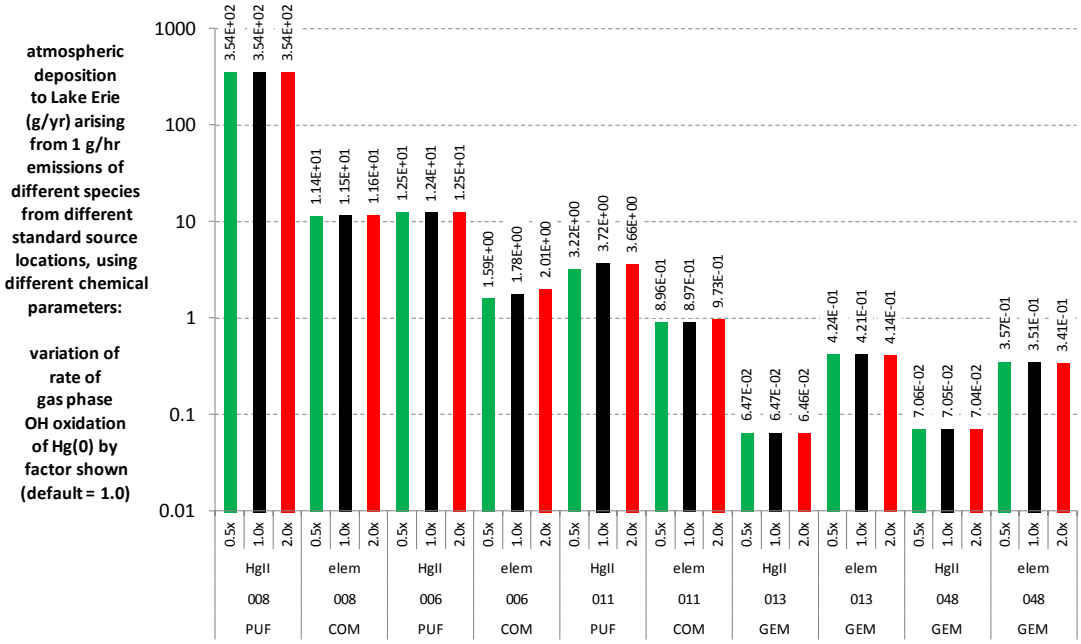

Figure 77. Atmospheric deposition to Lake Erie with gas-phase oxidation of Hg(0) by OH at 0.5, 1.0, and 2.0x the default rate, for emissions of Hg(II) and Hg(0), from all five illustrative standard source locations

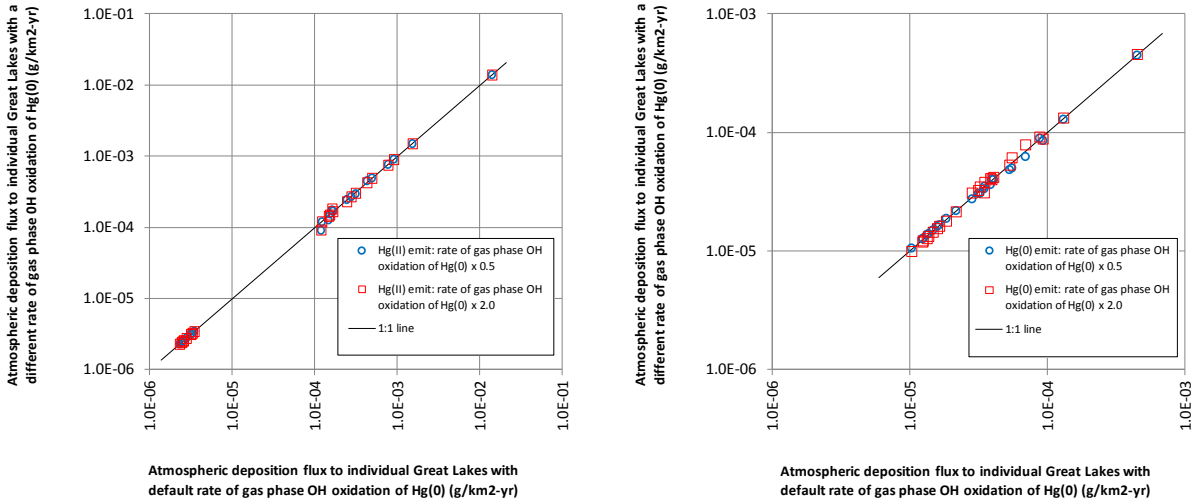

Figure 78. Atmospheric deposition to individual Great Lakes with gas-phase oxidation of Hg(0) by OH at 0.5, 1.0, and 2.0x the default rate, for emissions of Hg(II) and Hg(0), from all five illustrative standard source locations (scatterplots)

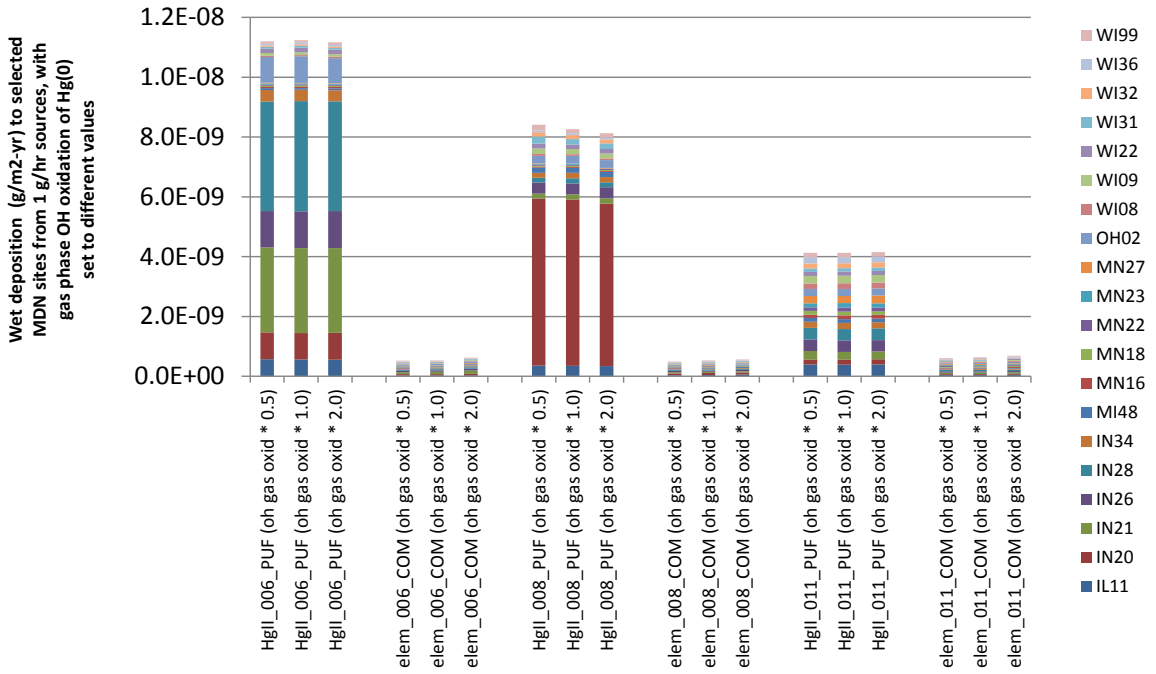

Figure 79.Atmospheric wet deposition to MDN sites in the Great Lakes region with gas-phase oxidation of Hg(0) by OH at 0.5, 1.0, and 2.0x the default rate, for emissions of Hg(II) & Hg(0), from the 3 U.S. illustrative SSL's

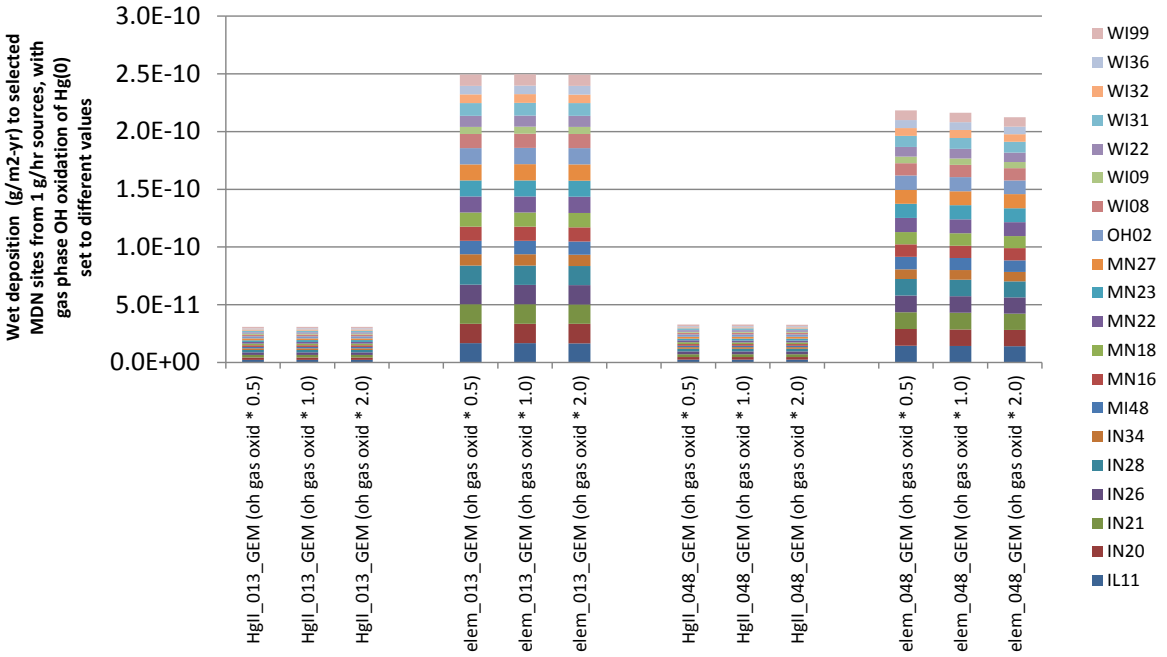

Figure 80.Atmospheric wet deposition to MDN sites in the Great Lakes region with gas-phase oxid. of Hg(0) by OH at 0.5, 1.0, & 2.0x the default rate, for emissions of Hg(II) & Hg(0), from SSL-13 (China) & SSL-48 (India)

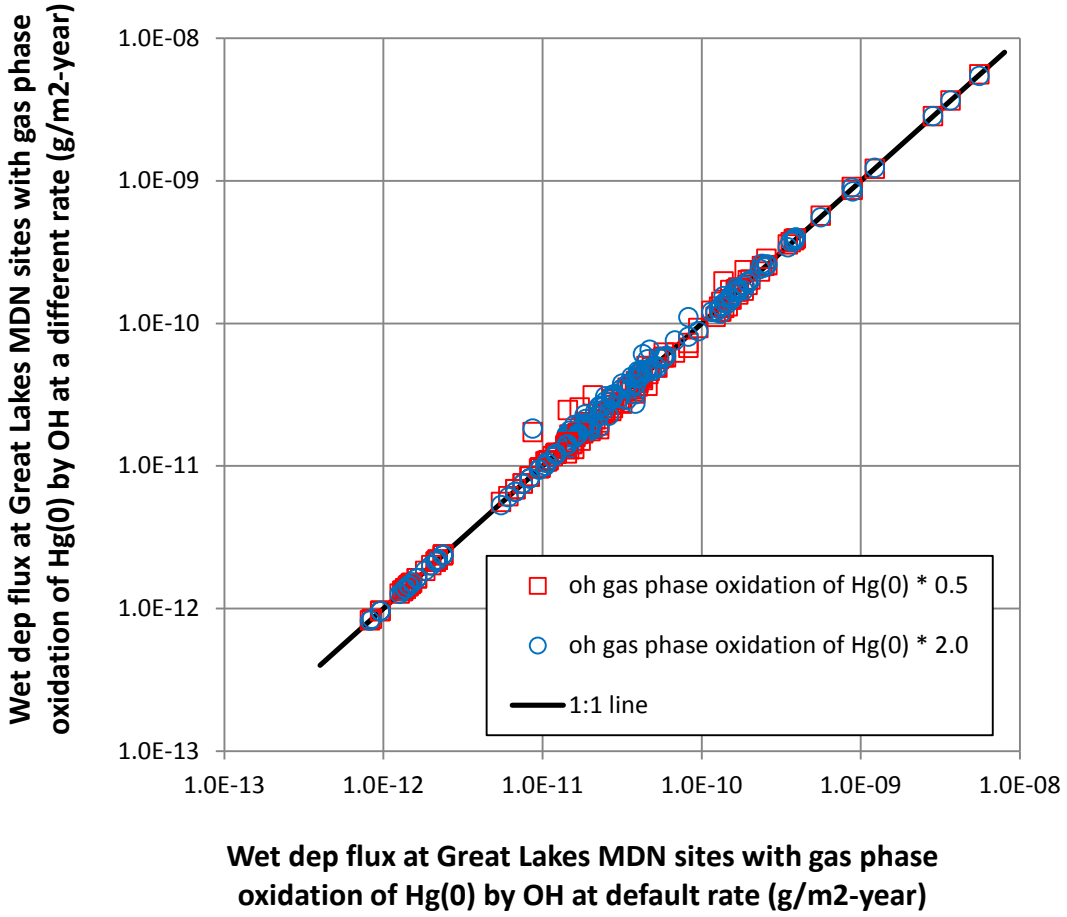

Figure 81.Atmospheric wet deposition to MDN sites in the Great Lakes region with gas-phase oxidation of Hg(0) by OH at 0.5, 1.0, and 2.0x the default rate, for emissions of Hg(II) & Hg(0), from all 5 illustrative SSL's (scatterplot)

2.6.7. Aqueous-phase reduction of Hg(II) by S(IV)

In this section, the rate of aqueous-phase reduction of Hg(II) by S(IV) is varied, and the influence of this variation on the fate and transport of emitted Hg(0) and Hg(II) is examined. It can be seen from Figure 82 through Figure 86 that the variation of this rate has little effect on the fate and transport of emitted Hg(0) or Hg(II). As discussed earlier, emissions of Hg(p) are not affected by this parameter.

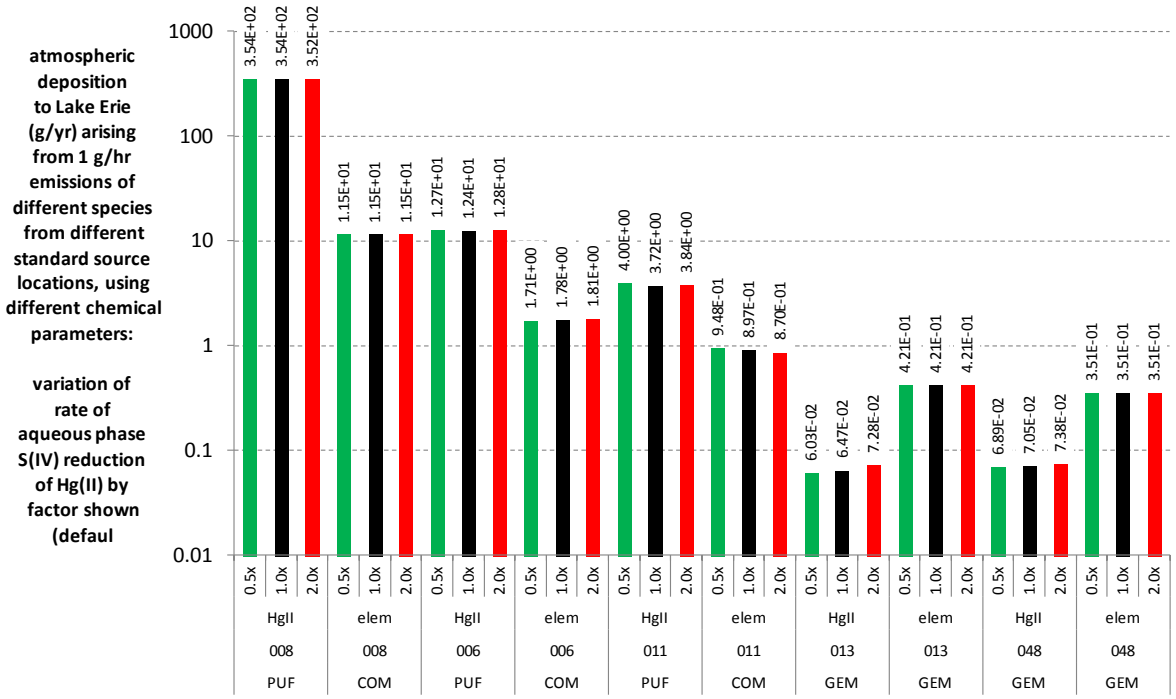

Figure 82. Atmospheric deposition to Lake Erie with aqueous-phase reduction of Hg(II) by S(IV) at 0.5, 1.0, and 2.0x the default rate, for emissions of Hg(II) and Hg(0), from all five illustrative standard source locations

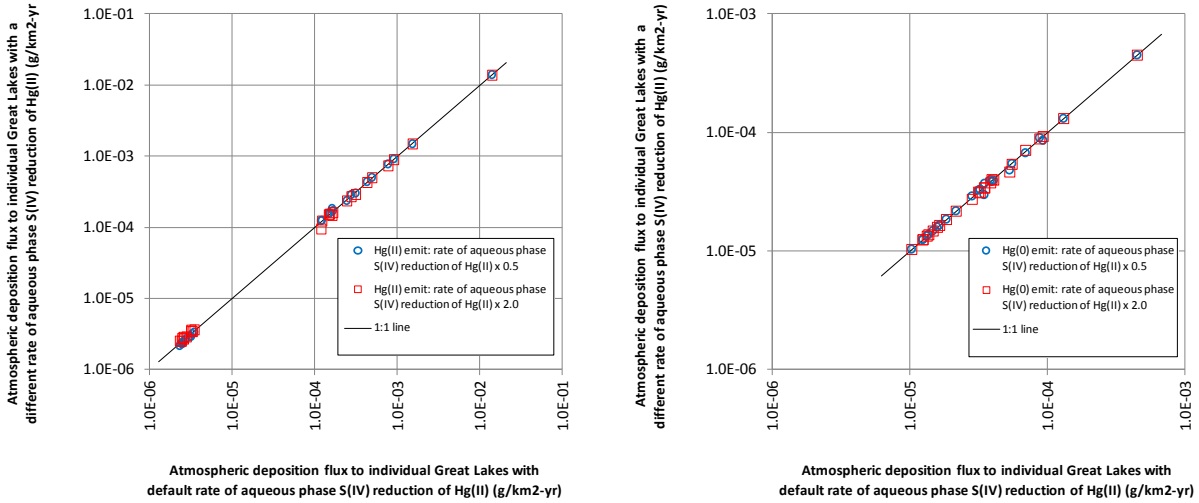

Figure 83. Atmospheric deposition to individual Great Lakes with aqueous-phase reduction of Hg(II) by S(IV) at 0.5, 1.0, and 2.0x the default rate, for emissions of Hg(II) and Hg(0), from all five illustrative standard source locations (scatterplots)

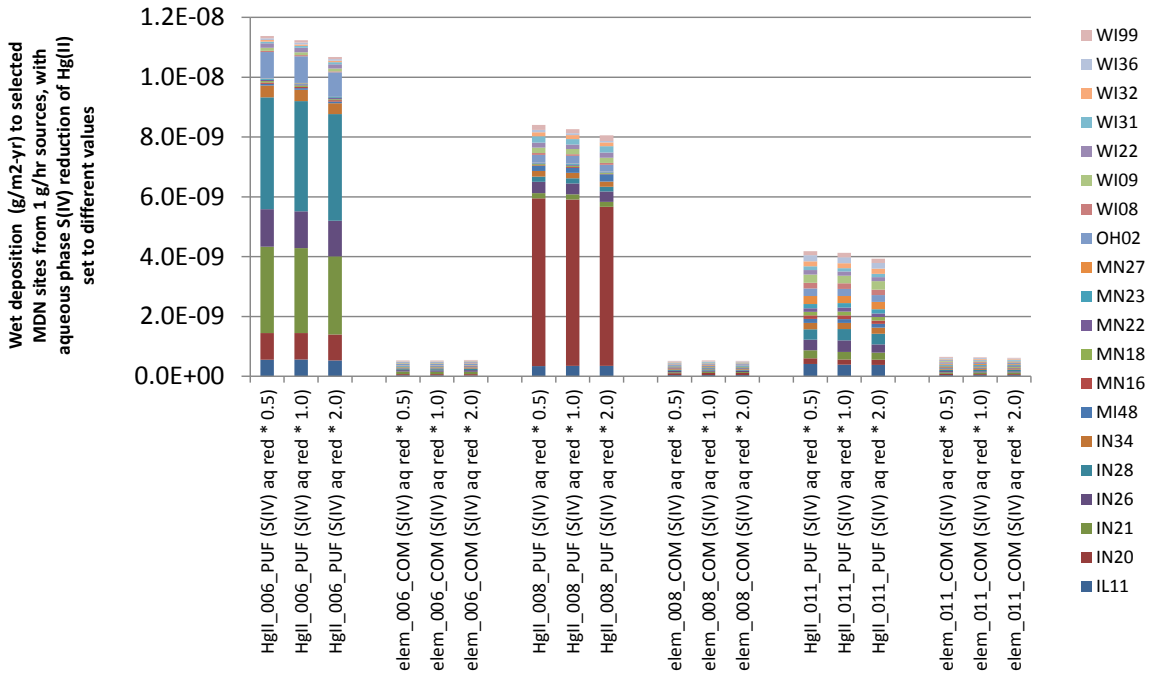

Figure 84.Atmospheric wet deposition to MDN sites in the Great Lakes region with aqueous-phase reduction of Hg(II) by S(IV) at 0.5, 1.0, and 2.0x the default rate, for emissions of Hg(II) & Hg(0), from the 3 U.S. illustrative SSL's

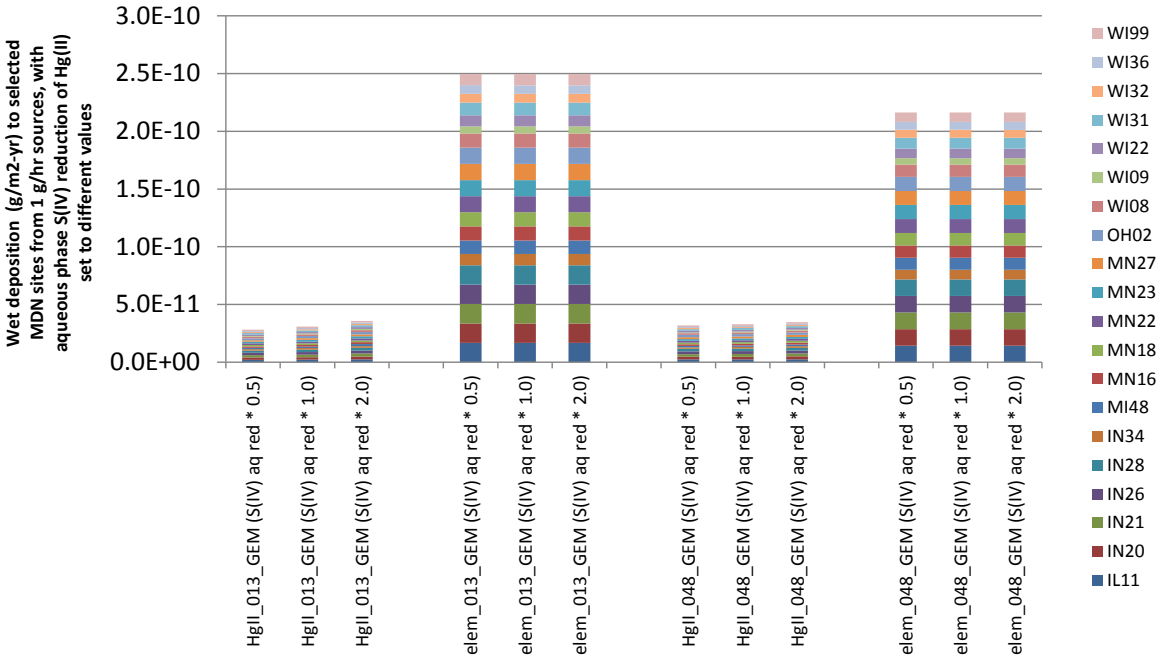

Figure 85.Atmospheric wet deposition to MDN sites in the Great Lakes region with aqueous-phase reduction of Hg(II) by S(IV) at 0.5, 1.0, & 2.0x the default rate, for emissions of Hg(II) & Hg(0), from SSL-13 (China) & SSL-48 (India)

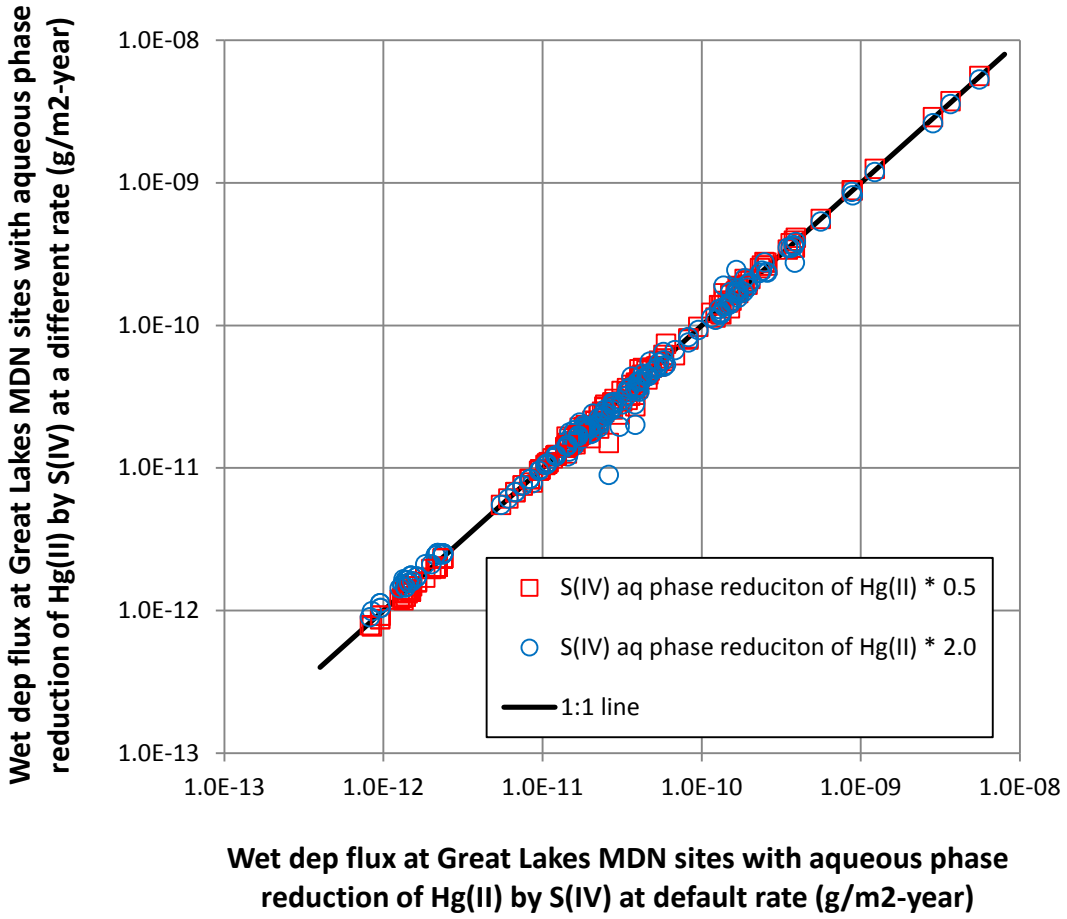

Figure 86.Atmospheric wet deposition to MDN sites in the Great Lakes region with aqueous-phase reduction of Hg(II) by S(IV) at 0.5, 1.0, and 2.0x the default rate, for emissions of Hg(II) & Hg(0), from all 5 illustrative SSL's (scatterplot)

2.6.8. Aqueous-soot adsorption partitioning factor for Hg(II)

In this section, the equilibrium constant for aqueous Hg(II)-soot partitioning is varied, and the influence of this variation on the fate and transport of emitted Hg(0) and Hg(II) is examined. It can be seen from Figure 87 through Figure 91that the variation of this rate has little effect on the fate and transport of emitted Hg(0) or Hg(II). As discussed earlier, emissions of Hg(p) are not affected by this parameter.

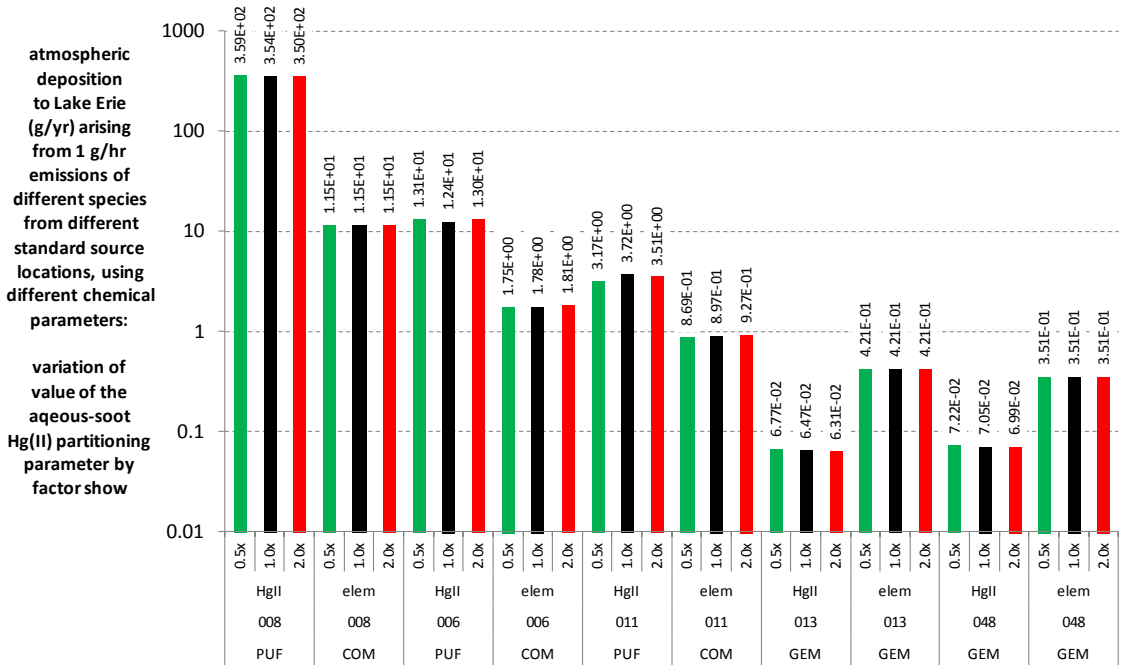

Figure 87. Atmospheric deposition to Lake Erie with the equilibrium constant for aqueous Hg(II)-soot partitioning S(IV) at 0.5, 1.0, and 2.0x the default value, for emissions of Hg(II) and Hg(0), from all five illustrative standard source locations

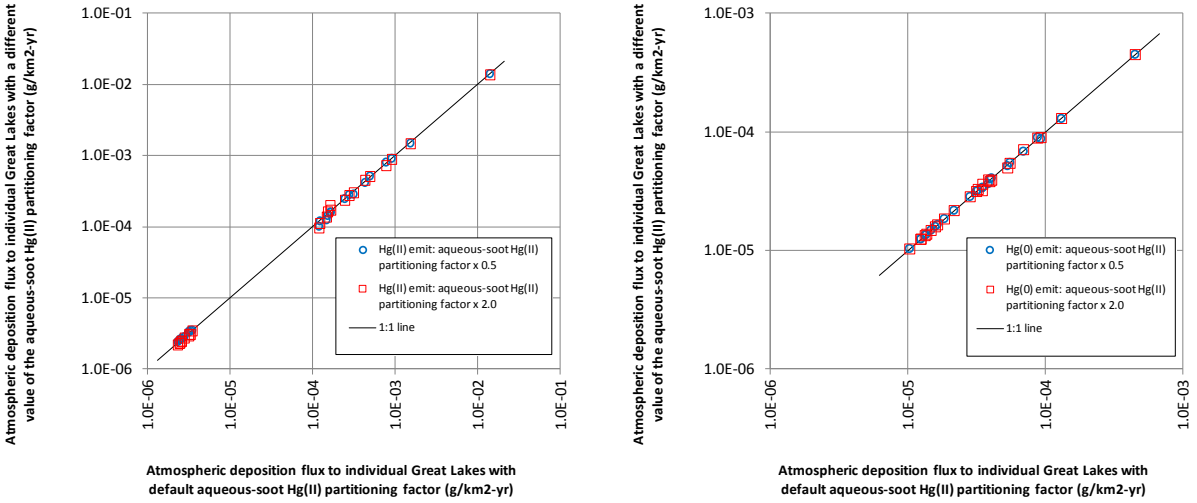

Figure 88. Atmospheric deposition to individual Great Lakes with the equilibrium constant for aqueous Hg(II)-soot partitioning S(IV) at 0.5, 1.0, and 2.0x the default value, for emissions of Hg(II) and Hg(0), from all five illustrative standard source locations (scatterplots)

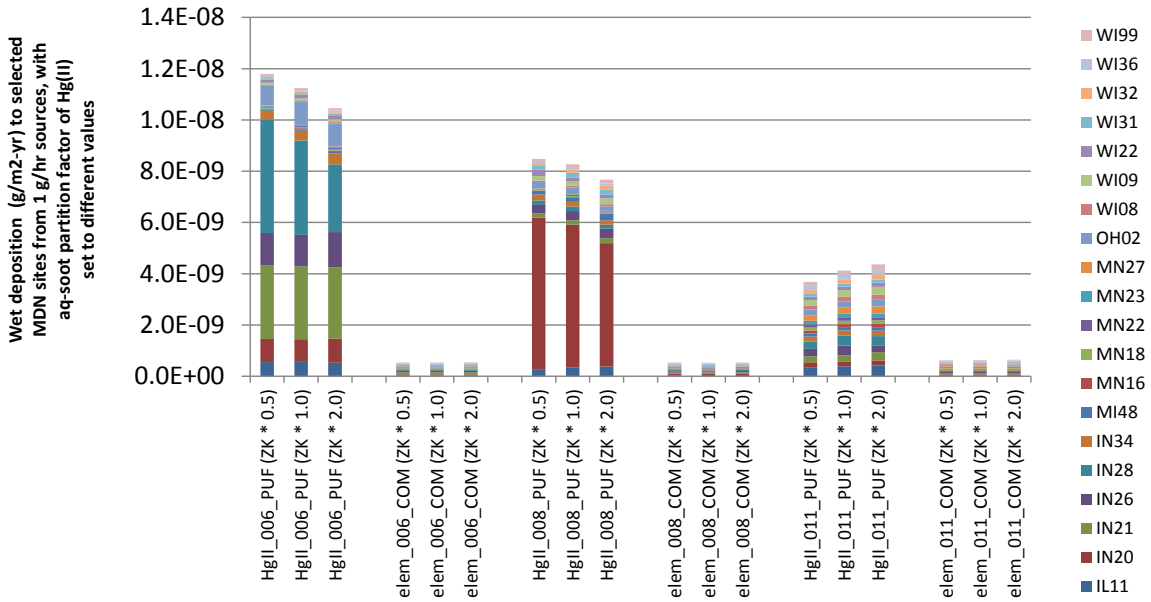

Figure 89. Atmospheric wet deposition to MDN sites in the Great Lakes region with the equilibrium constant for aqueous Hg(II)-soot partitioning S(IV) at 0.5, 1.0, and 2.0x the default value, for emissions of Hg(II) & Hg(0), from the 3 U.S. illustrative SSL's

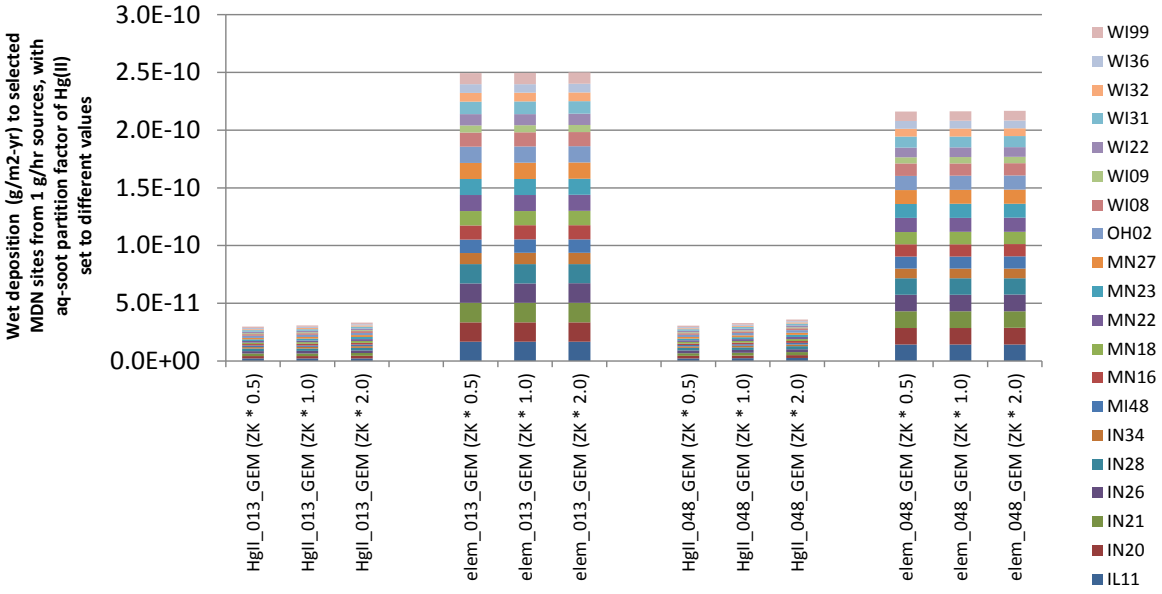

Figure 90. Atmospheric wet deposition to MDN sites in the Great Lakes region with the equilibrium constant for aqueous Hg(II)-soot partitioning S(IV) at 0.5, 1.0, and 2.0x the default value, for emissions of Hg(II) & Hg(0), from SSL-13 (China) & SSL-48 (India)

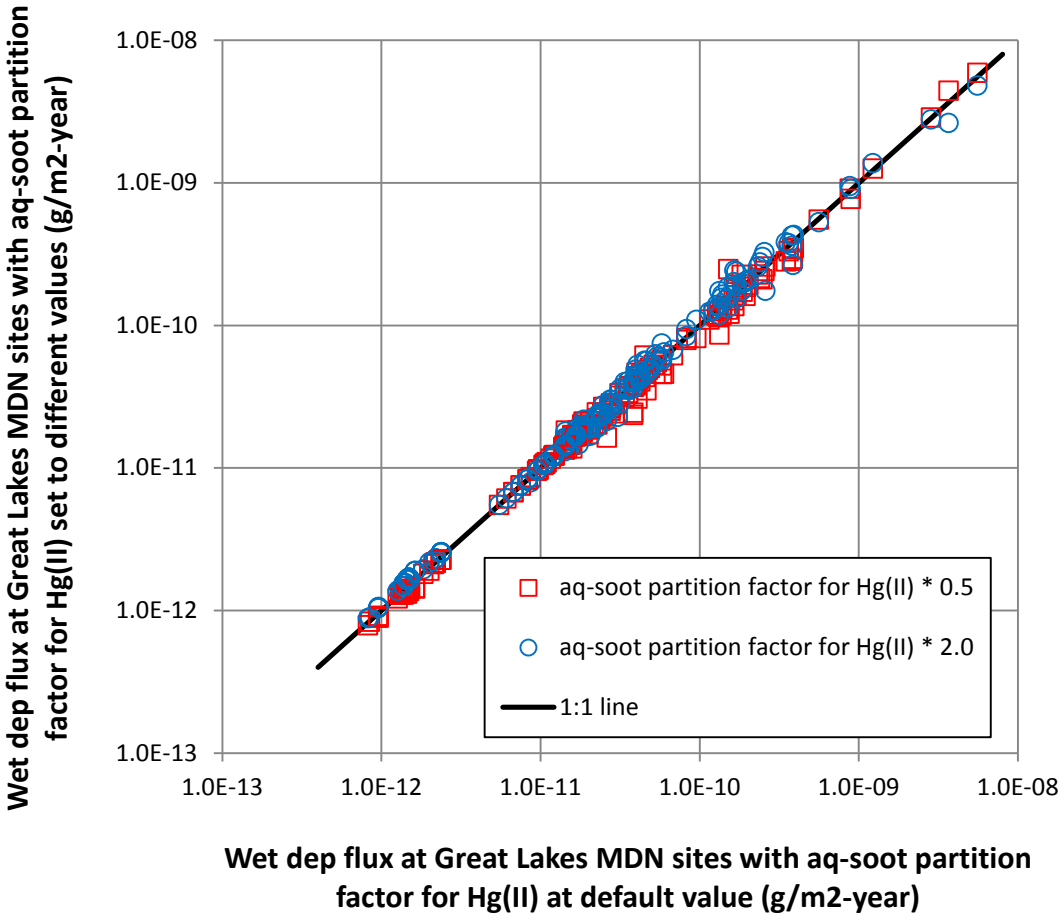

Figure 91. Atmospheric wet deposition to MDN sites in the Great Lakes region with the equilibrium constant for aqueous Hg(II)-soot partitioning S(IV) at 0.5, 1.0, and 2.0x the default value, for emissions of Hg(II) & Hg(0), from all 5 illustrative SSL's (scatterplot)

2.6.9. Aqueous-soot adsorption partitioning time constant for Hg(II)

In this section, the time constant for aqueous Hg(II)-soot partitioning is varied, and the influence of this variation on the fate and transport of emitted Hg(0) and Hg(II) is examined. It can be seen from Figure 87 through Figure 91that the variation of this rate has little effect on the fate and transport of emitted Hg(0) or Hg(II). As discussed earlier, emissions of Hg(p) are not affected by this parameter.

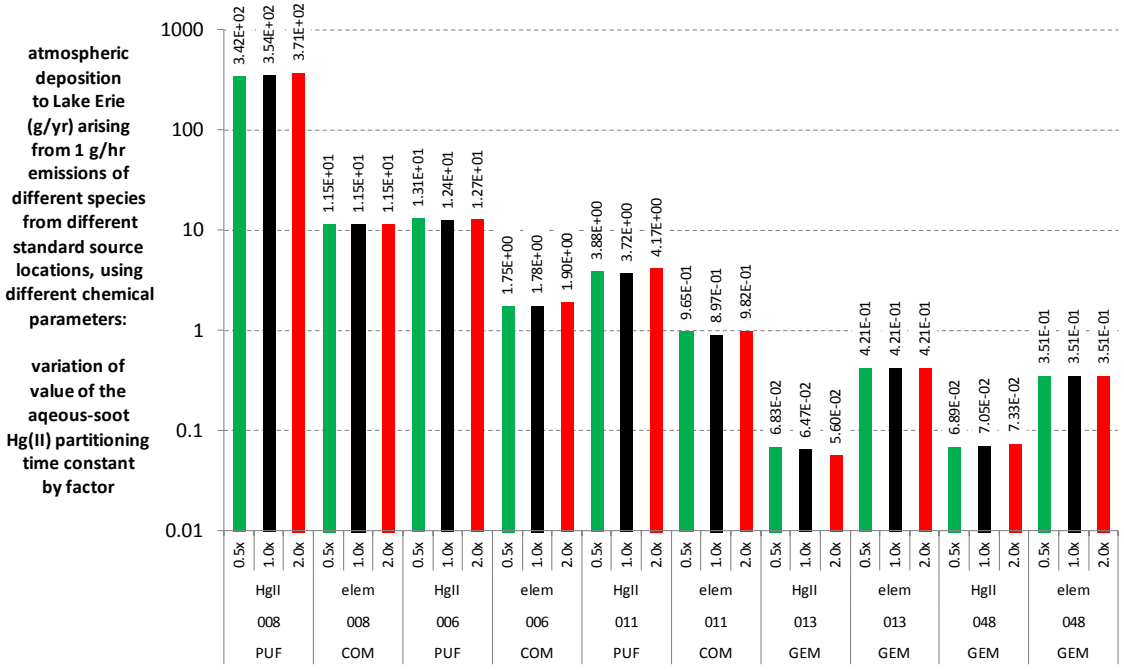

Figure 92. Atmospheric deposition to Lake Erie with the time constant for aqueous Hg(II)-soot partitioning S(IV) at 0.5, 1.0, and 2.0x the default value, for emissions of Hg(II) and Hg(0), from all five illustrative standard source locations

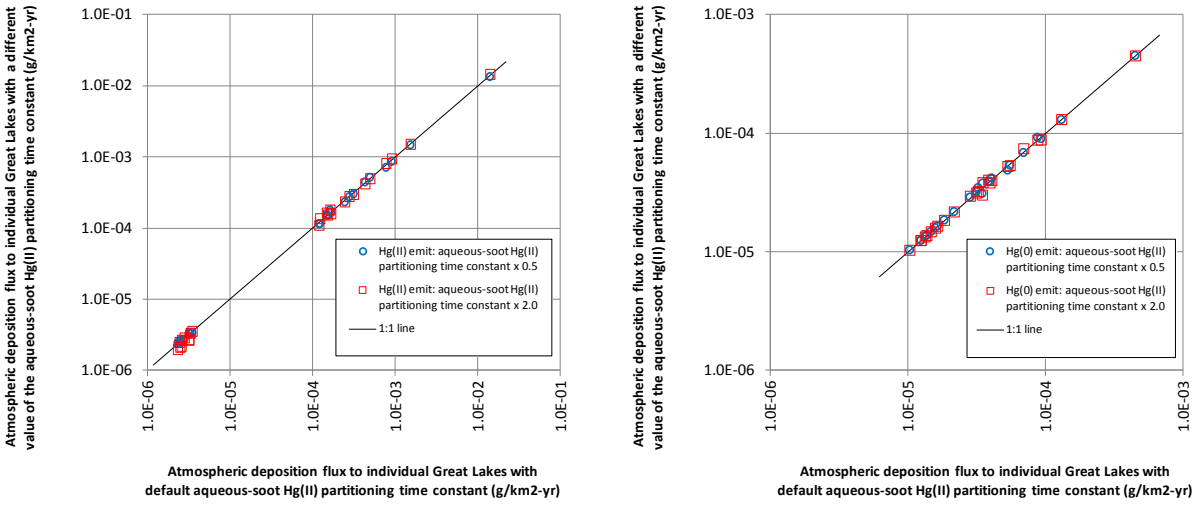

Figure 93. Atmospheric deposition to individual Great Lakes with the time constant for aqueous Hg(II)-soot partitioning S(IV) at 0.5, 1.0, and 2.0x the default value, for emissions of Hg(II) and Hg(0), from all five illustrative standard source locations (scatterplots)

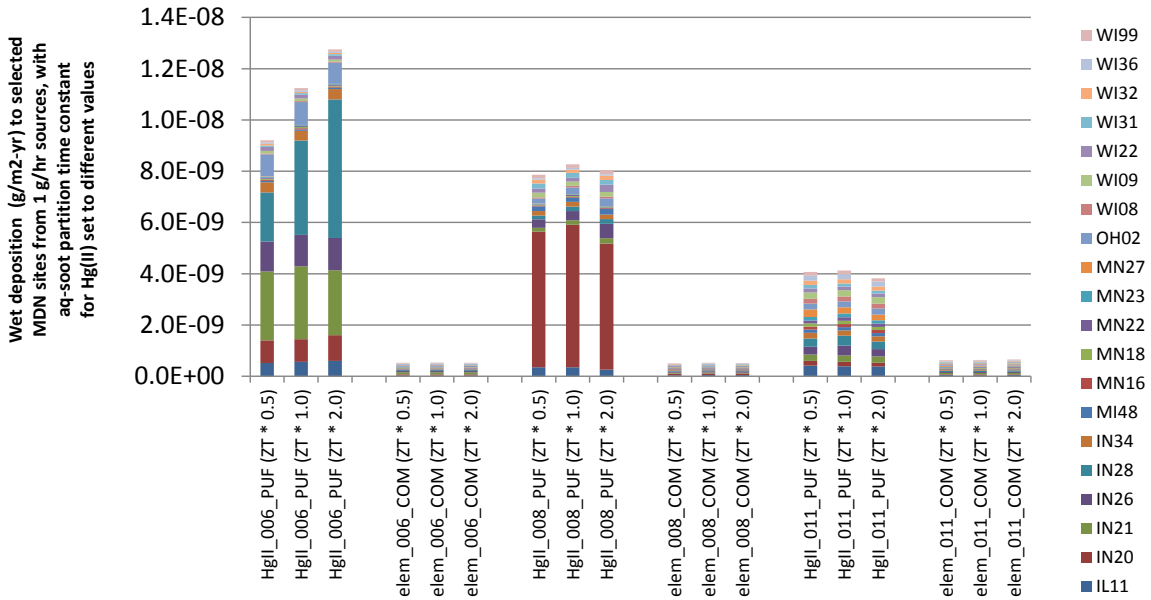

Figure 94. Atmospheric wet deposition to MDN sites in the Great Lakes region with the time constant for aqueous Hg(II)-soot partitioning S(IV) at 0.5, 1.0, and 2.0x the default value, for emissions of Hg(II) & Hg(0), from the 3 U.S. illustrative SSL's

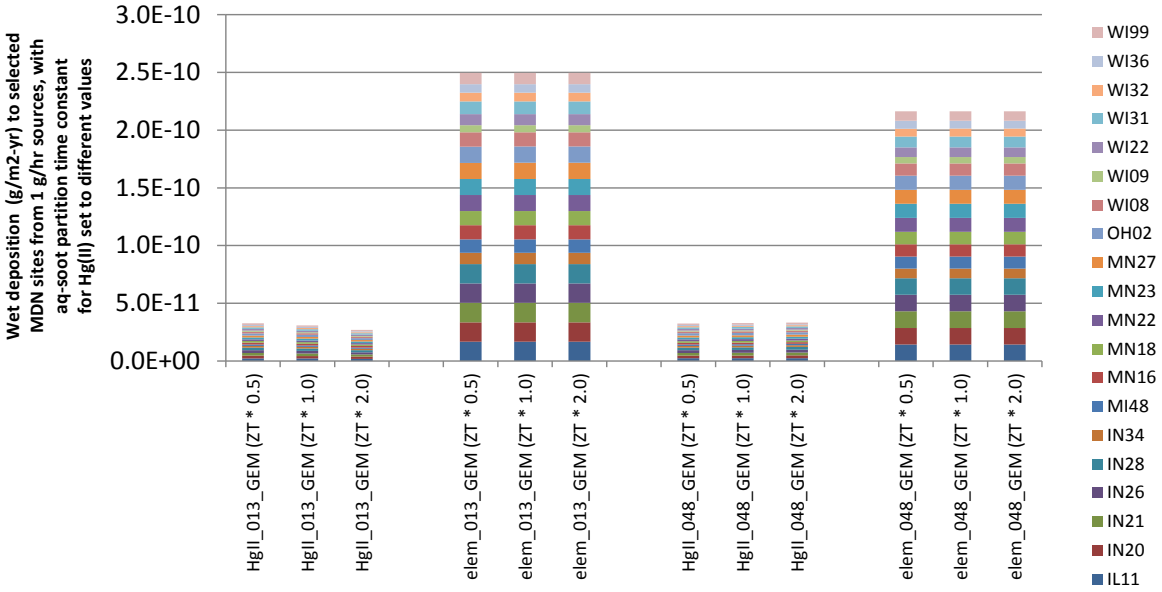

Figure 95. Atmospheric wet deposition to MDN sites in the Great Lakes region with the time constant for aqueous Hg(II)-soot partitioning S(IV) at 0.5, 1.0, and 2.0x the default value, for emissions of Hg(II) & Hg(0), from SSL-13 (China) & SSL-48 (India)

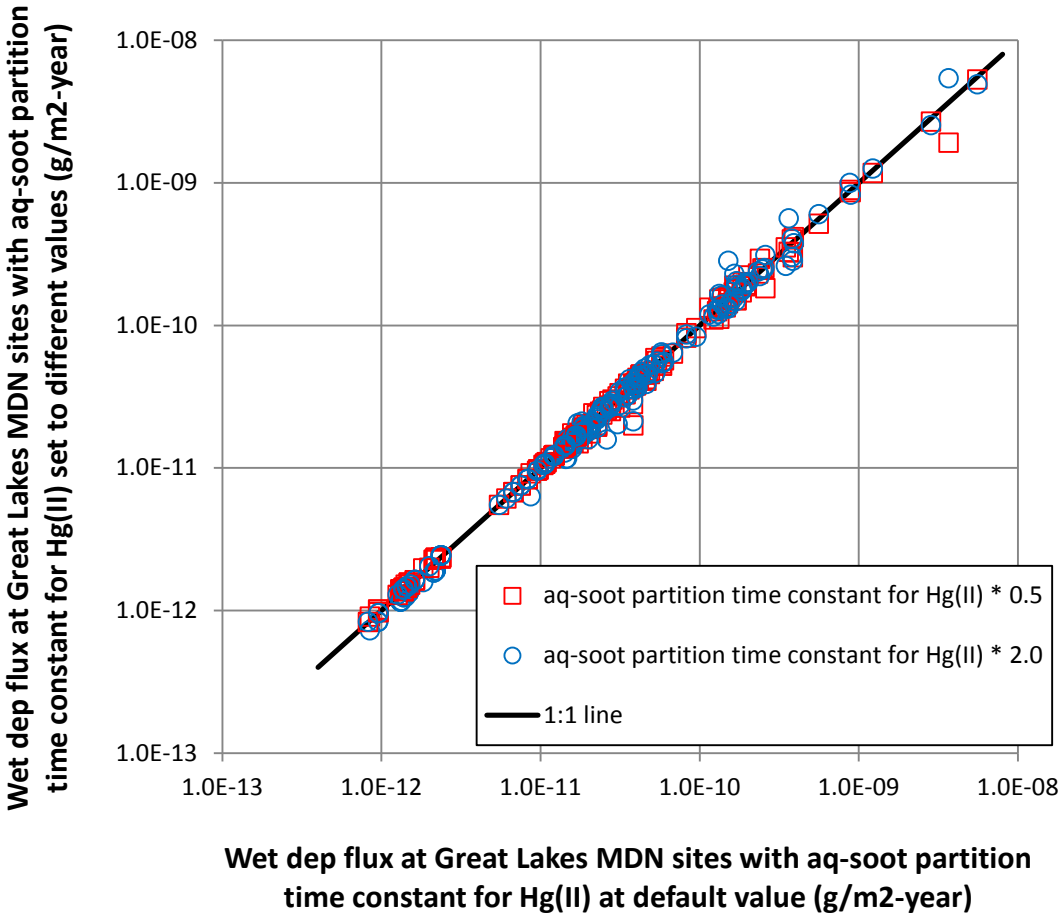

Figure 96. Atmospheric wet deposition to MDN sites in the Great Lakes region with the time constant for aqueous Hg(II)-soot partitioning S(IV) at 0.5, 1.0, and 2.0x the default value, for emissions of Hg(II) & Hg(0), from all 5 illustrative SSL's (scatterplot)

3. Synthesis of sensitivity analyses of illustrative source locations

3.1. Introduction

In this section, the numerous variations discussed above will be combined for each of the illustrative standard source locations. This will allow us to compare the influences of each perturbation on the overall simulation results.

In the graphs presented in the following sections, simulation names are constructed to give an abbreviated "cryptic" description of the nature of the simulation. The first part of any simulation name uses the standard naming convention, e.g., "elem_013_GEM" refers to a simulation with emissions of pure elemental mercury, Hg(0), from standard source location 13, using the GEM methodology. The types of basic runs (PUF, COM, and GEM) are described above in Section 2.2 (page 12).

Variations on the basic simulations are indicated by additional labels in the name, according to the following table.

Label text	Description	Notes
elem_dep_0	Dry deposition of Hg(0) set to zero	In default simulations, the dry deposition is estimated via a resistance method
wetr_010000	WETR in-cloud particle rainout coefficient set to 10,000	Default WETR = 40,000
wetr_160000	WETR in-cloud particle rainout coefficient set to 160,000	
elev_50	Release height set to 50m	Default is 250m
hvx2	Rate of reduction of Hg(II)-aq by *hv* multiplied by 2	In the default simulation, the rates of any given chemical transformation are not multiplied by 2 or 0.5
hvxp5	Rate of reduction of Hg(II)-aq by *hv* multiplied by 0.5	
o3gx2	Rate of oxidation of gas-phase Hg(0) by O_3 multiplied by 2	
o3gxp5	Rate of oxidation of gas-phase Hg(0) by O_3 multiplied by 0.5	
ohax2	Rate of aqueous phase oxidation of Hg(0) by OH multiplied by 2	
ohaxp5	Rate of aqueous phase oxidation of Hg(0) by OH multiplied by 0.5	
so2x2	Rate of aqueous phase reduction of Hg(II) by S(IV) multiplied by 2	
so2xp5	Rate of aqueous phase reduction of Hg(II) by S(IV) multiplied by 2	
zkx2	Aqueous Hg(II)-soot partition factor multiplied by 2	
zkxp5	Aqueous Hg(II)-soot partition factor multiplied by 0.5	
ztx2	Aqueous Hg(II)-soot partitioning time constant multiplied by 2	
ztxp5	Aqueous Hg(II)-soot partitioning time constant multiplied by 0.5	

In some of the run labels, a model version number is given, e.g., "v25ir". Variations between model versions are discussed and presented in the Appendix. For the purposes of the comparisons in this section, it can be safely assumed that any differences due to different model versions can be ignored.

Using the above information, it is possible to interpret what any given simulation was. For example, "HgII_008_PUF_v25ir_ o3gxp5" indicates that the simulation was for emissions of Hg(II), from standard source location #8, using the "PUF" methodology, with model version 25ir, in which the rate of gas-phase oxidation of Hg(0) by O_3 is multiplied by 0.5.

3.2. Standard Source Location 13 (China)

An overview of the influences on the atmospheric fate and transport of mercury emitted from SSL-13 (China) is shown in the figures below.

Figure 97 shows the results for emissions of Hg(0). It is seen from this figure that the various changes in parameters investigated here do not make a very significant difference in the predicted deposition of mercury to the Great Lakes.

Figure 98 shows the results for emissions of Hg(II). It is seen that variations in WETR and release height do make a significant difference, as well as a few of the chemical transformation variations. For example, it is seen that doubling the rate of Hg(II) reduction by S(IV) results in an increase in deposition flux to the Great Lakes. The increased reduction renders the mercury less vulnerable to wet and dry deposition, and thus more of the mercury reaches the Great Lakes region for potential deposition.

Figure 99 shows the results for emissions of Hg(p). There are fewer variations shown for Hg(p) emissions as the chemical transformation variations are not relevant for emissions of pure Hg(p), as discussed in Section 2.6.2 (page 55). The "elem_dep_0" simulation is shown as a QA/QC check – it should introduce no changes in the Hg(p) results, and it can be seen that it doesn't. It can be seen that differences in WETR make a big difference in the results for the Great Lakes. With a lower WETR, more of the emitted Hg(p) makes it to the Great Lakes region from this far-away source location. With a higher WETR, more of the emitted Hg(p) is wet-deposited before it reaches the Great Lakes region.

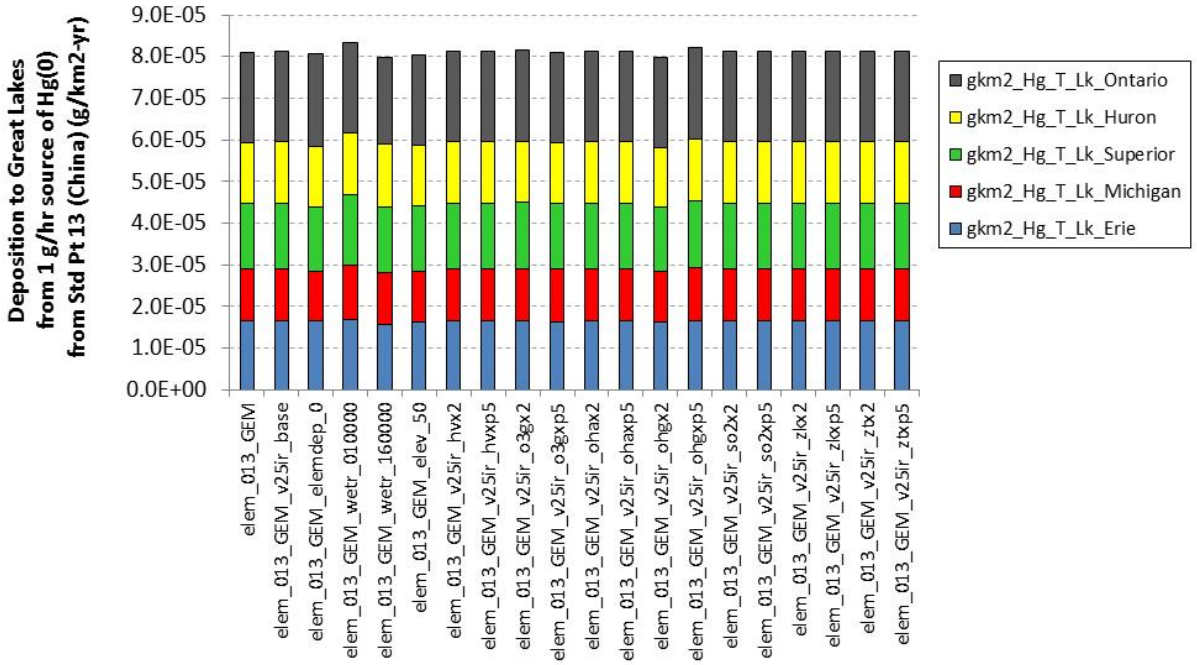

Figure 97. Modeled atmospheric mercury deposition flux to the Great Lakes arising from Hg(0) emissions from SSL-13 (China) using different simulation methodologies and/or parameters

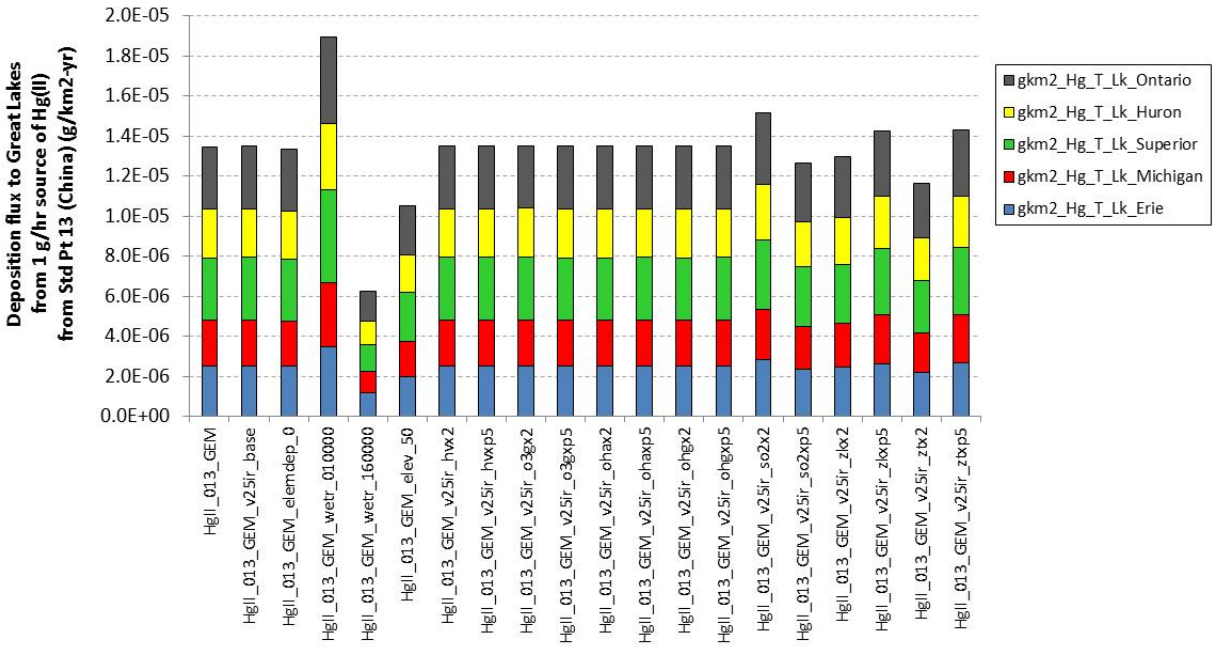

Figure 98. Modeled atmospheric mercury deposition flux to the Great Lakes arising from Hg(II) emissions from SSL-13 (China) using different simulation methodologies and/or parameters

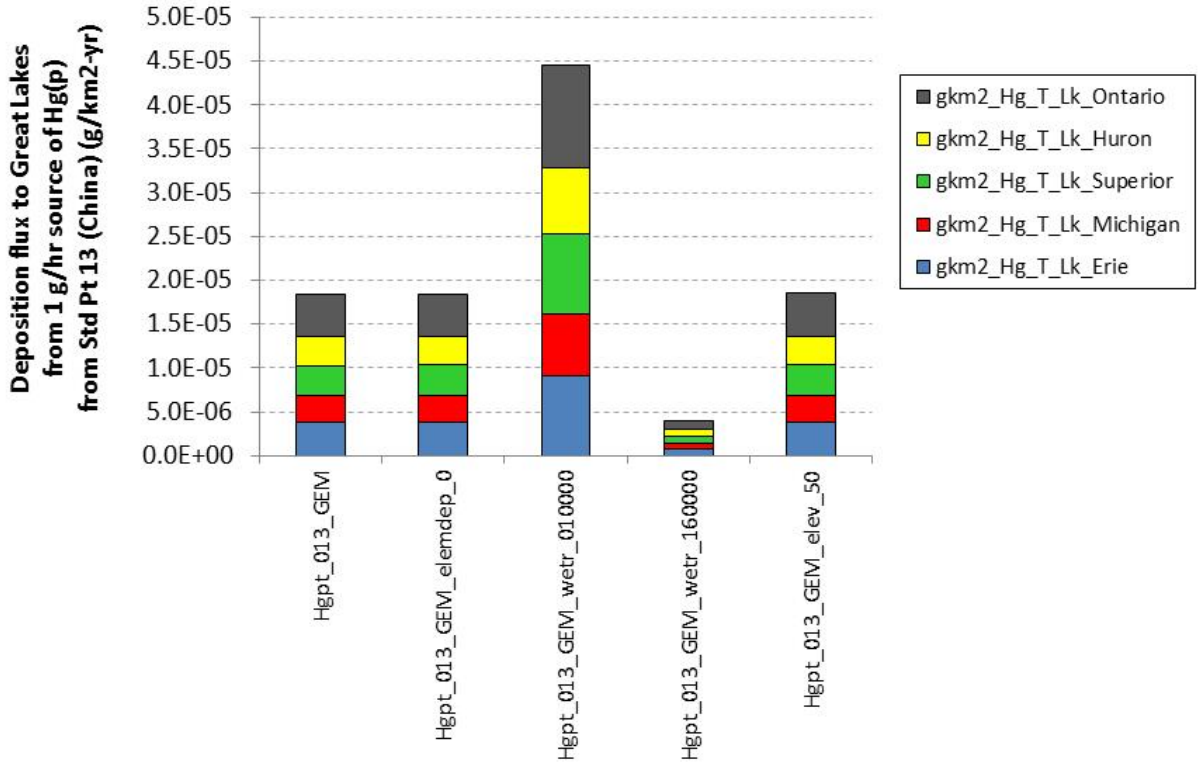

Figure 99. Modeled atmospheric mercury deposition flux to the Great Lakes arising from Hg(p) emissions from SSL-13 (China) using different simulation methodologies and/or parameters

3.3. Standard Source Location 48 (India)

An overview of the influences on the atmospheric fate and transport of mercury emitted from SSL-48 (India) is shown in the figures below.

Figure 100 shows the results for emissions of Hg(0). The WETR variations – affecting wet deposition – have a slightly larger impact than the results for SSL-13 (China). As with SSL-13, though, the chemical transformation variations do not appear to make a significant difference.

Figure 101 shows the results for emissions of Hg(II). It is seen that variations in WETR make the most significant difference. In contrast to SSL-13, changing the release height to 50m did not have a significant impact. Further, the influence of variations in the chemical transformation parameters was not as great as was seen for SSL-13.

Figure 102 shows the results for emissions of Hg(p). There are fewer variations shown for Hg(p) emissions as the chemical transformation variations are not relevant for emissions of pure Hg(p). The "elem_dep_0" simulation is shown as a QA/QC check – it should introduce no changes in the Hg(p) results, and it can be seen that it doesn't. Consistent with the results for SSL-13, differences in WETR make a big difference in the results for the Great Lakes. With a lower WETR, more of the emitted Hg(p) makes it to the Great Lakes region from this far-away source location. With a higher WETR, more of the emitted Hg(p) is wet-deposited before it reaches the Great Lakes region.

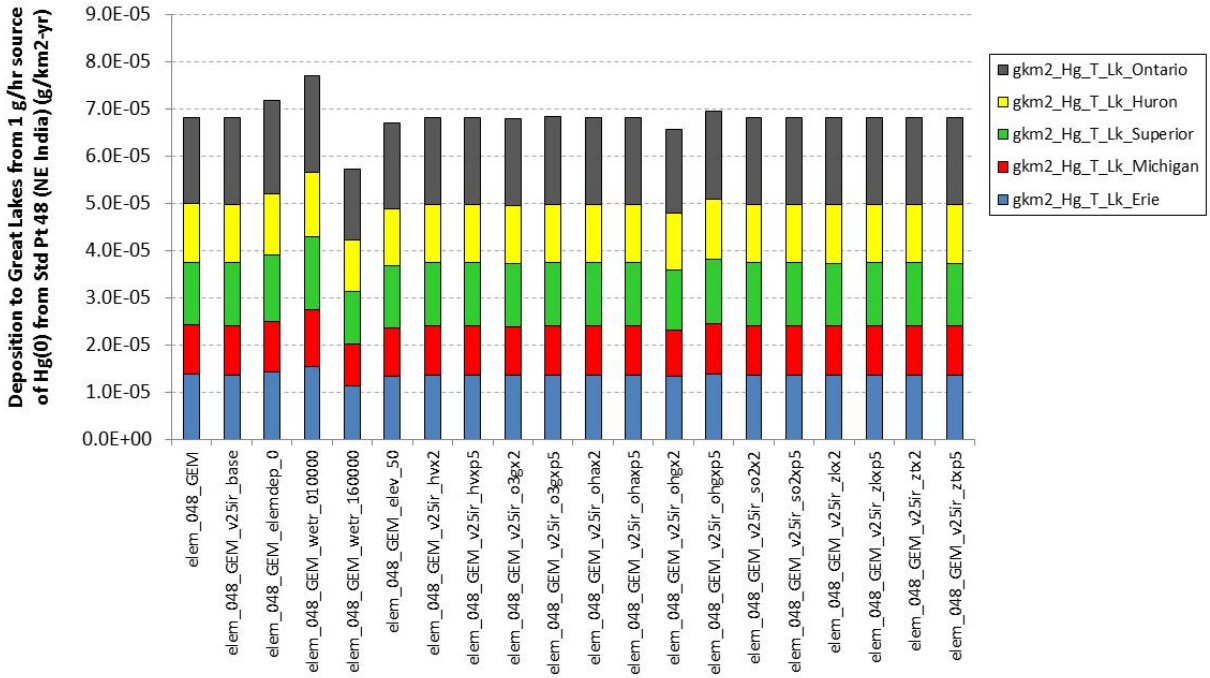

Figure 100. Modeled atmospheric mercury deposition flux to the Great Lakes arising from Hg(0) emissions from SSL-48 (India) using different simulation methodologies and/or parameters

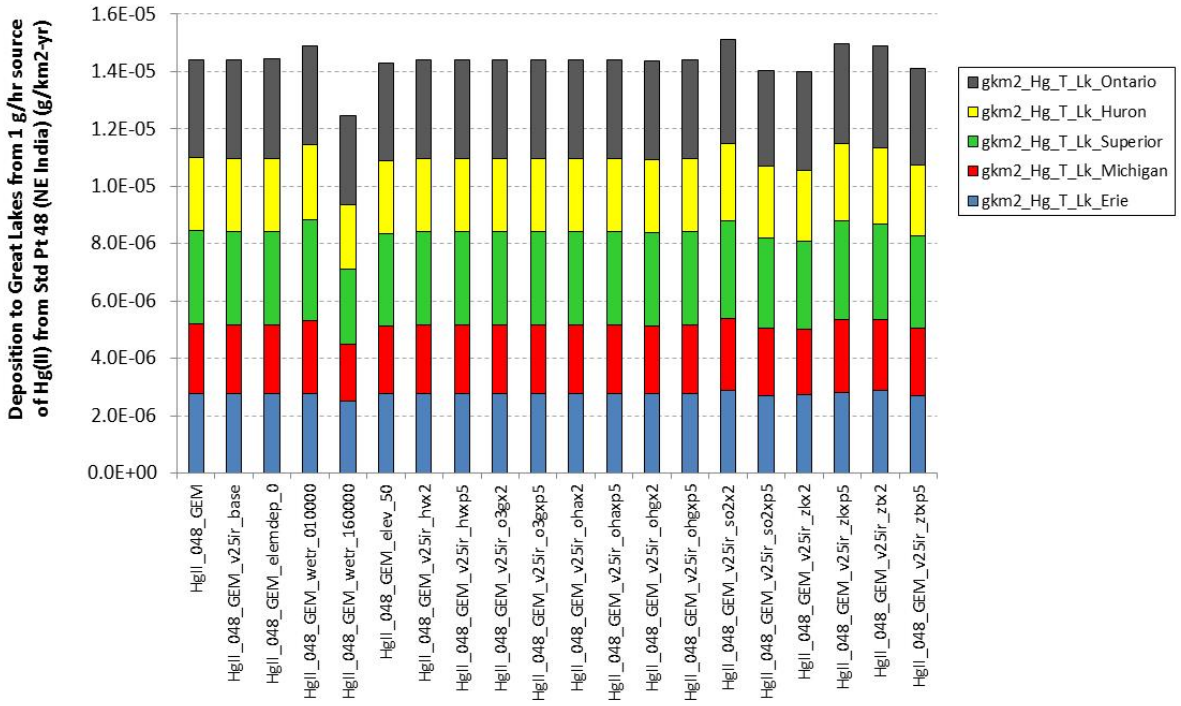

Figure 101. Modeled atmospheric mercury deposition flux to the Great Lakes arising from Hg(II) emissions from SSL-48 (India) using different simulation methodologies and/or parameters

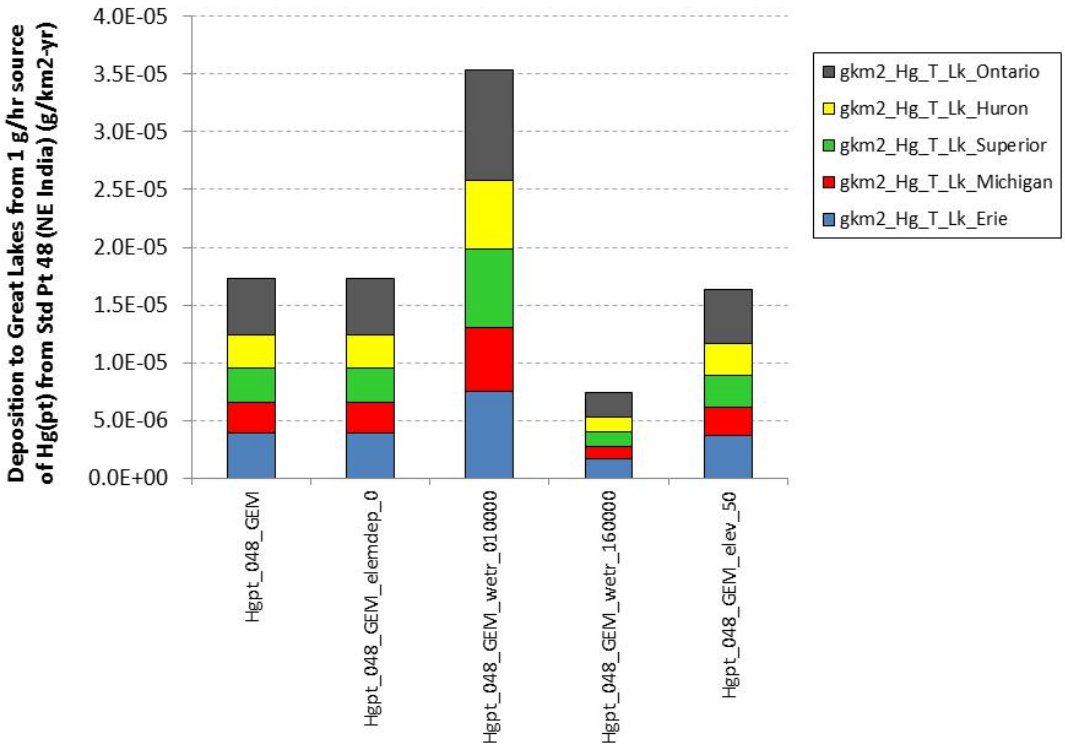

Figure 102. Modeled atmospheric mercury deposition flux to the Great Lakes arising from Hg(p) emissions from SSL-48 (India) using different simulation methodologies and/or parameters

3.4. Standard Source Location 11 (northeastern Texas)

An overview of the influences on the atmospheric fate and transport of mercury emitted from SSL-11 (northeastern Texas) is shown in the figures below.

Figure 103 shows the results for emissions of Hg(0). The input meteorological data – the default NARR vs. EDAS – has a big influence, as expected. Further, the simulation methodology (COM vs. PUF) also has a big influence, as expected. These differences were the rationale for using the NARR met data and COM methodology [for Hg(0)]. Of the other variations, the WETR changes – affecting wet deposition – have the most significant impact. A range of dispersion methodology variations is shown for the first time in this synthesis, as they are only relevant for PUF and COM simulations. Other than the overall methodology (PUF vs. COM) the other dispersion variations do not appear to influence the results significantly. The chemical transformation variations do not appear to make a significant difference.

Figure 104 shows the results for emissions of Hg(II). Similar to Hg(0), large variations are seen with the input meteorological data (the default NARR vs. EDAS). The PUF vs. COM variation did not make a large difference, and this is why the COM methodology was not deemed necessary for Hg(II). Like other comparisons, the variations in WETR make a significant difference. The puff scheme (ps10 vs.ps 12) appears to influence results. The reasons for this are discussed in Section 2.4.6 (page 39), and the differences found informed the choice of "default" puff scheme parameters

Figure 105 shows the results for emissions of Hg(p). As stated above, there are fewer variations shown for Hg(p) emissions as the chemical transformation variations are not relevant for emissions of pure Hg(p). The "elem_dep_0" simulation is shown as a QA/QC check – it should introduce no changes in the Hg(p) results, and it can be seen that it doesn't. As with Hg(II) above, the largest variations are seen with the input meteorological data (the default NARR vs. EDAS) and with WETR. In this case, the WETR influence on results is different than for SSL-13 and SSL-48. In this case, an increase in WETR leads to an increase in deposition to the Great Lakes. This is because the time scale for transport to the Great Lakes region from the source is relatively short, and there is less chance for the emitted mercury to be rained out along the way. Then, upon reaching the Great Lakes region, if there is precipitation, the increased value of WETR leads to increased wet deposition.

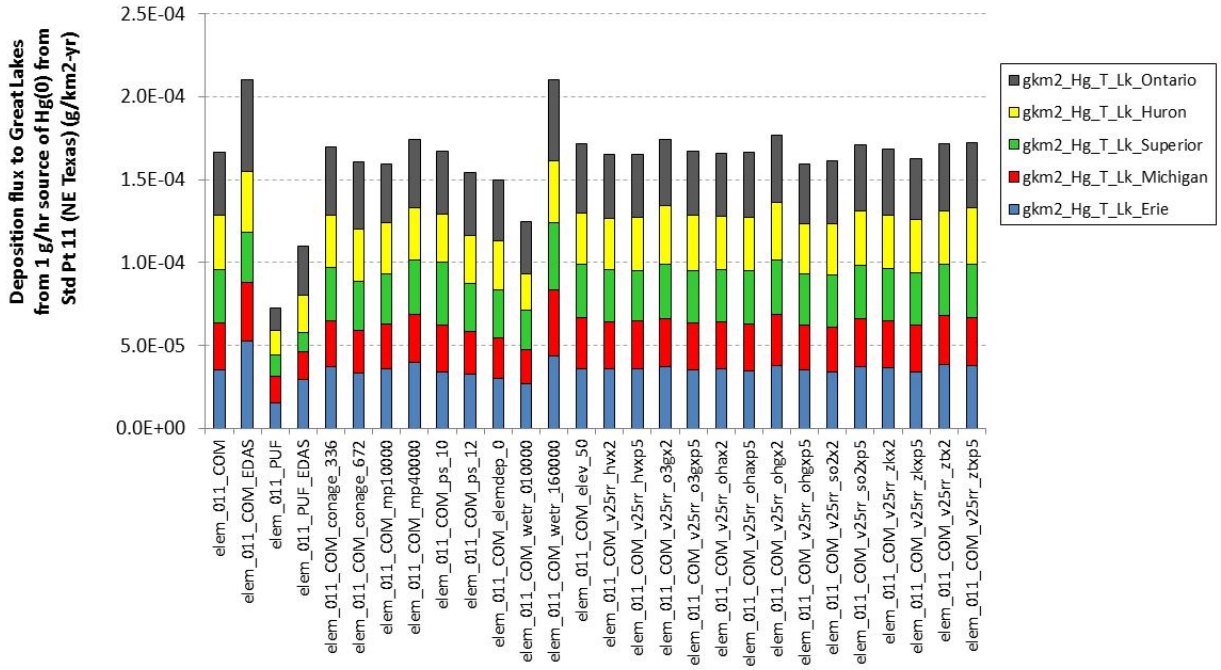

Figure 103. Modeled atmospheric mercury deposition flux to the Great Lakes arising from Hg(0) emissions from SSL-11 (Texas) using different simulation methodologies and/or parameters

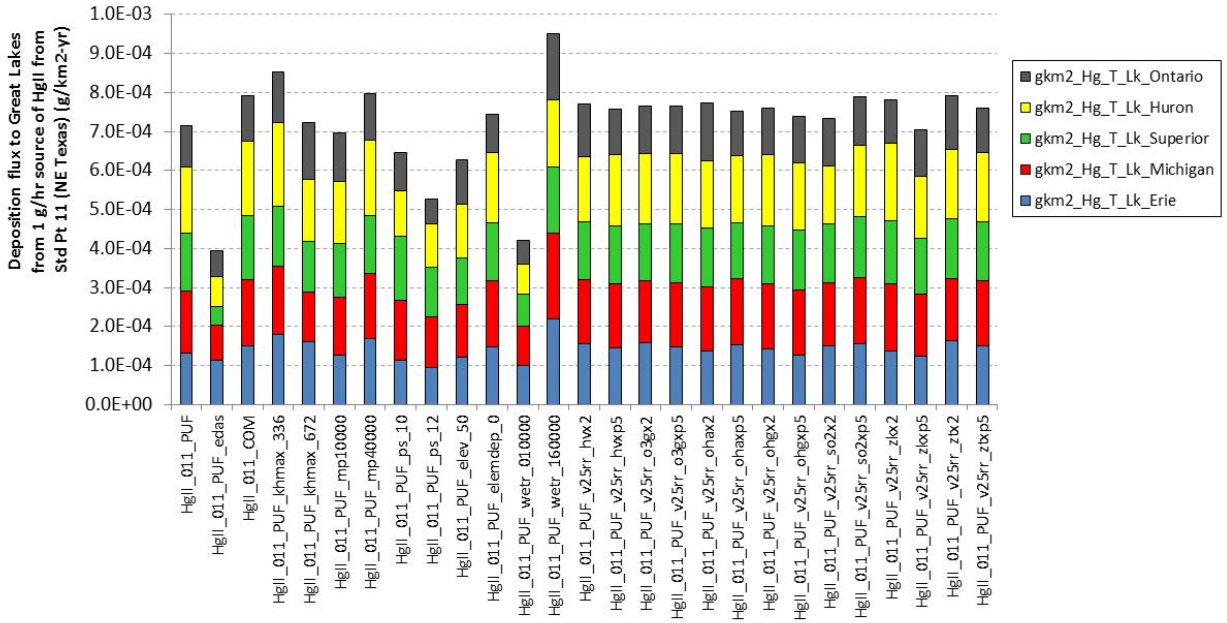

Figure 104. Modeled atmospheric mercury deposition flux to the Great Lakes arising from Hg(II) emissions from SSL-11 (Texas) using different simulation methodologies and/or parameters

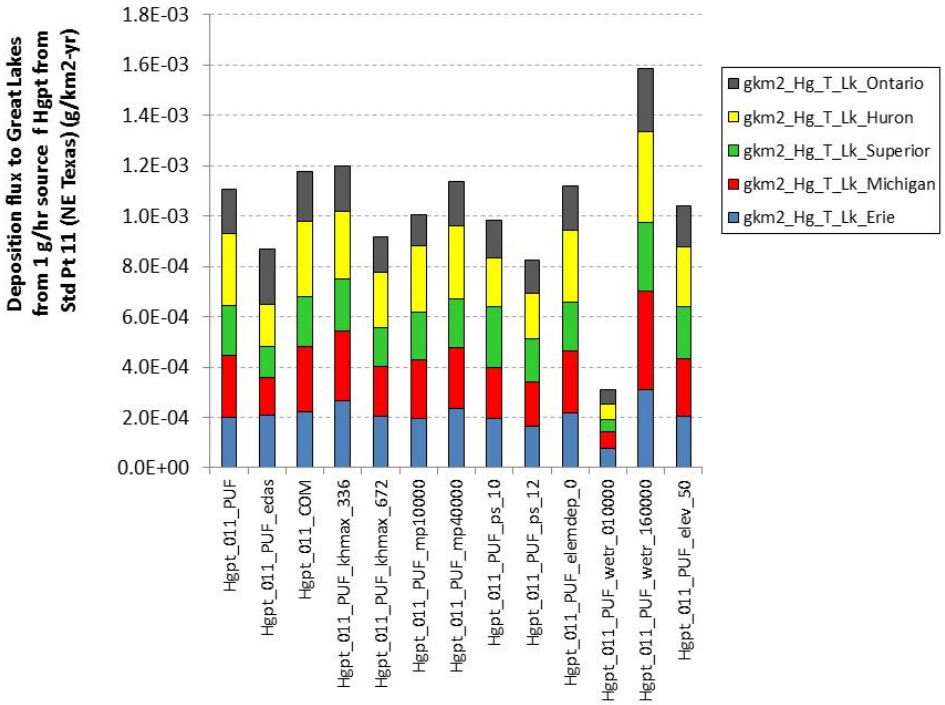

Figure 105. Modeled atmospheric mercury deposition flux to the Great Lakes arising from Hg(p) emissions from SSL-11 (Texas) using different simulation methodologies and/or parameters

3.5. Standard Source Location 6 (Ohio River Valley)

An overview of the influences on the atmospheric fate and transport of mercury emitted from SSL-6 (Ohio River Valley) is shown in the figures below.

Figure 106 shows the results for emissions of Hg(0). As with SSL-11, the input meteorological data – the default NARR vs. EDAS – has a big influence, as expected. Further, similar to SSL-11, the simulation methodology (COM vs. PUF) also has a big influence, as expected. As noted earlier, these differences were the rationale for using the NARR met data and COM methodology [for Hg(0)]. As seen in earlier comparisons, the WETR changes – affecting wet deposition – have a significant impact. The variation affecting the dry deposition of Hg(0) – "elemdep_0" – has a significant impact. As with SSL-11, a range of dispersion methodology variations are shown. Other than the overall methodology (PUF vs. COM) and the puff-scheme variations, the other dispersion variations do not appear to influence the results significantly. The chemical transformation variations do not appear to make a significant difference.

Figure 107 shows the results for emissions of Hg(II). Similar to Hg(0), large variations are seen with the input meteorological data (the default NARR vs. EDAS). As with SSL-11, the PUF vs. COM variation did not make a large difference, and this informed the decision that the COM methodology was not deemed necessary for Hg(II). Like other comparisons, the variations in WETR make a significant difference and the puff scheme (ps10 vs.ps 12) appears to influence results. The reasons for this are discussed in Section 2.4.6 (page 39), and the differences found informed the choice of "default" puff scheme parameters. The release elevation did have a big influence on the results. With a lower elevation, more of the Hg(II) deposited early in the transport path, and less mercury was potentially available for deposition if/when the air mass got to the Great Lakes.

Figure 108 shows the results for emissions of Hg(p). As stated above, there are fewer variations shown for Hg(p) emissions as the chemical transformation variations are not relevant for emissions of pure Hg(p). The "elem_dep_0" simulation is shown as a QA/QC check – it should introduce no changes in the Hg(p) results, and it can be seen that it doesn't. As with Hg(II) above, the largest variations are seen with the input meteorological data (the default NARR vs. EDAS) and with WETR. As with SSL-11, the WETR influence on results is different than for SSL-13 and SSL-48. As with SSL-11, an increase in WETR leads to an increase in deposition to the Great Lakes. The time scale for transport to the Great Lakes region from the source is likely even shorter, and there is less chance for the emitted mercury to be removed by wet deposition along the way. Then, upon reaching the Great Lakes region, if there is precipitation, the increased value of WETR leads to increased wet deposition.

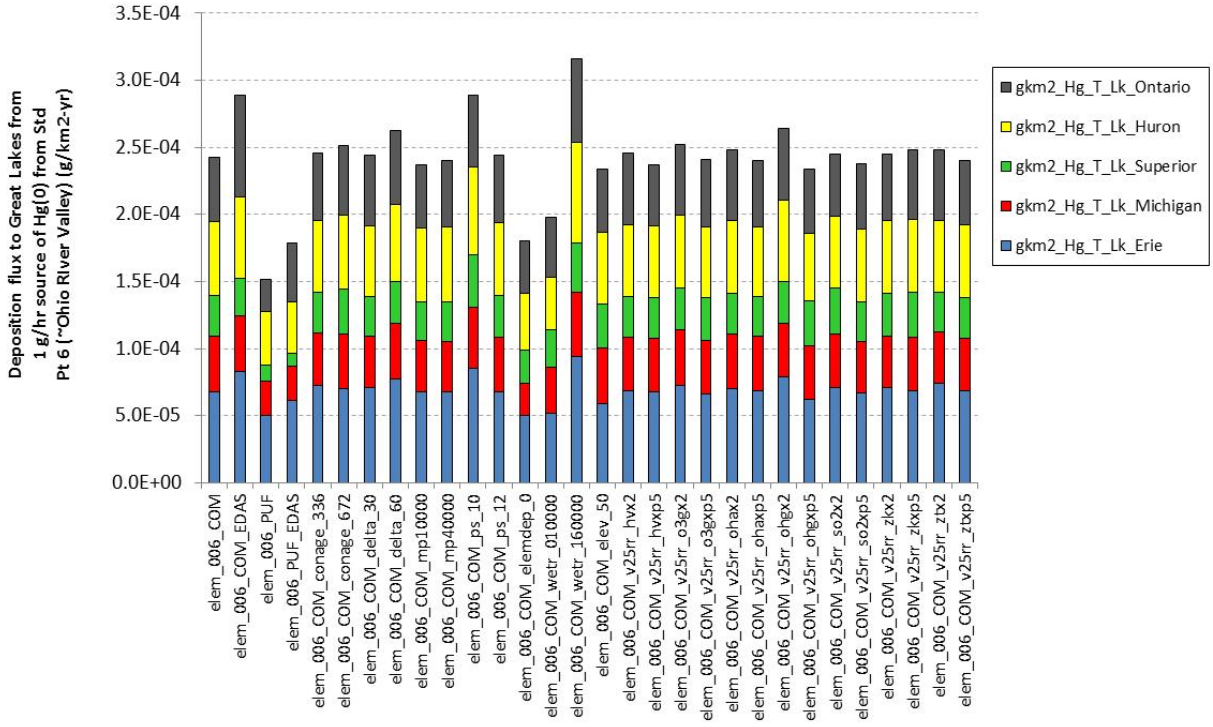

Figure 106. Modeled atmospheric mercury deposition flux to the Great Lakes arising from Hg(0) emissions from SSL-6 (Ohio River Valley) using different simulation methodologies and/or parameters

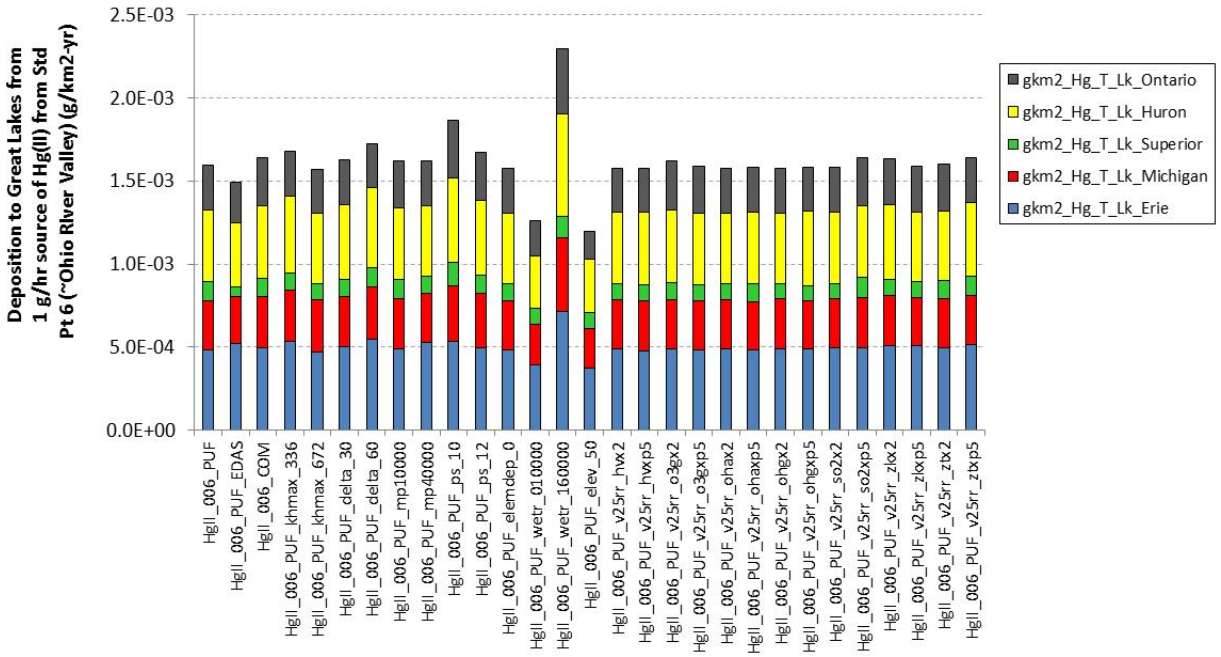

Figure 107. Modeled atmospheric mercury deposition flux to the Great Lakes arising from Hg(II) emissions from SSL-6 (Ohio River Valley) using different simulation methodologies and/or parameters

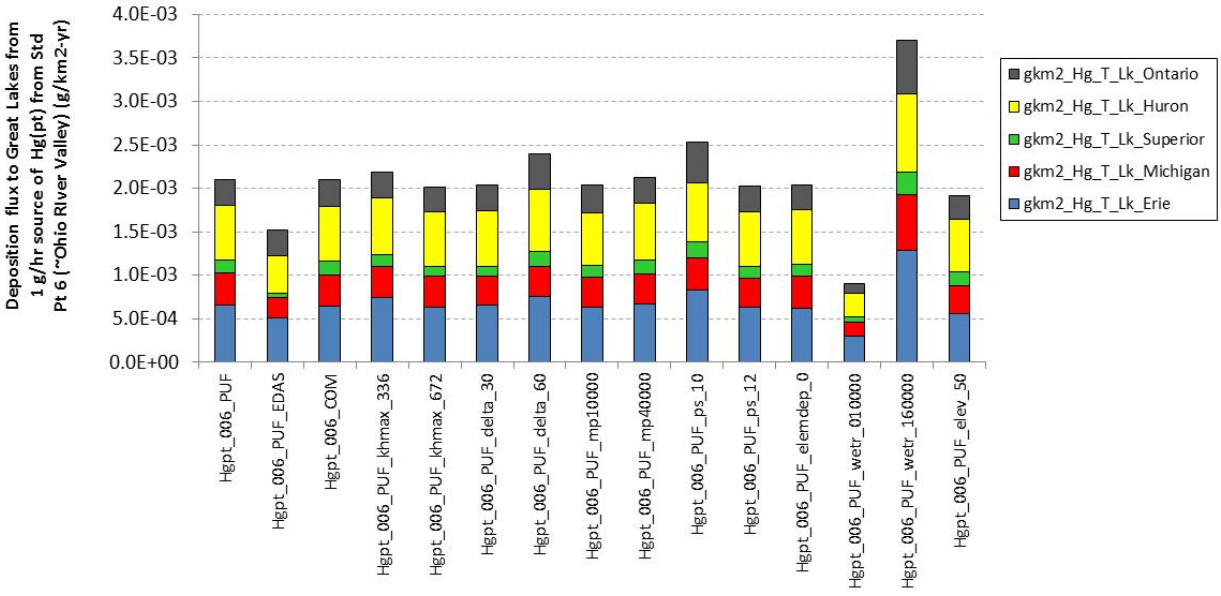

Figure 108. Modeled atmospheric mercury deposition flux to the Great Lakes arising from Hg(p) emissions from SSL-6 (Ohio River Valley) using different simulation methodologies and/or parameters

3.6. Standard Source Location 8 (western shore of Lake Erie)

An overview of the influences on the atmospheric fate and transport of mercury emitted from SSL-8 (western shore of Lake Erie) is shown in the figures below.

Figure 109 shows the results for emissions of Hg(0). The largest influences for this simulation are dry deposition (elemdep_0) and the release elevation (elev_50m). The biggest variation is for deposition flux to Lake Erie. In this case, the input meteorological data (NARR vs. EDAS) and the overall simulation methodology (PUF vs. COM) have a relatively small influence. The other dispersion variations do not appear to influence the results significantly. The chemical transformation variations do not appear to make a significant difference.

Figure 110 shows the results for emissions of Hg(II). Similar to Hg(0), large differences are seen for the variation in release elevation (50m vs. 250m). The input meteorological data (the default NARR vs. EDAS) also had a moderately large impact. Like many of the other comparisons, the variations in WETR made a difference. These were the largest influences observed for this case, and all other variations were relatively small.

Figure 111 shows the results for emissions of Hg(p). As stated above, there are fewer variations shown for Hg(p) emissions as the chemical transformation variations are not relevant for emissions of pure Hg(p). The “v25rr_base” and “max_oxid” simulations are shown as a QA/QC checks – they should introduce no changes in the Hg(p) results, and it can be seen that they don’t. The largest influence is seen with the variation in WETR, a parameter affecting scavenging of particles in precipitation. Similar to other species emissions at this site, the release height variation (50m vs. 250m) results in a relatively significant difference, but the effect can clearly be seen to impact the modeled deposition flux to other lakes in addition to Lake Erie.

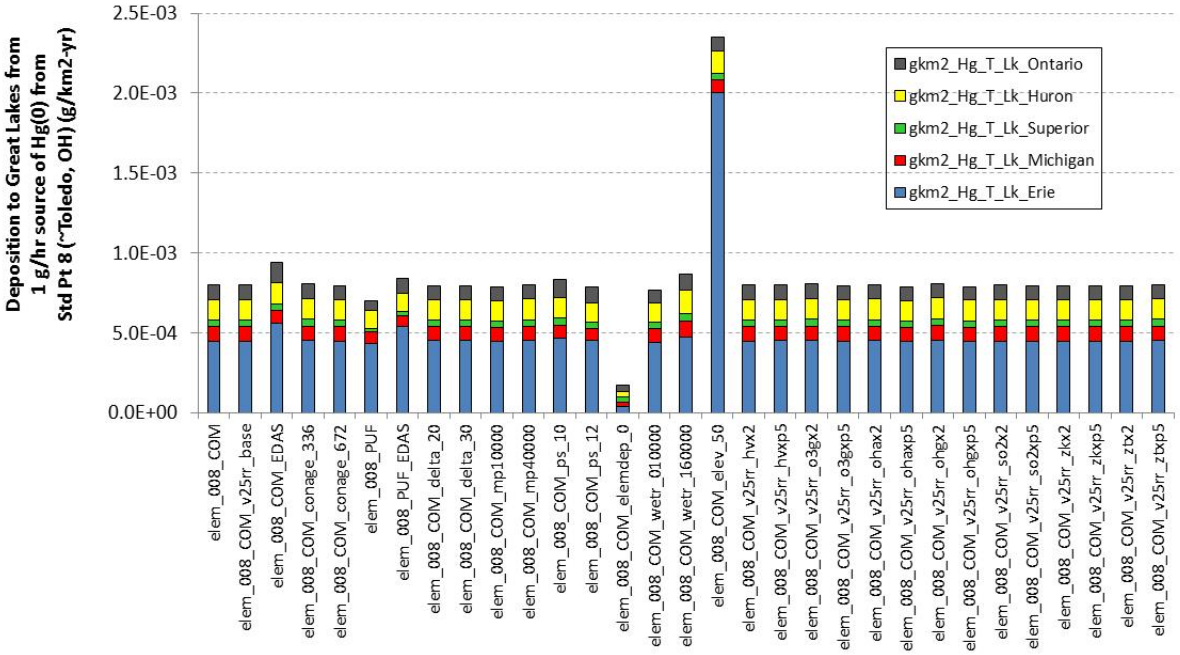

Figure 109. Modeled atmospheric mercury deposition flux to the Great Lakes arising from Hg(0) emissions from SSL-8 (Western shore of Lake Erie) using different simulation methodologies and/or parameters

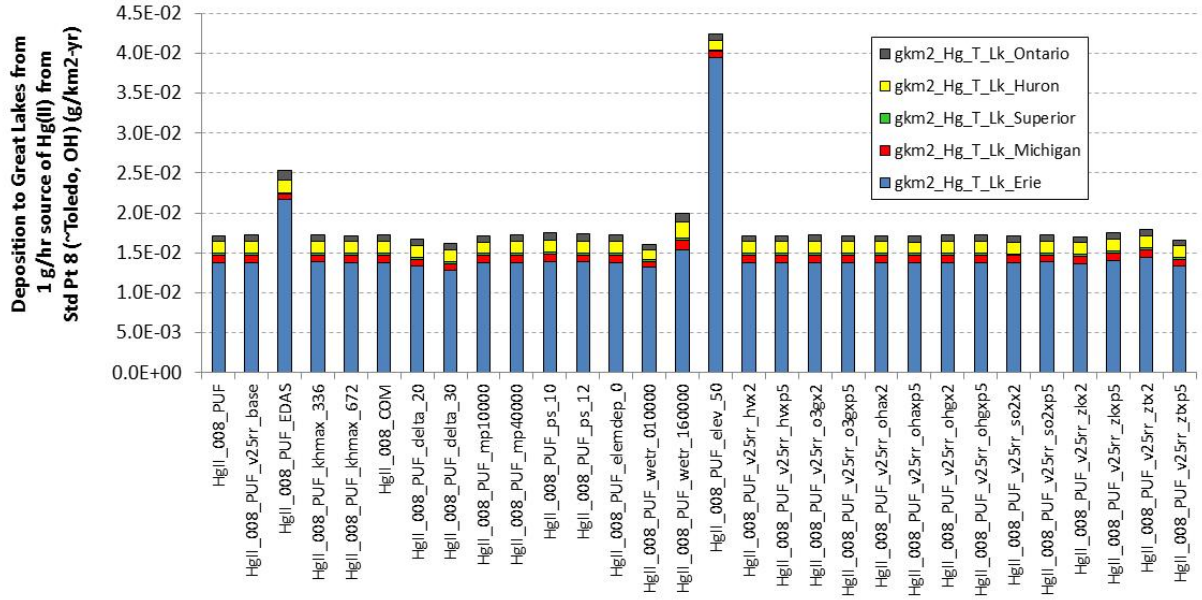

Figure 110. Modeled atmospheric mercury deposition flux to the Great Lakes arising from Hg(II) emissions from SSL-8 (Western shore of Lake Erie) using different simulation methodologies and/or parameters

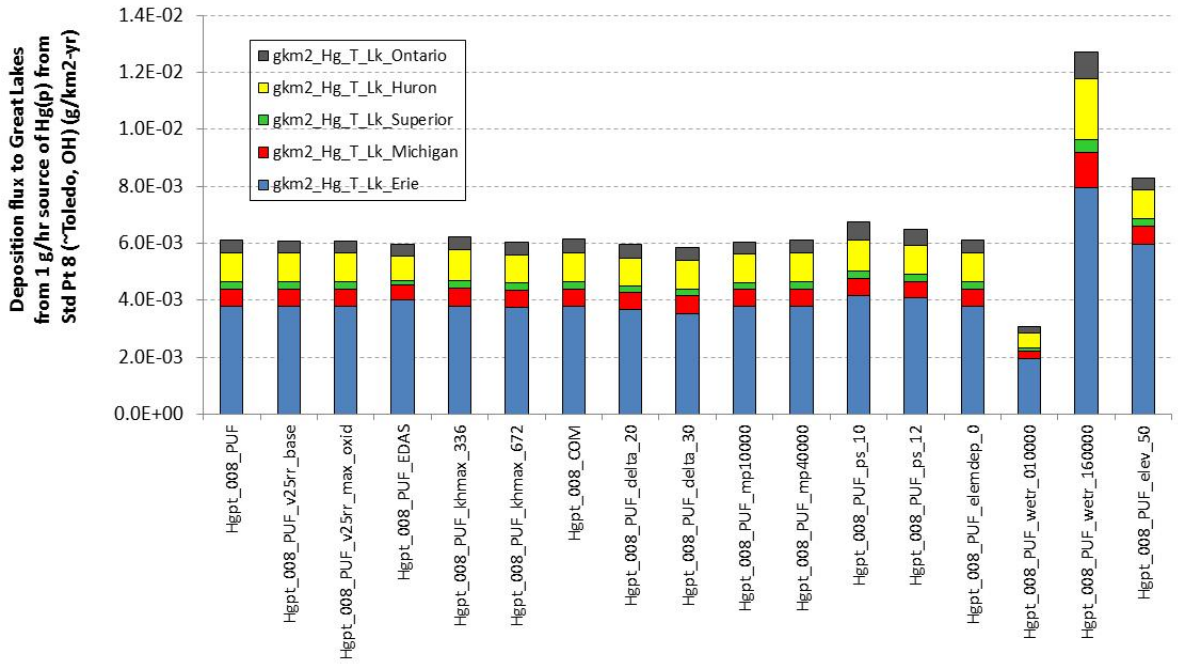

Figure 111. Modeled atmospheric mercury deposition flux to the Great Lakes arising from Hg(p) emissions from SSL-8 (Western shore of Lake Erie) using different simulation methodologies and/or parameters

3.7. Overall synthesis

A total of 474 different simulations were carried out for the five illustrative standard source locations (SSL's) examining the influence of variations on simulation results. About a third of these simulations (154) were carried out to examine numerical issues, as summarized in the Appendix. The remainder (320 simulations) examined the influence of different inputs, parameters, and algorithms on the model results. An overall summary of this investigation is provided here. Table 3 shows the fractional variations – expressed as a percent of the default value – for the most important variations examined, for each of the five SSL's, for emissions of pure Hg(0), Hg(II), and Hg(p). Graphical depictions of these same data are shown in Figure 112, Figure 113, and Figure 114, for Hg(0), Hg(II), and Hg(p), respectively. Based on an examination of the summary table and figures, the following overall conclusions can be made:

- Except as noted in the following bullets, for all illustrative standard source locations and for all mercury emission forms -- Hg(0), Hg(II), and Hg(p) -- the largest impacts on modeled Great Lakes deposition flux are generally seen for variations in the following :
    - the emissions release height [*emit elev (50m vs. 250m)*]
    - the particle rainout factor [*wetr (160,000 vs. 40,000)*]
    - the meteorological input data [*met data (edas vs. narr)*]

- For all mercury emission forms, the emissions release height shows the greatest variations for SSL-8, on the western shore of Lake Erie, and as discussed in the more detailed sections earlier, this is primarily due to the modeled deposition to Lake Erie, which is immediately adjacent to the emissions location. This makes intuitive sense as one would expect the emissions release height to have the greatest impact on concentrations and deposition nearby the source.

    - For Hg(0) and Hg(p), the release height is *only* important for SSL-8, i.e., the variations seen for the other SSL's for release height are relatively insignificant.
    - For Hg(II), the release height also shows moderate variations for other SSL's. This is because the near-field deposition of Hg(II) is relatively large. So, the increased near-field deposition due to a lower release height (50m vs. 250m) has a relatively bigger impact on the deposition further downwind.

- Increases in WETR, a parameter affecting wet deposition of particles, from the default value of 4.0E+04 m^3-air/m^3-water to 1.6E+05 m^3-air/m^3-water, for all emitted mercury forms results in:

    - lower deposition to the Great Lakes for distant sources (SSL-13, China, and SSL-48, India), as the increased wet deposition as the mercury is being transported to the Great Lakes has a bigger impact than the increased efficiency of wet deposition once the mercury arrives at the Great Lakes region
    - increased deposition to the Great Lakes for national, regional, and local sources (SSL-11, Texas, SSL-6, Ohio River Valley, and SSL-8, western shore of Lake Erie), as the increased wet deposition as the mercury is being transported to the Great Lakes has a lower

impact than the increased efficiency of wet deposition once the mercury arrives at the Great Lakes region

- The use of EDAS vs. the default NARR meteorological data to drive the HYSPLIT-Hg simulation only affects the simulations of SSL-11 (Texas), SSL-6 (Ohio River Valley), and SSL-8 (western shore of Lake Erie), as only the NCEP/NCAR 2.5 degree global reanalysis data is used to simulate the fate and transport of mercury emitted from the distant sources SSL-13 (China) and SSL-48 (India). For this variation, the effects on simulated Great Lakes deposition are significant, with relatively large positive and negative impacts.

- Setting the dry deposition of Hg(0) to zero has a moderately significant impact on the fate and transport of emitted Hg(0), but the impact appears to decrease as the distance to the Great Lakes increases. The largest impact (-79%) was seen for SSL-8 (Lake Erie shore). The impacts for SSL-6 (Ohio River Valley) and SSL-11 (Texas) were -26% and -10%, respectively, and the impacts for the most distant illustrative SSL's (China and India) were relatively small.

- In general, changes in the chemical transformation parameters did not generate large changes in simulated deposition to the Great Lakes. To examine these changes in a more detail, they have been plotted "alone" in Figure 115 for emissions of Hg(0) and Figure 116 for emissions of Hg(II). As discussed earlier, simulations of Hg(p) emissions in the HYSPLIT-Hg model are not influenced by changes in these chemical transformation parameters. Note that the scale in these figures is much smaller, as the maximum changes are only on the order of ~10%.

Table 3. Overall summary of influences of simulation variations on estimated deposition flux of mercury to the Great Lakes arising from the five different illustrative standard source locations

Emissions Location and Species		Met data and release height		Deposition Methodology		Chemistry and partitioning					Puff dispersion parameters		
Standard Source Location	Emissions species	Met data	Release elevation	Wet deposition of particles	Dry deposition of Hg(0)	Aqueous-phase Hg(II) reduction by S(IV)	Gas-phase oxidation of Hg(0) by OH	Gas-phase oxidation of Hg(0) by O3	Soot-HgII partitioning factor	Soot-HgII partitioning time constant	Maximum puff lifetime khmax and conage	Puff emissions and splitting frequency	Maximum number of puffs
		EDAS vs. NARR	50m vs. 250m	160,000 vs. 40,000	elemdep_0 vs. explicit calculation	SO2x2 vs. default	Ohgx2 vs. default	03gx2 vs. default	ZK * 2 (more partitioning)	ZT * 0.5 (faster partitioning)	672 hrs vs. 504 hrs	Puff scheme 10	40,000 vs. 20,000
#48 – India	Hg(0)		-2%	**-16%**	+5%	0%	-4%	0%	0%	0%			
	Hg(II)		-1%	**-14%**	0%	+5%	0%	0%	-3%	-2%			
	Hg(p)		-6%	**-57%**									
#13 – China	Hg(0)		-1%	-1%	-1%	0%	-2%	0%	0%	0%			
	Hg(II)		**-22%**	**-54%**	-1%	**+12%**	0%	0%	-4%	+6%			
	Hg(p)		+1%	**-78%**									
#11 – northeast Texas	Hg(0)	**+26%**	+3%	**+26%**	**-10%**	-3%	+6%	+4%	1%	+3%	-4%	0%	+4%
	Hg(II)	**-45%**	**-12%**	**+33%**	+4%	+3%	+6%	+7%	9%	+6%	+1%	**-10%**	**+11%**
	Hg(p)	**-21%**	-6%	**+43%**							-17%	**-11%**	+3%
#6 – Ohio River Valley	Hg(0)	**+19%**	-4%	**+30%**	**-26%**	+1%	+9%	+4%	+1%	-1%	+4%	**+19%**	-1%
	Hg(II)	-6%	**-25%**	**+40%**	-1%	-1%	-1%	+2%	+2%	+3%	-2%	**+17%**	+2%
	Hg(p)	**-28%**	-9%	**+76%**							-4%	**+20%**	+1%
#8 – western shore of Lake Erie	Hg(0)	**+18%**	**+195%**	+8%	**-79%**	0%	+1%	1%	0%	+1%	-1%	+5%	0%
	Hg(II)	**+47%**	**+146%**	**+16%**	0%	0%	0%	0%	-1%	-3%	0%	+2%	0%
	Hg(p)	-2%	**+36%**	**+109%**							-1%	**+11%**	0%

Shading key for above table:

Cell color and contents	Type of influence observed
	Variations of this type would have no influence on this simulation
	Variations of this type could have an influence, but no significant influence was observed (less than 10%)
	Variations of this type showed a positive influence (greater deposition than default)
	Variations of this type showed a negative influence (lesser deposition than default)

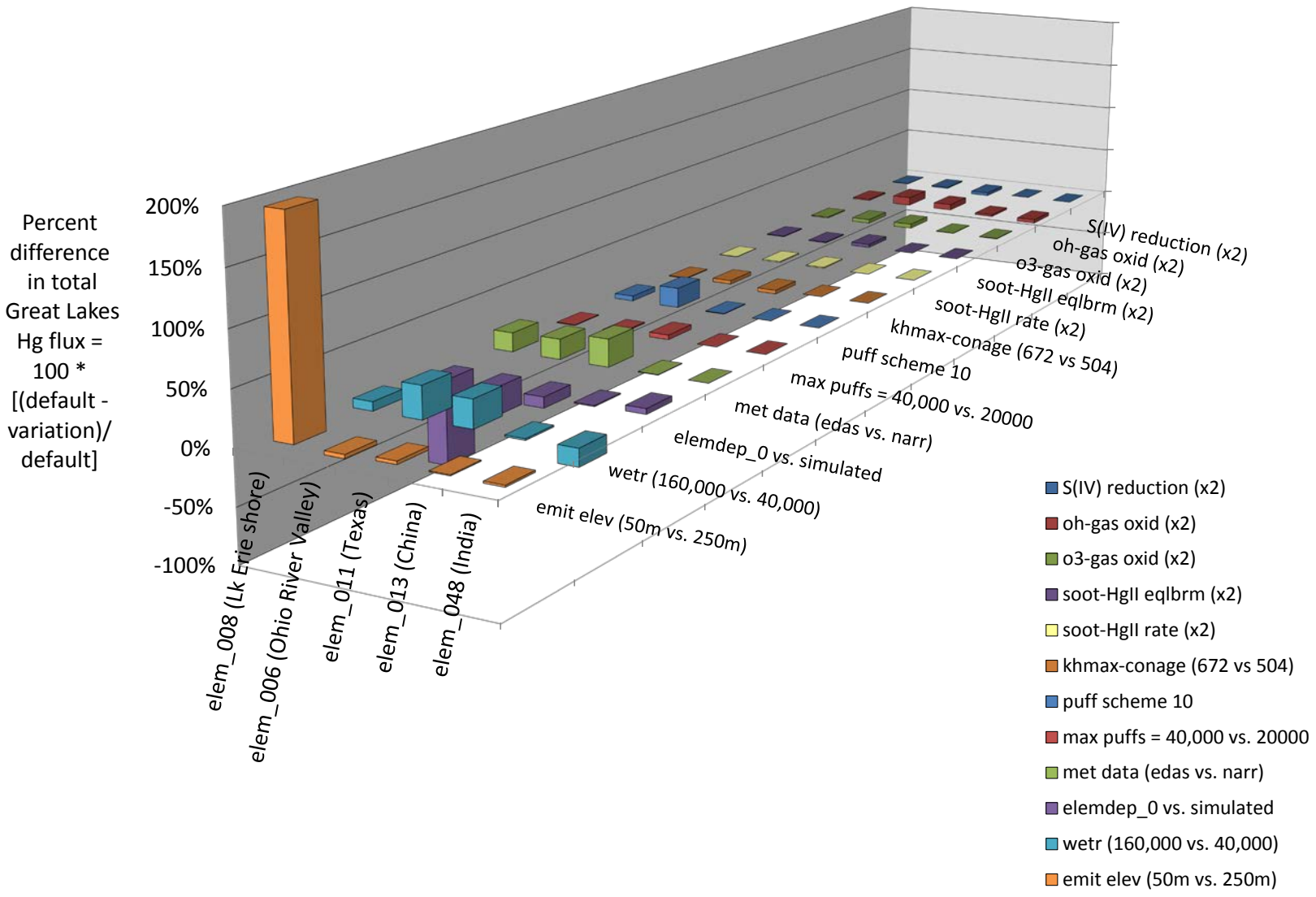

Figure 112. Overall summary of variations in modeled Great Lakes mercury deposition flux arising from different inputs, parameters and methodologies, from illustrative standard source locations, for emissions of Hg(0)

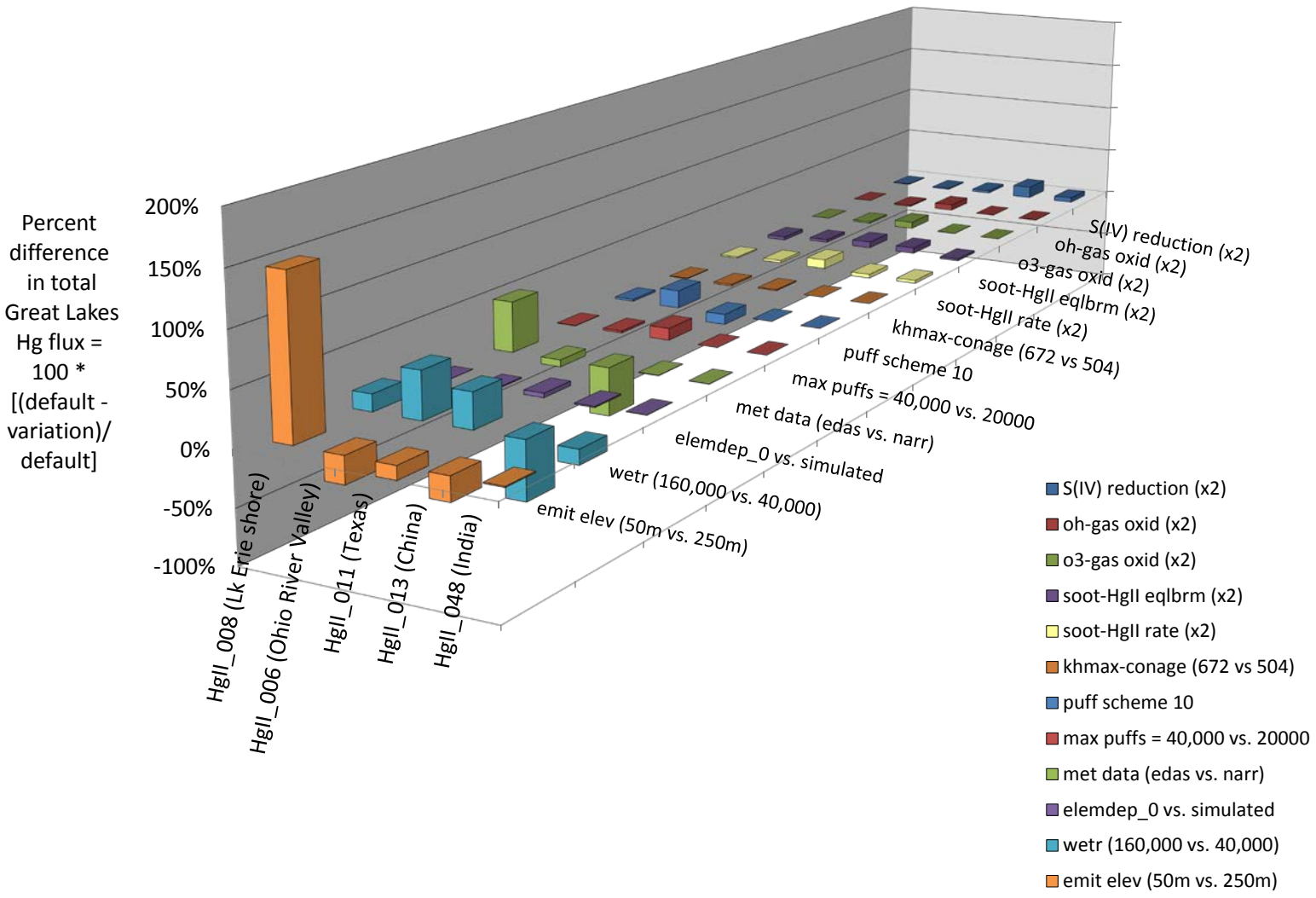

Figure 113. Overall summary of variations in modeled Great Lakes mercury deposition flux arising from different inputs, parameters and methodologies, from illustrative standard source locations, for emissions of Hg(II)

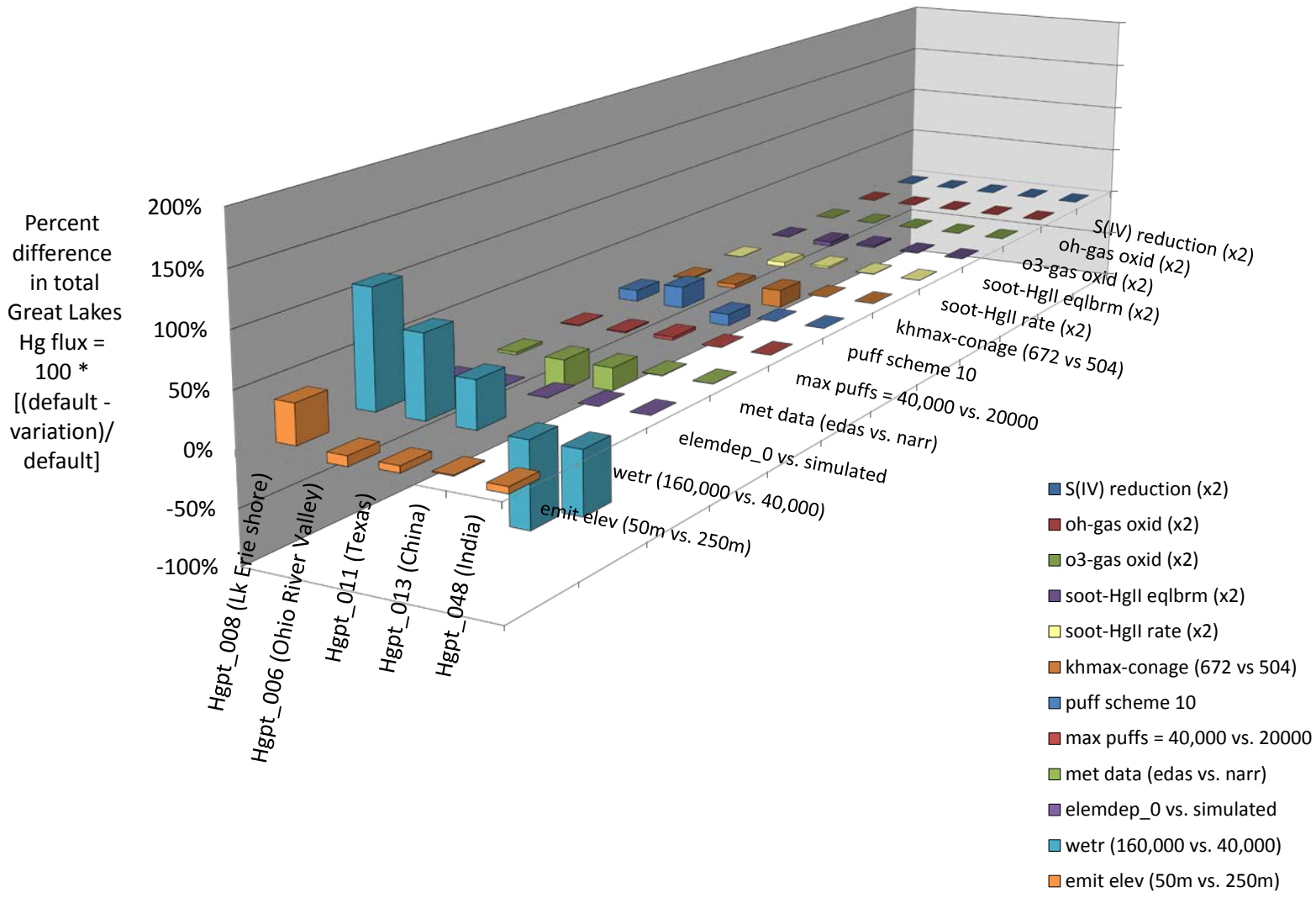

Figure 114. Overall summary of variations in modeled Great Lakes mercury deposition flux arising from different inputs, parameters and methodologies, from illustrative standard source locations, for emissions of Hg(p)

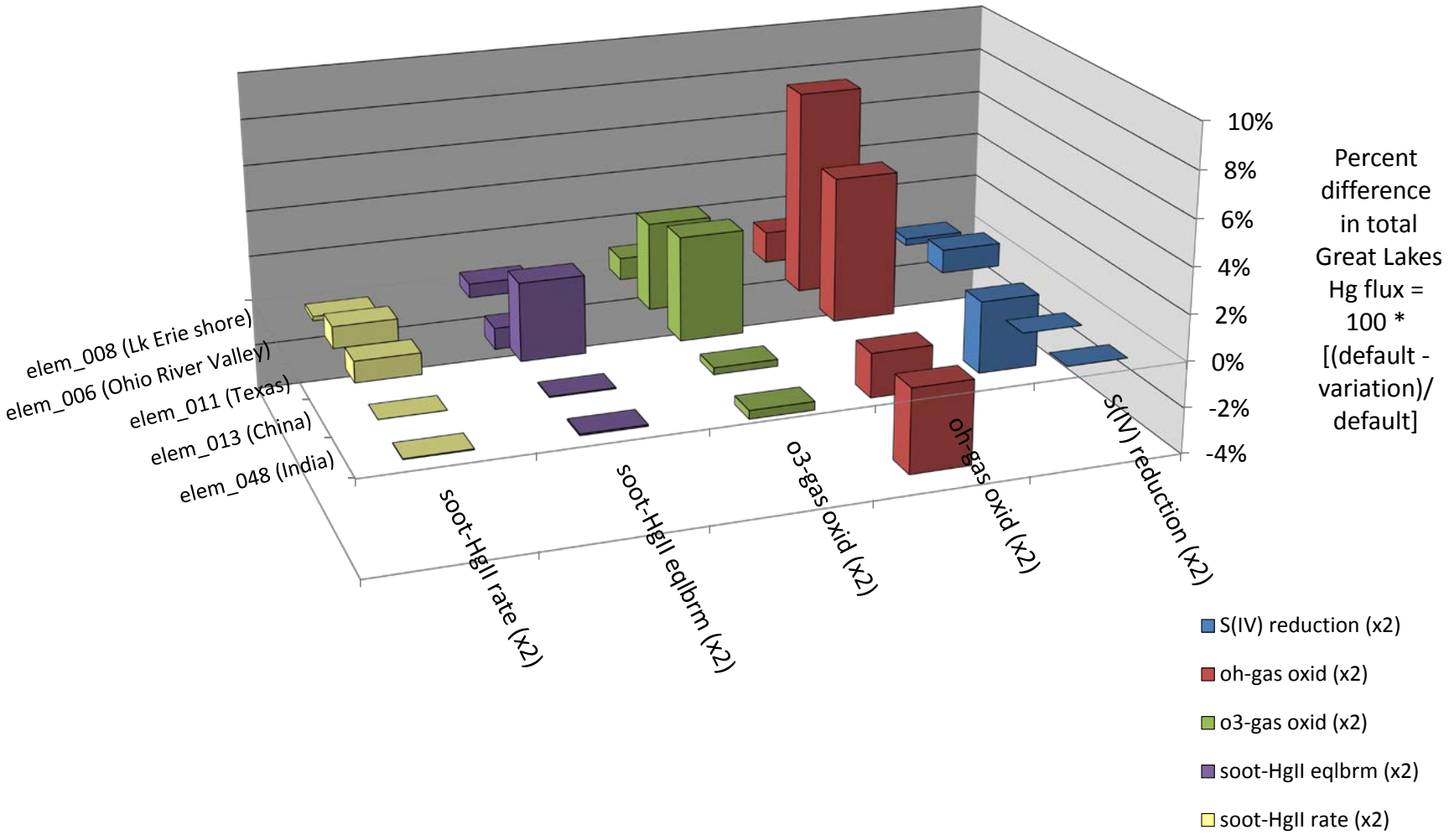

Figure 115. Overall summary of variations in modeled Great Lakes mercury deposition flux arising from different chemical transformation parameters, from illustrative standard source locations, for emissions of Hg(0)

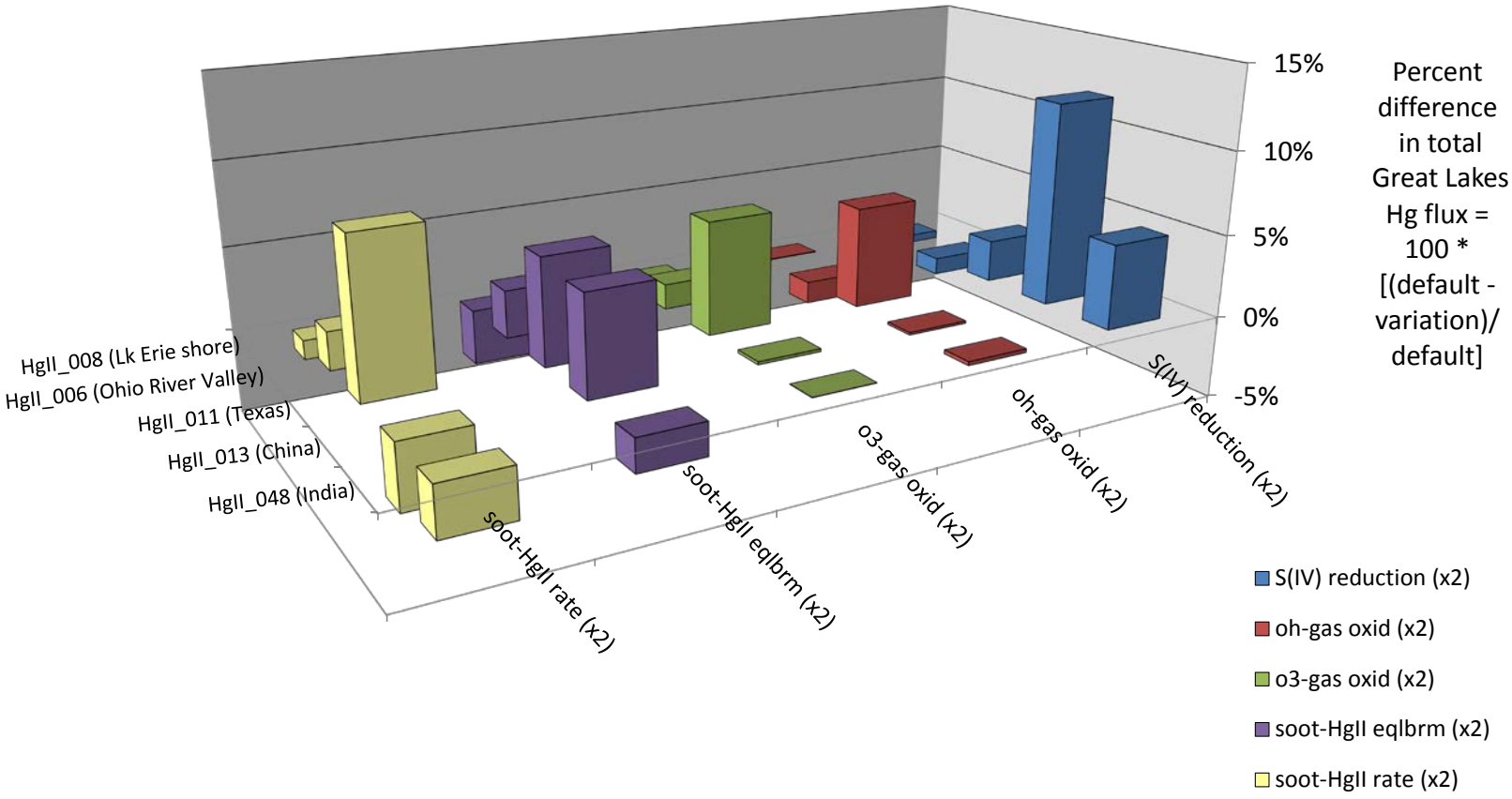

Figure 116. Overall summary of variations in modeled Great Lakes mercury deposition flux arising from different chemical transformation parameters, from illustrative standard source locations, for emissions of Hg(II)

4. Sensitivity of full simulations

4.1. Full simulations selected for analysis

As discussed above, only a few different overall variations in the "full" analysis could be undertaken, due to computational resource constraints. Accordingly, there were only 3 primary variations investigated. In addition, numerous sub-variations based on these two primary variations were explored.

The first primary variation was the use of NARR meteorological data instead of EDAS meteorological data to drive the simulation in the CONUS. As discussed above, the EDAS dataset (with 40km resolution) was used in the FY10 analysis over the Continental US (incl. southern Canada and northern Mexico), and the NCEP-NCAR Global Reanalysis dataset (with 2.5 degree) resolution was used outside of this region. We will refer to this base simulation, which used 136 standard source locations (SSL's), as "**EDAS-136**".To investigate the influence of input meteorological data, i.e., the data provided to the HYSPLIT-Hg model during the simulation, the NCEP-NCAR North American Regional Reanalysis ("NARR") dataset (with 36km resolution) was used instead of the EDAS dataset. The global dataset used, i.e., the NCEP-NCAR Global Reanalysis, was not changed. The NARR dataset is believed to have more accurate precipitation data than the EDAS dataset during 2005, and this was borne out by examining the model-predicted precipitation at mercury wet deposition measurement sites in the Great Lakes region (Figure 3, above). We will refer to this first primary simulation variation, which used the same 136 SSL's, as "**NARR-136**". This variation required 75 new Hg(0) COM-type simulations, and 75 new Hg(II) and Hg(p) PUF-type simulations (a total of 225 new simulations). The results for the 61 SSL's in the FY10 baseline analysis that were modeled using GEM-type simulations could be "re-used" as the only meteorological dataset used for these runs was the NCEP/NCAR Global Reanalysis.

The second primary variation involved adding additional standard source locations to the analysis, in the eastern Great Lakes region. One of the findings of the FY10 analysis was that the model predictions were less consistent with Mercury Deposition Network wet deposition data at sites east of the Great Lakes. It was hypothesized that this could have been because there were few standard source locations chosen in that region. The reason that fewer standard source locations were used was that the region was generally downwind of the Great Lakes, and impacts of sources in that region were likely less significant. Thus, it was decided to devote less computational resources to sources in that region. For this second primary variation, 15 additional locations were added to original 136 locations (for a total of 151 locations), to investigate what influence this might have on the consistency of model predictions with ambient measurements, in the eastern Great Lakes region. This simulation variation will be referred to as "**NARR-151**". This variation required an additional 45 simulations: 15 COM-type simulations for Hg(0) and 15 PUF-type simulations, each, for Hg(II) and Hg(p).

The third primary variation included an additional 28 standard source locations that were simulated for a complementary project analyzing mercury deposition to the Gulf of Mexico. This variation required an additional 84 simulations: 28 COM-type simulations for Hg(0) and 28 PUF-type simulations, each, for Hg(II) and Hg(p). These simulations were carried out with the identical methodology, and so they could

be readily added to this Great Lakes analysis. With these 28 locations added to the NARR-151 simulation, the resulting analysis will be referred to as "**NARR-179**". The NARR-179 analysis is not expected to be significantly different than the NARR-151 analysis for the Great Lakes, but this expectation will be examined below.

Maps of existing and newly added standard source locations, along with the locations of key model evaluation wet deposition (MDN) sites are shown in Figure 117 and Figure 118.

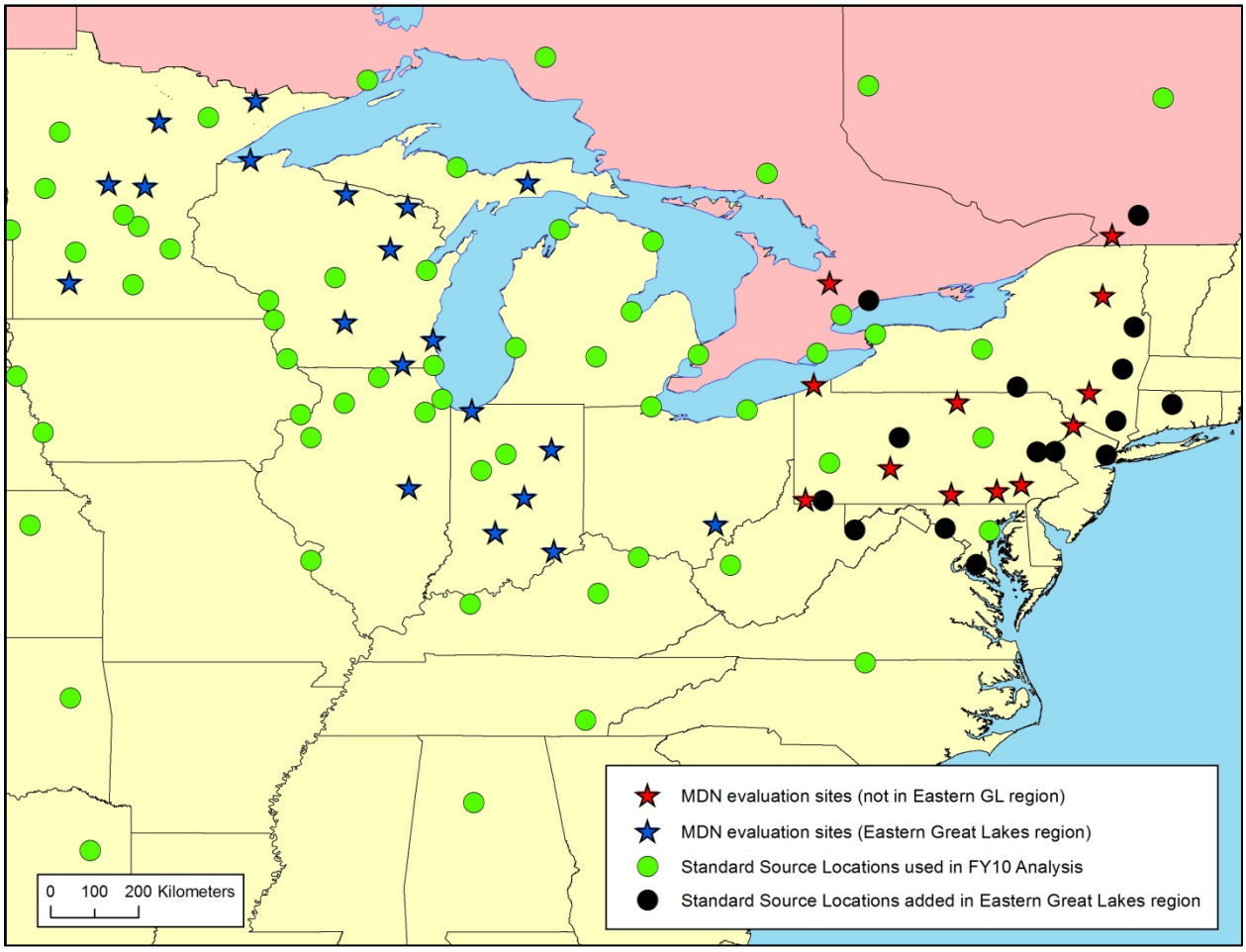

Figure 117. Standard source locations in the Great Lakes region, including 15 added sites in the eastern Great Lakes region

Additional sub-variations based on the above three primary analyses will be discussed in more detail when they arise, but will be briefly mentioned here. One sub-variation was the variation of total global anthropogenic terrestrial re-emissions from the baseline value of 750 metric tons/year to a much higher value (2000 metric tons/year), and the total global anthropogenic oceanic re-emissions from the baseline value of 1250 metric tons/year to a much higher value (2000 metric tons/year). An additional sub-variation was the method of adjusting precipitation data at the model evaluation sites. These sub-variations included adjusting the EDAS or NARR dataset, adjusting the NCEP/NCAR global dataset, adjusting both, and making no adjustments. A final set of sub-variations was considered involving the

interpolation methodology, including the number of standard source locations used, and the method of creating a weighted average result for a given source and receptor.

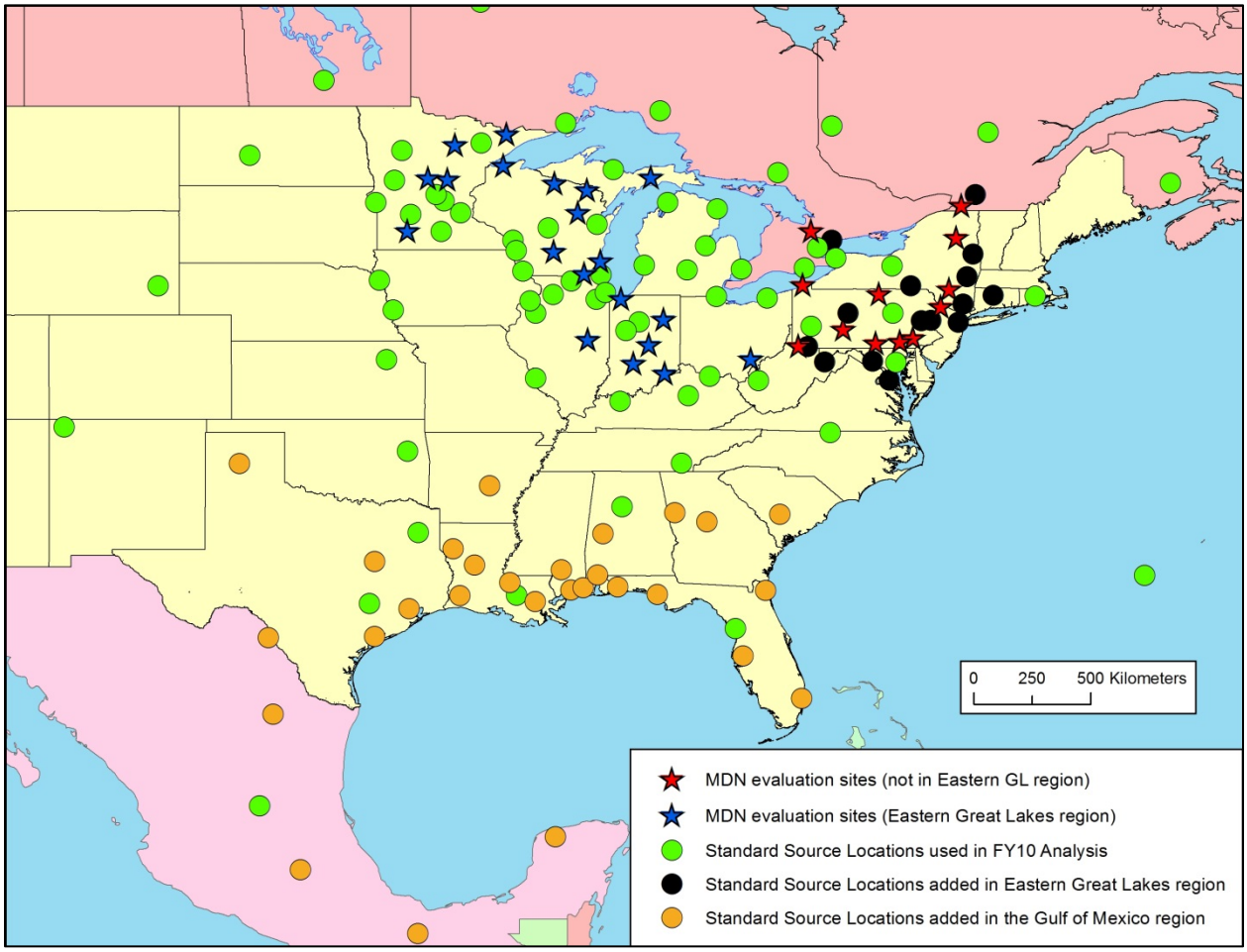

Figure 118. Additional standard source locations added for a complementary Gulf of Mexico analysis, along with the locations added in the eastern Great Lakes region

4.2. Model evaluation

The primary model evaluation approach used in the FY10 baseline analysis was to consider data from wet deposition measurement sites in the Mercury Deposition Network (MDN) in the Great Lakes region. A total of 32 sites with data for 2005 were used, including 20 in the western and central Great Lakes region and 12 in the eastern Great Lakes region, generally downwind of the Great Lakes. The essential evaluation results are shown below for the EDAS-136 analysis (Figure 119), the NARR-136 analysis (Figure 120), the NARR-151 analysis (Figure 121) and the NARR-179 analysis (Figure 122). As in the FY10 baseline analysis, we have considered different methods in comparing the model predictions with the ambient measurements. In one method, no adjustment was made to any of the model-predicted wet deposition estimates. In another, the portion of the wet deposition estimates at the MDN sites that was estimated using the EDAS-40km or NARR-36km dataset was adjusted proportionally to balance out the precipitation "error" in the EDAS-40km or NARR-36km data. In a third method, a comparable adjustment was made for the proportion of the wet mercury deposition at the MDN sites for which the NCEP/NCAR Global Reanalysis was utilized. In a fourth method, both of the adjustments in the previous two methods were made. In this FY11 analysis, we also considered variations introduced by basing the adjustment on the precipitation measured at the MDN site by the rain-gauge, versus basing the adjustment on maximum value of the precipitation measured by the rain gauge and the mercury collector itself. The various datasets and precipitation comparisons are discussed in more detail above (e.g., see page **Error! Bookmark not defined.**).

It is recognized that the impact of the precipitation "errors" in the meteorological datasets will introduce complex, non-linear deviations in the simulations. For example, over- or under-estimates of precipitation along the transport path of an air parcel making its way from the emissions source to the MDN site will have an impact on the modeled wet deposition at the MDN site, even if the model-input and measured precipitation matched perfectly at the site. So, the approaches described above involving the measured/model-input precipitation ratio at any given site are clearly oversimplifications. This simple methodology can be considered to provide an approximate estimate of the order of magnitude of the uncertainty introduced by the inherent precipitation biases in the input meteorological data.
In the model evaluation figures below, the values and "error bars" shown are the average and range, respectively, of the estimates made using the various adjustment methods discussed above. In the figures (and in the summary, Table 4), best-fit linear regressions for the central/western Great Lakes MDN sites and eastern Great Lakes region MDN sites are shown, along with the "slope", "intercept", and "R^2" of the regression in each case. If the modeled data matched the measurements perfectly, the slope would be "1", the intercept "0", and the R2 would be "1".

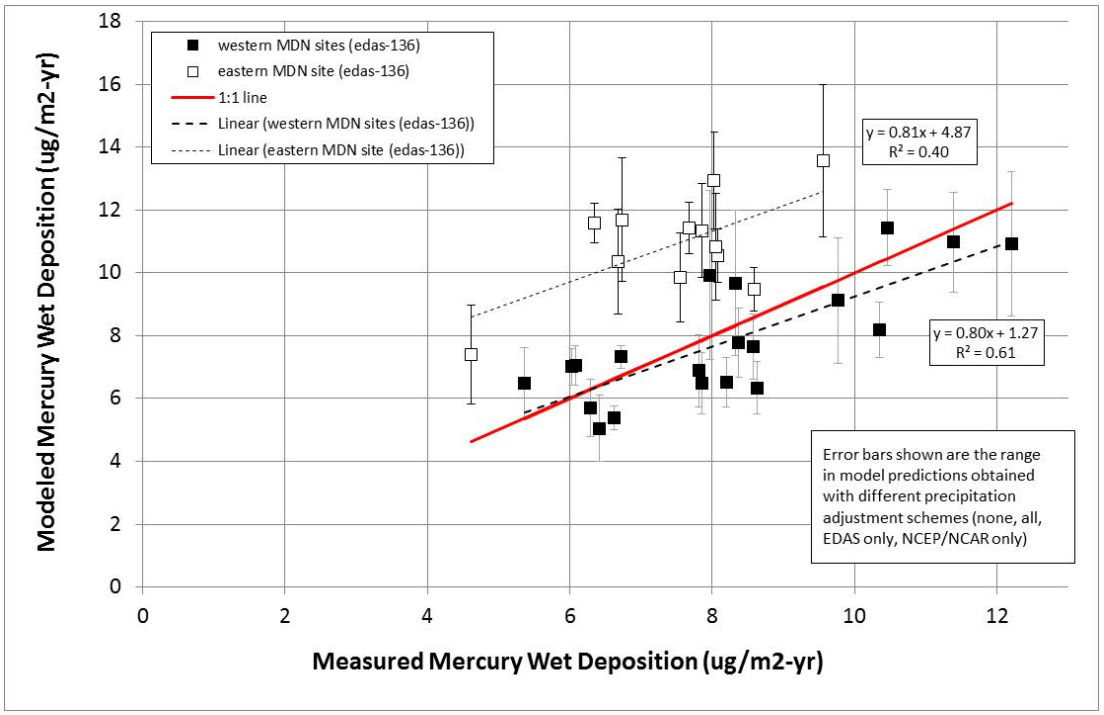

Figure 119. Comparison of model predictions with wet deposition measurements in the Great Lakes region using the EDAS-136 analysis

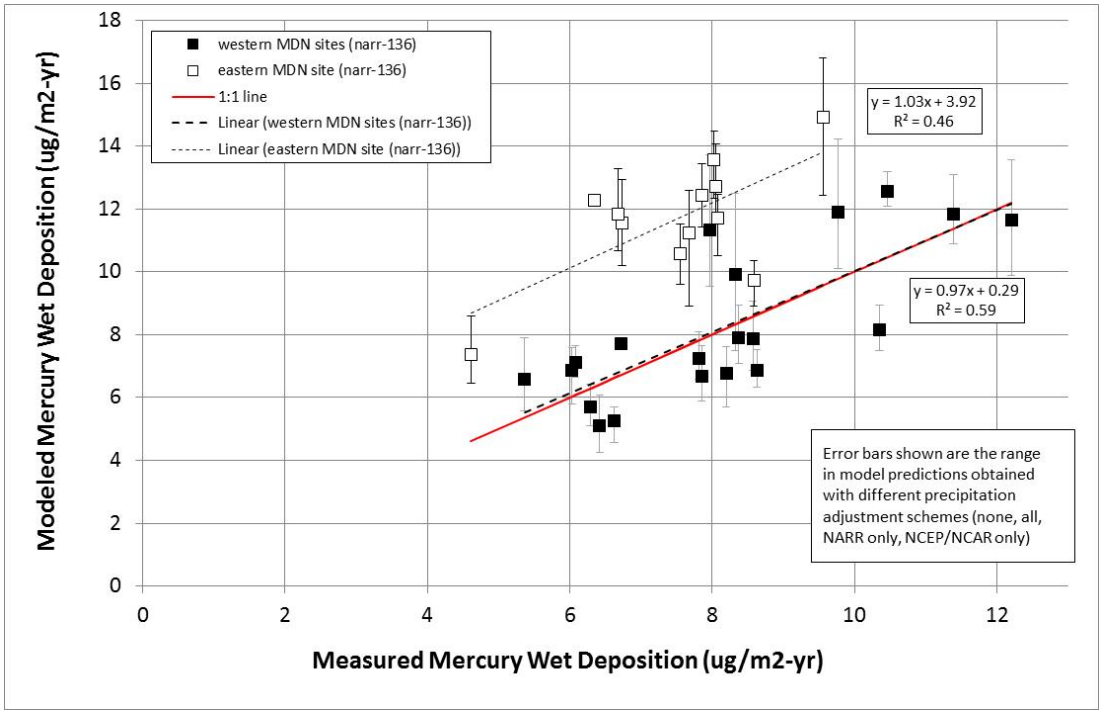

Figure 120. Comparison of model predictions with wet deposition measurements in the Great Lakes region using the NARR-136 analysis

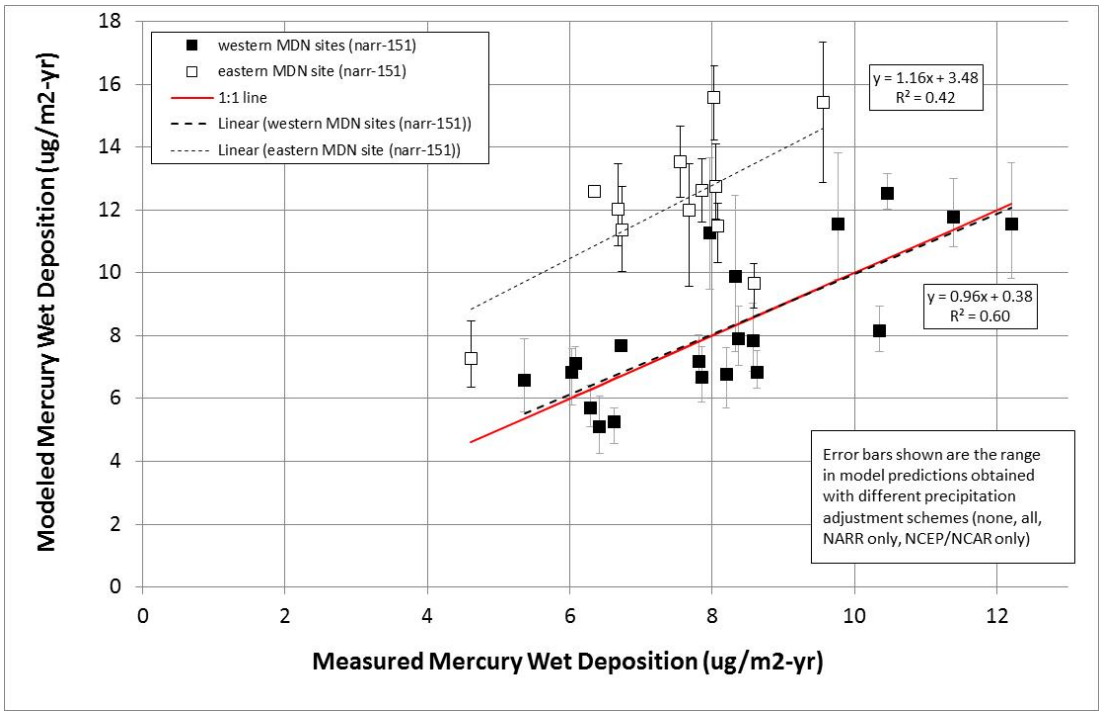

Figure 121. Comparison of model predictions with wet deposition measurements in the Great Lakes region using the NARR-151 analysis

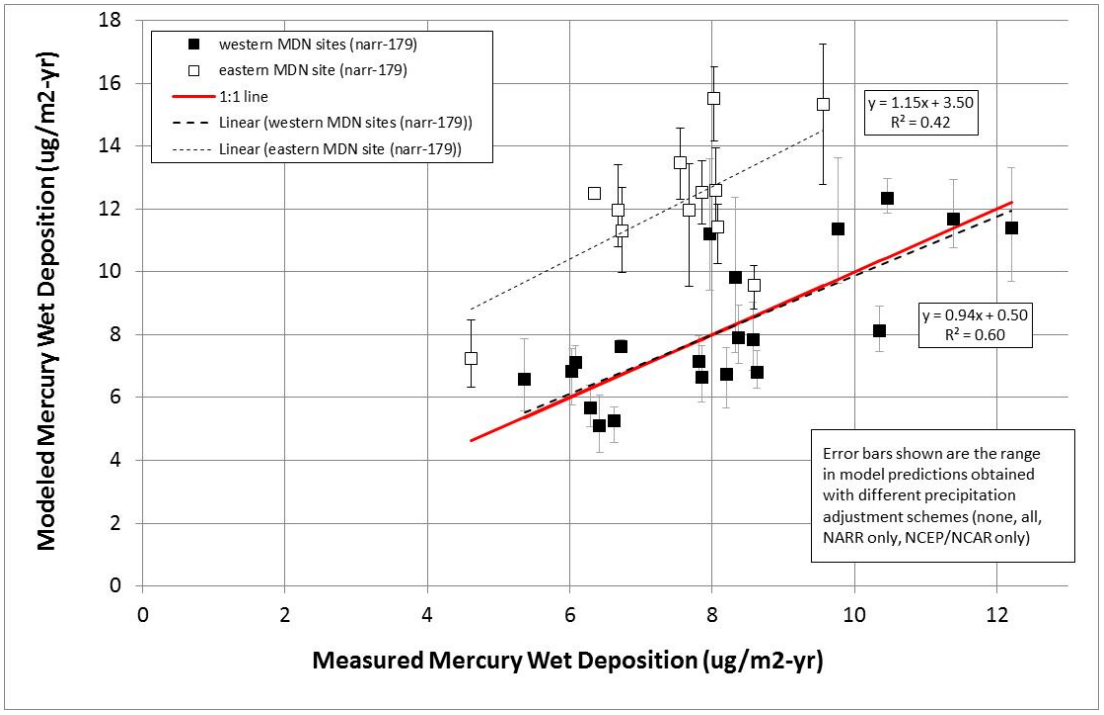

Figure 122. Comparison of model predictions with wet deposition measurements in the Great Lakes region using the NARR-179 analysis

The following overall findings can be observed from the model evaluation figures and Table 4 below:

- The consistency of the model-predicted and ambient measurements for the 20 MDN sites in the central and western Great Lakes region – already very reasonable in the EDAS-136 (baseline, FY10) analysis – improved slightly in the new variations. The slope went from 0.80 in the EDAS-136 baseline to 0.94-0.97 (very close to the ideal, "1") in the new variations using the NARR meteorological data. The "intercept" (the value of wet deposition where the best-fit straight line crosses the axis) improved from 1.27 $\mu g/m^2$-yr in the EDAS-136 baseline down to 0.29-0.50 $\mu g/m^2$-yr, getting much closer to the ideal, "0".

- For the central and western GL region MDN sites, the primary improvement was seen by changing from the EDAS to the NARR meteorological dataset, i.e., in comparing the EDAS-136 with the NARR-136 analysis. Adding additional standard source locations (i.e., the NARR-151 and NARR-179 analyses) did not result in further improvements, and in fact, showed very slightly worse performance than the NARR-136 analysis.

- For the 12 sites in the eastern Great Lakes region, the results got slightly better with the various NARR-based analyses as compared to the EDAS-136 analysis. The slope generally got closer to "1" (e.g., 1.03 in the NARR-136 analysis), the intercept got smaller, and the correlation coefficient R^2 got bigger.

- However, the model performance for these 12 sites in the eastern Great Lakes region did not improve significantly, and the tendency of the modeling analysis to over-predict the wet deposition flux at these sites remained.

Table 4. Characteristics of linear regressions comparing modeled and measured values at MDN sites in the Great Lakes region

Overall simulation variation	Central and Western GL Region MDN sites (n=20)			Eastern GL Region MDN sites (n=12)		
	Slope	Intercept	R^2	Slope	intercept	R^2
EDAS-136	0.80	1.27	0.61	0.81	4.87	0.40
NARR-136	0.97	0.29	0.59	1.03	3.92	0.46
NARR-151	0.96	0.38	0.60	1.16	3.48	0.42
NARR-179	0.94	0.50	0.60	1.15	3.50	0.42

4.3. Overall deposition to the Great Lakes and source-attribution for the largest contributors

The various calculation methodologies described above were used to estimate the atmospheric mercury deposition to each of the Great Lakes and their watersheds. The overall results for Lake Erie and the Lake Erie watershed are shown in Figure 123 and Figure 124, respectively. In these figures, the left panel shows the atmospheric mercury deposition flux ($\mu g/m^2$-yr) for each calculation variation and the right panel shows the percent-of-total modeled flux for the same variations. Source attribution for the estimated deposition is estimated for anthropogenic emissions from the U.S., Canada, Mexico, China, India, and all other countries (as a group), as well as ocean-re-emissions of previously deposited anthropogenic mercury and natural emissions.

It can be seen from these figures that the patterns for Lake Erie and the Lake Erie watershed are similar. Examination of the left panel in each figure shows that the NARR-136 results show less deposition than the EDAS-136 results. The largest difference is seen to be in the contribution from the U.S. As might be expected, the addition of extra standard source locations (SSL's) in the Gulf of Mexico (GOM) region (NARR-GOM) did not introduce significant changes into the estimated deposition. The addition of additional standard source locations in the eastern Great Lakes region (NARR-151) caused a slight decrease in deposition to Lake Erie but little is changed for deposition to its watershed. The inclusion of the additional GOM SSL's did not introduce any changes from this NARR-151 simulation (i.e., comparison of NARR-179 vs. NARR-151). The use of significantly larger terrestrial and ocean-based re-emissions of previously deposited anthropogenic mercury (2000 Mg/yr vs. 1250 Mg/yr for ocean re-emissions; 2000 Mg/year vs. 750 Mg/yr for terrestrial re-emissions) caused an increased deposition in all variations of roughly 20%.

Examination of the right panel in each of the figures show that there is an decrease in the U.S.-caused fraction of the deposition in the NARR-136 vs. EDAS-136 results, with the decrease being much greater for the watershed than for direct deposition to Lake Erie. While there are bigger variations seen for the watershed allocation fractions than for the lake allocation fractions, the overall pattern of the deposition allocations is not changed dramatically. For Lake Erie, the U.S.-caused fraction of deposition is the largest contributor, on the order of 35-45%. China contributes on the order of 10-15% in all of the calculation variations. Contribution ranges for other countries and for ocean re-emissions and for natural emissions are similarly consistent among the different variations. This finding suggests that the overall source-attribution results are reasonable robust. Even relatively significant changes in calculation methodology, the relative contributions from key contributors are not dramatically changed. This is an important finding for policy considerations.

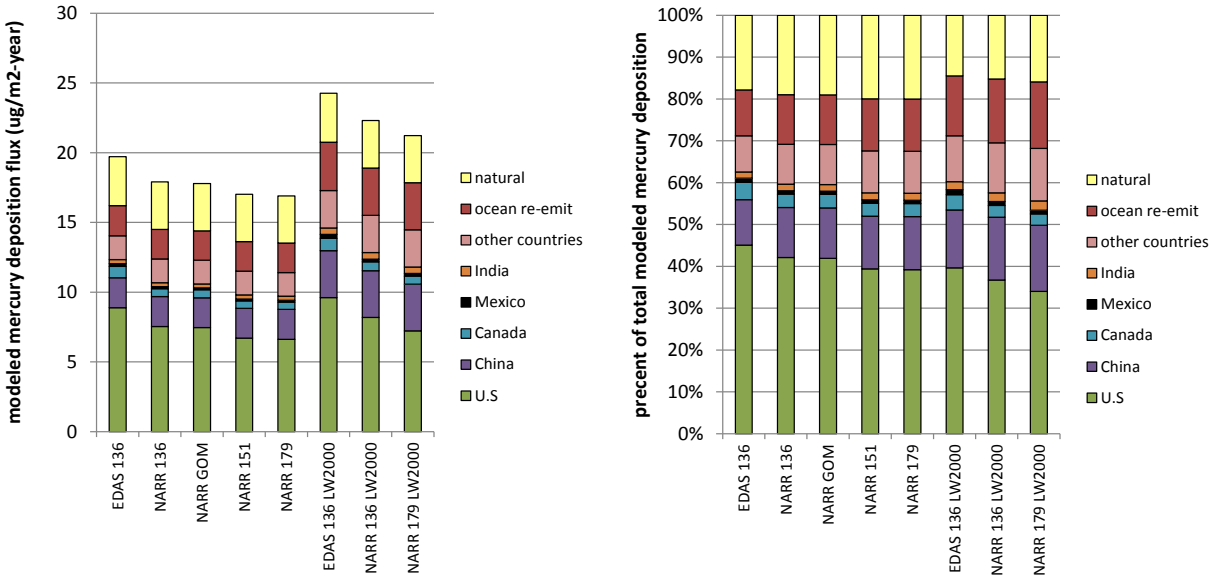

Figure 123. Modeled mercury deposition to Lake Erie

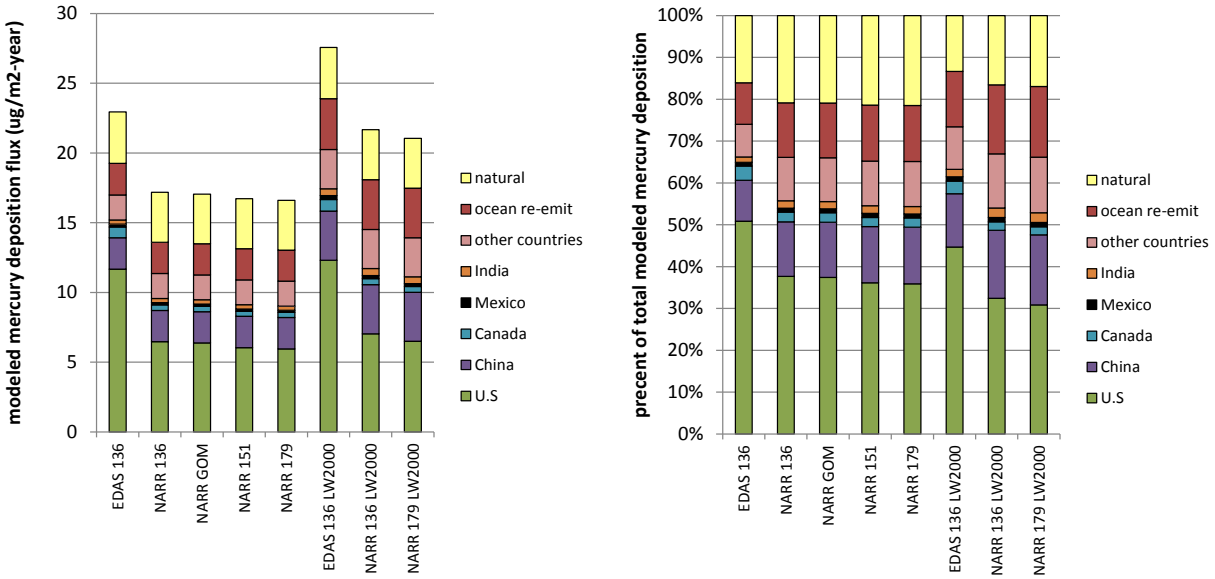

Figure 124. Modeled mercury deposition to the Lake Erie watershed

Comparable data for atmospheric mercury deposition to Lake Michigan are shown in Figure 125 and Figure 126 below. The responses of the simulated deposition to changes in methodology are similar to that observed for Lake Erie, described above. First, there is a decrease in deposition – primarily due to decreased U.S.-attributed deposition – in the change from EDAS to NARR meteorological data. Additional standard source locations cause even less change in simulated deposition than the minor changes seen for Lake Erie. The use of higher re-emissions estimates causes higher fluxes, as would be expected. Similar to Lake Erie, examination of the right-hand panels in the figures shows that the overall source-attribution fractions are not dramatically affected over the range of methodological variations examined. The largest difference is seen between the earlier EDAS-driven baseline (EDAS-136) and the NARR-driven analysis with increased re-emissions, with U.S. contributions falling from ~42% to about ~23%.

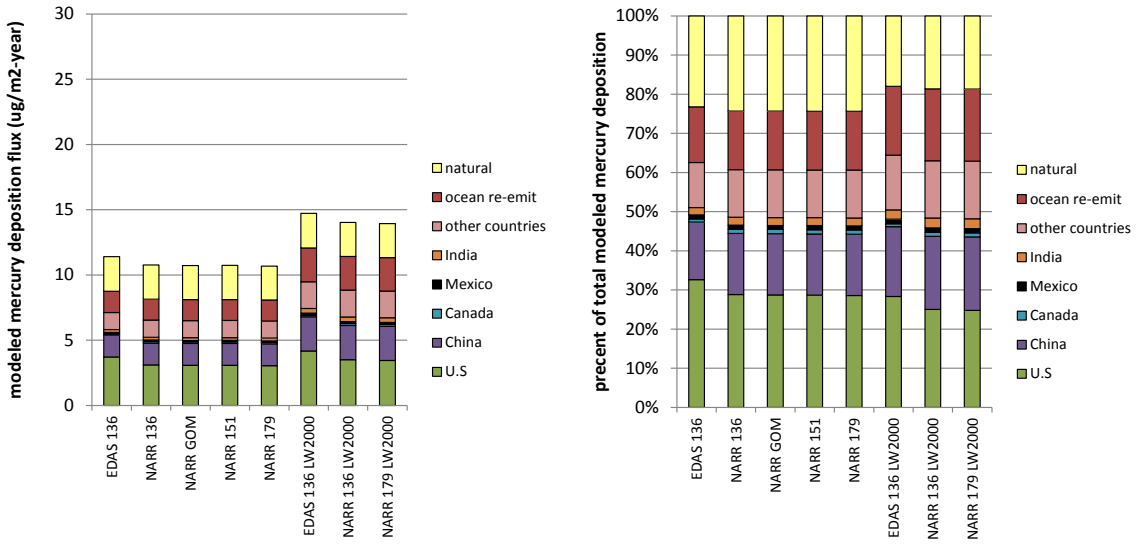

Figure 125. Modeled mercury deposition to Lake Michigan

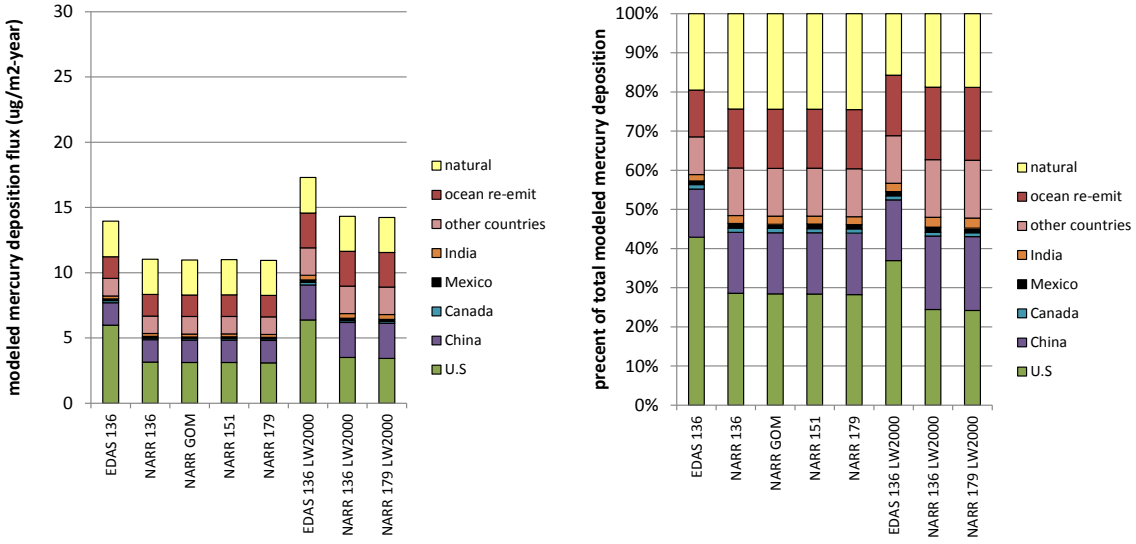

Figure 126. Modeled mercury deposition to the Lake Michigan watershed

Analogous data for atmospheric mercury deposition to Lake Superior are shown in Figure 127 and Figure 128 below. For Lake Superior and its watershed, the simulated deposition is not significantly changed when NARR rather than EDAS meteorological data are used to drive the HYSPLIT-Hg model. Like Erie and Michigan, additional SSL's do not significantly change the results, but increased re-emissions does lead to higher deposition fluxes. Examination of the right-hand panels in the figures shows that the overall source-attribution fractions are not dramatically affected over the range of methodological variations examined. The U.S. contribution is ~10% for all of the variations.

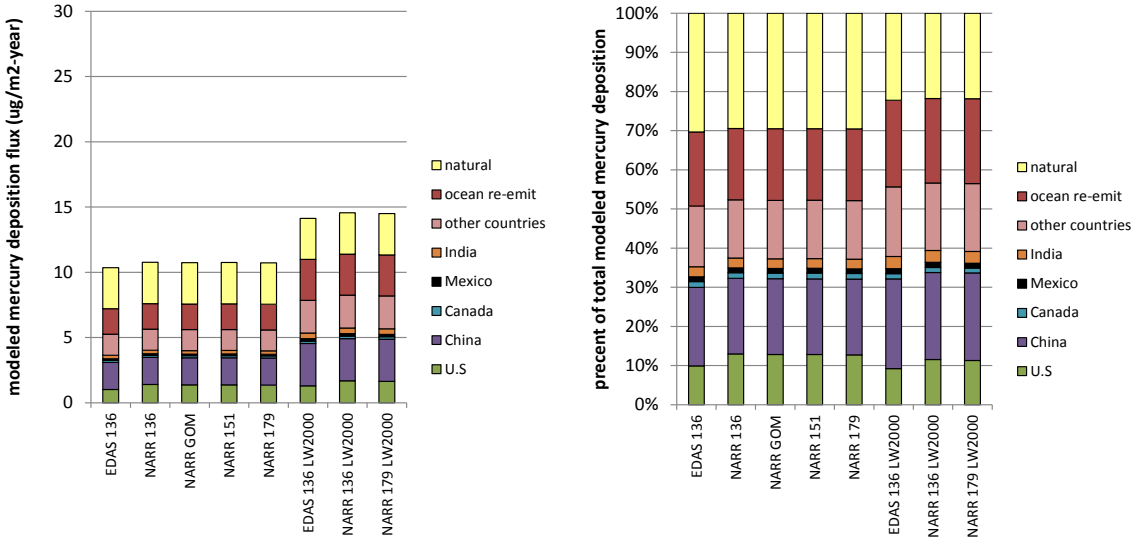

Figure 127. Modeled mercury deposition to Lake Superior

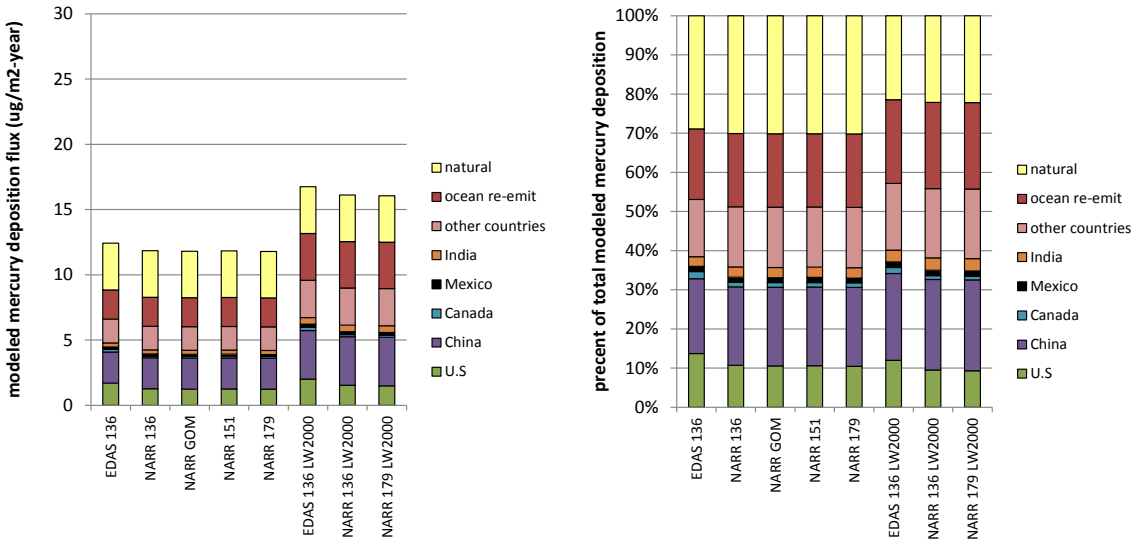

Figure 128. Modeled mercury deposition to the Lake Superior watershed

Data for atmospheric mercury deposition to Lake Huron are shown in Figure 129 and Figure 130 below. For Lake Huron's watershed, the simulated deposition to the watershed is decreased in changing from EDAS to NARR meteorological data, but the deposition to the lake itself is slightly increased. Similar to the other lakes discussed above, additional SSL's do not significantly change the results, but increased re-emissions does lead to higher deposition fluxes. Examination of the right-hand panels in the figures shows that the overall source-attribution fractions are not dramatically affected over the range of methodological variations examined. The U.S. contribution is on the order of ~20% for most of the variations. The largest difference in U.S. contribution fraction is between the EDAS-136 and the NARR-179-LW2000 (increased re-emissions), falling from ~27% down to ~16%.

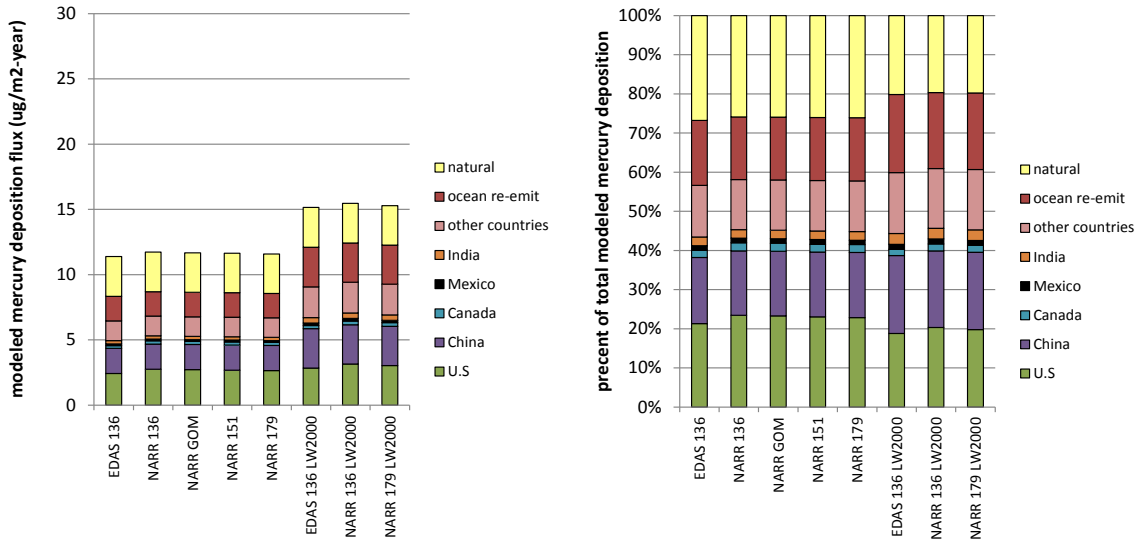

Figure 129. Modeled mercury deposition to Lake Huron

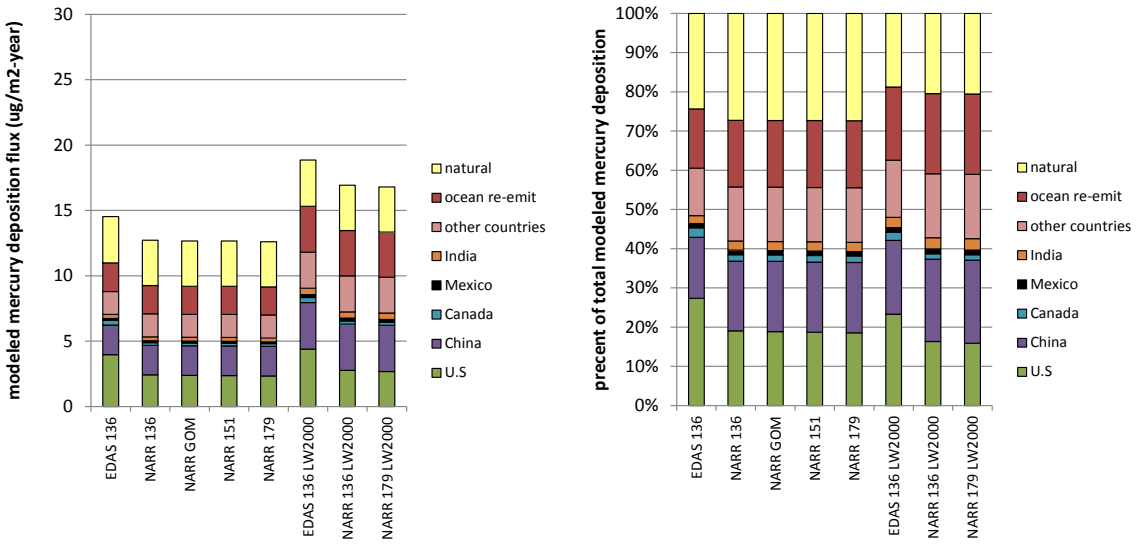

Figure 130. Modeled mercury deposition to the Lake Huron watershed

Model results for atmospheric mercury deposition to Lake Ontario are shown in Figure 131 and Figure 132 below. The results are similar to Lake Huron's, in that the watershed deposition shows a decrease moving from EDAS to NARR meteorological data, but deposition to the lake itself does not show a significant change. For Lake Ontario, the additional SSL's in the eastern Great Lakes region (e.g., NARR-151 vs. NARR-136) causes a small reduction in modeled deposition. As would be expected, increased re-emissions lead to higher deposition fluxes. As with the other lakes, the right-hand panels in the figures show that the overall source-attribution fractions are not dramatically affected over the range of methodological variations examined. The U.S. contribution is on the order of ~20%-25% for most of the variations. The largest difference in U.S. contribution fraction is for the watershed, between the EDAS-136 and the NARR-179-LW2000 (increased re-emissions), falling from ~34% down to ~18%.

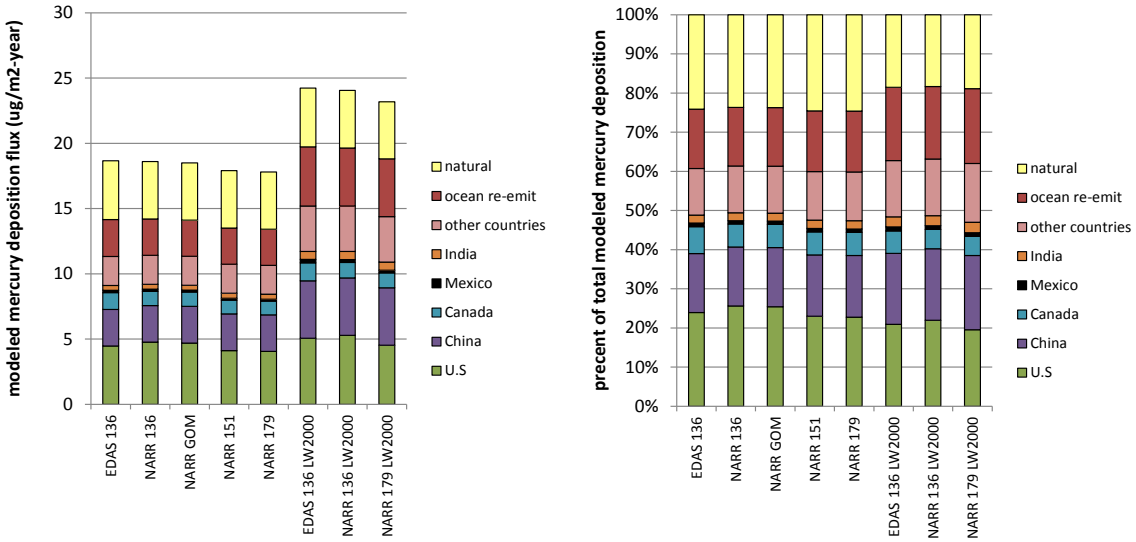

Figure 131. Modeled mercury deposition to Lake Ontario

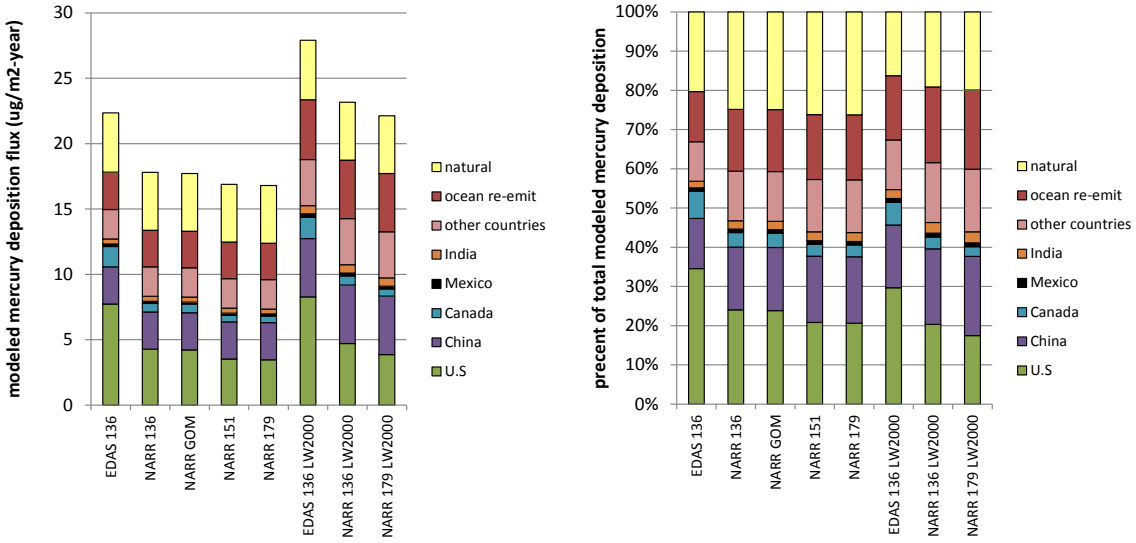

Figure 132. Modeled mercury deposition to the Lake Ontario watershed

Overall model results for atmospheric mercury deposition to the Great Lakes Basin – defined as the sum of the deposition to all five lakes and their watersheds – is shown in Figure 133 below. These overall results follow a similar pattern, in general, to the individual-lake results presented above. There is decreased deposition moving from EDAS to NARR meteorological data, largely due to decreased U.S.-attributed deposition. Additional SSL's do not cause significant variations. As with all the individual-lake results, increased re-emissions lead to higher deposition fluxes, but the right-hand panel shows that the overall source-attribution fractions are not dramatically affected over the range of methodological variations examined. The U.S. contribution is on the order of ~20%-25% for most of the variations. The largest difference in U.S. contribution fraction is between the EDAS-136 and the NARR-179-LW2000 (increased re-emissions), falling from ~32% down to ~19%.

It can be seen from examination of the figure below and from preceding figures in this section that For the Great Lakes Basin as a whole, and in for the individual Great Lakes and their watersheds, the doubling of mercury re-emissions from 2000 Mg/year to 4000 Mg/year causes an increase in deposition flux on the order of ~25%

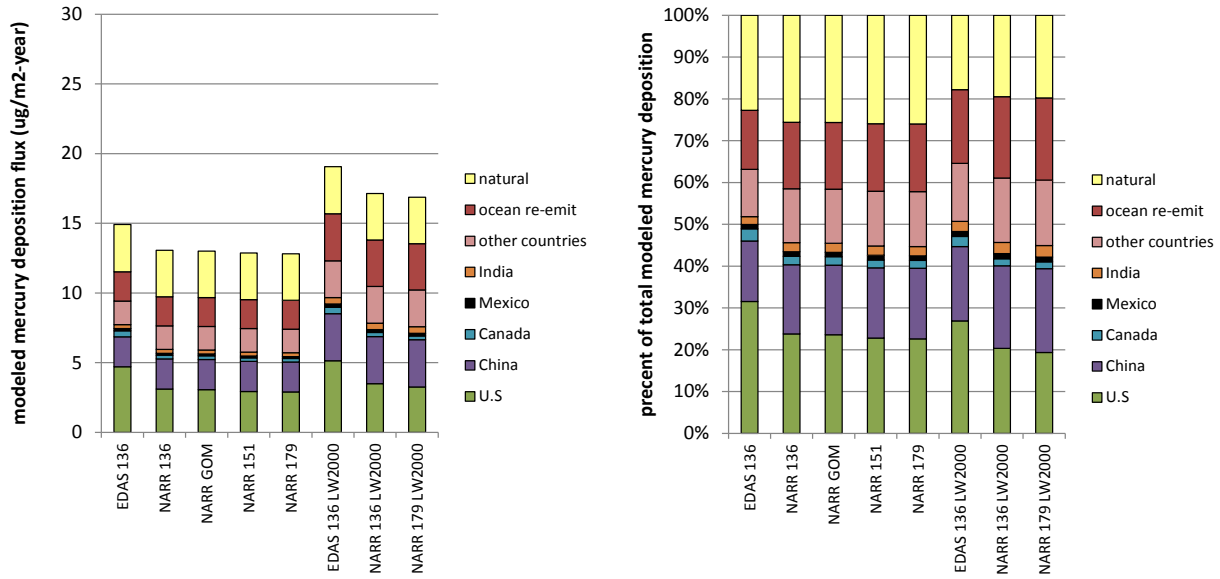

Figure 133. Modeled mercury deposition to the Great Lakes Basin

4.4. Deposition arising from emissions at different distances from the lakes

Modeling results showing the deposition flux – amount and fraction – arising from different distance ranges from the centroid of each lake and watershed are shown in Figure 134 through Figure 143 below. The results are very similar to those presented in the previous section, and it is seen that in the cases in which switching from EDAS to NARR makes a difference, the largest contributor to this difference is the change in contribution from emissions sources less than 500km from the centroid of the lake or watershed. As with the overall results presented above, additional standard source locations do not in general introduce significant changes in the results. The exception is the Lake Ontario watershed, which, as discussed earlier, would be expected to be influenced by additional SSL's in the eastern Great Lakes region. Increased re-emissions leads to increased fluxes, but does not lead to large differences in the fractions attributed to each distance range (right-hand panels of each figure). The largest impact of nearby sources (<500 km) is seen for Lake Erie and its watershed, for which ~30-35% of the modeled deposition arises from emissions less than 500 km from the center of the lake or the watershed. The smallest model-estimated contribution from nearby sources is seen for Lake Superior and its watershed, for which only about ~2-3% of the modeled deposition comes from such sources.

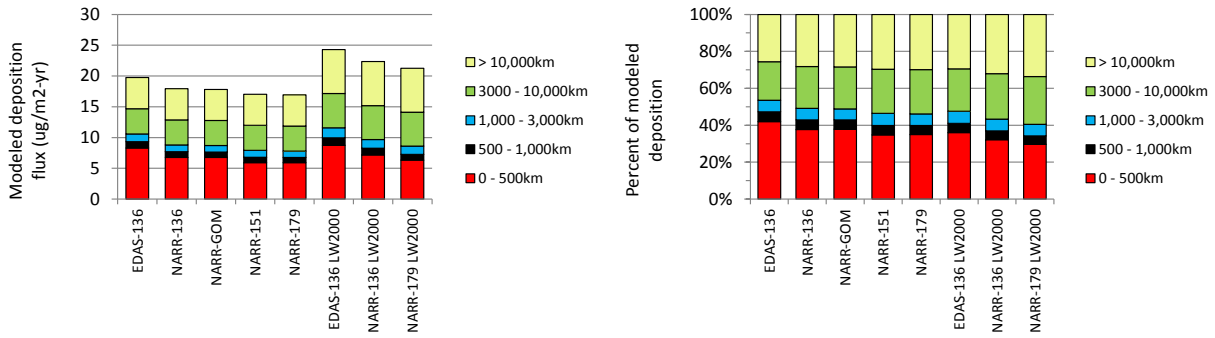

Figure 134. Mercury deposition arising from emissions at different distances from the center of Lake Erie

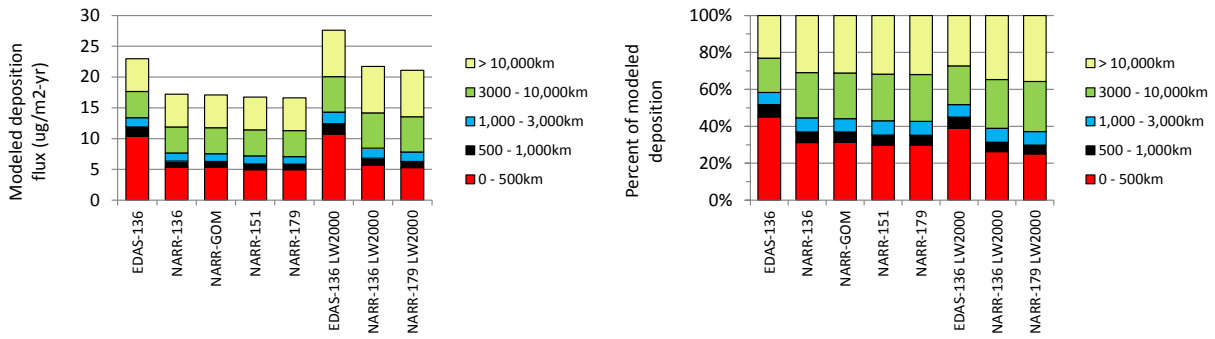

Figure 135. Mercury deposition arising from emissions at different distances from the center of the Lake Erie watershed

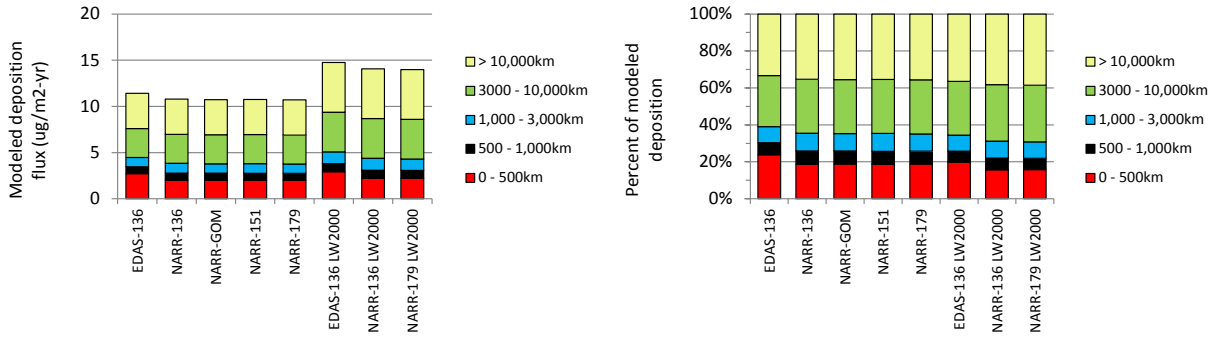

Figure 136. Mercury deposition arising from emissions at different distances from the center of Lake Michigan

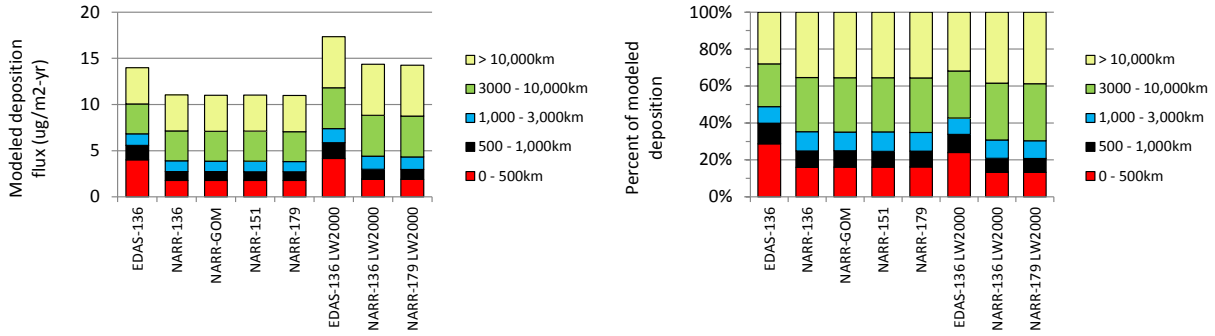

Figure 137. Mercury deposition arising from emissions at different distances from the center of the Lake Michigan watershed

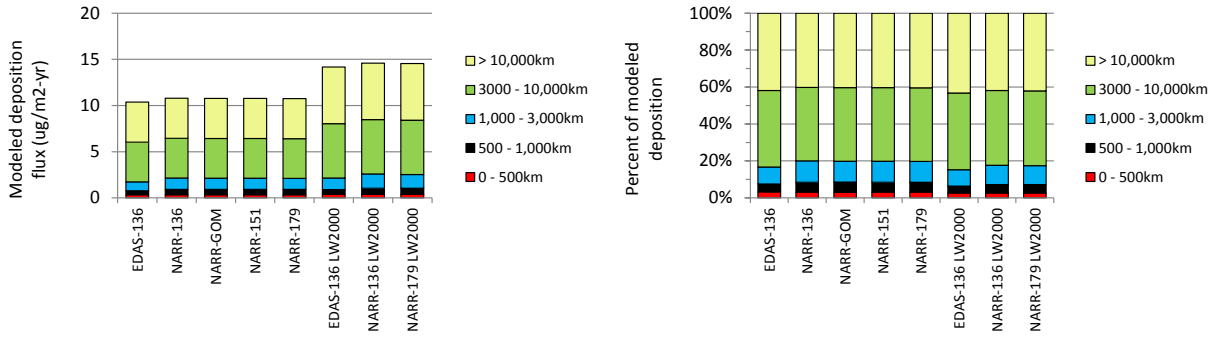

Figure 138. Mercury deposition arising from emissions at different distances from the center of Lake Superior

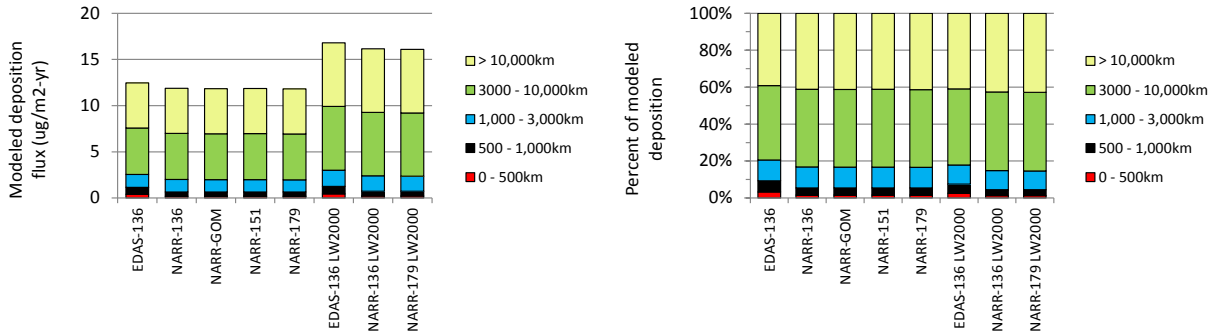

Figure 139. Mercury deposition arising from emissions at different distances from the center of the Lake Superior watershed

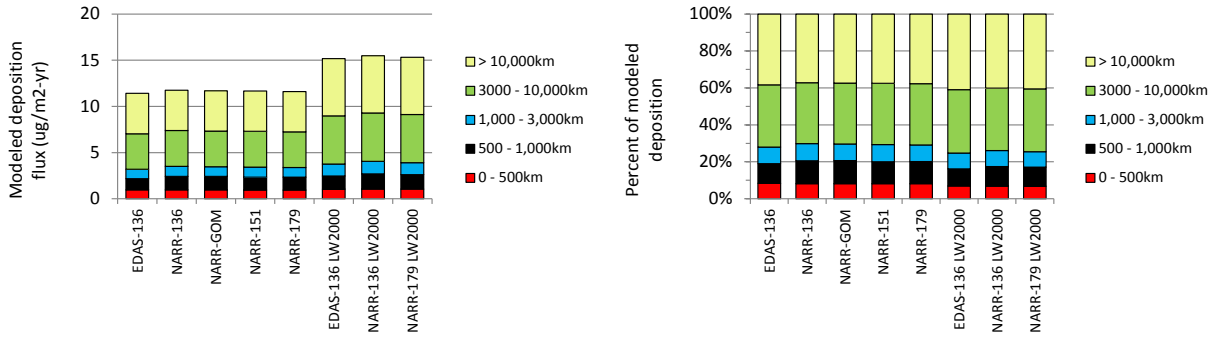

Figure 140. Mercury deposition arising from emissions at different distances from the center of Lake Huron

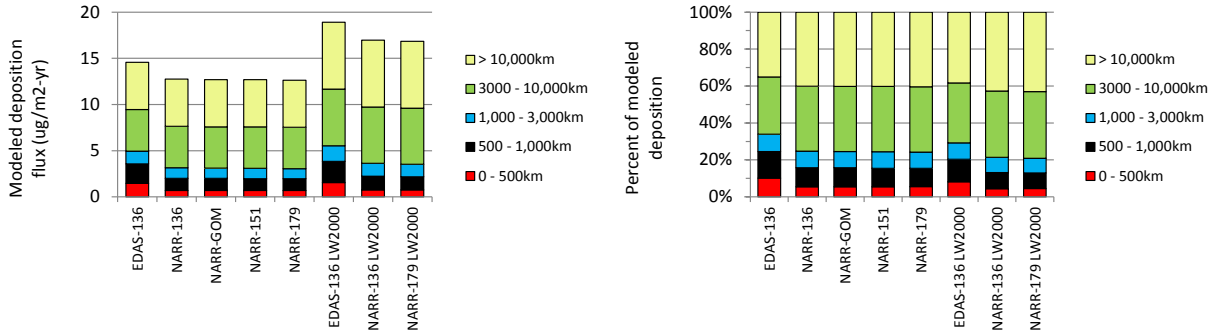

Figure 141. Mercury deposition arising from emissions at different distances from the center of the Lake Huron watershed

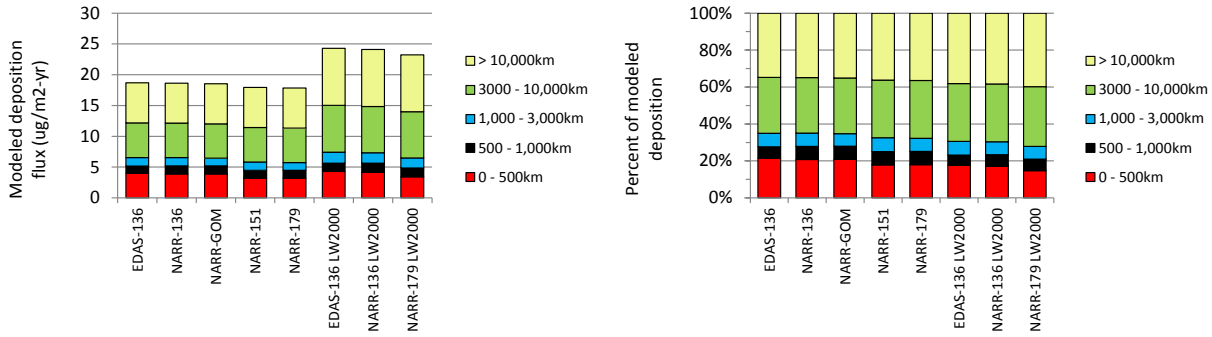

Figure 142. Mercury deposition arising from emissions at different distances from the center of Lake Ontario

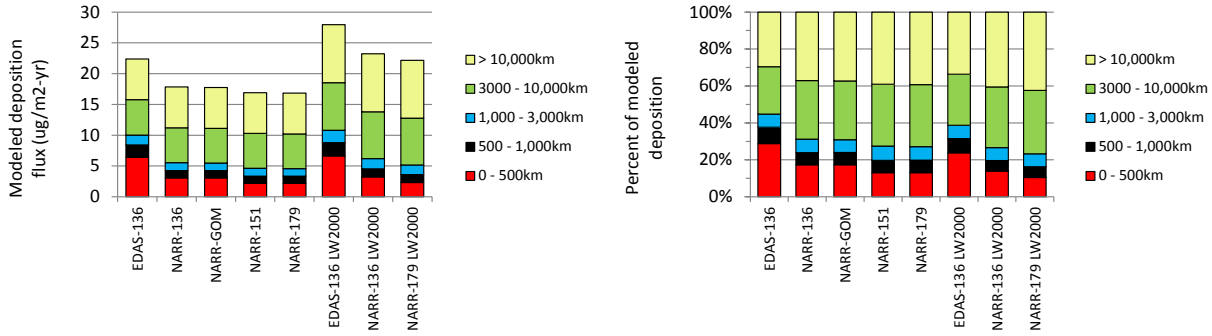

Figure 143. Mercury deposition arising from emissions at different distances from the center of the Lake Ontario watershed

4.5. Influence of different interpolation methodologies

As described in the FY10 report (Cohen et al., 2011), an interpolation procedure is used to estimate detailed source-receptor relationships. The impact of any given source – at other locations – on the Great Lakes was estimated based on a weighted average of the impacts of the nearest explicitly modeled *standard source locations* nearest to that given source. This procedure is illustrated conceptually in Figure 144.

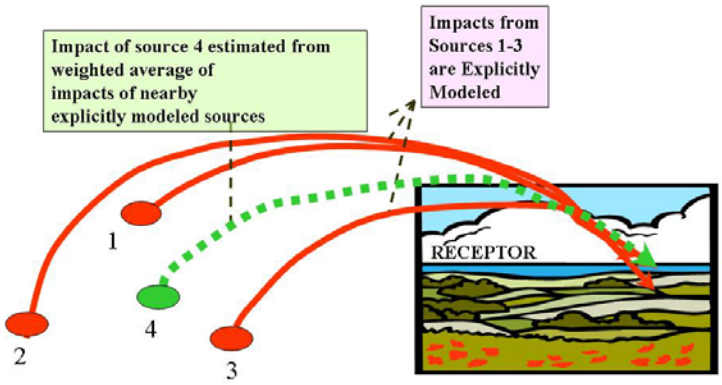

Figure 144. Spatial interpolation schematic

As further described in Cohen et al (2011), the impact of a source emitting a mixture of Hg^0, Hg(II), and Hg(p) was estimated based on a linear combination of these pure-component unit emissions simulations. An example of this procedure is illustrated in Figure 145.

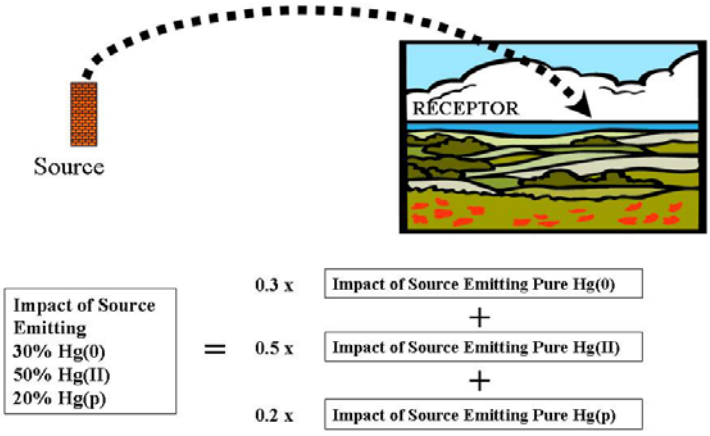

Figure 145. Chemical Interpolation

In this section, the influence of the spatial interpolation methodology on the modeling results is examined, for the NARR-179 analysis. The spatial interpolation approach in this work is characterized by three parameters: (a) the number of closest standard source locations (SSL's) used in the weighted average; (b) the exponent on the angular orientation weighting factor; and (c) the exponent on the distance-related weighting factor. In essence, if the exponent on a given factor is increased, its importance to the weighting procedure is increased. The default spatial interpolation methodology used the 3 closest SSL's, with exponents of "2.0" for both the angular orientation and distance weighting factors.

The interpolation parameters were varied in the following ways:

- Number of SSL's used for interpolation: 2, 3, 4
- Exponent on angular orientation weighting factor: 1.5, 2.0, 2.5
- Exponent on distance weighting factor: 1.5, 2.0, 2.5

The influence of these variations on the model-estimated atmospheric mercury deposition flux to each of the Great Lakes – from emissions in different distance ranges -- is presented in Figure 146 through Figure 150. In each case, the results of 27 different calculation procedures are given, representing each possible combination of the above parameters. Summary statistics for the overall total deposition flux for each lake are also provided in these figures. It can be seen from the figures that the variations in spatial interpolation parameters did not influence the modeling results in any significant way. For each lake, the standard deviation of the 27 variations was generally on the order of 1% of the mean deposition flux. It can be concluded from this analysis that the choice of spatial interpolation parameters – which is somewhat arbitrary -- does not influence the model-estimated deposition to the Great Lakes.

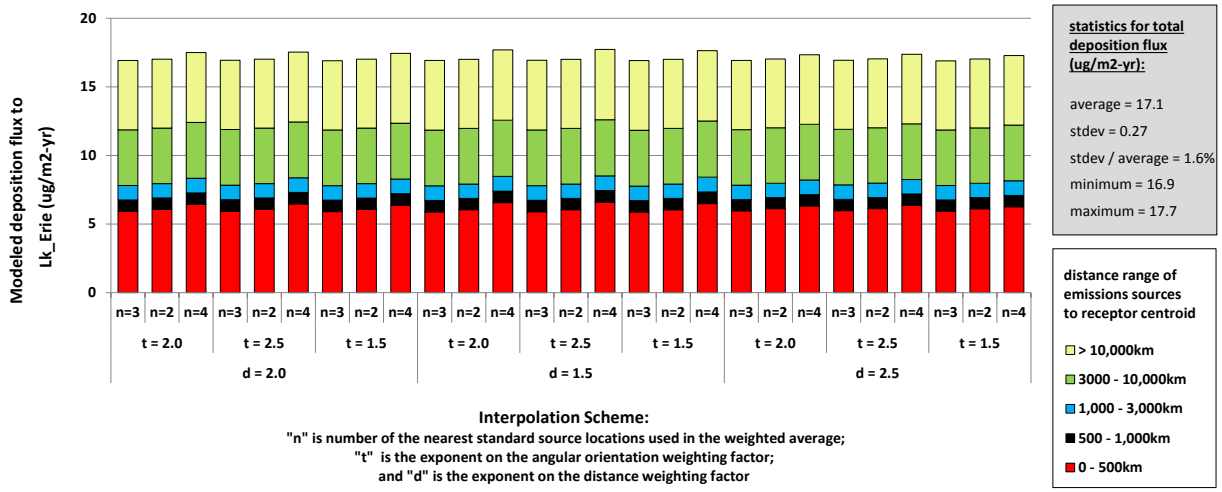

Figure 146. Influence of spatial interpolation variations on model-estimated deposition to Lake Erie

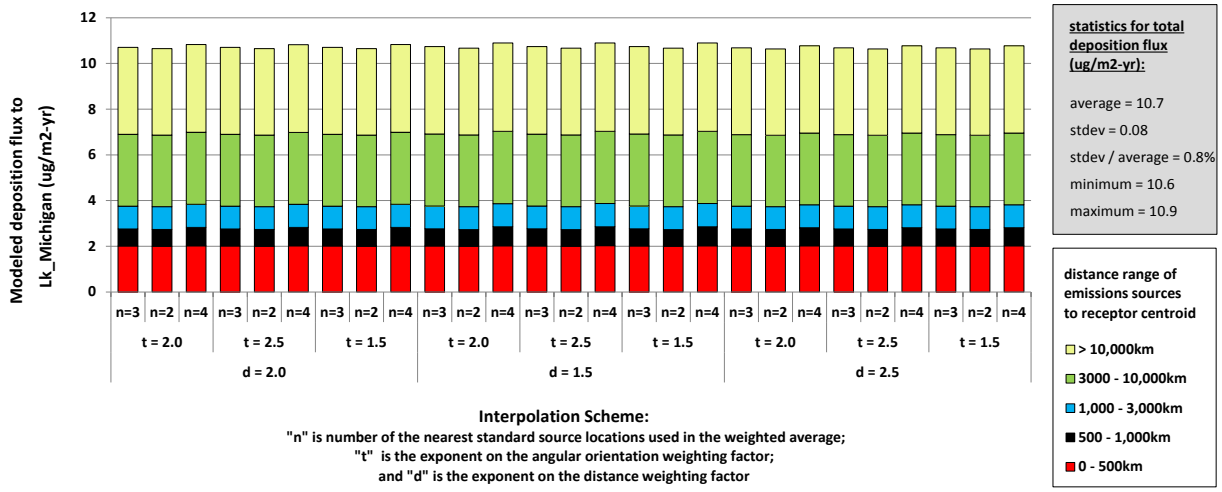

Figure 147. Influence of spatial interpolation variations on model-estimated deposition to Lake Michigan

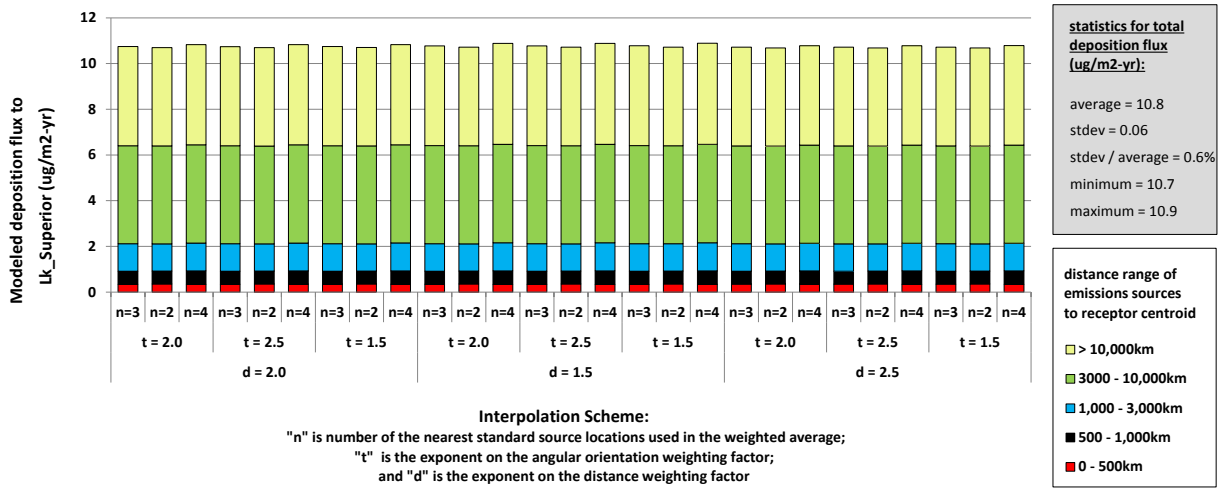

Figure 148. Influence of spatial interpolation variations on model-estimated deposition to Lake Superior

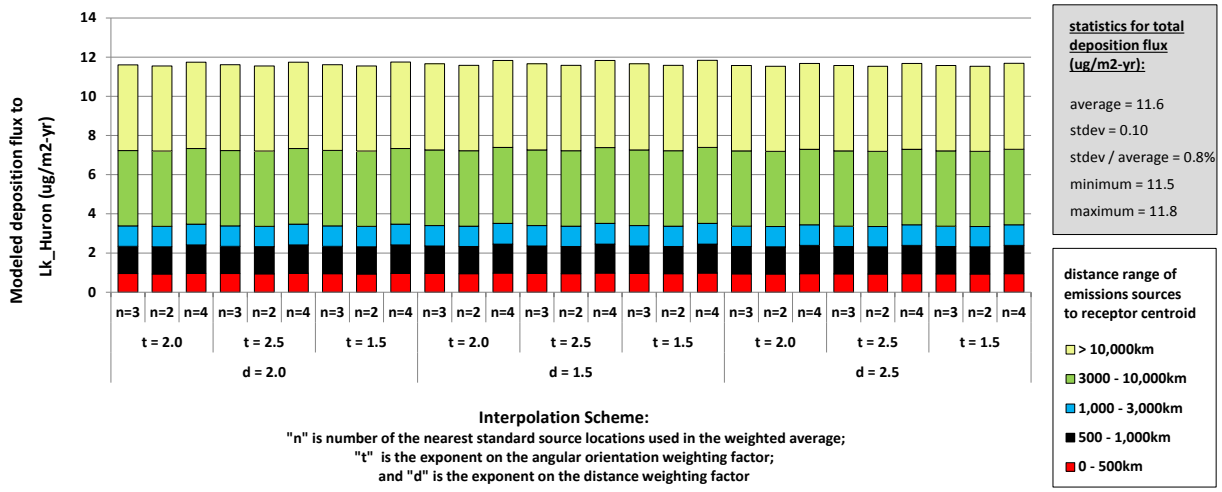

Figure 149. Influence of spatial interpolation variations on model-estimated deposition to Lake Huron

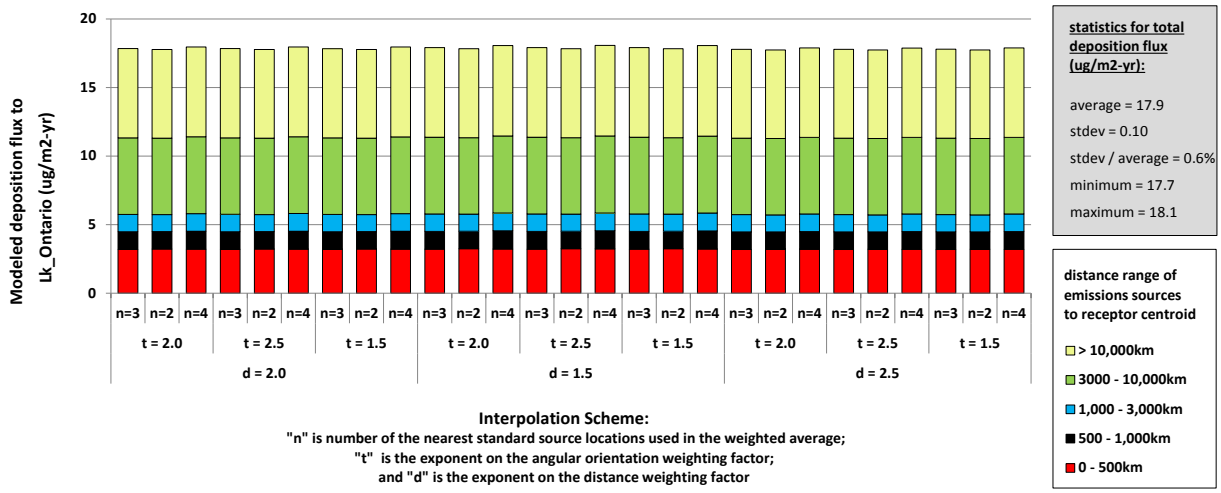

Figure 150. Influence of spatial interpolation variations on model-estimated deposition to Lake Ontario

5. Conclusions

The influence of variations in inputs, parameters, and algorithms on the model-estimated atmospheric mercury deposition – including source-attribution – to the Great Lakes has been examined. Due to computational resource constraints, only a few different overall variations in the "full" analysis could be undertaken. However, numerous variations – requiring 320 different 15-month simulations[1] -- were examined for a subset of five "illustrative" standard source locations (SSL's):

- SSL-8, on the western shore of Lake Erie, representing "local" impacts
- SSL-6, in the Ohio River Valley, representing "regional" impacts
- SSL-11, in northeast Texas, representing "national/continental" impacts
- SSL-13, in China, representing global impacts
- SSL-48, in India, also representing global impacts

Several different types of variations were investigated for these five illustrative SSL's, including input meteorological data, and dispersion, deposition, and chemical transformation methodologies. There were three variations that generally were found to cause the greatest changes in the modeling results:

- The choice of input meteorological data [NARR (North American Regional Reanalysis) vs. EDAS (Eta Data Assimilation System)]. While the EDAS data were used in the FY10 baseline analysis (Cohen et al, 2011), the NARR data appeared to be more accurate in its estimates of precipitation.

- Variations in the "WETR" parameter – affecting the wet deposition of atmospheric particles. This had contrasting influences for local-national vs. global sources. Increasing this particle wet deposition factor by a factor of 4 caused:

    - lower deposition to the Great Lakes for distant sources (SSL-13, China, and SSL-48, India), as the increased wet deposition as the mercury is being transported to the Great Lakes has a bigger impact than the increased efficiency of wet deposition once the mercury arrives at the Great Lakes region

    - increased deposition to the Great Lakes for national, regional, and local sources (SSL-11, Texas, SSL-6, Ohio River Valley, and SSL-8, western shore of Lake Erie), as the increased wet deposition as the mercury is being transported to the Great Lakes has a lower impact than the increased efficiency of wet deposition once the mercury arrives at the Great Lakes region

[1] An additional 154 simulations were carried out for these five illustrative standard source locations to examine a number of different numerical issues. A summary of the findings for these simulations is presented in the Appendix. In general, it was found that the numerical issues investigated did not significantly impact the results, with most variations on the order of a few percent of less.

- Variations in the emissions release height, primarily for the "local" impacts examined, i.e., the deposition to Lake Erie arising from emissions on its western shore (SSL-8). This finding was expected, as it is well known that local deposition can be significantly affected by release height. The default release height used in the modeling was 250 meters, characteristic of typical stack heights for coal-fired power plants, the largest mercury-emissions source category in the Great Lakes and surrounding region. It was found that changing the release height from 250m to 50m had a significant impact on the modeled Lake Erie deposition from the shoreline SSL-8. This result suggests that the impact of nearby sources to the Great Lakes may have been underestimated to a certain extent. However, the estimates for the sources with the largest mercury emissions and impacts (which typically have higher stack heights) were not strongly affected.

- Variations in dispersion and chemical transformation parameters were found to have relatively small influences

As discussed in the report, the NARR meteorological dataset is believed to be more accurate than then comparable EDAS dataset for 2005, and so the changes resulting from the use of the NARR rather than EDAS dataset to drive the HYSPLIT-Hg model can be viewed more as an "improvement" in the results rather than strictly a representation of the uncertainty associated with the choice of meteorological data.

Similarly, the impacts associated with variations in release height, while significant for near-field deposition impacts, should not be thought of strictly as an uncertainty. This is because the emissions release height used as the default was chosen to be representative of the mercury sources with the largest impacts. Thus, while a different (e.g., lower) release height was found to influence the results immediately downwind of the source, this would generally affect sources with relatively small impacts. Moreover, most of the emissions impacting the Great Lakes are not immediately upwind of a given lake. Therefore, this issue is not expected to have an overly significant impact on the overall results.

The variation if the particle-wet-deposition parameter (WETR), found to exert significant influence over the modeling results in some cases, does represent more of an uncertainty in the simulation. The "true" value of this parameter is not known accurately. However, variations in this parameter primarily affected emissions of Hg(p), which accounted for only 2% of the total emissions used as input for the analysis. Therefore, the impact on the overall results of this uncertainty is not expected to be significant.

As noted above, only a few variations in the "full-analysis" could be examined, due to computational constraints. The primary variations examined – requiring a total of 354 additional 15-month HYSPLIT-Hg simulations -- were the following:

- the use of NARR vs. EDAS meteorological data to drive the HYSPLIT-Hg model
- the use of additional standard source locations (SSL's) to reduce errors in spatial interpolation
- the use of significantly increased re-emissions
- variations in spatial interpolation methodology

The use of significantly increased mercury re-emissions (global total of 4000 Mg/year vs. 2000 Mg/year) resulted in overall total modeled mercury deposition fluxes to the Great Lakes that were increased by ~25%. The use of different spatial interpolation methodologies did not influence the results significantly.

The NARR-based analysis had results that were more consistent with mercury wet deposition measurement in the Great Lakes region. Additional SSL's resulted in only minor additional improvements in the model performance, as judged by consistency with wet deposition measurements. However, while improved, the model performance for 12 sites in the eastern Great Lakes region did not improve significantly, and the tendency of the modeling analysis to over-predict the wet deposition flux at these sites remained. The overall Great Lakes deposition results from the NARR-based analysis were somewhat different than those from the EDAS-based analysis. The most common difference was a decrease in model-estimated deposition from local and regional sources in the NARR-based simulations relative to the EDAS-based simulations.

An overall summary of the modeling results is provided below in Figure 151, which shows the overall source-attribution results for the largest variations in modeling methodology, i.e., NARR vs. EDAS, and doubling the mercury re-emissions rate. While the overall fractions of the deposition contributed by key source types and regions were impacted somewhat by the simulation variations, the source-attribution results were not dramatically affected. This suggests that the results are reasonably robust, at least from the perspective of the relative importance of different source types and source regions to the deposition of mercury to the Great Lakes basin.

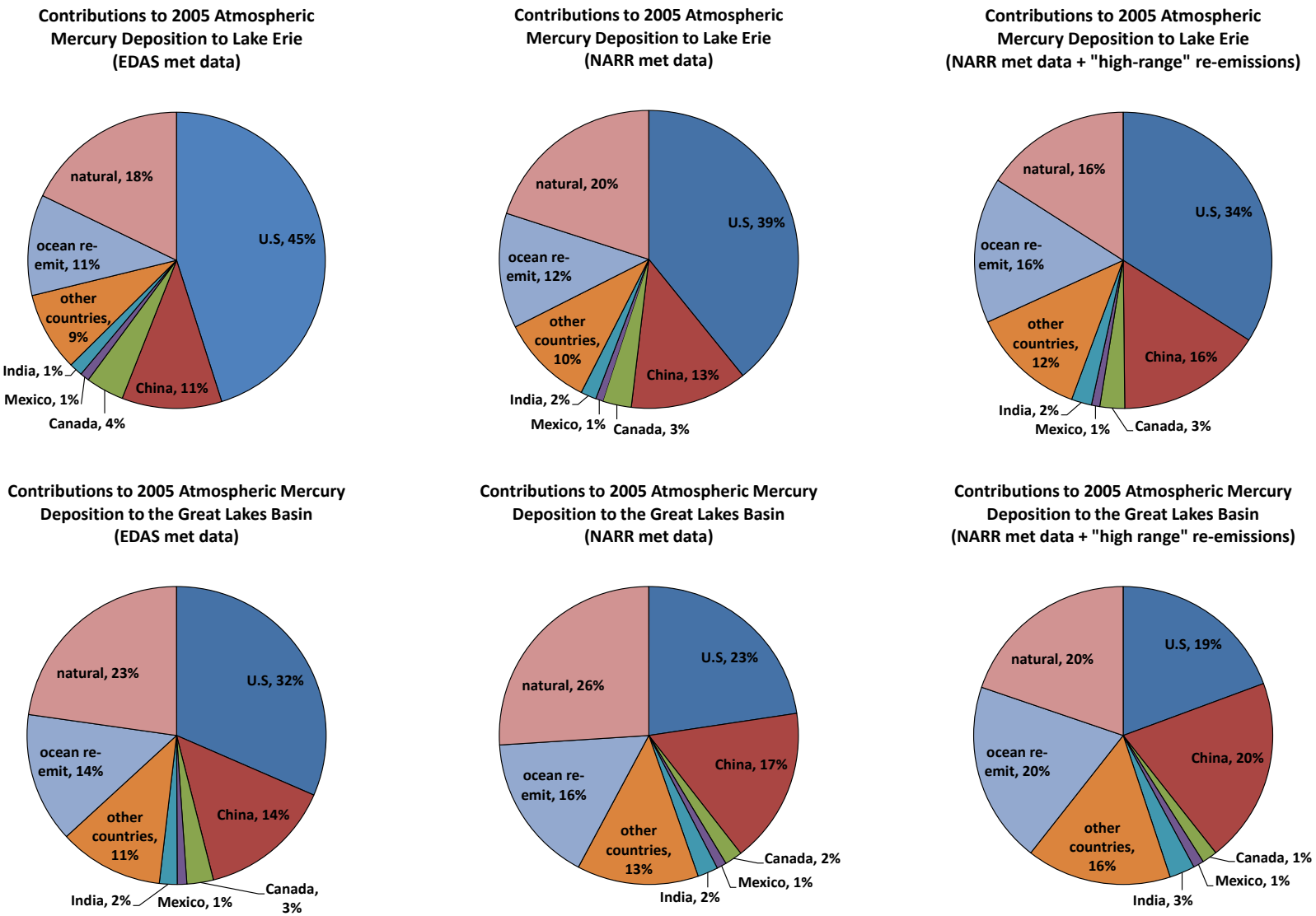

Figure 151. Overall source attribution results for Lake Erie (top row) and the Great Lakes Basin (bottom row) for largest variations in modeling methodology; 2005 baseline (left); key variations showing the largest differences (center & right)

6. References

Bullock, O.R., and Brehme, K. (2002). Atmospheric mercury simulation using the CMAQ model: formulation description and analysis of wet deposition results. *Atmos. Environ.* **36**, 2135-2146.

Calhoun, J., and Prestbo, E. (2001). Kinetic study of the gas phase oxidation of elemental mercury by molecular chlorine. Frontier Geosciences, Inc., Seattle, WA (as cited by Bullock and Brehme, 2002).

Cohen, M., R. Draxler, R. Artz (2011). *Modeling Atmospheric Mercury Deposition to the Great Lakes. Final Report for work conducted with FY2010 funding from the Great Lakes Restoration Initiative.* NOAA Air Resources Laboratory, Silver Spring, MD. Dec 16, 2011. 160 pages. Available at: http://www.arl.noaa.gov/documents/reports/GLRI_FY2010_Atmospheric_Mercury_Final_Report_2011_Dec_16.pdf

Draxler, R. R., Hess, G.D. (1998). An overview of the HYSPLIT_4 Modelling System for Trajectories, Dispersion and Deposition. *Australian Met. Mag.* 47: 295-308.

Draxler, R.R., Hess, G.D. (2010) . NOAA Technical Memorandum ERL ARL-224. DESCRIPTION OF THE HYSPLIT_4 MODELING SYSTEM. NOAA Air Resources Laboratory. Available at: http://www.arl.noaa.gov/documents/reports/arl-224.pdf

Evers, D., J. Wiener, et al. (2011a). Mercury in the Great Lakes region: bioaccumulation, spatiotemporal patterns, ecological risks, and policy. *Ecotoxicology* 20(7): 1487-1499.

Evers, D.C., Wiener, J.G., Driscoll, C.T., Gay, D.A., Basu, N., Monson, B.A., Lambert, K.F., Morrison, H.A., Morgan, J.T., Williams, K.A., Soehl, A.G. (2011b). *Great Lakes Mercury Connections: The Extent and Effects of Mercury Pollution in the Great Lakes Region*. Biodiversity Research Institute. Gorham, Maine. Report BRI 2011-18. 44 pages. http://www.briloon.org/mercuryconnections/greatlakes

Gardfeldt, K. and Jonnson, M. (2003). Is bimolecular reduction of Hg(II)-complexes possible in aqueous systems of environmental importance? *J. Phys. Chem. A* **107**, 4478-4482.

Hall, B., and Bloom, N.S. (1993). Report to the Electric Power Research Institute, Palo Alto, CA. As cited in Seigneur et al., 1994.

Hall, B. (1995). The gas phase oxidation of elemental mercury by ozone. *Water, Air, and Soil Pollution* **80**, 301-315.

Lin, C. and Pehkonen, S. (1997). The chemistry of atmospheric mercury: a review. *Atmos. Environ.* **33**, 2067-2079.

Lin, C., and Pehkonen, S. (1998). Oxidation of elemental mercury by aqueous chlorine (HOCl/OCl-): implications for tropospheric mercury chemistry. *J. Geophys. Res.* **103 (D21)** 28093-28102.

Munthe, J. (1992). The aqueous oxidation of elemental mercury by ozone. *Atmos. Environ.* **26A**, 1461-1468.

Seigneur, C., Wrobel, J., and Constantinou, E. (1994). A chemical kinetic mechanism for atmospheric inorganic mercury. *Environ Sci Technol* **28**, 1589-1597.

Seigneur, C., Abeck, H., Chia, G., Reinhard, M., Bloom, N., Prestbo, E., and Saxena, P. (1998). Mercury adsorption to elemental carbon (soot) particles and atmospheric particulate matter. *Atmos. Environ.* **32**, 2649-2657.

Sommar, J., Gardfeldt, K., Stromberg, D., and Feng, X. (2001). A kinetic study of the gas-phase reaction between the hydroxyl radical and atomic mercury. *Atmos. Environ.* **35**, 3049-3054.

Tokos, J., Hall, B., Calhoun, J., and Prestbo, E. (1998). Homogeneous gas-phase reaction of Hg0 with H2O2, O3, CH3I, and (CH3)3 S: implications for atmospheric Hg cycling. *Atmos. Environ.* **32**, 823-827.

Van Loon, L., Mader, E., and Scott, S. (2000). Reduction of the aqueous mercuric ion by sulfite: UV spectrum of HgSO3 and its intramolecular redox reaction. *J. Phys. Chem. A* **104**, 1621-1626.

Xiao, Z.F., Munthe, J., Stromberg, D., and Lindqvist, O. (1994). Photochemical Behavior of Inorganic Mercury Compounds in Aqueous Solution. Chapter VI-6, pages 581-592, in *Mercury Pollution Integration and Synthesis*, edited by Watras, C.J., CRC Press, Boca Raton, FL.

7. Appendix: Sensitivity to Computational Environment and Numerical Methodologies

7.1. Introduction

During the course of this work, there were changes to the computational environment, and small differences in results could be observed. The types of changes included the following:

- Installation of a new, upgraded operating system on the Linux-based 16-processor workstation being used to carry out the simulations;
- Upgrading the Intel Fortran compiler being used to create executables;
- Use of different optimization schemes during compilation
- Different procedures for handling arrays with the HYSPLIT-Hg program

As the objective of this phase of the work was to examine the sensitivity of the simulations to inputs and physicochemical parameters, it was important to examine the variations introduced by these numerical and computational environment changes. If the influence of these changes was too large, it would significantly complicate the interpretation of results of the numerous sensitivity investigations described in the main body of this report. As will be shown in some detail in this Appendix, the computational environment and numerical methodologies did have an observable effect, but the variations in results were generally very small, on the order of a few percent or less. Thus, it was concluded that the analyses in the main body of the report were valid and could be interpreted in a straightforward way. In other words, the differences observed in the sensitivity analyses presented above were essentially all due to changes in inputs and parameters, and not due to changes in the computational environment and numerical methodologies.

In the following sections, results are presented for each of the five illustrative standard source locations (SSL's) examined in the main body of this report: SSL-48 (India), SSL-13 (China), SSL-11 (northeast Texas), SSL-6 (Ohio River Valley), and SSL-8 (western shore of Lake Erie). As in the main body of the report, results will be presented for model-estimated deposition to the Great Lakes as well as model-estimated wet-deposition flux at MDN sites in the Great Lakes region. A total of 154 different simulations were performed examining potential numerical influences. However, before these results are presented, a description of the various computational / numerical variations that were investigated will be presented, to serve as a basis for interpreting the results for each SSL.

Compilation Variations

The INTEL Fortran compiler was used to compile the Fortran source code to create executables on the Linux workstation used for model simulations. There are numerous options that the user can specify that will impact the way the code is compiled and the resulting executable. There were four primary variations investigated, involving the "optimization" employed during compilation, described in the

following table. An additional compilation variations analyzed included the option to improve floating point consistency "-fltconsistency". This was used in some of the compilations, as described below.

Optimization Scheme	Description
0	Disables all optimization in the code generation; array bounds checks included unless disabled
1	Disables some optimizations which increase code size for a small speed benefit
2	Optimizes for maximum speed; this is the default optimization for the INTEL Fortran Compiler
3	Enables more aggressive optimizations that may not improve performance on some programs

Treatment of Meteorological Arrays

One of the key issues investigated in this numerical methodology involved the way the HYSPLIT model used meteorological data arrays in simulating advection of 3-dimensional puffs. The investigation was motivated by the discovery of a small, rarely encountered "bug" in the code. In practice, the "bug" would not be likely to create any significant problems for the simulation, but since computational differences were being examined, an investigation of this issue was undertaken.

The "bug" was in the way the HYSPLIT program determined what meteorological data to use for a given 3-D puff. During a simulation, one of the basic operations performed for each puff at each time step was "advection", i.e., the puff was moved downwind, based on the wind speed and wind direction in the meteorological data in its path. During execution, the HYSPLIT model does not normally load a full meteorological grid domain, but loads only a subset of the domain necessary to carry out the advection of puffs currently in the simulation. When the puffs get close to the edge of the sub-domain, the sub-domain is expanded. In the original version of HYSPLIT, the subgrid is expanded by a factor of 1.5 in each horizontal dimension. For example, if the subgrid were 10 x 10, the expanded subgrid would be 15 x 15.

In the original version of HYSPLIT-Hg used in this study, the maximum subgrid array dimensions – before expansion -- were limited by the dimensions of the smallest full grid dimensions. In this study, the NARR meteorological data has horizontal dimensions of 225 x 156, and the NCEP/NCAR global reanalysis dataset had dimensions of 144 x 73. Thus, the largest initial NARR subgrid that the HYSPLIT model would consider – before any necessary expansion -- at any given time was one with dimensions 144 x 73. If expansion was required, the initial version expanded by 1.5x, and so the resulting subgrid maximum would be 216 x 109, a subgrid that was actually smaller than the actual full size of the NARR grid (225 x 156). In a few rare cases, puffs were advected to a place where the program identified that they were somewhere on the NARR grid, but, were not within this 216 x 109 maximum subgrid. In that situation, an array bounds violation would occur.

The "bug" was rarely encountered, and in many simulations, was never encountered. Nevertheless, the issue could result in an array bounds violation during execution. Unless instructed to do so, a Fortran program does not check the indices of an array being referenced. So, it is possible that indices are specified that are actually outside the dimensions of the array. When that happens, the program simply goes to that spot in memory – where the array element would be if the array was actually that big – and pulls the data from that spot. This is obviously a situation to be avoided at all costs. The tradeoff is that if

the program is required to check all array bounds for validity, the execution time is increased dramatically. In practice, a common approach, and one used in the this study, is to do debugging and checking using array-bounds checks during execution, but for "production" runs where lots of results are being generated, to turn array-bounds checking off. So, one of the label-components you will see in the following sections is "no_check" indicating that array bounds checking was turned off.

The grid expansion factor – 1.5x in the original HYSPLIT algorithm – was varied to examine its influence on the computations. The 1.5x expansion was labeled "orig", a 1.7x expansion was labeled "1p7x", a 10x expansion was labeled "10x", and an immediate expansion to the full NARR grid was labeled "full". In all cases, the resulting grid was limited to the maximum size of the NARR grid (225 x 156). In some of the run labels in the data presented below, you will see these label-components specified, i.e., "orig", "1p7x", "10x", and "full". The impact of these changes would be expected to alter the frequency and consequences of occasional array bounds violations, should they occur.

In a related variation, the code logic that stipulated that the maximum initial subgrid size was the minimum full grid size was lifted, and the maximum initial subgrid was only limited by the size of the actual grid. This change is indicated in the descriptions of the model versions below.

Model Versions

In the results presented below, results for a number of different model versions are shown. A brief description of these versions is described in the table below.

Model version	Description
base	Used to indicate a base simulation to which others are compared
V3	Refers to model version 24a; simulation conducted in Feb 2012 immediately after reconstruction of workstation, which had suffered a complete collapse
v25i	New version of HYSPLIT-Hg in which chemical rate parameters were converted to input parameters, as opposed to be hard-wired into the code; this was done for convenience in carrying out the sensitivity studies
v25q	With max subgrid equal to min full grid, and compiled with "-fltconsistency", potentially vulnerable to array bounds violations
v25r	With maximum initial subgrid *not* limited to minimum full grid; compiled with "-fltconsistency"; believed to be less vulnerable to array bounds violations
v25v	Additional changes to meteorological data array handling; improved bounds checks; less vulnerable to array bounds violations; "-fltconsistency"
v25w	Additional diagnostic outputs – should have no impact on results; "-fltconsistency"
v25x	New version of array bounds checking and correction, max subgrid = min full grid; "-fltconsistency"
v25y	Additional diagnostic outputs – should have no impact on results; "-fltconsistency"
v25z	Another array handling methodology, believed to be somewhat vulnerable to array bounds violations; "-fltconsistency"
v25aa	Max subgrid = min full grid; same array bounds checking and correction as v25x; "-fltconsistency";
v25ab	A different version of array bounds checking and correction; different algorithms for setting grid sizes; "-fltconsistency"

Additional Run Label Components

In a few cases, additional run label components are included. For example, “mp10000” means the MAXPUFF parameter is set to 10,000. This might be seen in an examination of a GEM (global Eulerian model) simulation, in which the MAXPUFF parameter should be irrelevant. So, a GEM simulation with “mp10000” should be identical to any other GEM simulation. “WETR_040000” can also be seen in a few runs. This was the default version of the WETR parameter – described in the main body of the report – and so a run with this specified should not differ from the default or base simulation. “Max_Oxid” is also seen, referring to the maximum oxidation chemical mechanism scheme, which should have no impact on simulations of pure Hg(p) emissions, as described in the main body of this report.

How to parse a simulation label

In all of the results presented in the following sections, a given simulation is described by a label.

As an example, consider a simulation labeled “HgII_006_PUF_v25aa2_TEST_43_full_no_check”

This simulation involved emissions of pure Hg(II), from standard source location #6 (Ohio River Valley), employing the PUF dispersion methodology, using model version v25aa, with optimization scheme set to “2”, with grid expansion set to “full”, and with no array bounds checking.

In the main body of the report, run labels generally were abbreviated to include only the emissions species, the standard source location, and the dispersion methodology, e.g., in the above example, the label would just have been “HgII_006_PUF”

7.2. Standard Source Location #48 (India)

The graphs below show comparisons for a number of different simulations for emissions from standard source location #48, in India. In almost all cases, it is seen that the computational variations have very little influence on the overall results for deposition to the Great Lakes or to wet deposition to MDN sites in the Great Lakes region. The largest differences in the results appear to occur for differences in the compiler optimization schemes.

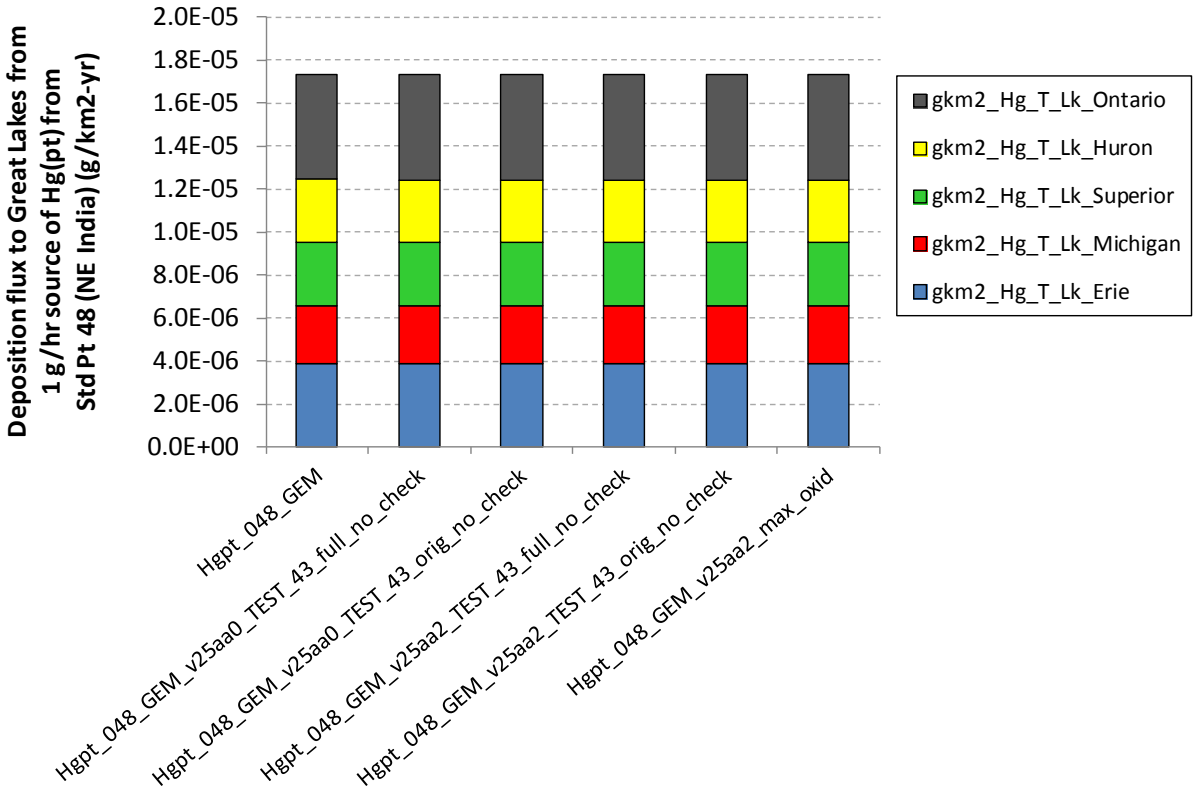

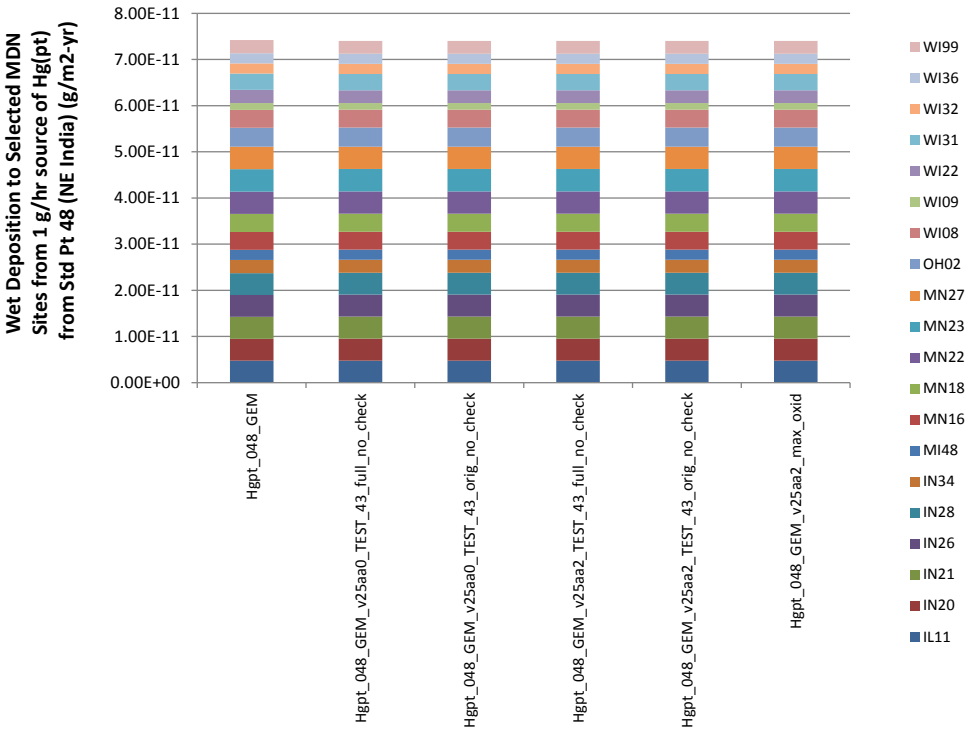
Wet Deposition to Selected MDN Sites from 1 g/hr source of Hg(pt) from Std Pt 48 (NE India) (g/m2-yr)
8.00E-11
7.00E-11
6.00E-11
5.00E-11
4.00E-11
3.00E-11
2.00E-11
1.00E-11
0.00E+00
Hgpt_048_GEM
Hgpt_048_GEM_v25aa0_TEST_43_full_no_check
Hgpt_048_GEM_v25aa0_TEST_43_orig_no_check
Hgpt_048_GEM_v25aa2_TEST_43_full_no_check
Hgpt_048_GEM_v25aa2_TEST_43_orig_no_check
Hgpt_048_GEM_v25aa2_max_oxid
WI99
WI36
WI32
WI31
WI22
WI09
WI08
OH02
MN27
MN23
MN22
MN18
MN16
MI48
IN34
IN28
IN26
IN21
IN20
IL11

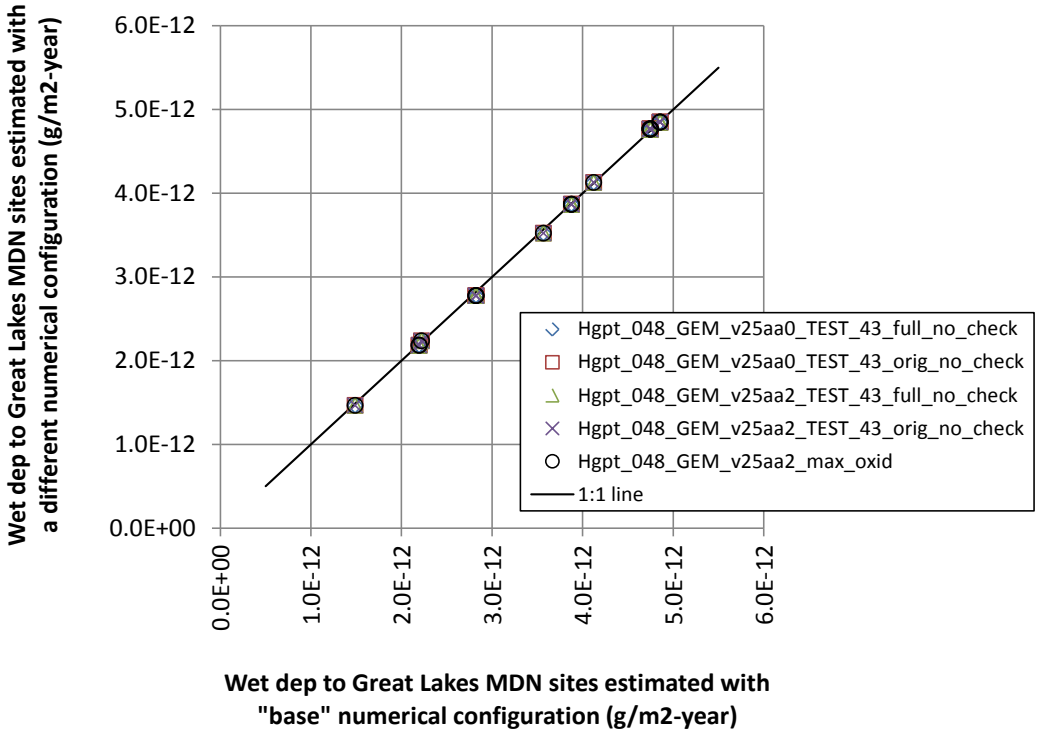
Wet dep to Great Lakes MDN sites estimated with a different numerical configuration (g/m2-year)
6.0E-12
5.0E-12
4.0E-12
3.0E-12
2.0E-12
1.0E-12
0.0E+00
0.0E+00
1.0E-12
2.0E-12
3.0E-12
4.0E-12
5.0E-12
6.0E-12
Hgpt_048_GEM_v25aa0_TEST_43_full_no_check
Hgpt_048_GEM_v25aa0_TEST_43_orig_no_check
Hgpt_048_GEM_v25aa2_TEST_43_full_no_check
Hgpt_048_GEM_v25aa2_TEST_43_orig_no_check
Hgpt_048_GEM_v25aa2_max_oxid
1:1 line
Wet dep to Great Lakes MDN sites estimated with "base" numerical configuration (g/m2-year)

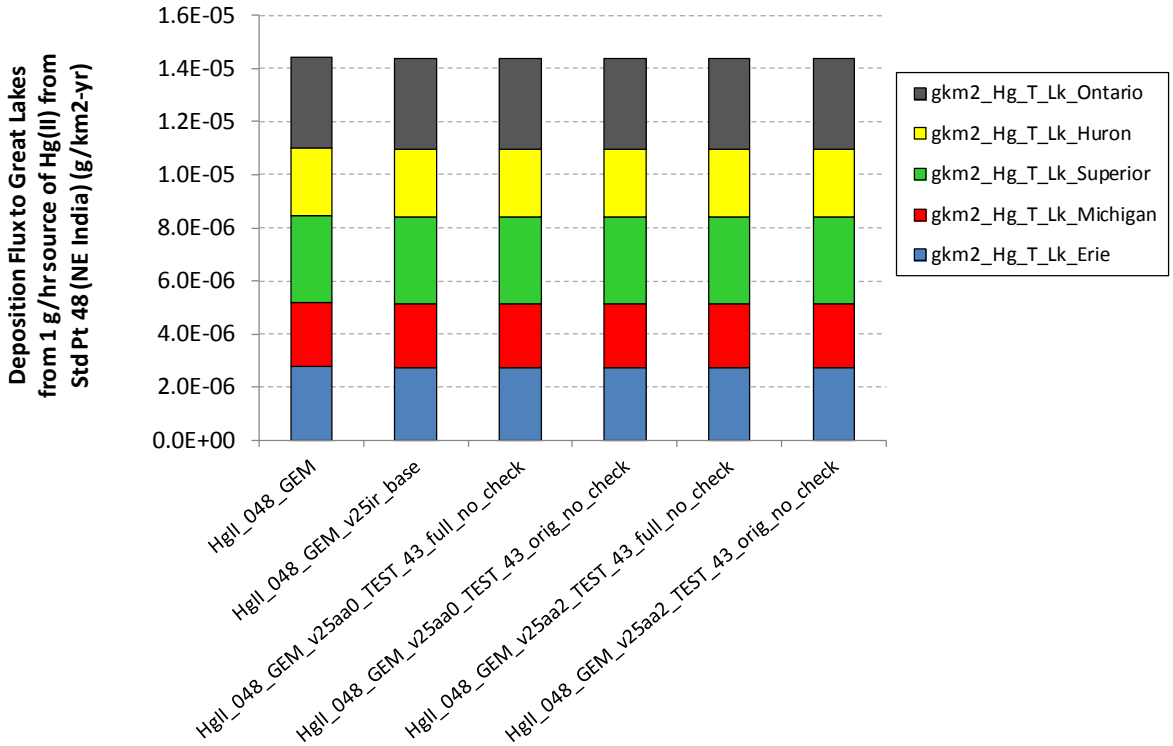
Deposition Flux to Great Lakes from 1 g/hr source of Hg(II) from Std Pt 48 (NE India) (g/km2-yr)
1.6E-05
1.4E-05
1.2E-05
1.0E-05
8.0E-06
6.0E-06
4.0E-06
2.0E-06
0.0E+00
gkm2_Hg_T_Lk_Ontario
gkm2_Hg_T_Lk_Huron
gkm2_Hg_T_Lk_Superior
gkm2_Hg_T_Lk_Michigan
gkm2_Hg_T_Lk_Erie
HgII_048_GEM
HgII_048_GEM_v25ir_base
HgII_048_GEM_v25aa0_TEST_43_full_no_check
HgII_048_GEM_v25aa0_TEST_43_orig_no_check
HgII_048_GEM_v25aa2_TEST_43_full_no_check
HgII_048_GEM_v25aa2_TEST_43_orig_no_check

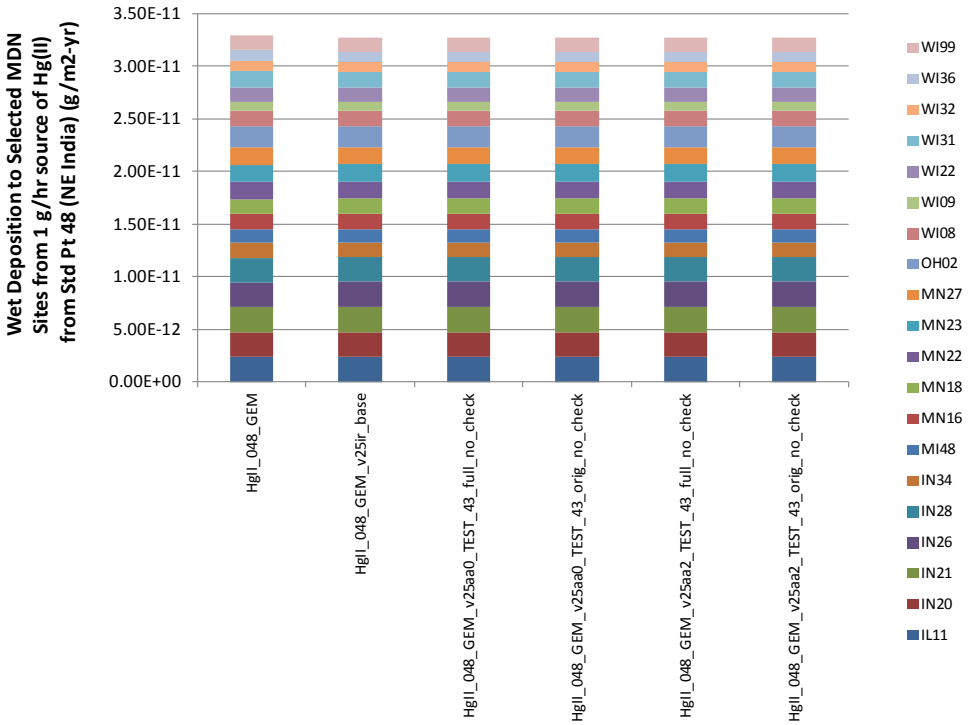
Wet Deposition to Selected MDN Sites from 1 g/hr source of Hg(II) from Std Pt 48 (NE India) (g/m2-yr)
3.50E-11
3.00E-11
2.50E-11
2.00E-11
1.50E-11
1.00E-11
5.00E-12
0.00E+00
WI99
WI36
WI32
WI31
WI22
WI09
WI08
OH02
MN27
MN23
MN22
MN18
MN16
MI48
IN34
IN28
IN26
IN21
IN20
IL11
HgII_048_GEM
HgII_048_GEM_v25ir_base
HgII_048_GEM_v25aa0_TEST_43_full_no_check
HgII_048_GEM_v25aa0_TEST_43_orig_no_check
HgII_048_GEM_v25aa2_TEST_43_full_no_check
HgII_048_GEM_v25aa2_TEST_43_orig_no_check

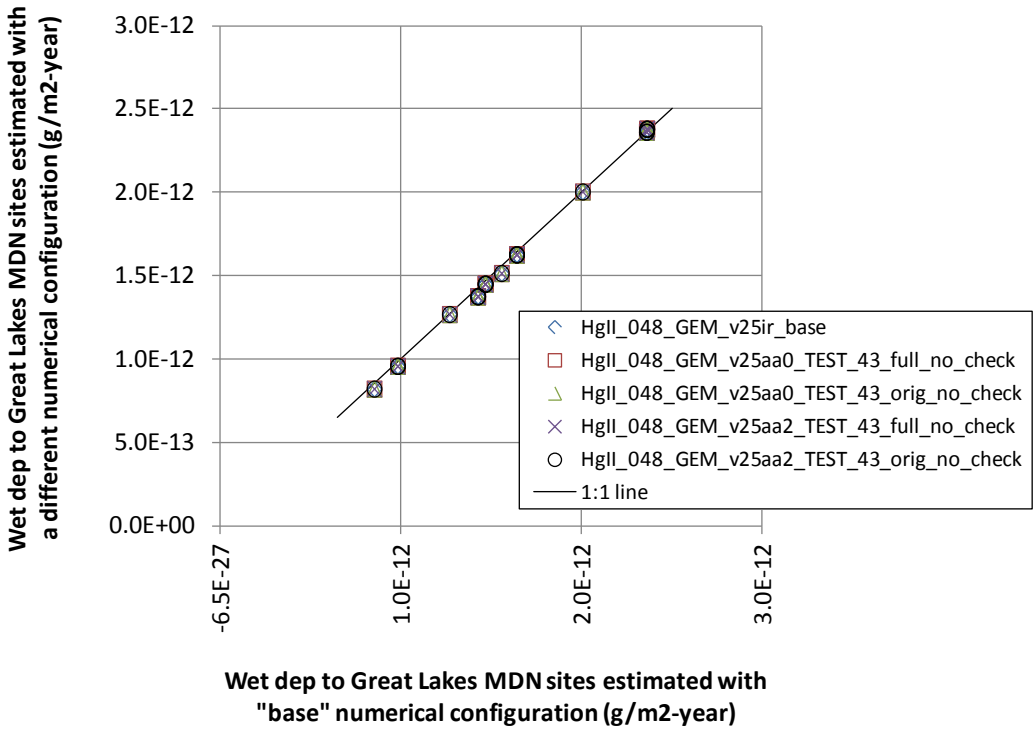
Wet dep to Great Lakes MDN sites estimated with a different numerical configuration (g/m2-year)
3.0E-12
2.5E-12
2.0E-12
1.5E-12
1.0E-12
5.0E-13
0.0E+00
-6.5E-27
1.0E-12
2.0E-12
3.0E-12
HgII_048_GEM_v25ir_base
HgII_048_GEM_v25aa0_TEST_43_full_no_check
HgII_048_GEM_v25aa0_TEST_43_orig_no_check
HgII_048_GEM_v25aa2_TEST_43_full_no_check
HgII_048_GEM_v25aa2_TEST_43_orig_no_check
1:1 line
Wet dep to Great Lakes MDN sites estimated with "base" numerical configuration (g/m2-year)

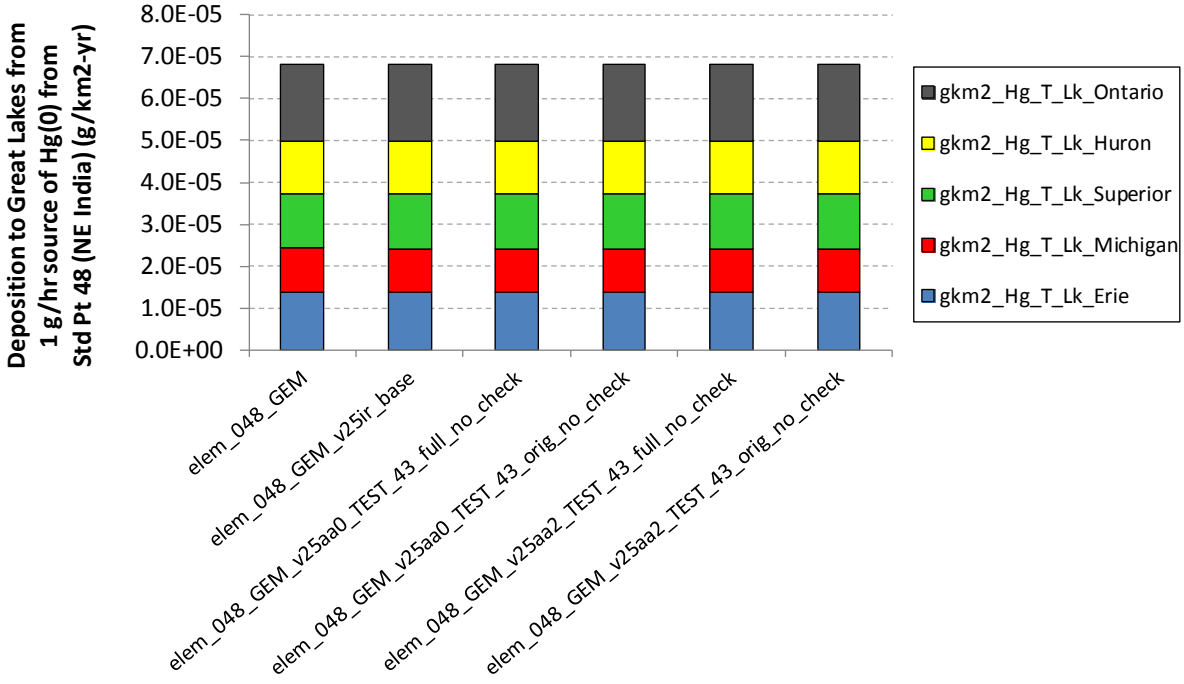
Deposition to Great Lakes from 1 g/hr source of Hg(0) from Std Pt 48 (NE India) (g/km2-yr)
8.0E-05
7.0E-05
6.0E-05
5.0E-05
4.0E-05
3.0E-05
2.0E-05
1.0E-05
0.0E+00
gkm2_Hg_T_Lk_Ontario
gkm2_Hg_T_Lk_Huron
gkm2_Hg_T_Lk_Superior
gkm2_Hg_T_Lk_Michigan
gkm2_Hg_T_Lk_Erie
elem_048_GEM
elem_048_GEM_v25ir_base
elem_048_GEM_v25aa0_TEST_43_full_no_check
elem_048_GEM_v25aa0_TEST_43_orig_no_check
elem_048_GEM_v25aa2_TEST_43_full_no_check
elem_048_GEM_v25aa2_TEST_43_orig_no_check

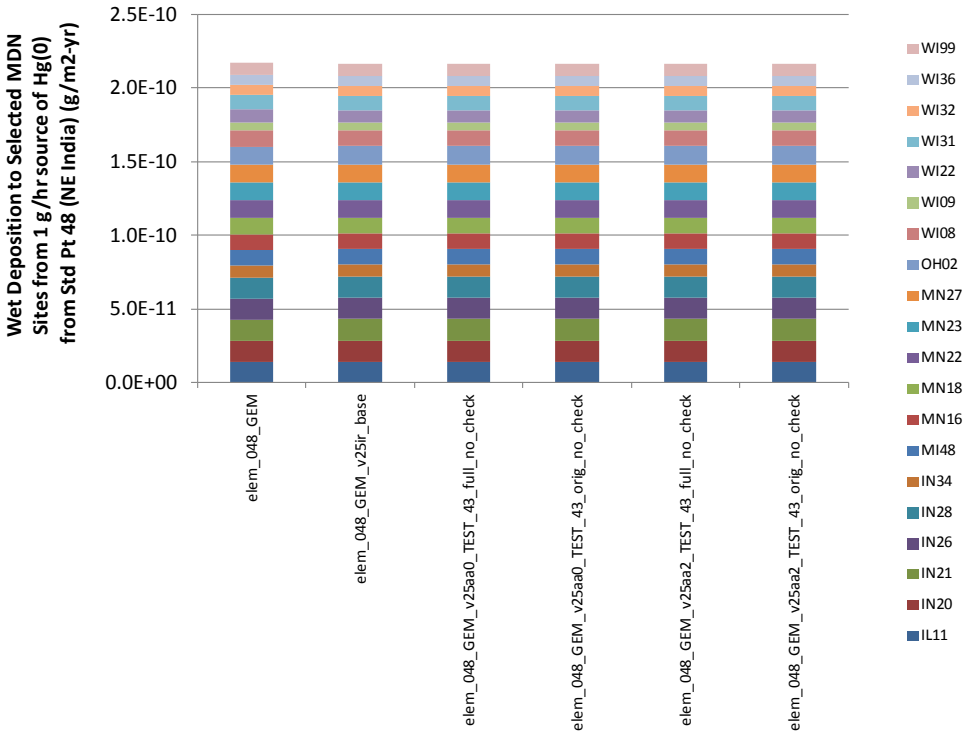
Wet Deposition to Selected MDN Sites from 1 g/hr source of Hg(0) from Std Pt 48 (NE India) (g/m2-yr)
2.5E-10
2.0E-10
1.5E-10
1.0E-10
5.0E-11
0.0E+00
elem_048_GEM
elem_048_GEM_v25ir_base
elem_048_GEM_v25aa0_TEST_43_full_no_check
elem_048_GEM_v25aa0_TEST_43_orig_no_check
elem_048_GEM_v25aa2_TEST_43_full_no_check
elem_048_GEM_v25aa2_TEST_43_orig_no_check
WI99
WI36
WI32
WI31
WI22
WI09
WI08
OH02
MN27
MN23
MN22
MN18
MN16
MI48
IN34
IN28
IN26
IN21
IN20
IL11

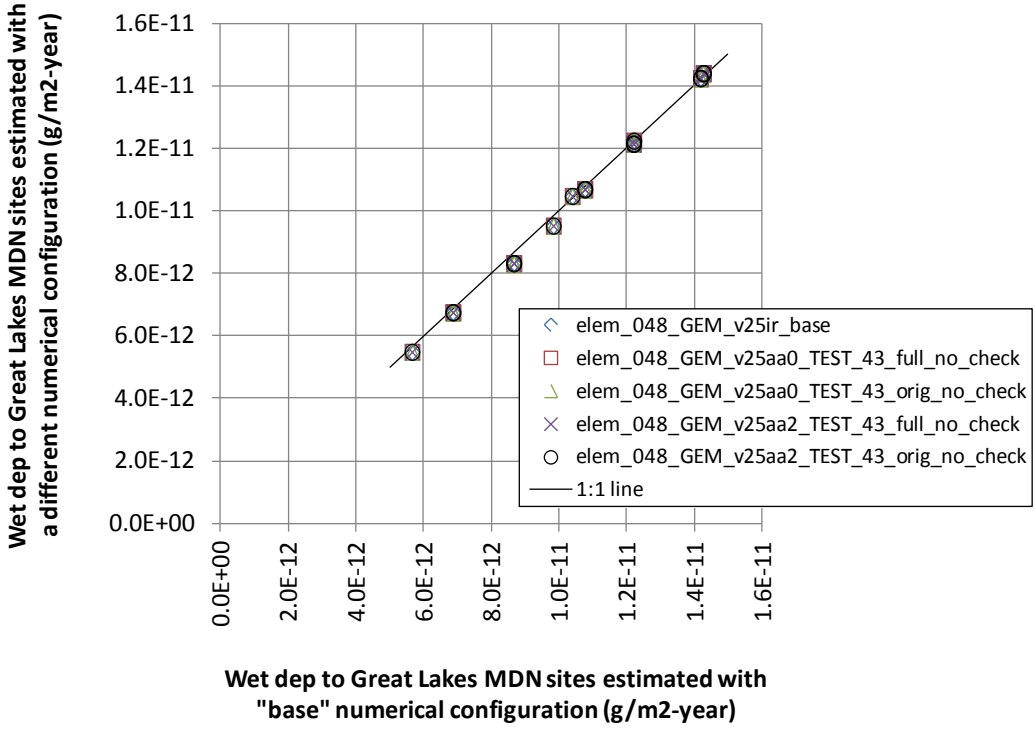
Wet dep to Great Lakes MDN sites estimated with a different numerical configuration (g/m2-year)
1.6E-11
1.4E-11
1.2E-11
1.0E-11
8.0E-12
6.0E-12
4.0E-12
2.0E-12
0.0E+00
0.0E+00
2.0E-12
4.0E-12
6.0E-12
8.0E-12
1.0E-11
1.2E-11
1.4E-11
1.6E-11
elem_048_GEM_v25ir_base
elem_048_GEM_v25aa0_TEST_43_full_no_check
elem_048_GEM_v25aa0_TEST_43_orig_no_check
elem_048_GEM_v25aa2_TEST_43_full_no_check
elem_048_GEM_v25aa2_TEST_43_orig_no_check
1:1 line
Wet dep to Great Lakes MDN sites estimated with "base" numerical configuration (g/m2-year)

7.3. Standard Source Location #13 (China)

The graphs below show comparisons for a number of different simulations for emissions from standard source location #13, in China. In almost all cases, it is seen that the computational variations have very little influence on the overall results for deposition to the Great Lakes or to wet deposition to MDN sites in the Great Lakes region. The largest differences in the results appear to occur for differences in the compiler optimization schemes.

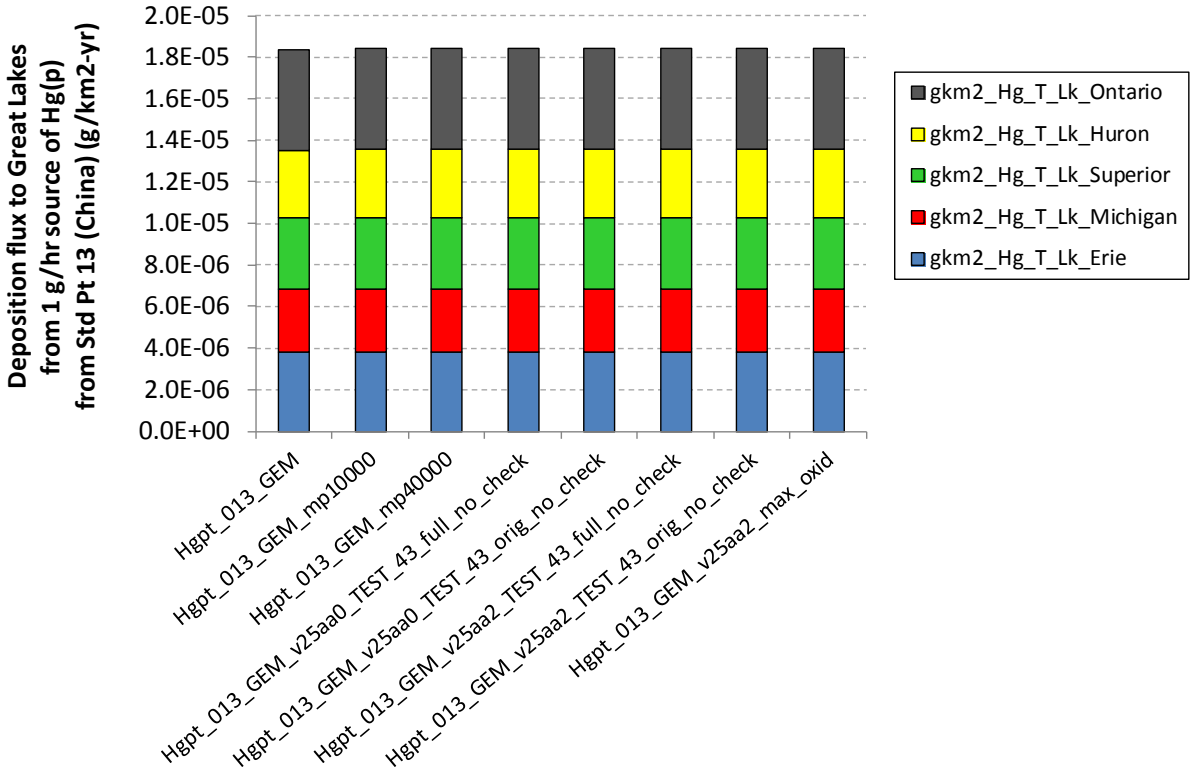

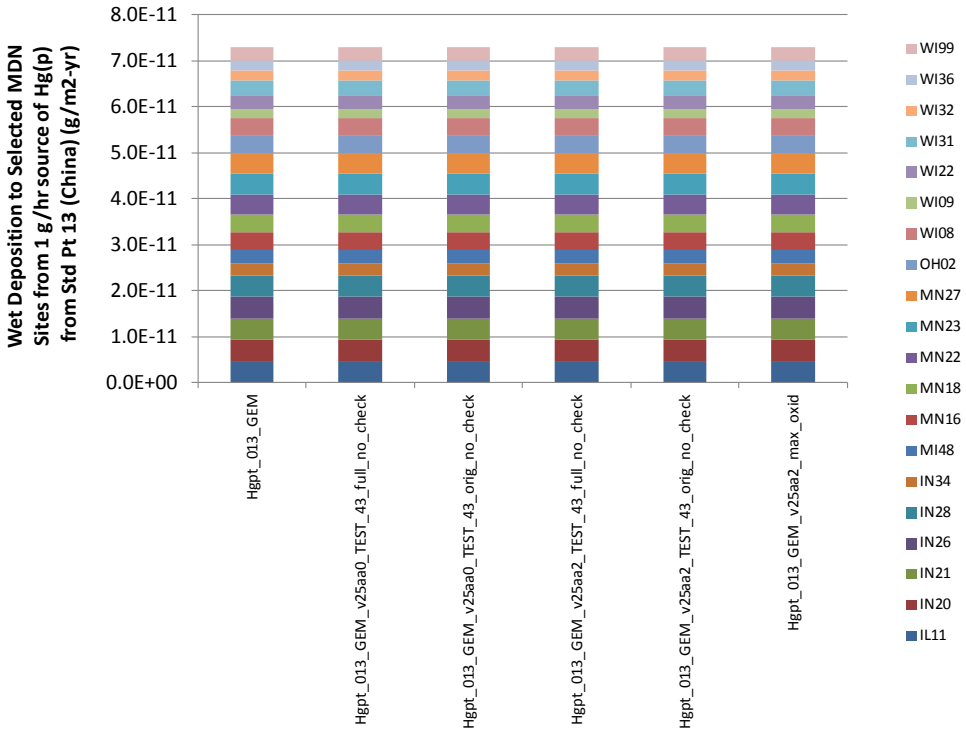
Wet Deposition to Selected MDN Sites from 1 g/hr source of Hg(p) from Std Pt 13 (China) (g/m2-yr)
8.0E-11
7.0E-11
6.0E-11
5.0E-11
4.0E-11
3.0E-11
2.0E-11
1.0E-11
0.0E+00
Hgpt_013_GEM
Hgpt_013_GEM_v25aa0_TEST_43_full_no_check
Hgpt_013_GEM_v25aa0_TEST_43_orig_no_check
Hgpt_013_GEM_v25aa2_TEST_43_full_no_check
Hgpt_013_GEM_v25aa2_TEST_43_orig_no_check
Hgpt_013_GEM_v25aa2_max_oxid
WI99
WI36
WI32
WI31
WI22
WI09
WI08
OH02
MN27
MN23
MN22
MN18
MN16
MI48
IN34
IN28
IN26
IN21
IN20
IL11

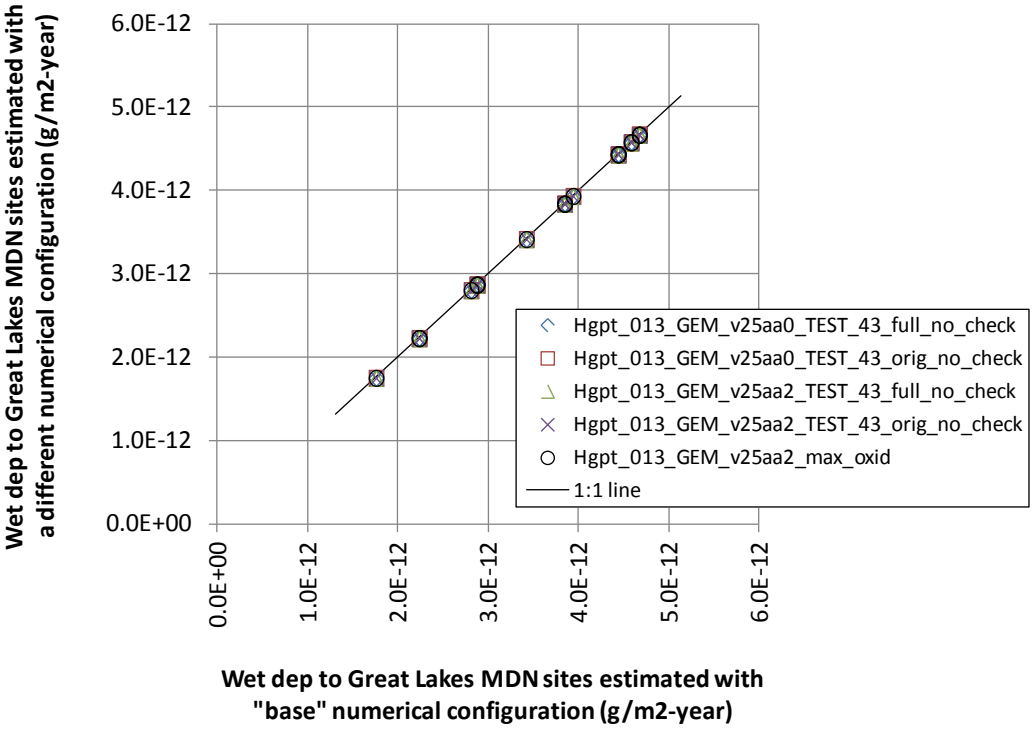
Wet dep to Great Lakes MDN sites estimated with a different numerical configuration (g/m2-year)
6.0E-12
5.0E-12
4.0E-12
3.0E-12
2.0E-12
1.0E-12
0.0E+00
0.0E+00
1.0E-12
2.0E-12
3.0E-12
4.0E-12
5.0E-12
6.0E-12
Hgpt_013_GEM_v25aa0_TEST_43_full_no_check
Hgpt_013_GEM_v25aa0_TEST_43_orig_no_check
Hgpt_013_GEM_v25aa2_TEST_43_full_no_check
Hgpt_013_GEM_v25aa2_TEST_43_orig_no_check
Hgpt_013_GEM_v25aa2_max_oxid
1:1 line
Wet dep to Great Lakes MDN sites estimated with "base" numerical configuration (g/m2-year)

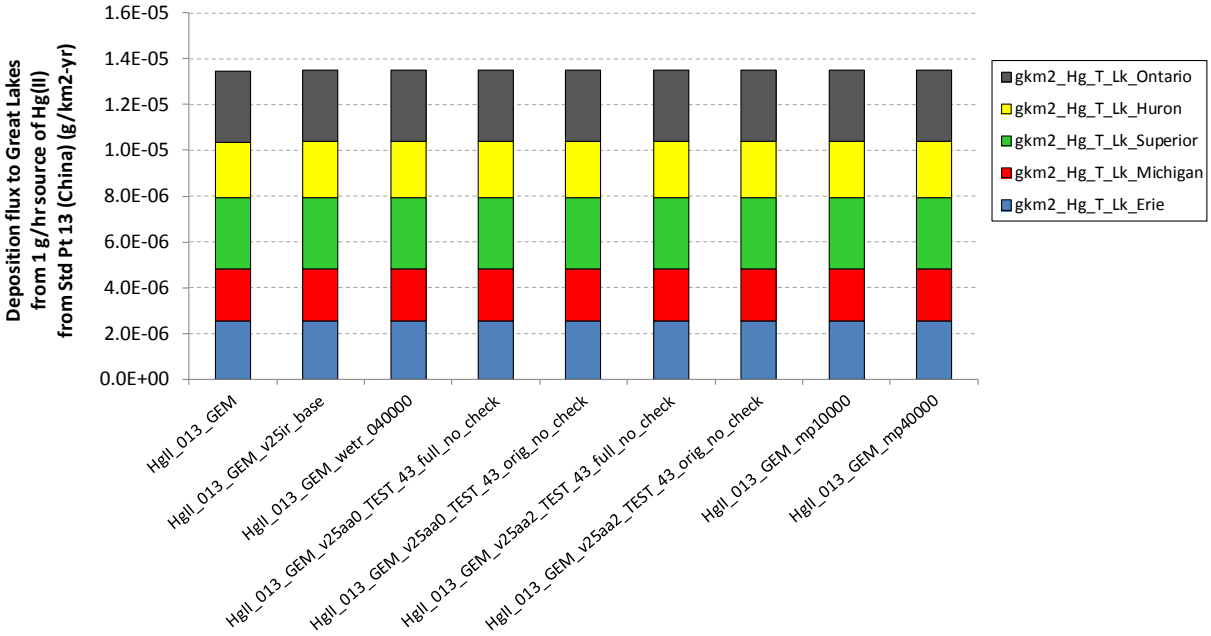
Deposition flux to Great Lakes from 1 g/hr source of Hg(II) from Std Pt 13 (China) (g/km2-yr)
1.6E-05
1.4E-05
1.2E-05
1.0E-05
8.0E-06
6.0E-06
4.0E-06
2.0E-06
0.0E+00
gkm2_Hg_T_Lk_Ontario
gkm2_Hg_T_Lk_Huron
gkm2_Hg_T_Lk_Superior
gkm2_Hg_T_Lk_Michigan
gkm2_Hg_T_Lk_Erie
HgII_013_GEM
HgII_013_GEM_v25ir_base
HgII_013_GEM_wetr_040000
HgII_013_GEM_v25aa0_TEST_43_full_no_check
HgII_013_GEM_v25aa0_TEST_43_orig_no_check
HgII_013_GEM_v25aa2_TEST_43_full_no_check
HgII_013_GEM_v25aa2_TEST_43_orig_no_check
HgII_013_GEM_mp10000
HgII_013_GEM_mp40000

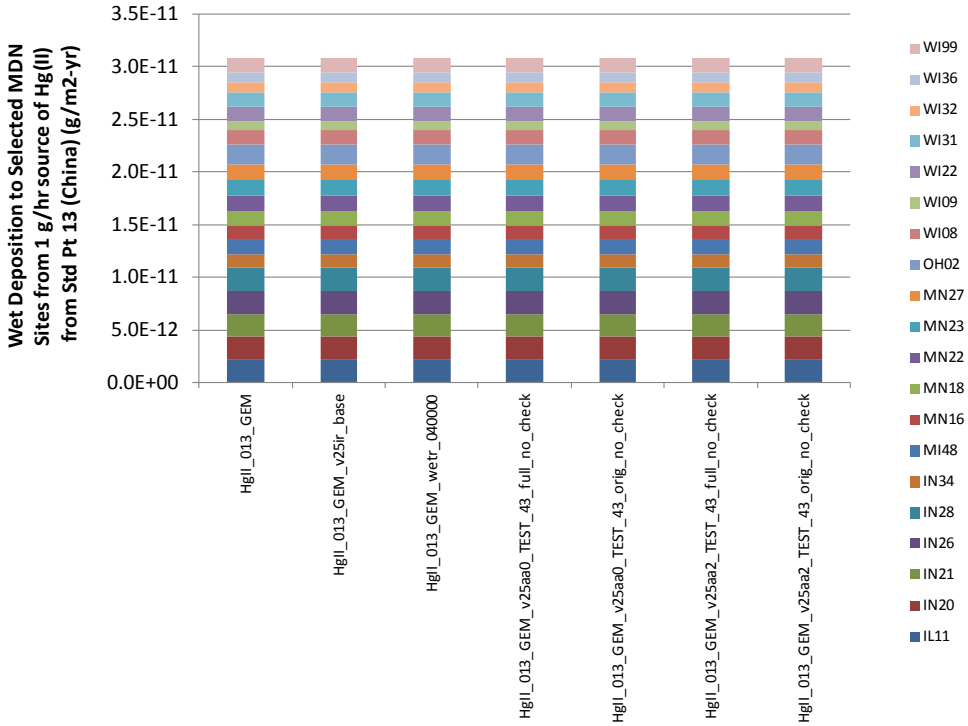
Wet Deposition to Selected MDN Sites from 1 g/hr source of Hg(II) from Std Pt 13 (China) (g/m2-yr)
3.5E-11
3.0E-11
2.5E-11
2.0E-11
1.5E-11
1.0E-11
5.0E-12
0.0E+00
WI99
WI36
WI32
WI31
WI22
WI09
WI08
OH02
MN27
MN23
MN22
MN18
MN16
MI48
IN34
IN28
IN26
IN21
IN20
IL11
HgII_013_GEM
HgII_013_GEM_v25ir_base
HgII_013_GEM_wetr_040000
HgII_013_GEM_v25aa0_TEST_43_full_no_check
HgII_013_GEM_v25aa0_TEST_43_orig_no_check
HgII_013_GEM_v25aa2_TEST_43_full_no_check
HgII_013_GEM_v25aa2_TEST_43_orig_no_check

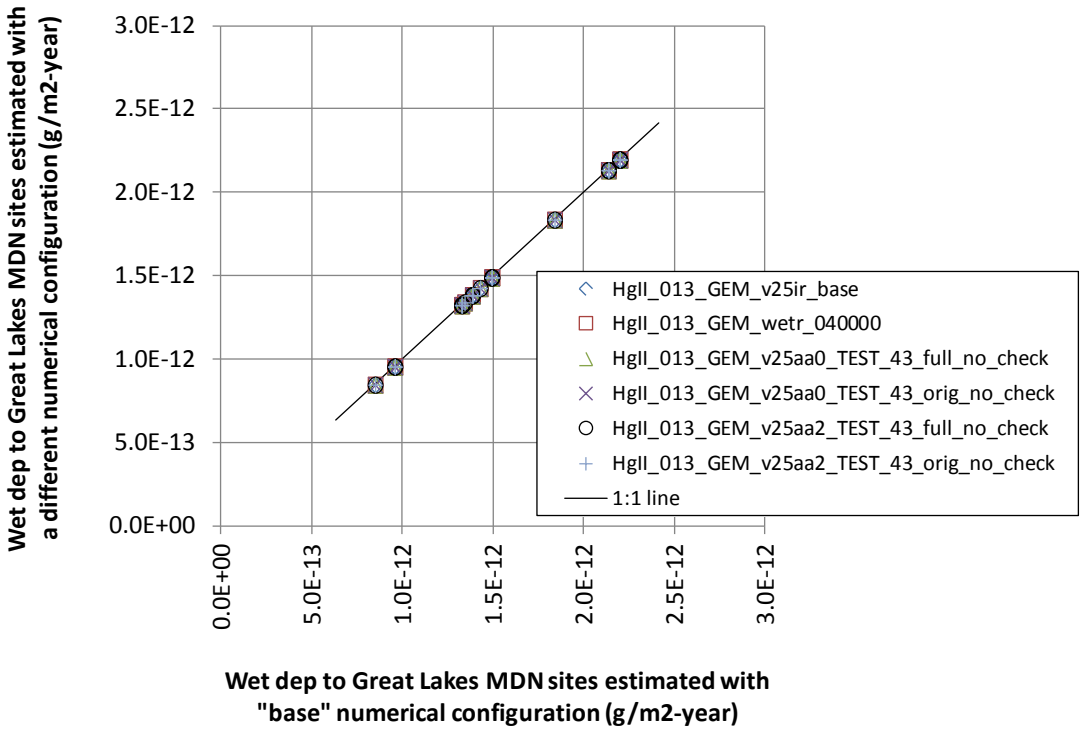
Wet dep to Great Lakes MDN sites estimated with a different numerical configuration (g/m2-year)
3.0E-12
2.5E-12
2.0E-12
1.5E-12
1.0E-12
5.0E-13
0.0E+00
0.0E+00
5.0E-13
1.0E-12
1.5E-12
2.0E-12
2.5E-12
3.0E-12
HgII_013_GEM_v25ir_base
HgII_013_GEM_wetr_040000
HgII_013_GEM_v25aa0_TEST_43_full_no_check
HgII_013_GEM_v25aa0_TEST_43_orig_no_check
HgII_013_GEM_v25aa2_TEST_43_full_no_check
HgII_013_GEM_v25aa2_TEST_43_orig_no_check
1:1 line
Wet dep to Great Lakes MDN sites estimated with "base" numerical configuration (g/m2-year)

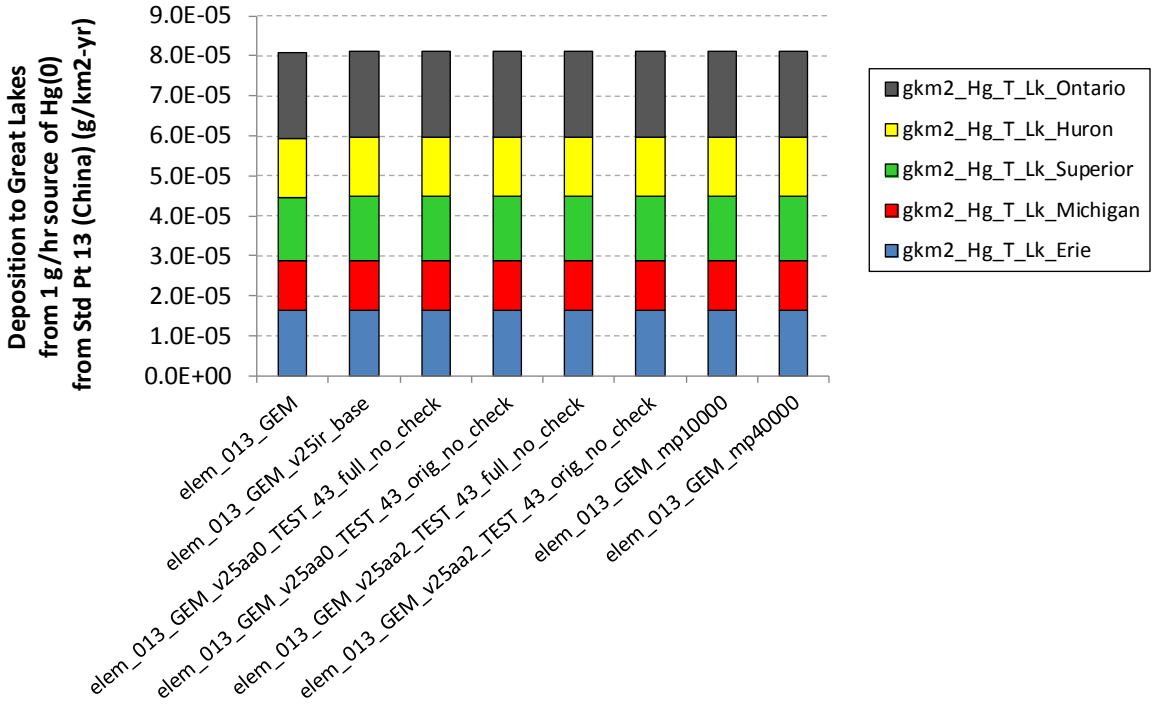
Deposition to Great Lakes from 1 g/hr source of Hg(0) from Std Pt 13 (China) (g/km2-yr)
9.0E-05
8.0E-05
7.0E-05
6.0E-05
5.0E-05
4.0E-05
3.0E-05
2.0E-05
1.0E-05
0.0E+00
gkm2_Hg_T_Lk_Ontario
gkm2_Hg_T_Lk_Huron
gkm2_Hg_T_Lk_Superior
gkm2_Hg_T_Lk_Michigan
gkm2_Hg_T_Lk_Erie
elem_013_GEM
elem_013_GEM_v25ir_base
elem_013_GEM_v25aa0_TEST_43_full_no_check
elem_013_GEM_v25aa0_TEST_43_orig_no_check
elem_013_GEM_v25aa2_TEST_43_full_no_check
elem_013_GEM_v25aa2_TEST_43_orig_no_check
elem_013_GEM_mp10000
elem_013_GEM_mp40000

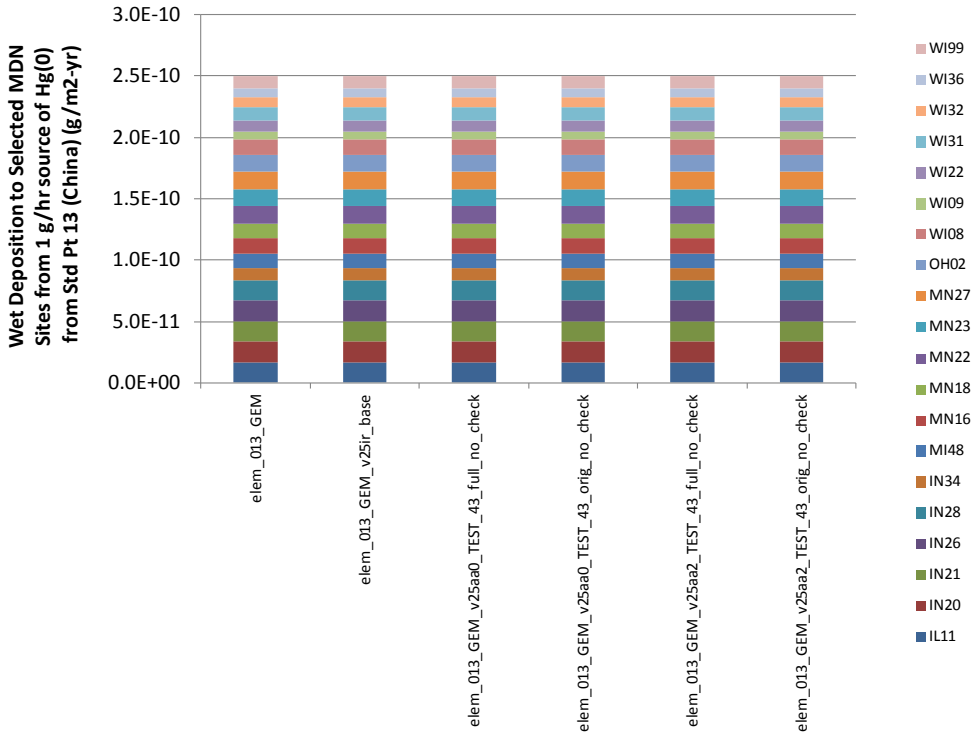
Wet Deposition to Selected MDN Sites from 1 g/hr source of Hg(0) from Std Pt 13 (China) (g/m2-yr)
3.0E-10
2.5E-10
2.0E-10
1.5E-10
1.0E-10
5.0E-11
0.0E+00
elem_013_GEM
elem_013_GEM_v25ir_base
elem_013_GEM_v25aa0_TEST_43_full_no_check
elem_013_GEM_v25aa0_TEST_43_orig_no_check
elem_013_GEM_v25aa2_TEST_43_full_no_check
elem_013_GEM_v25aa2_TEST_43_orig_no_check
WI99
WI36
WI32
WI31
WI22
WI09
WI08
OH02
MN27
MN23
MN22
MN18
MN16
MI48
IN34
IN28
IN26
IN21
IN20
IL11

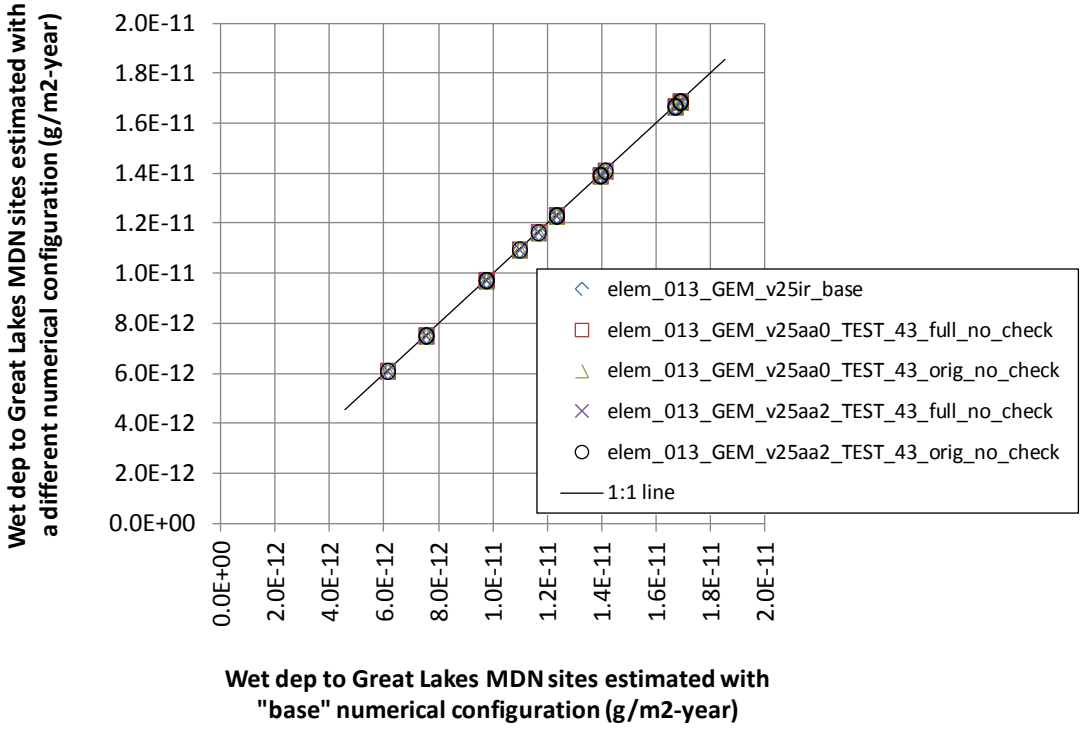
Wet dep to Great Lakes MDN sites estimated with a different numerical configuration (g/m2-year)
2.0E-11
1.8E-11
1.6E-11
1.4E-11
1.2E-11
1.0E-11
8.0E-12
6.0E-12
4.0E-12
2.0E-12
0.0E+00
0.0E+00
2.0E-12
4.0E-12
6.0E-12
8.0E-12
1.0E-11
1.2E-11
1.4E-11
1.6E-11
1.8E-11
2.0E-11
elem_013_GEM_v25ir_base
elem_013_GEM_v25aa0_TEST_43_full_no_check
elem_013_GEM_v25aa0_TEST_43_orig_no_check
elem_013_GEM_v25aa2_TEST_43_full_no_check
elem_013_GEM_v25aa2_TEST_43_orig_no_check
1:1 line
Wet dep to Great Lakes MDN sites estimated with "base" numerical configuration (g/m2-year)

7.4. Standard Source Location #11 (northeast Texas)

The graphs below show comparisons for a number of different simulations for emissions from standard source location #11, in northeast Texas. In almost all cases, it is seen that the computational variations have very little influence on the overall results for deposition to the Great Lakes or to wet deposition to MDN sites in the Great Lakes region. The largest differences in the results appear to occur for differences in the compiler optimization schemes.

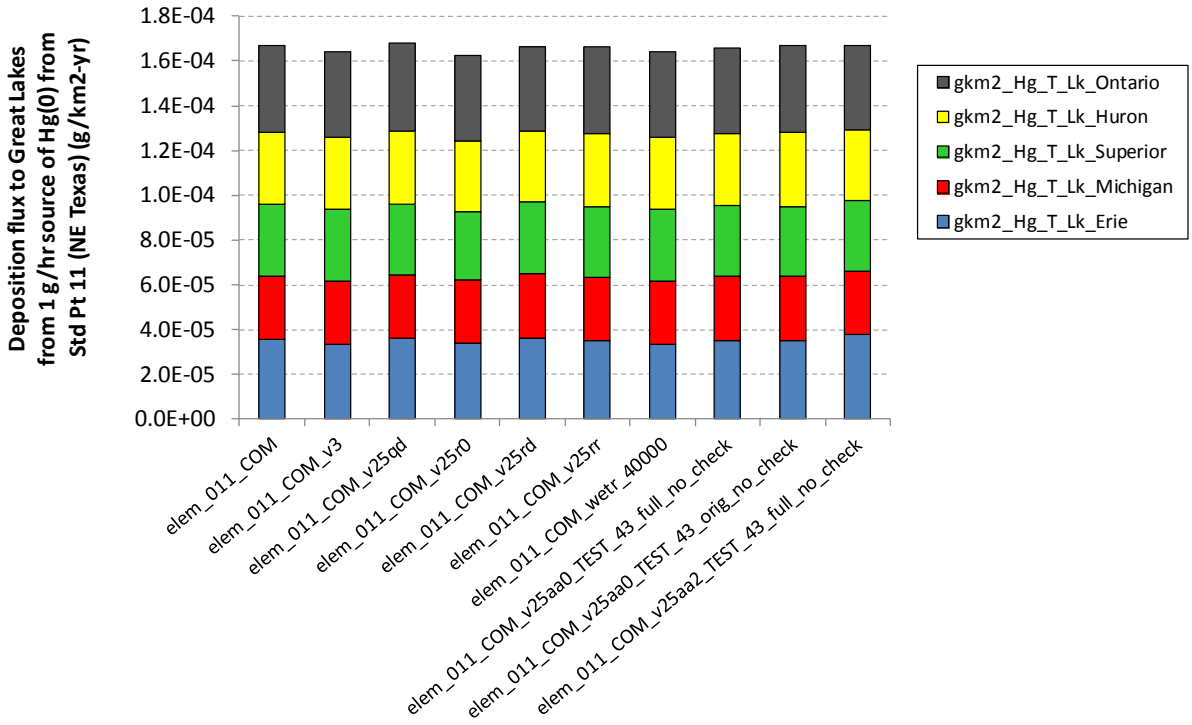

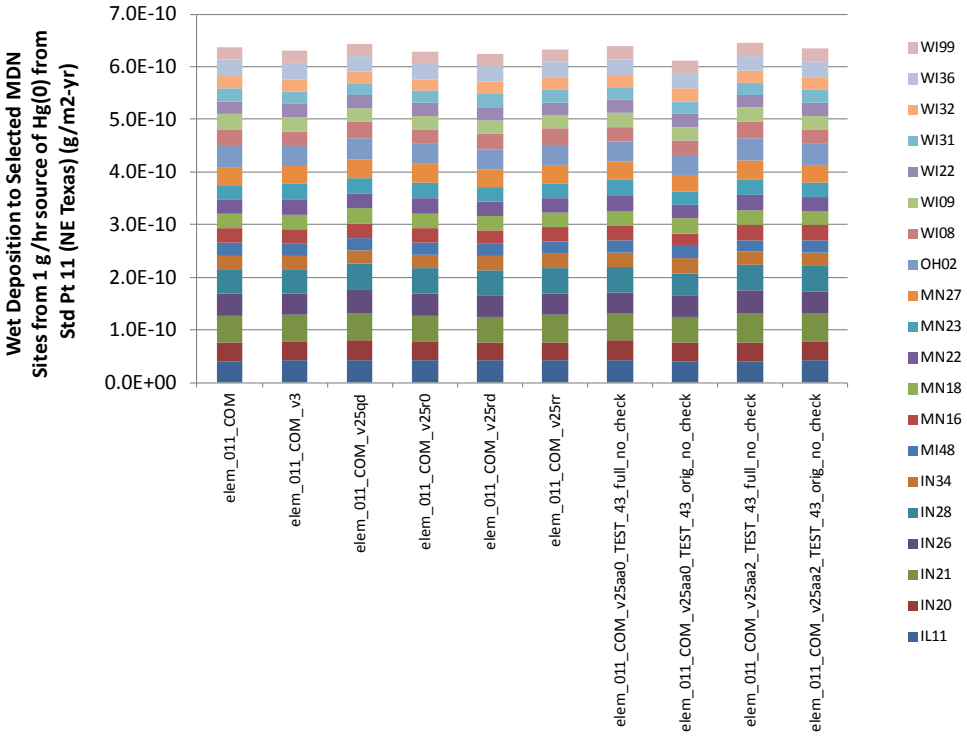
Wet Deposition to Selected MDN Sites from 1 g/hr source of Hg(0) from Std Pt 11 (NE Texas) (g/m2-yr)
7.0E-10
6.0E-10
5.0E-10
4.0E-10
3.0E-10
2.0E-10
1.0E-10
0.0E+00
elem_011_COM
elem_011_COM_v3
elem_011_COM_v25qd
elem_011_COM_v25r0
elem_011_COM_v25rd
elem_011_COM_v25rr
elem_011_COM_v25aa0_TEST_43_full_no_check
elem_011_COM_v25aa0_TEST_43_orig_no_check
elem_011_COM_v25aa2_TEST_43_full_no_check
elem_011_COM_v25aa2_TEST_43_orig_no_check
WI99
WI36
WI32
WI31
WI22
WI09
WI08
OH02
MN27
MN23
MN22
MN18
MN16
MI48
IN34
IN28
IN26
IN21
IN20
IL11

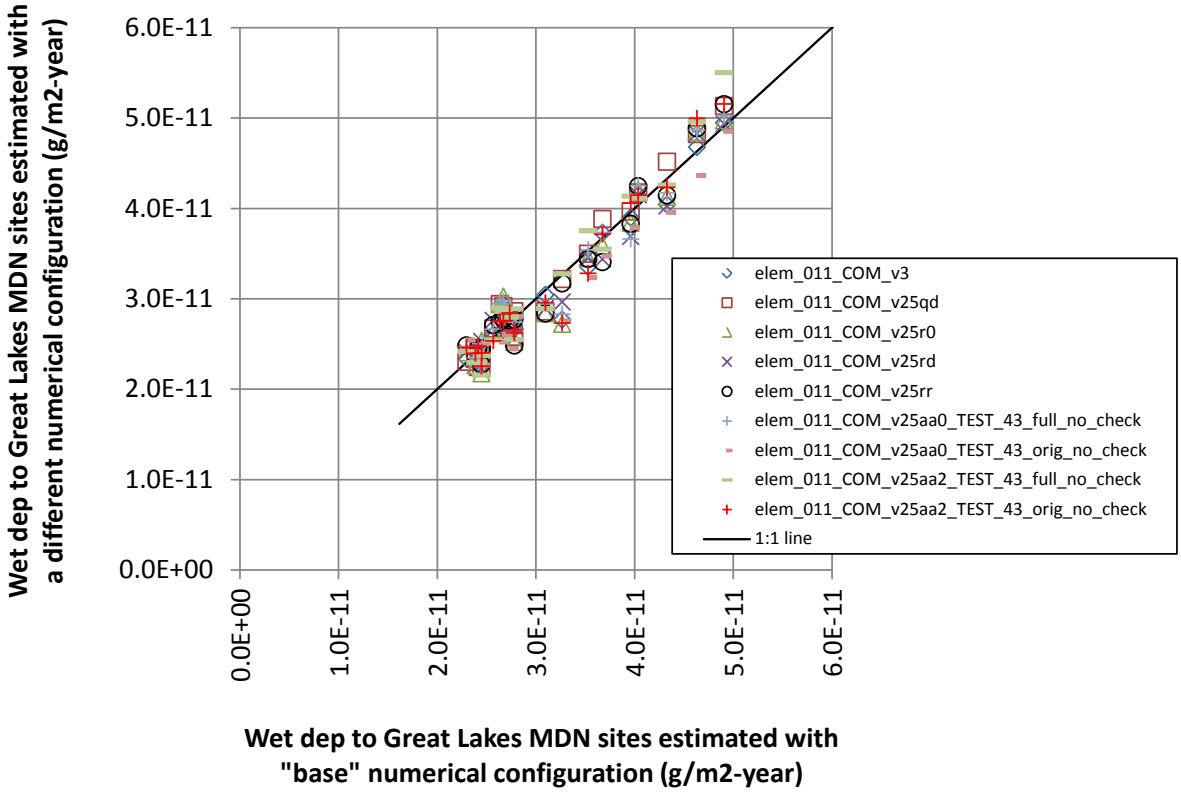
Wet dep to Great Lakes MDN sites estimated with a different numerical configuration (g/m2-year)
6.0E-11
5.0E-11
4.0E-11
3.0E-11
2.0E-11
1.0E-11
0.0E+00
0.0E+00
1.0E-11
2.0E-11
3.0E-11
4.0E-11
5.0E-11
6.0E-11
elem_011_COM_v3
elem_011_COM_v25qd
elem_011_COM_v25r0
elem_011_COM_v25rd
elem_011_COM_v25rr
elem_011_COM_v25aa0_TEST_43_full_no_check
elem_011_COM_v25aa0_TEST_43_orig_no_check
elem_011_COM_v25aa2_TEST_43_full_no_check
elem_011_COM_v25aa2_TEST_43_orig_no_check
1:1 line
Wet dep to Great Lakes MDN sites estimated with "base" numerical configuration (g/m2-year)

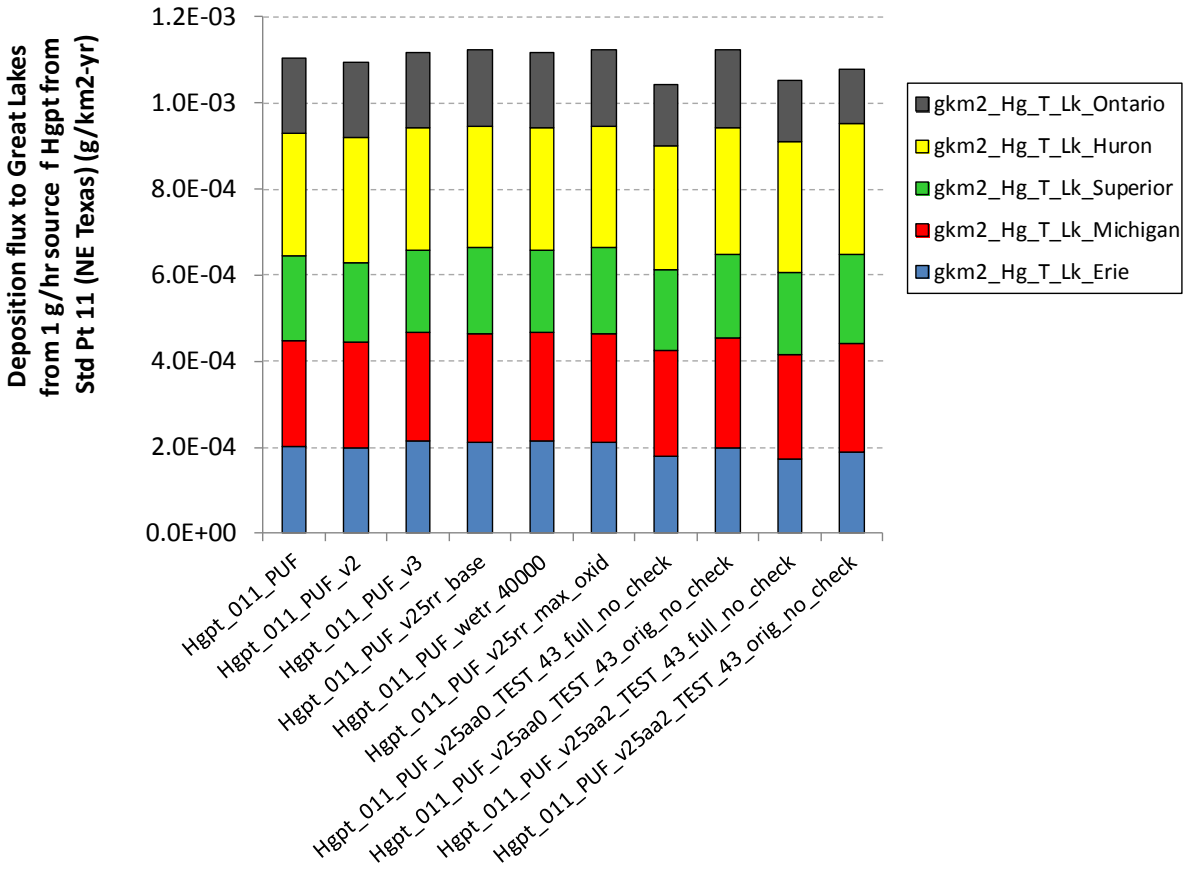
Deposition flux to Great Lakes from 1 g/hr source f Hgpt from Std Pt 11 (NE Texas) (g/km2-yr)
1.2E-03
1.0E-03
8.0E-04
6.0E-04
4.0E-04
2.0E-04
0.0E+00
gkm2_Hg_T_Lk_Ontario
gkm2_Hg_T_Lk_Huron
gkm2_Hg_T_Lk_Superior
gkm2_Hg_T_Lk_Michigan
gkm2_Hg_T_Lk_Erie
Hgpt_011_PUF
Hgpt_011_PUF_v2
Hgpt_011_PUF_v3
Hgpt_011_PUF_v25rr_base
Hgpt_011_PUF_wetr_40000
Hgpt_011_PUF_v25rr_max_oxid
Hgpt_011_PUF_v25aa0_TEST_43_full_no_check
Hgpt_011_PUF_v25aa0_TEST_43_orig_no_check
Hgpt_011_PUF_v25aa2_TEST_43_full_no_check
Hgpt_011_PUF_v25aa2_TEST_43_orig_no_check

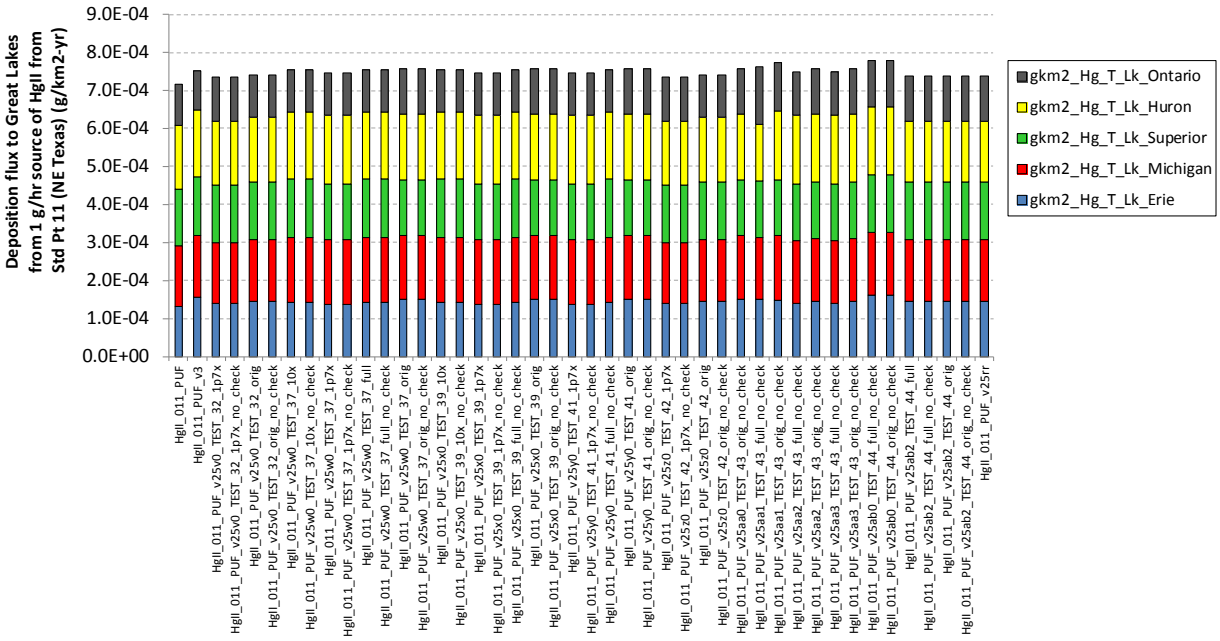
Deposition flux to Great Lakes from 1 g/hr source of HgII from Std Pt 11 (NE Texas) (g/km2-yr)
9.0E-04
8.0E-04
7.0E-04
6.0E-04
5.0E-04
4.0E-04
3.0E-04
2.0E-04
1.0E-04
0.0E+00
gkm2_Hg_T_Lk_Ontario
gkm2_Hg_T_Lk_Huron
gkm2_Hg_T_Lk_Superior
gkm2_Hg_T_Lk_Michigan
gkm2_Hg_T_Lk_Erie

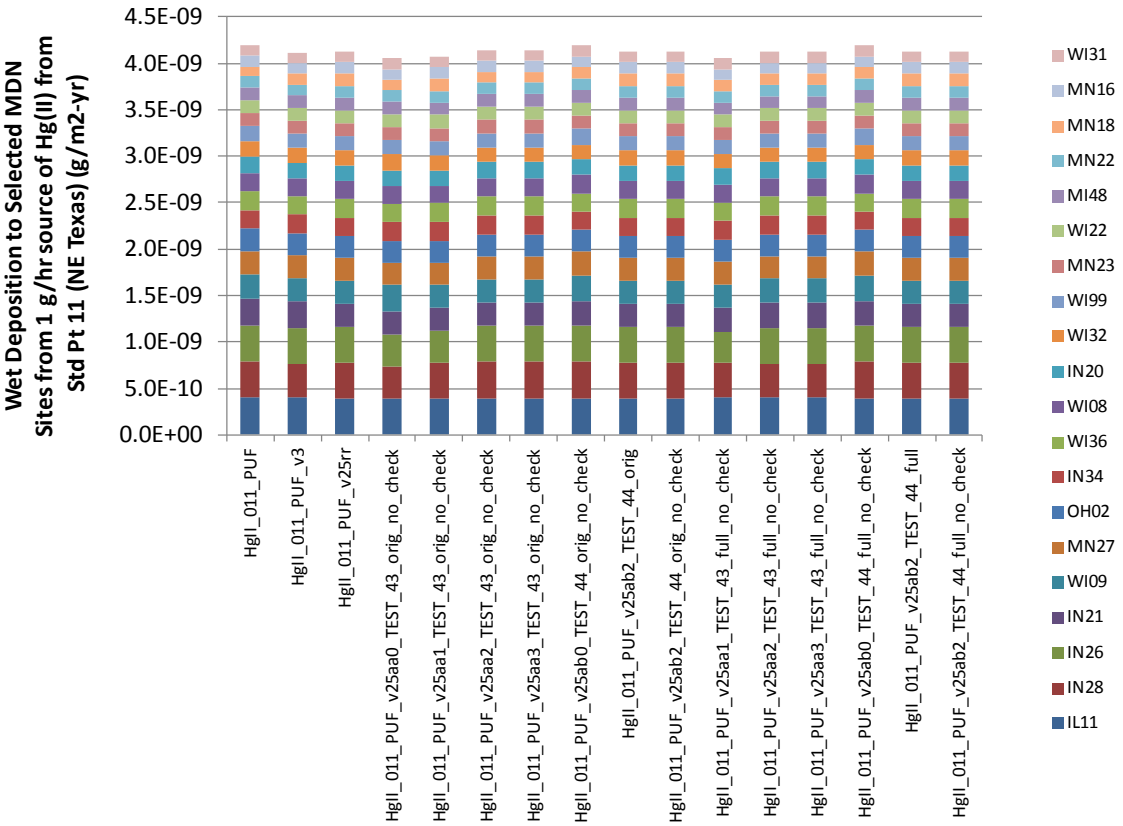
Wet Deposition to Selected MDN Sites from 1 g/hr source of Hg(II) from Std Pt 11 (NE Texas) (g/m2-yr)
4.5E-09
4.0E-09
3.5E-09
3.0E-09
2.5E-09
2.0E-09
1.5E-09
1.0E-09
5.0E-10
0.0E+00
HgII_011_PUF
HgII_011_PUF_v3
HgII_011_PUF_v25rr
HgII_011_PUF_v25aa0_TEST_43_orig_no_check
HgII_011_PUF_v25aa1_TEST_43_orig_no_check
HgII_011_PUF_v25aa2_TEST_43_orig_no_check
HgII_011_PUF_v25aa3_TEST_43_orig_no_check
HgII_011_PUF_v25ab0_TEST_44_orig_no_check
HgII_011_PUF_v25ab2_TEST_44_orig
HgII_011_PUF_v25ab2_TEST_44_orig_no_check
HgII_011_PUF_v25aa1_TEST_43_full_no_check
HgII_011_PUF_v25aa2_TEST_43_full_no_check
HgII_011_PUF_v25aa3_TEST_43_full_no_check
HgII_011_PUF_v25ab0_TEST_44_full_no_check
HgII_011_PUF_v25ab2_TEST_44_full
HgII_011_PUF_v25ab2_TEST_44_full_no_check
WI31
MN16
MN18
MN22
MI48
WI22
MN23
WI99
WI32
IN20
WI08
WI36
IN34
OH02
MN27
WI09
IN21
IN26
IN28
IL11

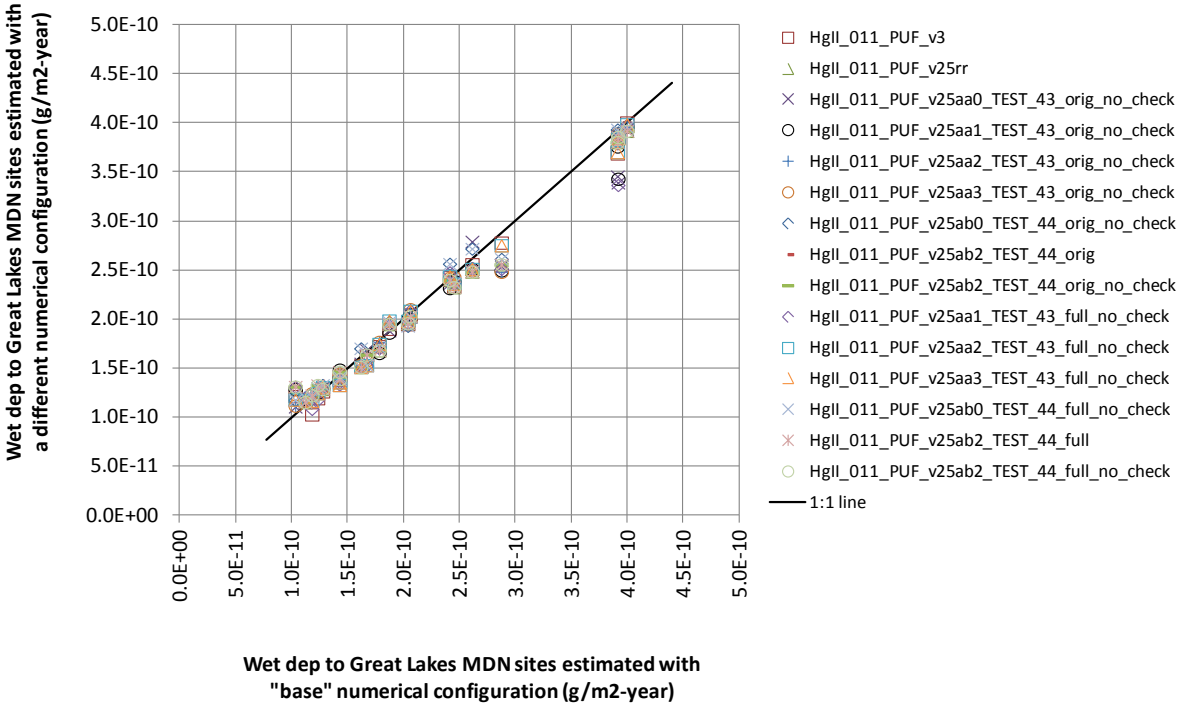
Wet dep to Great Lakes MDN sites estimated with a different numerical configuration (g/m2-year)
5.0E-10
4.5E-10
4.0E-10
3.5E-10
3.0E-10
2.5E-10
2.0E-10
1.5E-10
1.0E-10
5.0E-11
0.0E+00
0.0E+00
5.0E-11
1.0E-10
1.5E-10
2.0E-10
2.5E-10
3.0E-10
3.5E-10
4.0E-10
4.5E-10
5.0E-10
Wet dep to Great Lakes MDN sites estimated with "base" numerical configuration (g/m2-year)
HgII_011_PUF_v3
HgII_011_PUF_v25rr
HgII_011_PUF_v25aa0_TEST_43_orig_no_check
HgII_011_PUF_v25aa1_TEST_43_orig_no_check
HgII_011_PUF_v25aa2_TEST_43_orig_no_check
HgII_011_PUF_v25aa3_TEST_43_orig_no_check
HgII_011_PUF_v25ab0_TEST_44_orig_no_check
HgII_011_PUF_v25ab2_TEST_44_orig
HgII_011_PUF_v25ab2_TEST_44_orig_no_check
HgII_011_PUF_v25aa1_TEST_43_full_no_check
HgII_011_PUF_v25aa2_TEST_43_full_no_check
HgII_011_PUF_v25aa3_TEST_43_full_no_check
HgII_011_PUF_v25ab0_TEST_44_full_no_check
HgII_011_PUF_v25ab2_TEST_44_full
HgII_011_PUF_v25ab2_TEST_44_full_no_check
1:1 line

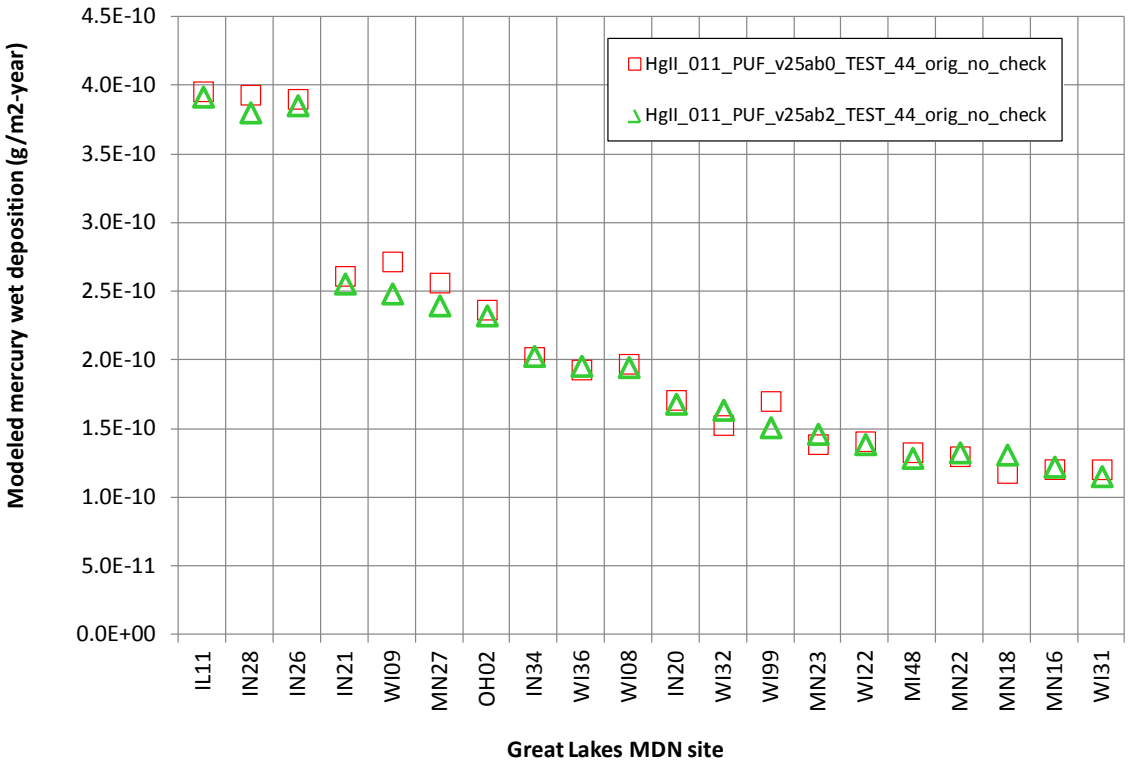
Modeled mercury wet deposition (g/m2-year)
4.5E-10
4.0E-10
3.5E-10
3.0E-10
2.5E-10
2.0E-10
1.5E-10
1.0E-10
5.0E-11
0.0E+00
HgII_011_PUF_v25ab0_TEST_44_orig_no_check
HgII_011_PUF_v25ab2_TEST_44_orig_no_check
IL11
IN28
IN26
IN21
WI09
MN27
OH02
IN34
WI36
WI08
IN20
WI32
WI99
MN23
WI22
MI48
MN22
MN18
MN16
WI31
Great Lakes MDN site

7.5. Standard Source Location #6 (Ohio River Valley)

The graphs below show comparisons for a number of different simulations for emissions from standard source location #6, in the Ohio River Valley. In almost all cases, it is seen that the computational variations have very little influence on the overall results for deposition to the Great Lakes or to wet deposition to MDN sites in the Great Lakes region. The largest differences in the results appear to occur for differences in the compiler optimization schemes.

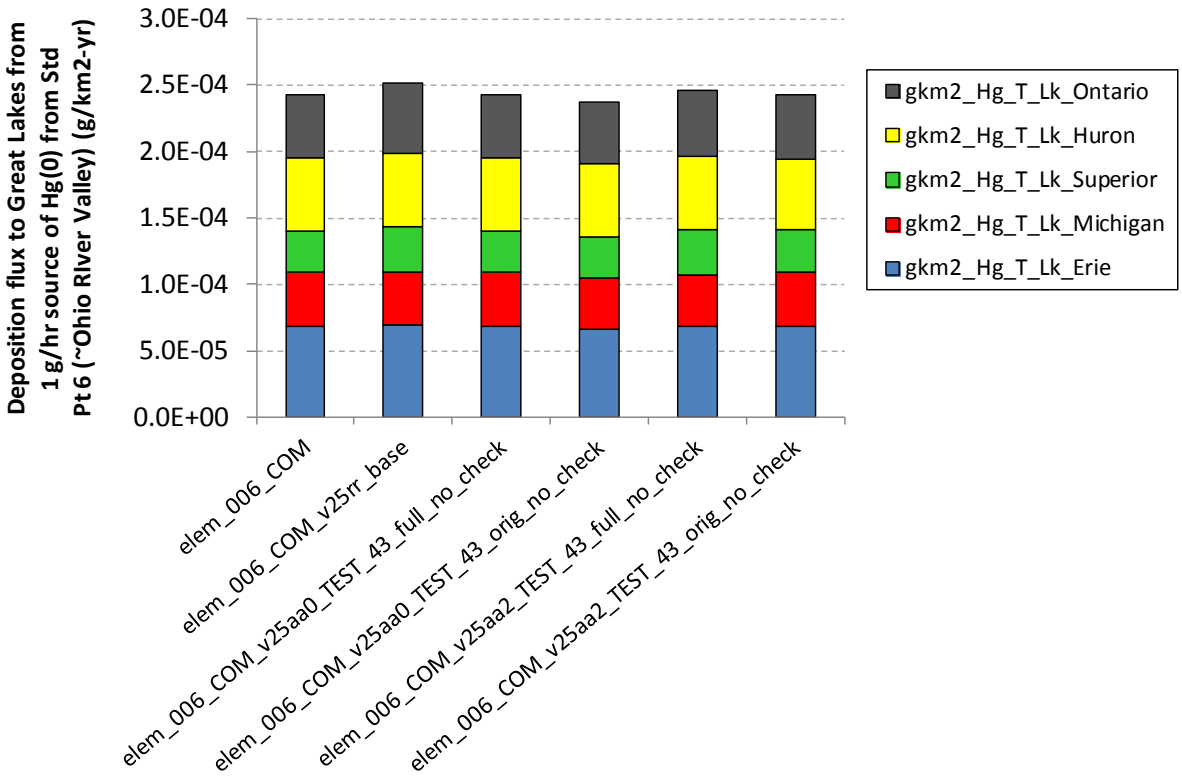

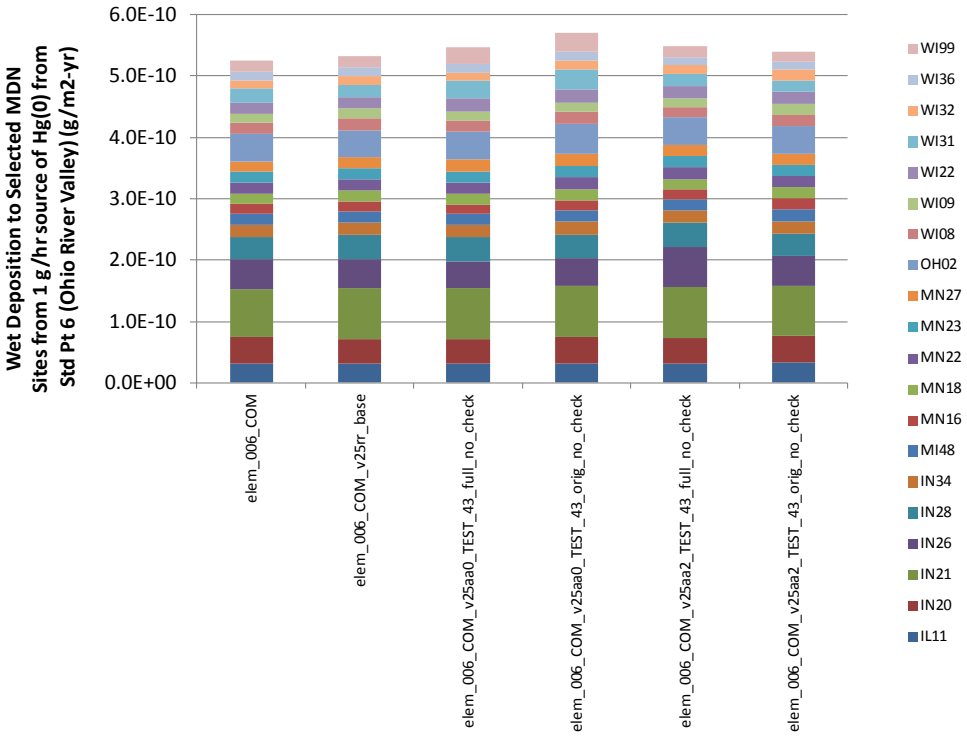
Wet Deposition to Selected MDN Sites from 1 g/hr source of Hg(0) from Std Pt 6 (Ohio River Valley) (g/m2-yr)
6.0E-10
5.0E-10
4.0E-10
3.0E-10
2.0E-10
1.0E-10
0.0E+00
elem_006_COM
elem_006_COM_v25rr_base
elem_006_COM_v25aa0_TEST_43_full_no_check
elem_006_COM_v25aa0_TEST_43_orig_no_check
elem_006_COM_v25aa2_TEST_43_full_no_check
elem_006_COM_v25aa2_TEST_43_orig_no_check
WI99
WI36
WI32
WI31
WI22
WI09
WI08
OH02
MN27
MN23
MN22
MN18
MN16
MI48
IN34
IN28
IN26
IN21
IN20
IL11

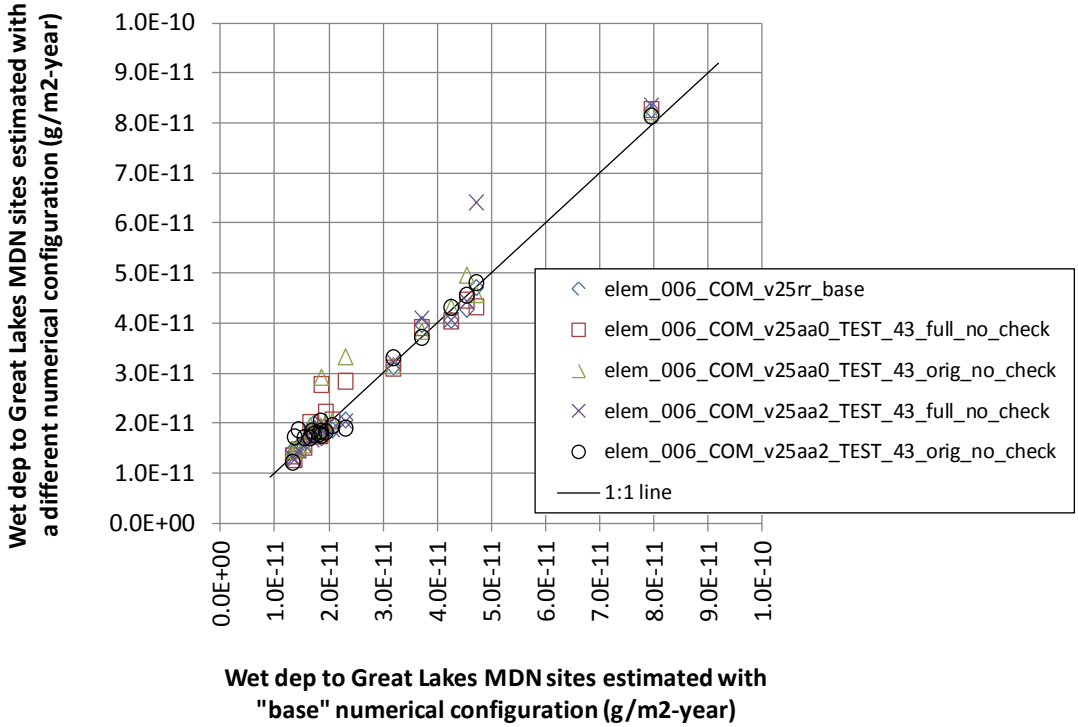
Wet dep to Great Lakes MDN sites estimated with a different numerical configuration (g/m2-year)
1.0E-10
9.0E-11
8.0E-11
7.0E-11
6.0E-11
5.0E-11
4.0E-11
3.0E-11
2.0E-11
1.0E-11
0.0E+00
0.0E+00
1.0E-11
2.0E-11
3.0E-11
4.0E-11
5.0E-11
6.0E-11
7.0E-11
8.0E-11
9.0E-11
1.0E-10
elem_006_COM_v25rr_base
elem_006_COM_v25aa0_TEST_43_full_no_check
elem_006_COM_v25aa0_TEST_43_orig_no_check
elem_006_COM_v25aa2_TEST_43_full_no_check
elem_006_COM_v25aa2_TEST_43_orig_no_check
1:1 line
Wet dep to Great Lakes MDN sites estimated with "base" numerical configuration (g/m2-year)

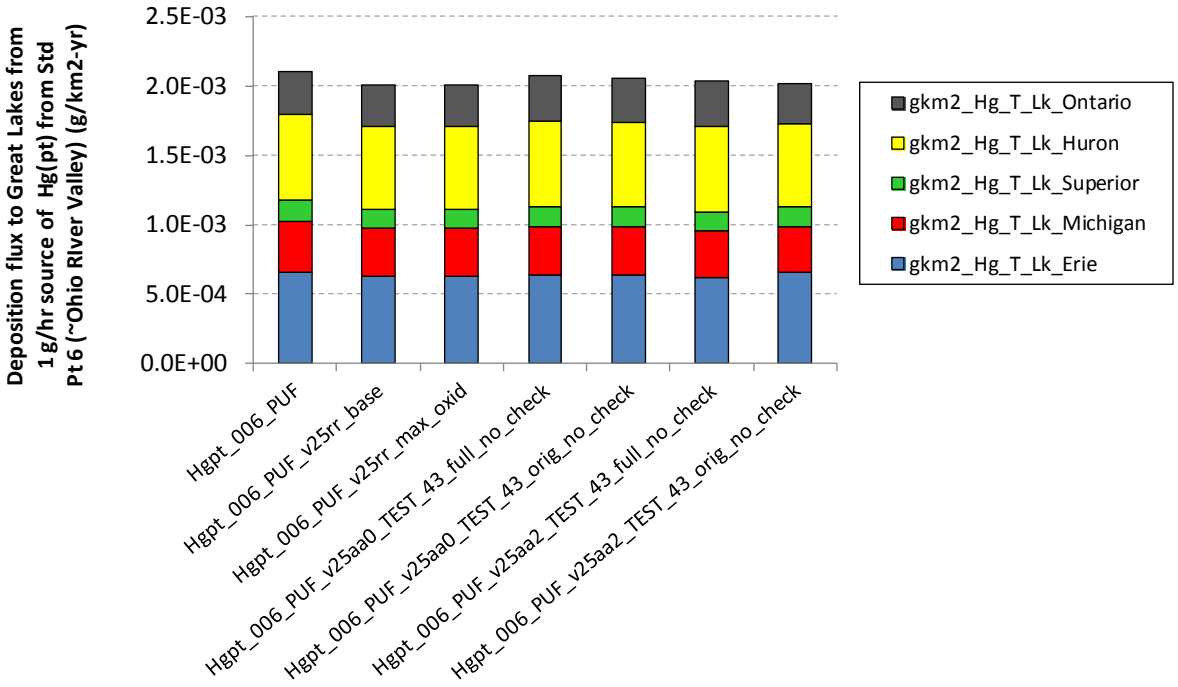
Deposition flux to Great Lakes from 1 g/hr source of Hg(pt) from Std Pt 6 (~Ohio River Valley) (g/km2-yr)
2.5E-03
2.0E-03
1.5E-03
1.0E-03
5.0E-04
0.0E+00
gkm2_Hg_T_Lk_Ontario
gkm2_Hg_T_Lk_Huron
gkm2_Hg_T_Lk_Superior
gkm2_Hg_T_Lk_Michigan
gkm2_Hg_T_Lk_Erie
Hgpt_006_PUF
Hgpt_006_PUF_v25rr_base
Hgpt_006_PUF_v25rr_max_oxid
Hgpt_006_PUF_v25aa0_TEST_43_full_no_check
Hgpt_006_PUF_v25aa0_TEST_43_orig_no_check
Hgpt_006_PUF_v25aa2_TEST_43_full_no_check
Hgpt_006_PUF_v25aa2_TEST_43_orig_no_check

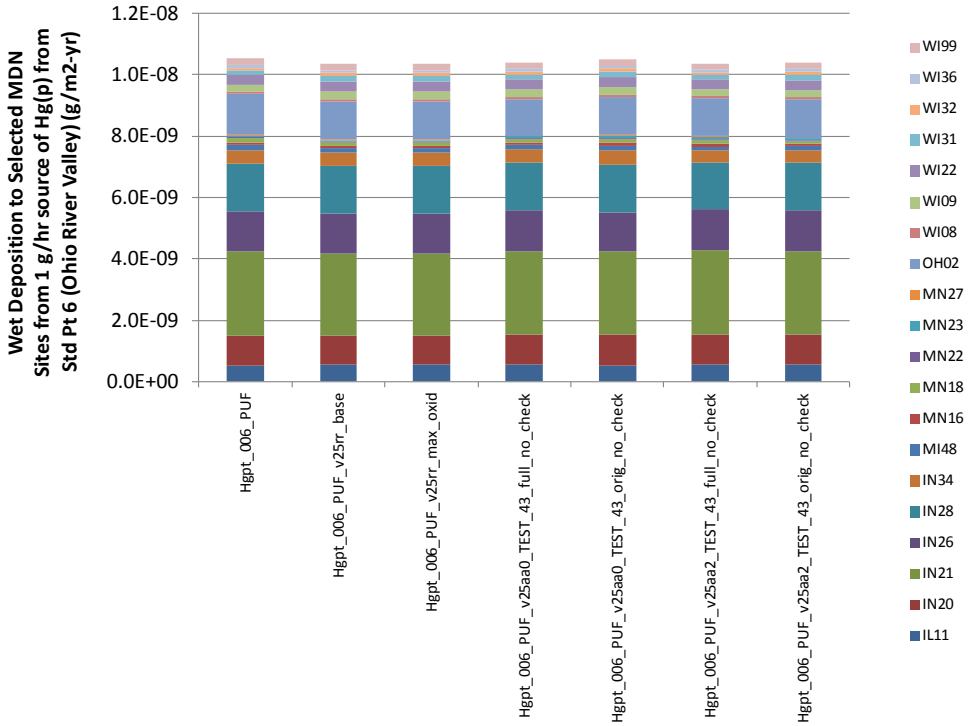
Wet Deposition to Selected MDN Sites from 1 g/hr source of Hg(p) from Std Pt 6 (Ohio River Valley) (g/m2-yr)
1.2E-08
1.0E-08
8.0E-09
6.0E-09
4.0E-09
2.0E-09
0.0E+00
WI99
WI36
WI32
WI31
WI22
WI09
WI08
OH02
MN27
MN23
MN22
MN18
MN16
MI48
IN34
IN28
IN26
IN21
IN20
IL11
Hgpt_006_PUF
Hgpt_006_PUF_v25rr_base
Hgpt_006_PUF_v25rr_max_oxid
Hgpt_006_PUF_v25aa0_TEST_43_full_no_check
Hgpt_006_PUF_v25aa0_TEST_43_orig_no_check
Hgpt_006_PUF_v25aa2_TEST_43_full_no_check
Hgpt_006_PUF_v25aa2_TEST_43_orig_no_check

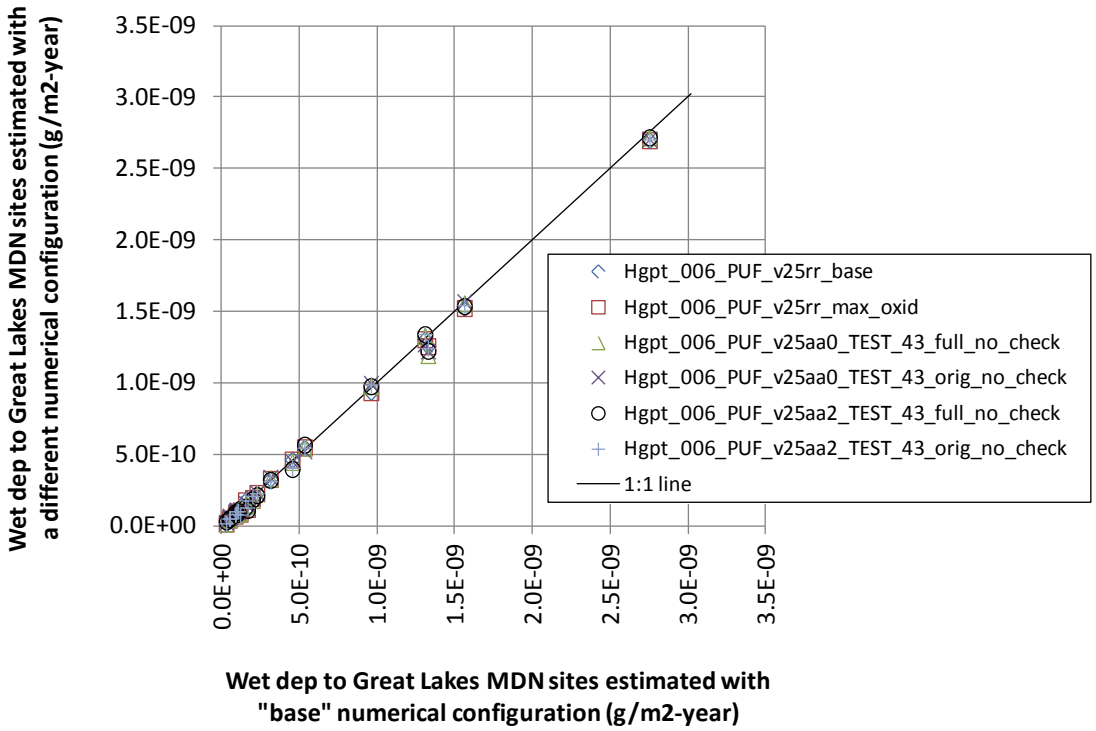
Wet dep to Great Lakes MDN sites estimated with a different numerical configuration (g/m2-year)
3.5E-09
3.0E-09
2.5E-09
2.0E-09
1.5E-09
1.0E-09
5.0E-10
0.0E+00
0.0E+00
5.0E-10
1.0E-09
1.5E-09
2.0E-09
2.5E-09
3.0E-09
3.5E-09
Hgpt_006_PUF_v25rr_base
Hgpt_006_PUF_v25rr_max_oxid
Hgpt_006_PUF_v25aa0_TEST_43_full_no_check
Hgpt_006_PUF_v25aa0_TEST_43_orig_no_check
Hgpt_006_PUF_v25aa2_TEST_43_full_no_check
Hgpt_006_PUF_v25aa2_TEST_43_orig_no_check
1:1 line
Wet dep to Great Lakes MDN sites estimated with "base" numerical configuration (g/m2-year)

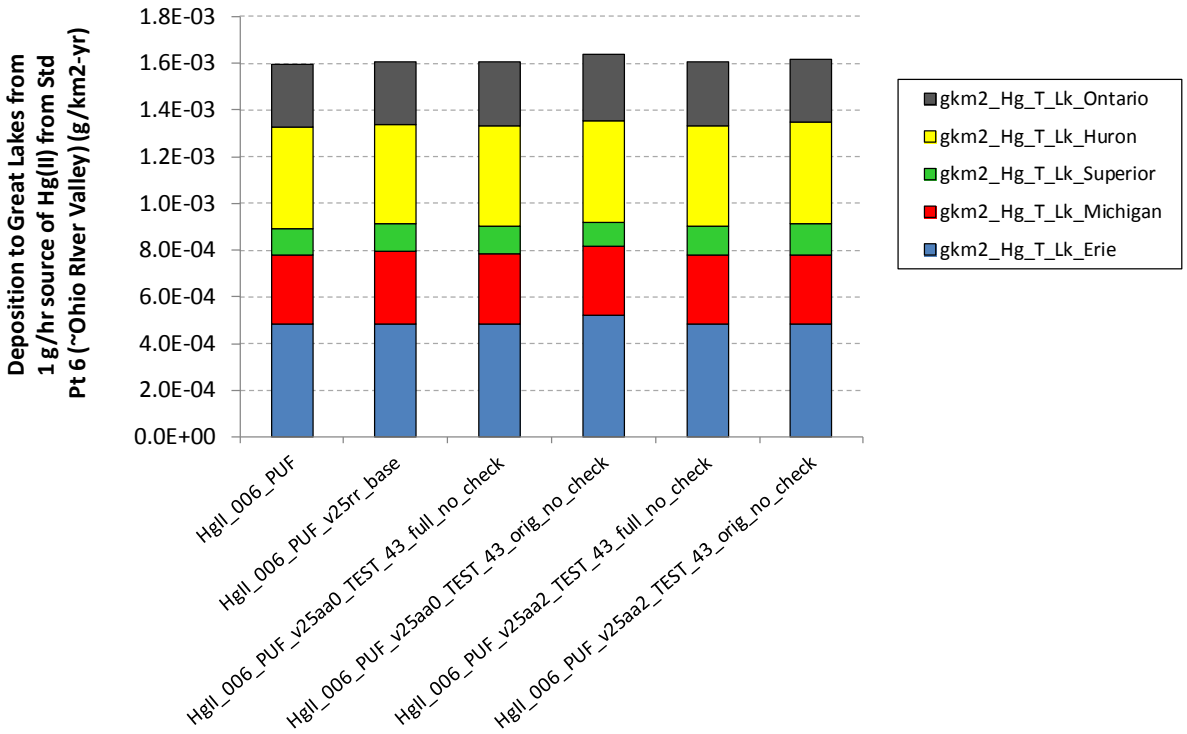
Deposition to Great Lakes from 1 g/hr source of Hg(II) from Std Pt 6 (~Ohio River Valley) (g/km2-yr)
1.8E-03
1.6E-03
1.4E-03
1.2E-03
1.0E-03
8.0E-04
6.0E-04
4.0E-04
2.0E-04
0.0E+00
HgII_006_PUF
HgII_006_PUF_v25rr_base
HgII_006_PUF_v25aa0_TEST_43_full_no_check
HgII_006_PUF_v25aa0_TEST_43_orig_no_check
HgII_006_PUF_v25aa2_TEST_43_full_no_check
HgII_006_PUF_v25aa2_TEST_43_orig_no_check
gkm2_Hg_T_Lk_Ontario
gkm2_Hg_T_Lk_Huron
gkm2_Hg_T_Lk_Superior
gkm2_Hg_T_Lk_Michigan
gkm2_Hg_T_Lk_Erie

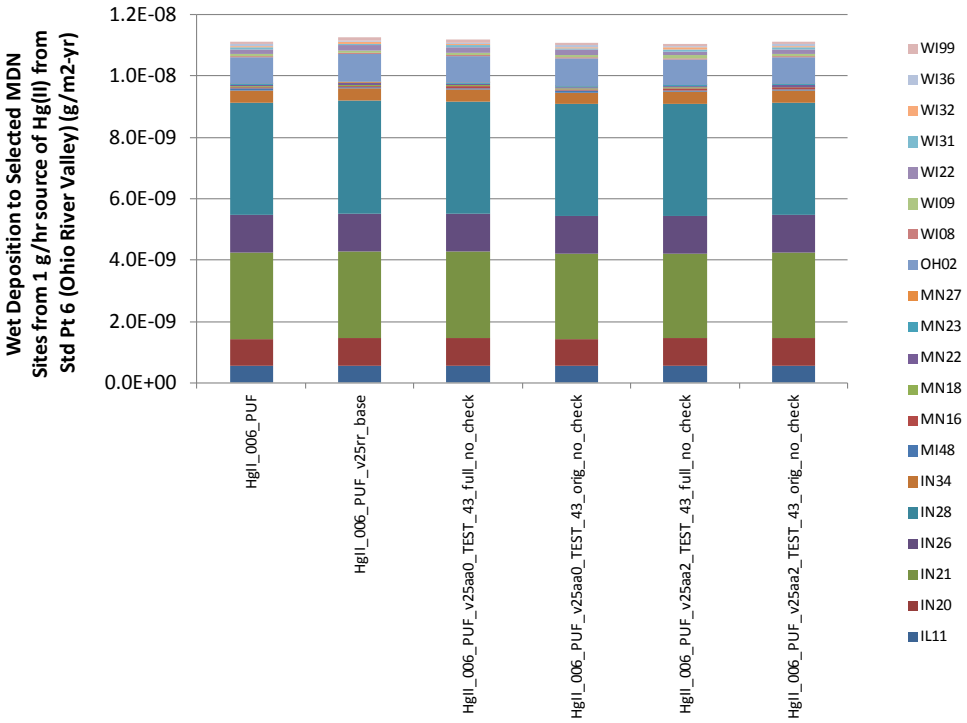
Wet Deposition to Selected MDN Sites from 1 g/hr source of Hg(II) from Std Pt 6 (Ohio River Valley) (g/m2-yr)
1.2E-08
1.0E-08
8.0E-09
6.0E-09
4.0E-09
2.0E-09
0.0E+00
HgII_006_PUF
HgII_006_PUF_v25rr_base
HgII_006_PUF_v25aa0_TEST_43_full_no_check
HgII_006_PUF_v25aa0_TEST_43_orig_no_check
HgII_006_PUF_v25aa2_TEST_43_full_no_check
HgII_006_PUF_v25aa2_TEST_43_orig_no_check
WI99
WI36
WI32
WI31
WI22
WI09
WI08
OH02
MN27
MN23
MN22
MN18
MN16
MI48
IN34
IN28
IN26
IN21
IN20
IL11

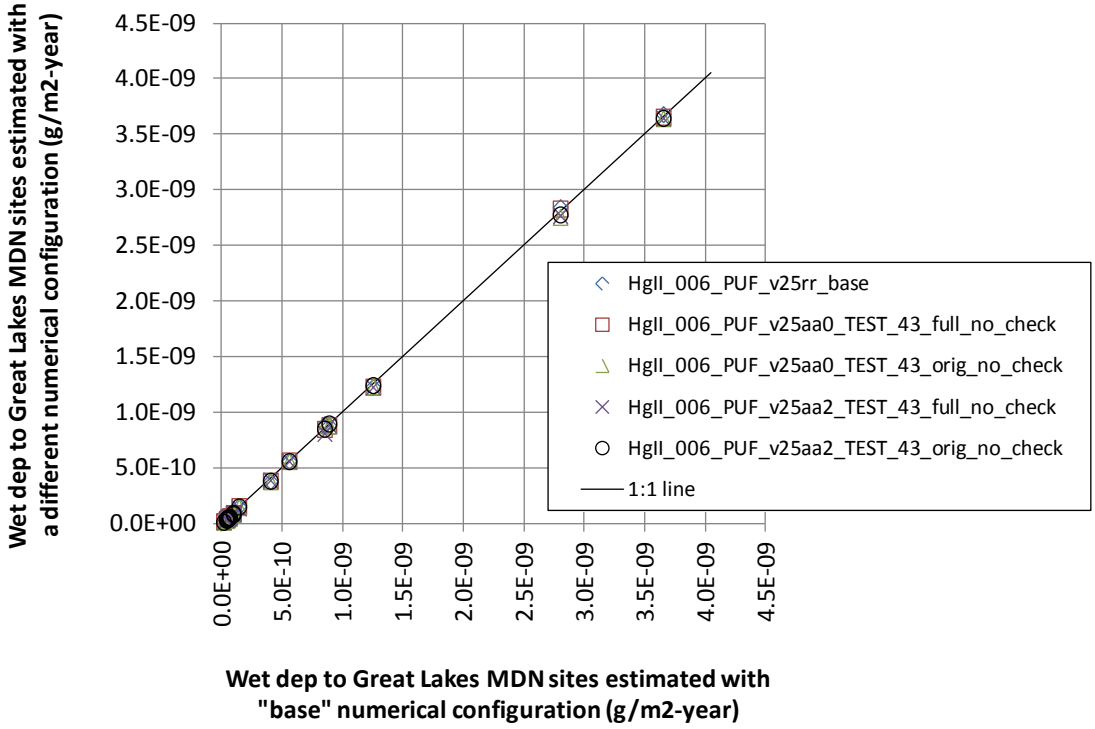
Wet dep to Great Lakes MDN sites estimated with a different numerical configuration (g/m2-year)
4.5E-09
4.0E-09
3.5E-09
3.0E-09
2.5E-09
2.0E-09
1.5E-09
1.0E-09
5.0E-10
0.0E+00
0.0E+00
5.0E-10
1.0E-09
1.5E-09
2.0E-09
2.5E-09
3.0E-09
3.5E-09
4.0E-09
4.5E-09
HgII_006_PUF_v25rr_base
HgII_006_PUF_v25aa0_TEST_43_full_no_check
HgII_006_PUF_v25aa0_TEST_43_orig_no_check
HgII_006_PUF_v25aa2_TEST_43_full_no_check
HgII_006_PUF_v25aa2_TEST_43_orig_no_check
1:1 line
Wet dep to Great Lakes MDN sites estimated with "base" numerical configuration (g/m2-year)

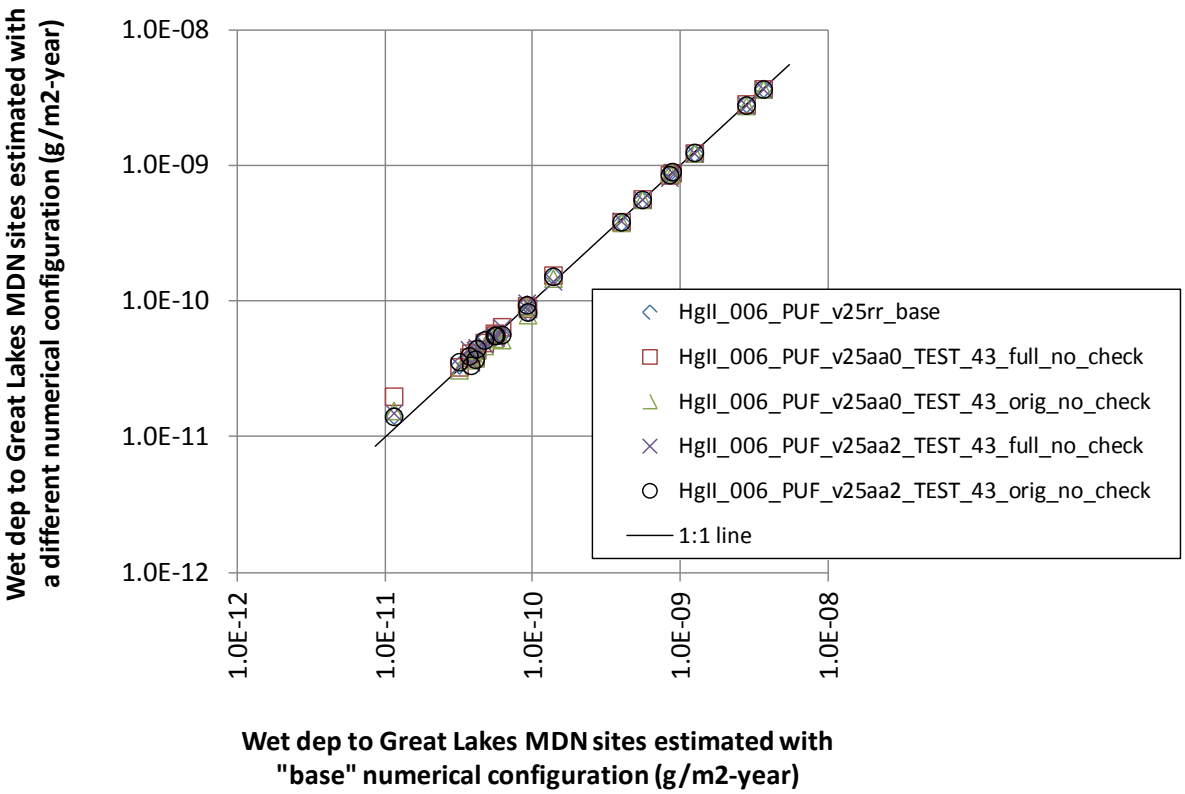
Wet dep to Great Lakes MDN sites estimated with a different numerical configuration (g/m2-year)
1.0E-08
1.0E-09
1.0E-10
1.0E-11
1.0E-12
1.0E-12
1.0E-11
1.0E-10
1.0E-09
1.0E-08
Wet dep to Great Lakes MDN sites estimated with "base" numerical configuration (g/m2-year)
HgII_006_PUF_v25rr_base
HgII_006_PUF_v25aa0_TEST_43_full_no_check
HgII_006_PUF_v25aa0_TEST_43_orig_no_check
HgII_006_PUF_v25aa2_TEST_43_full_no_check
HgII_006_PUF_v25aa2_TEST_43_orig_no_check
1:1 line

7.6. Standard Source Location #8 (western shore of Lake Erie)

The graphs below show comparisons for a number of different simulations for emissions from standard source location #8, on the western shore of Lake Erie. In almost all cases, it is seen that the computational variations have very little influence on the overall results for deposition to the Great Lakes or to wet deposition to MDN sites in the Great Lakes region. The largest differences in the results appear to occur for differences in the compiler optimization schemes.

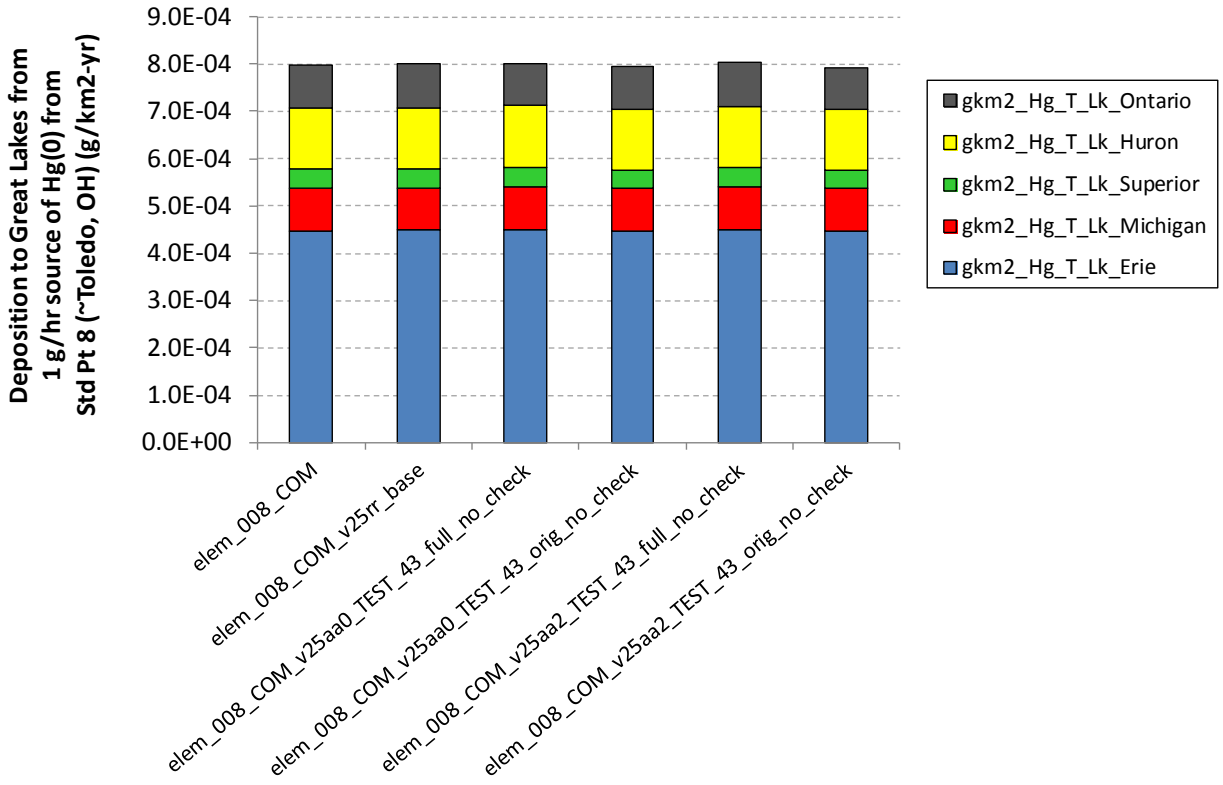

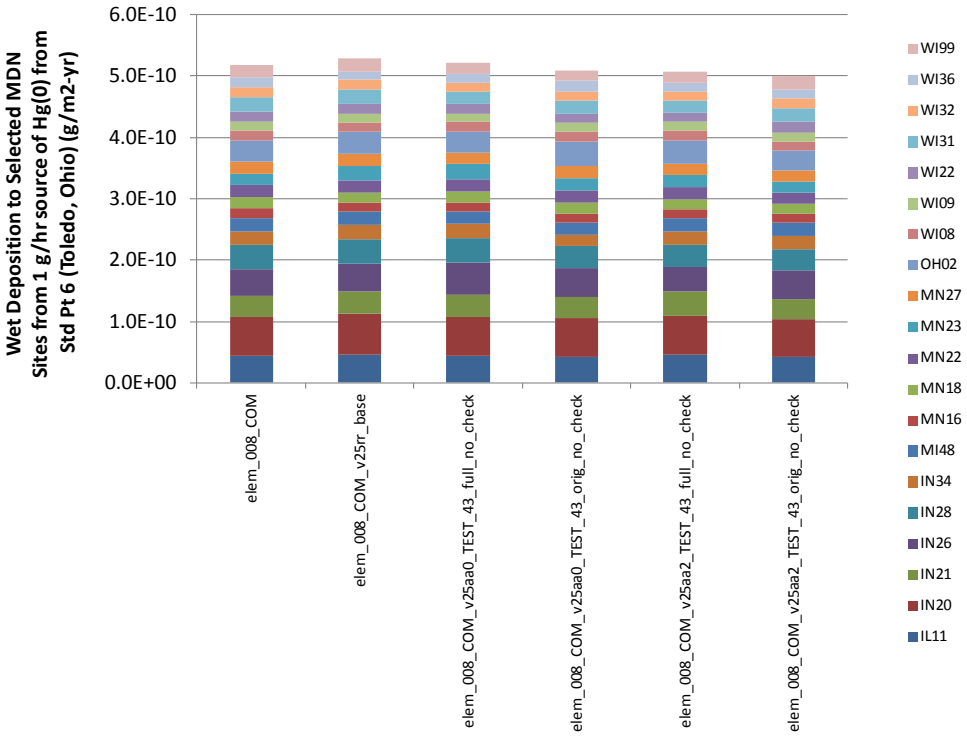
Wet Deposition to Selected MDN Sites from 1 g/hr source of Hg(0) from Std Pt 6 (Toledo, Ohio) (g/m2-yr)
6.0E-10
5.0E-10
4.0E-10
3.0E-10
2.0E-10
1.0E-10
0.0E+00
elem_008_COM
elem_008_COM_v25rr_base
elem_008_COM_v25aa0_TEST_43_full_no_check
elem_008_COM_v25aa0_TEST_43_orig_no_check
elem_008_COM_v25aa2_TEST_43_full_no_check
elem_008_COM_v25aa2_TEST_43_orig_no_check
WI99
WI36
WI32
WI31
WI22
WI09
WI08
OH02
MN27
MN23
MN22
MN18
MN16
MI48
IN34
IN28
IN26
IN21
IN20
IL11

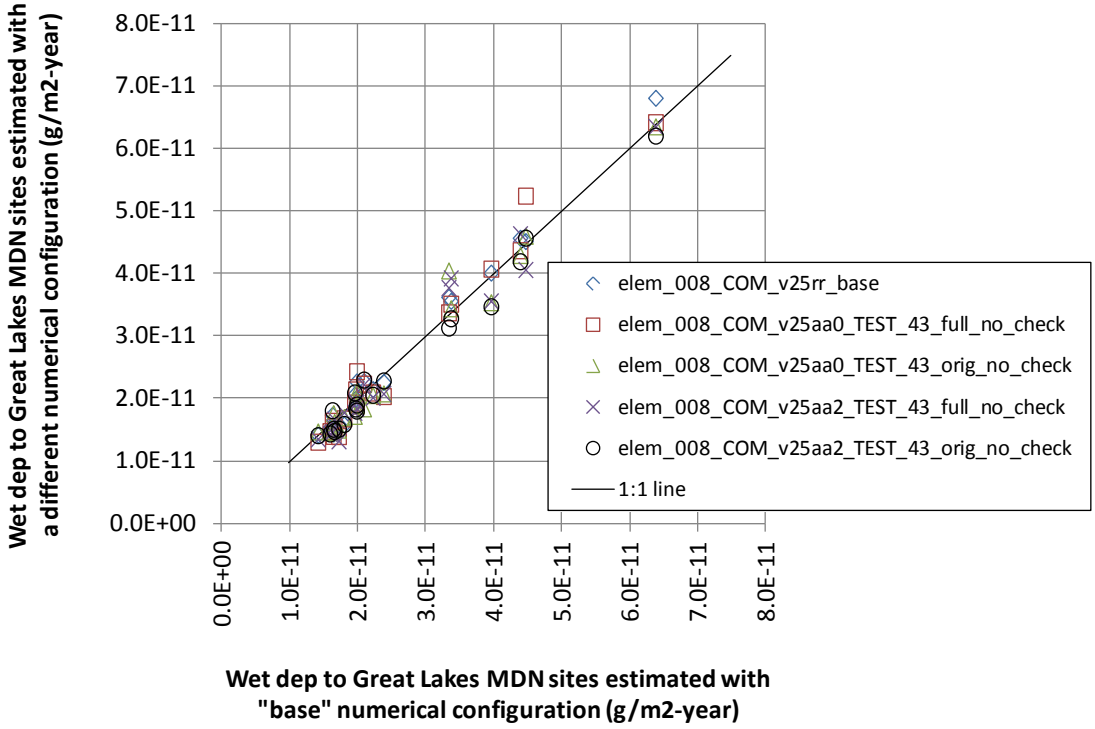
Wet dep to Great Lakes MDN sites estimated with a different numerical configuration (g/m2-year)
8.0E-11
7.0E-11
6.0E-11
5.0E-11
4.0E-11
3.0E-11
2.0E-11
1.0E-11
0.0E+00
0.0E+00
1.0E-11
2.0E-11
3.0E-11
4.0E-11
5.0E-11
6.0E-11
7.0E-11
8.0E-11
elem_008_COM_v25rr_base
elem_008_COM_v25aa0_TEST_43_full_no_check
elem_008_COM_v25aa0_TEST_43_orig_no_check
elem_008_COM_v25aa2_TEST_43_full_no_check
elem_008_COM_v25aa2_TEST_43_orig_no_check
1:1 line
Wet dep to Great Lakes MDN sites estimated with "base" numerical configuration (g/m2-year)

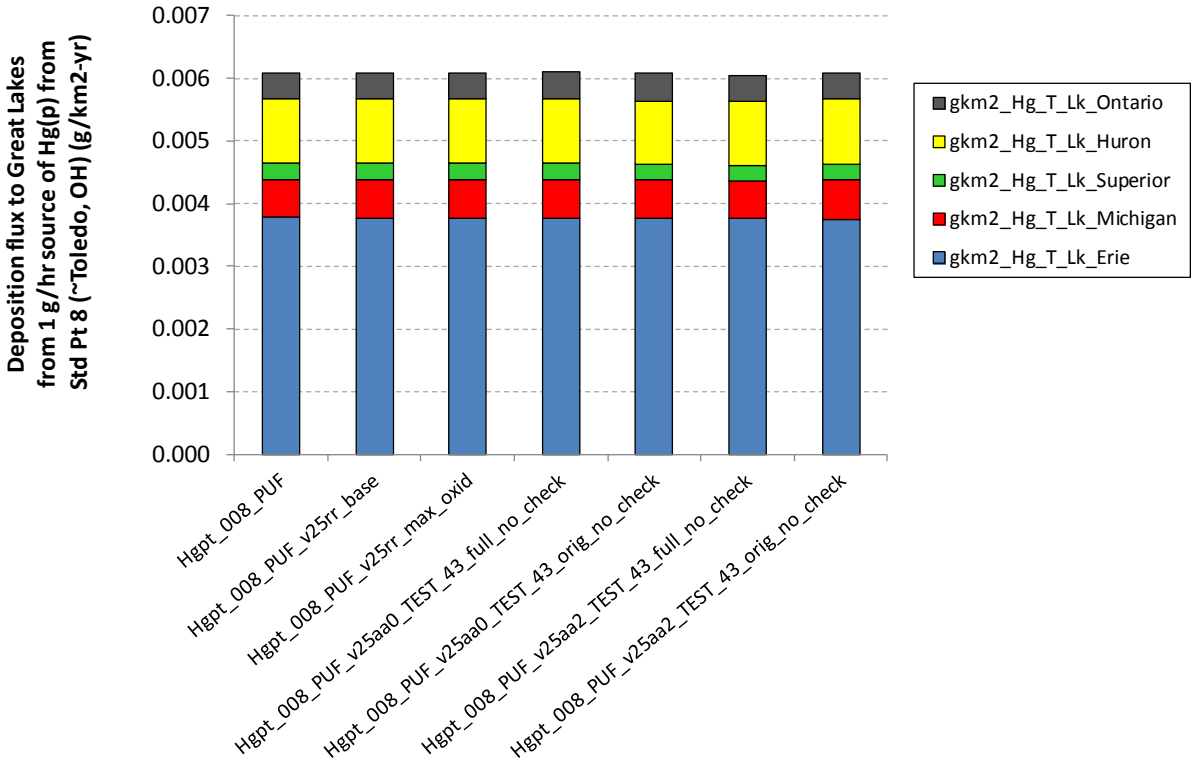
Deposition flux to Great Lakes from 1 g/hr source of Hg(p) from Std Pt 8 (~Toledo, OH) (g/km2-yr)
0.007
0.006
0.005
0.004
0.003
0.002
0.001
0.000
gkm2_Hg_T_Lk_Ontario
gkm2_Hg_T_Lk_Huron
gkm2_Hg_T_Lk_Superior
gkm2_Hg_T_Lk_Michigan
gkm2_Hg_T_Lk_Erie
Hgpt_008_PUF
Hgpt_008_PUF_v25rr_base
Hgpt_008_PUF_v25rr_max_oxid
Hgpt_008_PUF_v25aa0_TEST_43_full_no_check
Hgpt_008_PUF_v25aa0_TEST_43_orig_no_check
Hgpt_008_PUF_v25aa2_TEST_43_full_no_check
Hgpt_008_PUF_v25aa2_TEST_43_orig_no_check

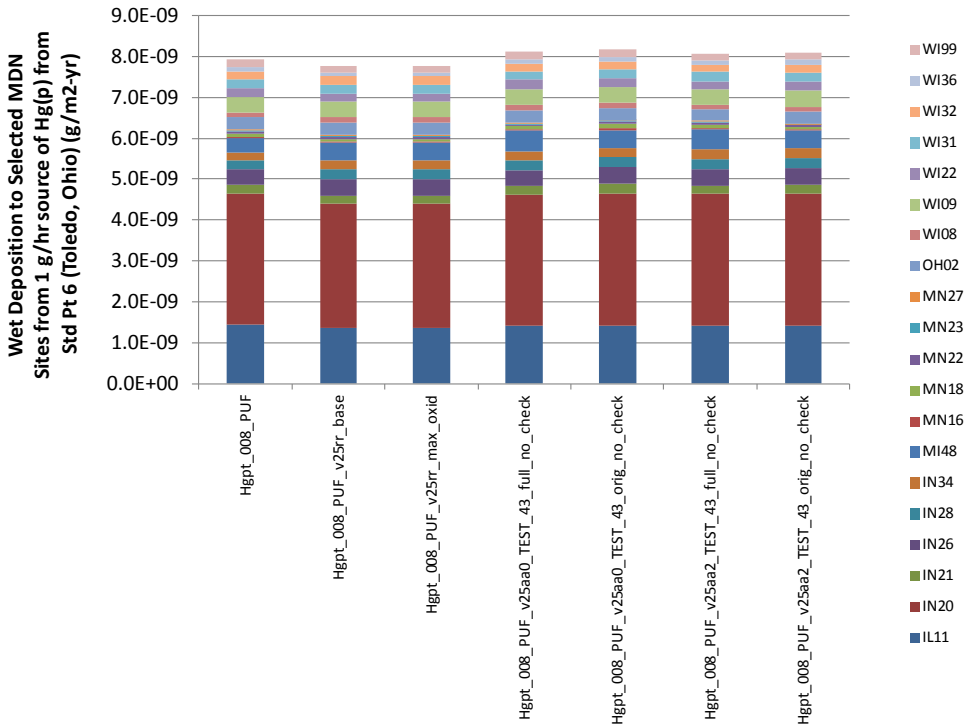
Wet Deposition to Selected MDN Sites from 1 g/hr source of Hg(p) from Std Pt 6 (Toledo, Ohio) (g/m2-yr)
9.0E-09
8.0E-09
7.0E-09
6.0E-09
5.0E-09
4.0E-09
3.0E-09
2.0E-09
1.0E-09
0.0E+00
WI99
WI36
WI32
WI31
WI22
WI09
WI08
OH02
MN27
MN23
MN22
MN18
MN16
MI48
IN34
IN28
IN26
IN21
IN20
IL11
Hgpt_008_PUF
Hgpt_008_PUF_v25rr_base
Hgpt_008_PUF_v25rr_max_oxid
Hgpt_008_PUF_v25aa0_TEST_43_full_no_check
Hgpt_008_PUF_v25aa0_TEST_43_orig_no_check
Hgpt_008_PUF_v25aa2_TEST_43_full_no_check
Hgpt_008_PUF_v25aa2_TEST_43_orig_no_check

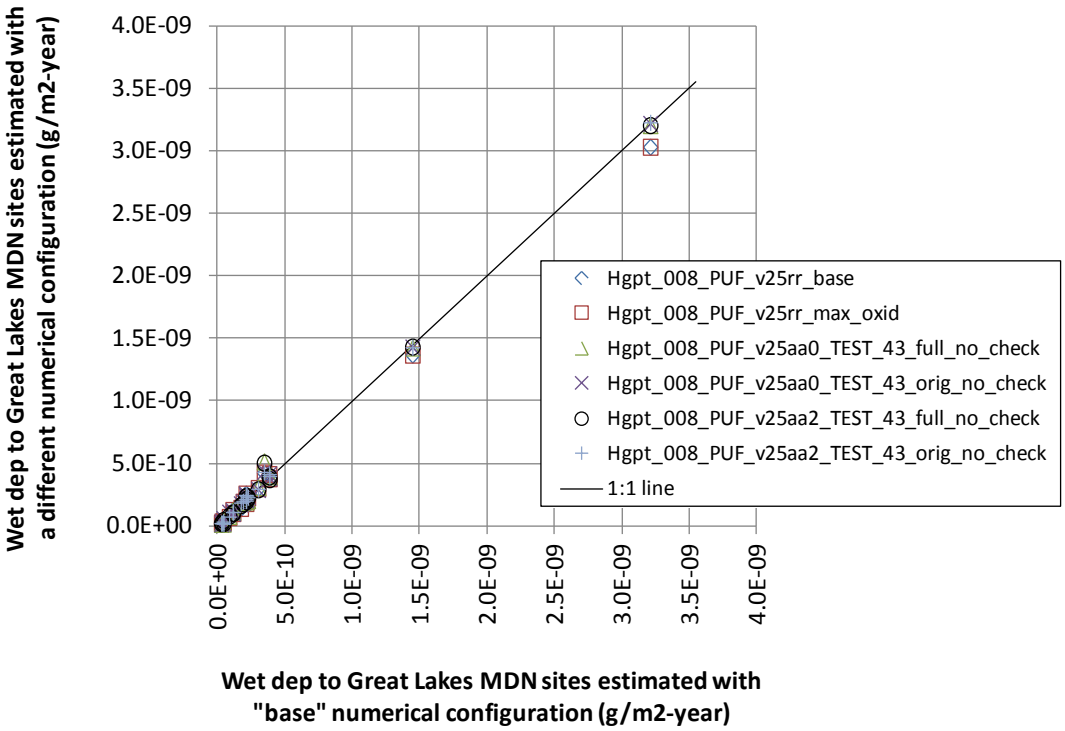
Wet dep to Great Lakes MDN sites estimated with a different numerical configuration (g/m2-year)
4.0E-09
3.5E-09
3.0E-09
2.5E-09
2.0E-09
1.5E-09
1.0E-09
5.0E-10
0.0E+00
0.0E+00
5.0E-10
1.0E-09
1.5E-09
2.0E-09
2.5E-09
3.0E-09
3.5E-09
4.0E-09
Hgpt_008_PUF_v25rr_base
Hgpt_008_PUF_v25rr_max_oxid
Hgpt_008_PUF_v25aa0_TEST_43_full_no_check
Hgpt_008_PUF_v25aa0_TEST_43_orig_no_check
Hgpt_008_PUF_v25aa2_TEST_43_full_no_check
Hgpt_008_PUF_v25aa2_TEST_43_orig_no_check
1:1 line
Wet dep to Great Lakes MDN sites estimated with "base" numerical configuration (g/m2-year)

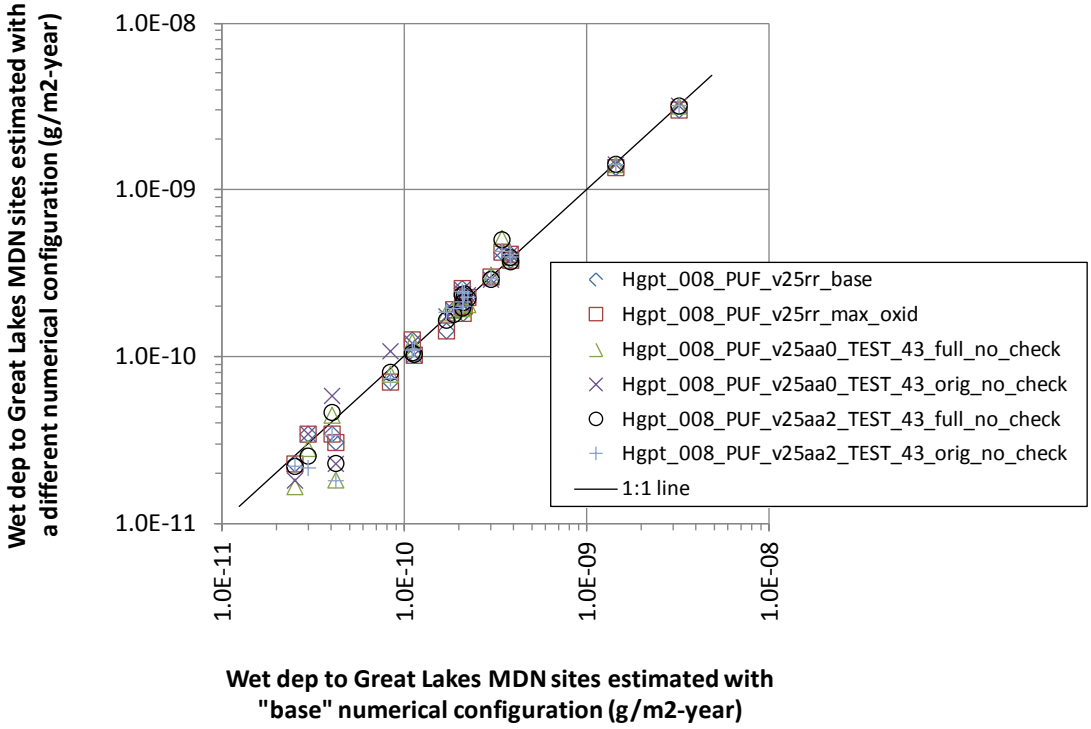
Wet dep to Great Lakes MDN sites estimated with a different numerical configuration (g/m2-year)
1.0E-08
1.0E-09
1.0E-10
1.0E-11
1.0E-11
1.0E-10
1.0E-09
1.0E-08
Hgpt_008_PUF_v25rr_base
Hgpt_008_PUF_v25rr_max_oxid
Hgpt_008_PUF_v25aa0_TEST_43_full_no_check
Hgpt_008_PUF_v25aa0_TEST_43_orig_no_check
Hgpt_008_PUF_v25aa2_TEST_43_full_no_check
Hgpt_008_PUF_v25aa2_TEST_43_orig_no_check
1:1 line
Wet dep to Great Lakes MDN sites estimated with "base" numerical configuration (g/m2-year)

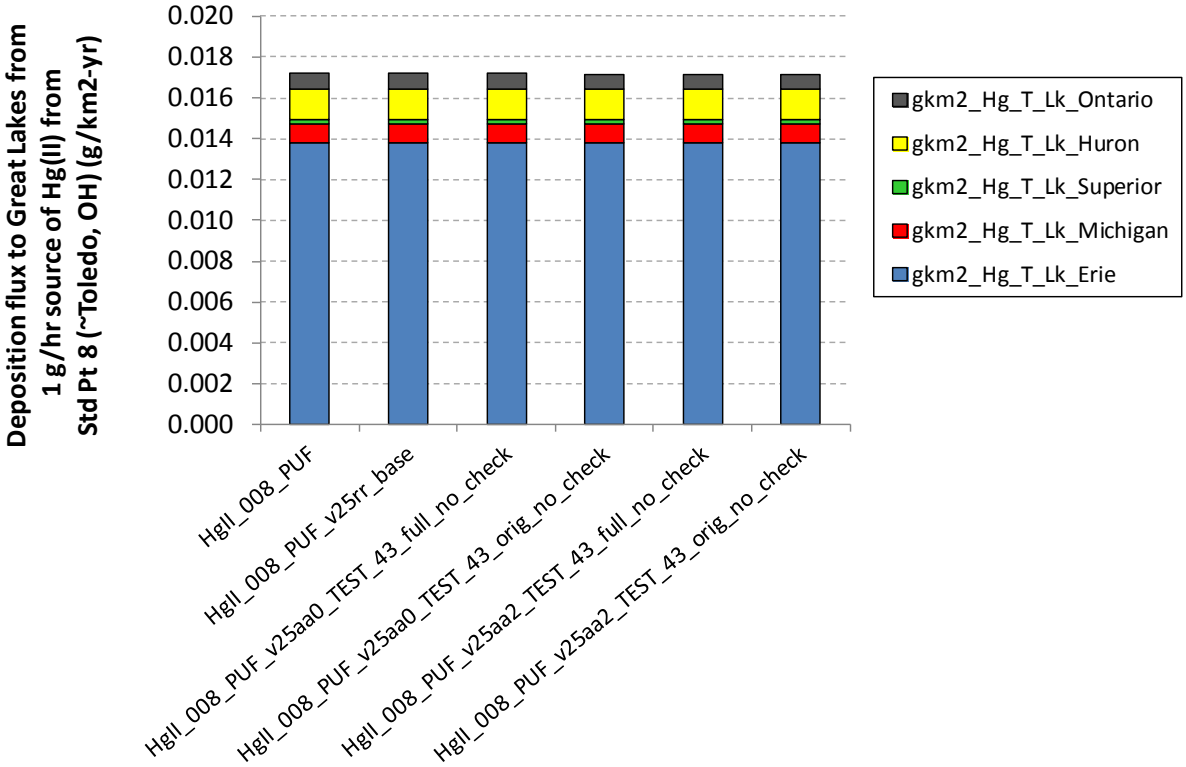
Deposition flux to Great Lakes from 1 g/hr source of Hg(II) from Std Pt 8 (~Toledo, OH) (g/km2-yr)
0.020
0.018
0.016
0.014
0.012
0.010
0.008
0.006
0.004
0.002
0.000
gkm2_Hg_T_Lk_Ontario
gkm2_Hg_T_Lk_Huron
gkm2_Hg_T_Lk_Superior
gkm2_Hg_T_Lk_Michigan
gkm2_Hg_T_Lk_Erie
HgII_008_PUF
HgII_008_PUF_v25rr_base
HgII_008_PUF_v25aa0_TEST_43_full_no_check
HgII_008_PUF_v25aa0_TEST_43_orig_no_check
HgII_008_PUF_v25aa2_TEST_43_full_no_check
HgII_008_PUF_v25aa2_TEST_43_orig_no_check

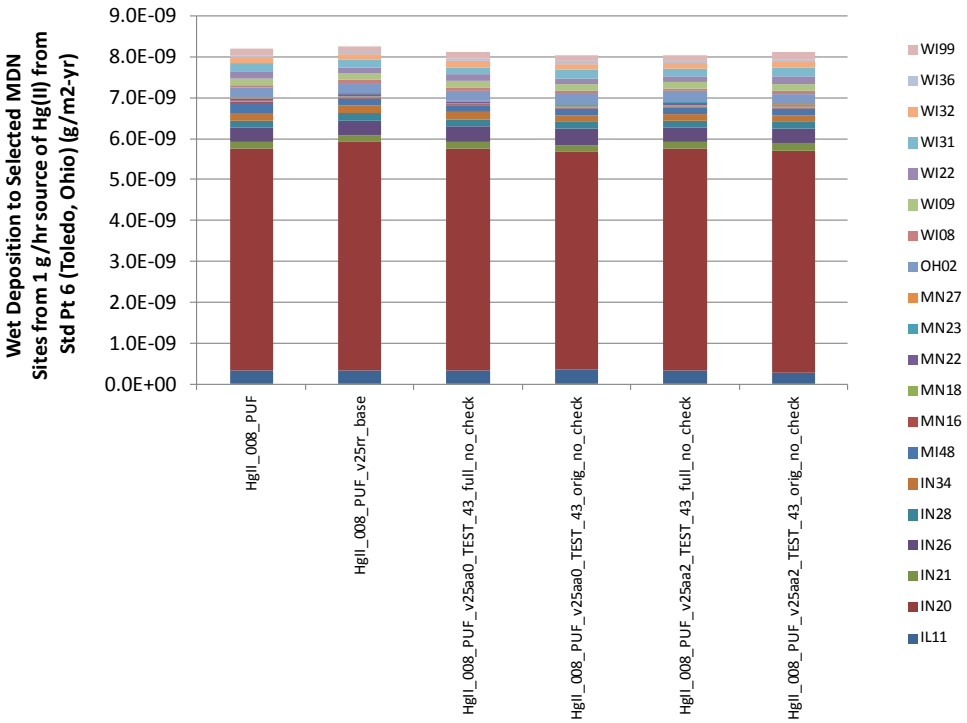
Wet Deposition to Selected MDN Sites from 1 g/hr source of Hg(II) from Std Pt 6 (Toledo, Ohio) (g/m2-yr)
9.0E-09
8.0E-09
7.0E-09
6.0E-09
5.0E-09
4.0E-09
3.0E-09
2.0E-09
1.0E-09
0.0E+00
WI99
WI36
WI32
WI31
WI22
WI09
WI08
OH02
MN27
MN23
MN22
MN18
MN16
MI48
IN34
IN28
IN26
IN21
IN20
IL11
HgII_008_PUF
HgII_008_PUF_v25rr_base
HgII_008_PUF_v25aa0_TEST_43_full_no_check
HgII_008_PUF_v25aa0_TEST_43_orig_no_check
HgII_008_PUF_v25aa2_TEST_43_full_no_check
HgII_008_PUF_v25aa2_TEST_43_orig_no_check

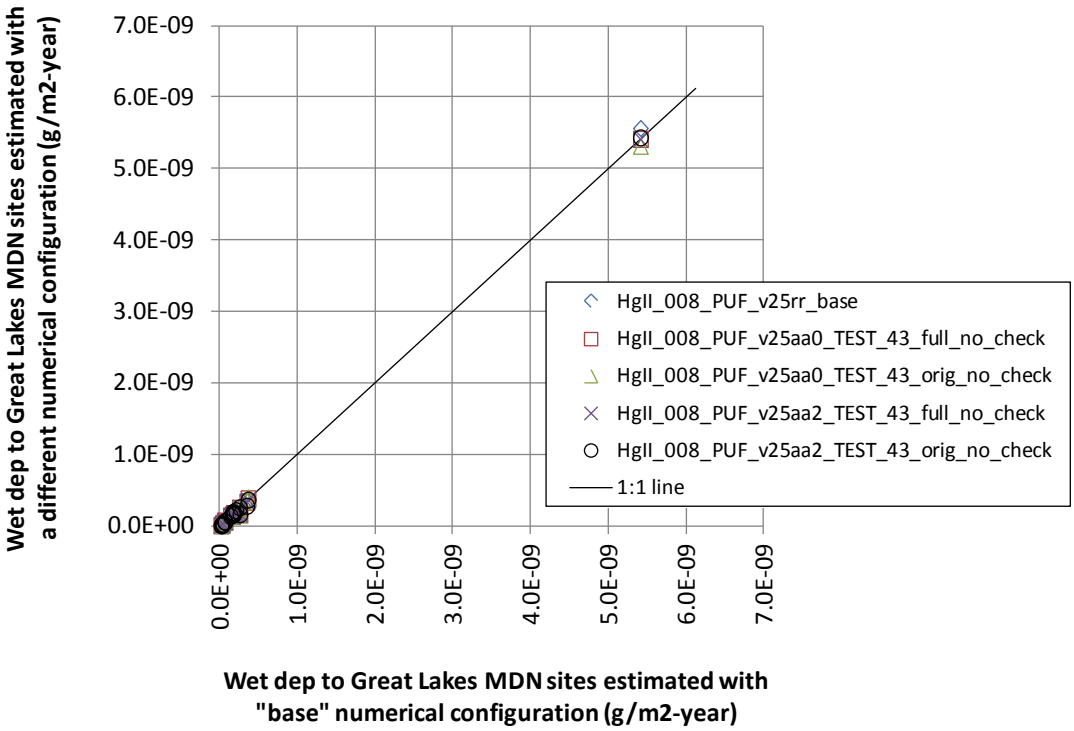
Wet dep to Great Lakes MDN sites estimated with a different numerical configuration (g/m2-year)
7.0E-09
6.0E-09
5.0E-09
4.0E-09
3.0E-09
2.0E-09
1.0E-09
0.0E+00
0.0E+00
1.0E-09
2.0E-09
3.0E-09
4.0E-09
5.0E-09
6.0E-09
7.0E-09
HgII_008_PUF_v25rr_base
HgII_008_PUF_v25aa0_TEST_43_full_no_check
HgII_008_PUF_v25aa0_TEST_43_orig_no_check
HgII_008_PUF_v25aa2_TEST_43_full_no_check
HgII_008_PUF_v25aa2_TEST_43_orig_no_check
1:1 line
Wet dep to Great Lakes MDN sites estimated with "base" numerical configuration (g/m2-year)

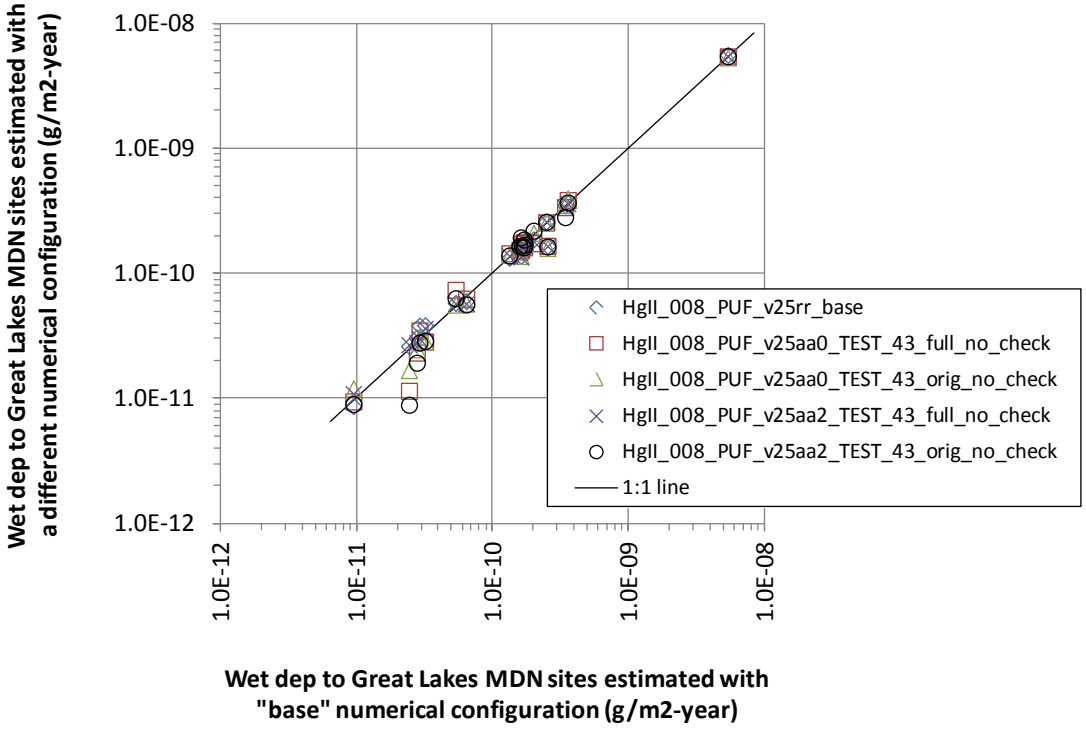
Wet dep to Great Lakes MDN sites estimated with a different numerical configuration (g/m2-year)
1.0E-08
1.0E-09
1.0E-10
1.0E-11
1.0E-12
1.0E-12
1.0E-11
1.0E-10
1.0E-09
1.0E-08
HgII_008_PUF_v25rr_base
HgII_008_PUF_v25aa0_TEST_43_full_no_check
HgII_008_PUF_v25aa0_TEST_43_orig_no_check
HgII_008_PUF_v25aa2_TEST_43_full_no_check
HgII_008_PUF_v25aa2_TEST_43_orig_no_check
1:1 line
Wet dep to Great Lakes MDN sites estimated with "base" numerical configuration (g/m2-year)